Doctoral Dissertations 1896 - February 2014

1-1-1977

Bounded coating flows of viscous and viscoelastic fluids.

Jehuda, Greener
University of Massachusetts Amherst

Follow this and additional works at: https://scholarworks.umass.edu/dissertations_1

BOUNDED COATING FLOWS OF VISCOUS
AND VISCOELASTIC FLUIDS

A Dissertation Presented

By

JEHUDA GREENER

Submitted to the Graduate School of the
University of Massachusetts in partial fulfillment
of the requirements for the degree of

DOCTOR OF PHILOSOPHY

December   1977

Polymer Science and Engineering

BOUNDED COATING FLOWS OF VISCOUS
AND VISCOELASTIC FLUIDS

A Dissertation Presented
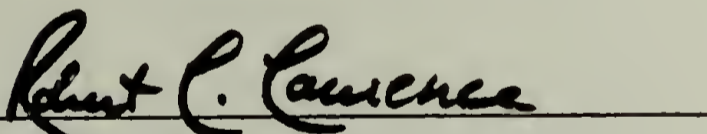
By

JEHUDA GREENER
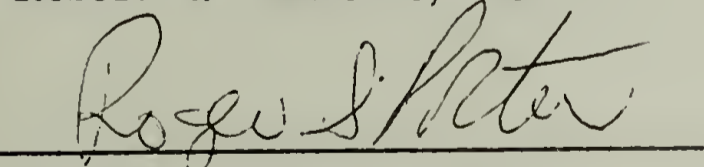
Approved as to style and content by:
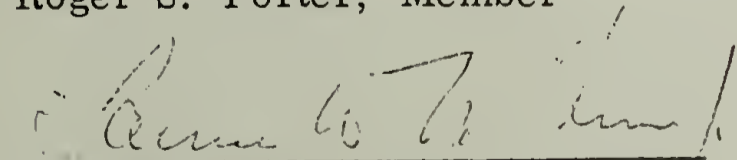
Stanley Middle

Stanley Middleman
Chairperson of Committee
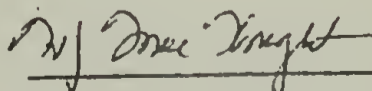
Robert C. Laurence

Robert L. Laurence, Member

Roger S. Porter

Roger S. Porter, Member

Lawrence W. McKenna

Lawrence W. McKenna, Member

W. J. MacKnight

W.J. MacKnight, Department Head
Polymer Science and Engineering

iii

ACKNOWLEDGEMENTS

ABSTRACT

Bounded Coating Flows of Viscous
and Viscoelastic Fluids

February   1978

Jehuda Greener
B.S.(Ch.E.) Technion, Haifa (Isreal)
M.S., University of Massachusetts
Ph.D., University of Massachusetts

Directed by: Professor Stanley Middleman

A theoretical and experimental study of bounded coating flows is presented.   These flows are characterized by lubrication-like kinematics and by high capillary numbers in the vicinity of free surfaces and are encountered in numerous coating applications.

Two systems were studied in detail: blade coating and roll coating. These systems were represented by simple but realistic prototypes: the rigid planar blade coater, the sheet-and-roll system and the system of half-immersed counter rotating rollers. Hydrodynamic models have been developed for each system, utilizing the lubrication approximation and with a special consideration given to the effect of fluid rheology; Lubrication analyses were carried out for several non-Newtonian constitutive models (the power-law fluid, the second-order fluid and the Criminale-Ericksen-Filbey (CEF) equation) yielding useful performance relations for the systems

under consideration. These relations gave predictions mainly for the coating thickness and the hydrodynamic loading. In addition to the kinematic lubrication approximation, the analytical work required a number of approximations, dynamic constitutive and geometric which were explicitly stated and rationalized. Some calculations (for the CEF model) were carried out through a regular perturbation scheme.

Experiments were conducted with a simulated rigid planar blade coater in which the coating thickness was measured for several fluids both Newtonian and viscoelastic and the effect of the inclination of the blade relative to the web was studied. The Newtonian data were generally in agreement with the lubrication solution. Also, the viscoelastic fluids were found to produce higher coating thickness than the Newtonian fluids consistent with the approximate analytical model.

The system of half-immersed counter rotating rollers was used for an experimental study of roll coating. In this experiment coating thickness data were gathered for rheologically different fluids. Data for Newtonian fluids, both in gravity-free and gravity-controlled regimes, were found in satisfactory agreement with the lubrication solution. Similar runs with viscoelastic fluids were inconclusive because of the onset of the "ribbing instability" under relatively low speed conditions.

An attempt to elucidate the dynamics in roll coating was made through a study of the submerged roll system which was shown to be

hydrodynamically similar to the sheet-and-roll system. An experimental study of the system was conducted in which pressure distributions were measured in the converging-diverging flow space for a Newtonian and a viscoelastic fluid. The Newtonian data were in agreement with a finite element solution of the problem. The results for the viscoelastic fluid, while qualitatively in conformity with the approximate theory, could not be critically evaluated because of the lack of an exact solution to the related problem.

The important question of stability in coating flows was considered through a study of the ribbing phenomenon. The related literature was surveyed and the few existing studies concerning this phenomenon were critically assessed. Some data for Newtonian and viscoelastic fluids have been reported. These data show clear phenomenological as well as quantitative differences between the Newtonian and the viscoelastic instabilities. A simple physical stability theory that is capable of explaining some of the observed differences has been presented.

TABLE OF CONTENTS

APPENDIX

LIST OF FIGURES

LIST OF TABLES

To my wife Helena
and to my parents.

CHAPTER I

INTRODUCTION

In the past, coating system design and optimization of process variables have been an art which advanced mainly through trial-and-error. With the advent of sophisticated process control equipment, the increase in production volume and the growing demand for low-tolerance high precision products, the need for more fundamental understanding of the dynamics of coating operations has emerged. Up-to-date process control equipment permits reliable monitoring and efficient control of many process variables and the only relevant question to be asked is: Which variables should be controlled and how?

An increase in total throughput and a decrease in processing cost while maintaining the product properties within specified tolerances is the classical goal of optimal production. This goal can normally be approached in many ways. The coating of a fluid onto a web can also be achieved through several alternative processes. But aside from the selection of a proper coating system for a specific application, a decision has to be made as to what operating conditions (e.g., system geometry, web speed, imposed pressure etc.) are to be used for obtaining a uniform coating at a specified thickness and at a desired throughput. The trial and error approach

becomes increasingly inefficient and the various questions facing the designer and the operator can be answered more readily (and less expensively) through a better understanding of the dynamics of the particular coating system.

> "Coating is a process whereby a liquid is applied continuously to a moving sheet in order to produce a uniform application of the fluid onto and/or within the sheet." (Middleman 1977)

The flows encountered in coating processes are called coating flows. Despite the obvious technological impact of such hydrodynamic systems, the related literature is relatively scant and it addresses itself primarily to the technological aspects of coating operations. Publications by Park (1969), Briston (1974), Booth (1968) and Lin (1974) are a characteristic sample of the technical literature in this area. In these publications the treatment is mainly descriptive-qualitative and it is oriented toward specific applications of the systems considered.

Only few attempts at hydrodynamic modeling of coating flows have been made. Ruschak (1974) and Ruschak and Scriven (1977) present analytical solutions to several free surface problems encountered in coating operations. The classical problem of withdrawal coating has been studied intensively in the last two decades (Cf: Middleman 1977) and is still subject to theoretical and experimental investigations. Some analyses of coating systems in which free surface effects are secondary have been carried out by Greener and Middleman (1974, 1975) and Middleman (1977). The present work is an extension of the latter publications.

This study addresses itself to modeling and experimental investigation of several bounded coating flow systems. By way of definition, these flows are hydrodynamically similar to lubrication flows and their performance is not controlled by surface tension effects. (More definite features are specified in Chapter II.) Also, inasmuch as many coating materials are polymeric by nature, a special consideration is given to the effect of fluid rheology.

Rheologists have developed a host of molecular and continuum theories to explain the behavior of macromolecular fluids under well defined flow conditions. These theories proved generally successful for so-called viscometric flows. Such flows, however, are rarely encountered in practice and many technologically important systems are kinematically complex and cannot be dealt with by conventional rheological approaches. Most, if not all, polymer processing flow systems, such as those found in extrusion, injection molding, fiber spinning and various coating processes are non-viscometric. The complexity of such flows is twofold:

a. The rate-of-deformation tensor is often spatially inhomogeneous and it contains mixed components of shear and elongation.

b. The strain (stretch) histories are not constant, i.e., these flows involve non-steady deformations in the Lagrangian sense.

Some current hypotheses suggest that flows containing mixed kinematic components may be fundamentally different from simple shear flows under

conditions of high deformation rates (Hinch 1974, Tanner 1976); This difference is proposed to arise from the highly orienting effect of the finite elongational components on the configuration of macromolecules in such flows. These flow, termed "strong flows", are gaining much attention both on the molecular and phenomenological levels.

Bounded coating flows, being kinematically nearly viscometric, are suitable for a study of first-order deviations from viscometric flow behavior. It is argued in Chapter II, however, that despite their nearly viscometric character, these flows may be much different dynamically from viscometric flows.

Aside from the fundamental aspects involved in the study of bounded coating flows, these flows are of considerable technological importance. This study attempts to establish some useful operation-performance relations for two important coating systems: blade coating and roll coating. The specific and immediate goals of this study are:

a. To develop simple hydrodynamic models for the systems under consideration with an emphasis on the effect of fluid viscoelasticity.

b. To test experimentally the analytical models for (rheologically) different fluids.

c. To pursue an experimental investigation of the "ribbing instability" observed in roll coating operations, and to modify existing stability criteria for non-Newtonian fluids.

The systems considered in this study are simplified versions of the usually more complex industrial devices. It is hoped, however, that this work will provide a theoretical and empirical basis for further refinements and modifications.

The dissertation is composed of three main units. Chapters I - IV are the introductory chapters, in which the subject is introduced, the modeling strategy presented and several topics of rather general nature are discussed. Chapters V - VIII, the core chapters, give an account of the original contributions of this study. Finally, in Chapter IX, a summary of this work, together with suggestions for future research, are presented.

In Chapter II, a rather general discussion of some hydrodynamic and rheological aspects of bounded coating flows is given. This discussion illustrates the formidable task involved in undertaking an explicit viscoelastic analysis for the flows under consideration. A brief state-of-the-art survey of viscoelastic lubrication flows is presented in Chapter III. This chapter discusses some rational approaches used to tackle viscoelastic flow problems encountered in lubrication-type systems. In Chapter IV, the mathematical model used throughout this study is presented and the various dynamic, kinematic and constitutive approximations are stated and discussed.

From Chapter V and on attention is centered on specific coating problems. Chapter V deals with blade coating. The problem is introduced, stated and analyzed for several constitutive models and a simple experiment

designed to test the various model results is reported. Some comments on the dynamic boundary conditions in blade coating conclude this chapter.

Chapter VI is concerned with the roll coating problem. Two model systems are considered explicitly: the sheet-and-roll system and the system of half-immersed counter-rotating rollers. Analyses for these systems are followed by a section which details the experimental work with the system of half-immersed counter-rotating rollers. Finally, a brief account of the reverse-roll coating problem is given. Chapter VII is a direct extension of Chapter VI. Here, the dynamics in the bounded regime in roll coating are studied through an investigation of the submerged roll system. Hydrodynamic analyses of this system are presented and an experimental study of the system is reported.

The "ribbing phenomenon", the most common hydrodynamic instability in coating operations, is considered in Chapter VIII. The related literature is surveyed and additional data for Newtonian and viscoelastic fluids are presented followed by a simplified stability analysis.

A concise summary of the analytical and experimental results of this work is given in Chapter IX together with some thoughts on potential future research directly extended from this dissertation.

CHAPTER II

BOUNDED COATING FLOWS:
HYDRODYNAMIC AND RHEOLOGICAL CONSIDERATIONS

II. 1   Characteristic Features

Coating flows can be crudely classified as flows encountered in industrial coating operations where a coating fluid is deposited, in some way, onto a moving web. Such a practical definition, however, lacks in providing insight as to the hydrodynamic-physical nature of the flows. It is thus fruitful to examine this class of flows in a more rigorous manner and establish a more meaningful framework for discussion.

Coating flows have several characteristic features which are found in many industrial coating processes. These features can serve as a basis for defining these flows and distinguishing them from other hydrodynamic systems.

a.   Lubrication flows - geometric and kinematic similarities. Many coating systems can be looked upon as "lubrication systems". That is to say that coating flows are, in effect, two dimensional flows with dominant shear components and with small but non-vanishing extension components. This statement does not apply universally to all coating processes and there are some coating systems which do not fall in the category of "lubrication flows" (e.g., blade-coaters with a large angle). The notion of

lubrication character, however, is in most cases conceptually useful and practically applicable. A more detailed discussion of hydrodynamic lubrication and its relation to coating flows is given in Chapter III. It is implicit from the above that fluid particles in coating flow systems are experiencing rapidly changing deformations in time. These transient kinematics are manifested by finite Lagrangian acclerations (finite extensional components in the rate-of-deformation tensor) and are of considerable importance when dealing with viscoelastic fluids.

b. Non-Newtonian fluids. Unlike lubrication systems in which fluids are mostly Newtonian in character, many fluids employed in industrial coating processes are polymeric by nature and thus rheologically non-Newtonian. Such fluids can be either purely viscous or viscoelastic; for neither case does the classical lubrication theory hold.

From a standpoint of the "Simple Fluid Theory" (Noll 1958) viscoelastic fluids are isotropic fluids with (fading but) relatively strong "memory", i.e., past deformations and the transient nature of these deformations contribute to the present state of the stress field. For such complex deformation histories as encountered in coating flows it is required, in principle, to employ a superior constitutive model that is capable of predicting the response of the fluid. It is, however, well known that the better the predictive capabilities of a constitutive model the less its algebraic tractability. Consequently, as will be seen later, one has to resort to

approximations and compromises. Undoubtedly, the introduction of non-Newtonian constitutive models adds to the complexity of the general flow equations, and thereby makes the analysis excessively difficult in some cases.

c. Free Surfaces. Such hydrodynamic boundaries are found in most, if not all, coating processes. Free surfaces are mathematically difficult to handle since their position is a-priori unknown and because of the need to introduce Cauchy-type boundary conditions to the system equations. The existence of free surfaces requires the consideration of surface tension forces and the assessment of their relative importance along the free boundaries. Furthermore, hydrodynamic instabilities which are common in many processes are usually manifested by the shape of the free surfaces and are strongly dependent on the free surface dynamics. This phenomenon is of paramount importance in certain coating operations and it is considered in Chapter VIII.

In some cases, such as withdrawal coating (or dip coating), free surface effects completely dominate the dynamics of the system (Middleman 1977). Indeed, a theoretical investigation of free surface flows encountered in coating operations had been carried out by Ruschak (1974) (see also Ruschak and Scriven 1977). In many cases, however, free surfaces play a minor role and have little effect on the performance of the system.

Coating flows in which the free surface dynamics are relatively unimportant, so long as the flow is stable, will be referred to as <u>bounded coating flows</u> as opposed to <u>free coating flows.</u> It is also stipulated, by way of definition, that bounded coating flows are kinematically equivalent to lubrication flows in clear distinction from free coating flows which cannot be regarded as lubrication flows in the classical sense. For the bounded coating flow systems that are considered in this study (blade and roll coaters) the surface tension is introduced into the analysis (at best) through a dynamic boundary condition for the pressure and it is found to have, generally, a marginal effect on the performance of the system.

Some aspects of the kinematics of bounded coating flows are considered in the next section where discussion is confined to the bounded flow regimes. This is followed by a general discussion of the dynamics presented in Section 3. Finally, in Section 4, Deborah-number effects in bounded coating flows are briefly assessed.

II. 2 Kinematics

A qualitative examination of the kinematic character of bounded coating flows is presented. The kinematics of flow provide, in general, a very valueable insight as to the kind of deformations experienced by the fluid in a particular system. It serves as a basis for selecting an appropriate constitutive model that will be the best compromise between realism and simplicity in describing the response of the fluid. The objective of

this section is to develop some kinematic formalism and basic analytic

tools for a more rigorous examination of coating flows.

Coating flows can be viewed as steady two-dimensional (planar) flows

with dominant shear components. The most general possible two-dimension-

al velocity field for an incompressible fluid is given by (Marrucci and

Astarita 1967)

$$u^1 = \dot{\epsilon} x^1 + \dot{\gamma}_1 x^2$$
$$u^2 = \dot{\gamma}_2 x^1 - \dot{\epsilon} x^2 \tag{II-1}$$
$$u^3 = 0$$

Where $\dot{\gamma}_1$, $\dot{\gamma}_2$ and $\dot{\epsilon}$ are some kinematic parameters and u^i are the

velocity vector components in x^i (a cartesian frame).

Lubrication flows (and therefore bounded coating flows) can be regard-

ed as a special subclass of the general flows defined by Eq. (II-1). Such

flows are subject to the following additional restriction

$$\dot{\epsilon}, \dot{\gamma}_2 \ll 1 \tag{II-2}$$

(This condition is not homogeneously valid!) It is, nevertheless, illuminat-

ing to proceed on with the general planar flow equations and later discuss

some special cases on their merits.

It was shown by Marrucci and Astarita (1967) that by a proper trans-

formation any flow field of the form given in Eq. (II-1) can be reduced to:

$$u^{1'} = \dot{\beta}_1 x^{2'}$$
$$u^{2'} = \dot{\beta}_2 x^{1'} \tag{II-3}$$
$$u^{3'} = 0$$

where:

$$x^{1'} = x^1 \cos\alpha - x^2 \sin\alpha$$

$$x^{2'} = x^1 \sin\alpha + x^2 \cos\alpha \qquad\qquad (II-4)$$

$$x^{3'} = x^3$$

and,

$$\sin\alpha = \frac{1}{\sqrt{2}} \sqrt{1 - \sqrt{\frac{\dot{\gamma}^2}{\dot{\gamma}^2 + \dot{\epsilon}^2}}}$$

$$\dot{\gamma} = \frac{1}{2}(\dot{\gamma}_1 + \dot{\gamma}_2)$$

$$\qquad\qquad (II-5)$$

$$\dot{\beta}_1 = \frac{1}{2}(\dot{\gamma}_1 - \dot{\gamma}_2) + \sqrt{\dot{\gamma}^2 + \dot{\epsilon}^2}$$

$$\dot{\beta}_2 = \frac{1}{2}(\dot{\gamma}_2 - \dot{\gamma}_1) + \sqrt{\dot{\gamma}^2 + \dot{\epsilon}^2}$$

The transformation in Eq. (II-4) is in effect a rotation by an angle α about the x^3 axis.

The field in the rotated system ($u^{i'}$) is a combination of pure shear flow (PSF) and simple shear flow (SSF). These two cases are obtained under two extreme conditions; when $\dot{\beta}_2 = 0$ (or $\dot{\epsilon} = \dot{\gamma}_2 = 0$) the flow is SSF and for $\dot{\beta}_1 = \dot{\beta}_2$ (or $\dot{\gamma}_1 = \dot{\gamma}_2 = 0$) the PSF limit is approached (in the $x^{i'}$ frame).

In general, Eq. (II-3) represents a spectrum of flow situations that range from SSF to PSF depending on the relative magnitude of $\dot{\beta}_1$ and $\dot{\beta}_2$. It is implicit from the condition given in Eq. (II-2) that bounded coating flows will lie close to the SSF limit in this spectrum. One can actually

argue that these flows are perturbations about the SSF case with $\dot{\epsilon}/\dot{\gamma}_1$ and $\dot{\gamma}_2/\dot{\gamma}_1$ as some perturbation parameters. The kinematic parameters $\dot{\gamma}_1$, $\dot{\gamma}_2$ and $\dot{\epsilon}$ will not be, in general, spatially uniform (Crowley et al. 1976) and thus the restriction given in Eq. (II-2) will not be uniformly valid.

After the general planer flow field has been defined in the original frame (x^i) and the rotated frame $(x^{i'})$ attention can be focused on some relevant kinematic tensors.

It is useful to restrict the following discussion to the original coordinate system (x^i) for which the kinematic parameters are more readily interpretable. For the velocity field given in Eq. (II-1) the rate-of-deformation tensor, can be easily obtained:

$$\underset{\sim}{\Delta} = \nabla \underline{u} + \nabla^{\mathsf{T}}\underline{u}$$

$$= \begin{pmatrix} 2\dot{\epsilon} & \dot{\gamma}_1 + \dot{\gamma}_2 & 0 \\ \dot{\gamma}_1 + \dot{\gamma}_2 & -2\dot{\epsilon} & 0 \\ 0 & 0 & 0 \end{pmatrix} \qquad \text{(II-6)}$$

and the vorticity tensor, $\underset{\sim}{\omega}$, is given by:

$$\underset{\sim}{\omega} = (\nabla \underline{u} - \nabla^{\mathsf{T}}\underline{u})$$

$$= \begin{pmatrix} 0 & -\dot{\gamma}_1 + \dot{\gamma}_2 & 0 \\ -\dot{\gamma}_2 + \dot{\gamma}_1 & 0 & 0 \\ 0 & 0 & 0 \end{pmatrix} \qquad \text{(II-7)}$$

It is apparent from Eq. (II-6) that whenever the condition in Eq. (II-2) is imposed one faces a simple shear flow in effect. Such an argument is indeed valid when dealing with purely viscous fluids for which the deformation fields are solely represented by $\underset{\sim}{\Delta}$.

For viscoelastic fluids the strain tensors are more appropriate measures of the deformation field since they represent in some way the strain history in the field.

The motion of a particle in the general planar flow field (Eq. (II-1)) can be obtained by solving the following simultaneous equations:

$$\frac{\partial x^i}{\partial s} = -u^i \tag{II-8}$$

with $\quad x^i = \xi^i \ @ \ s = 0$

x^i is the position of the particle at the instant of observation, t, ξ^i is the coordinate that gives the position of the particle at some past time, t + s, where s is the "backward running elapsed time". As is stated by the initial condition in Eq. (II-8) the coordinates x^i and ξ^i will coincide at the instant of observation (s = 0). Solution of Eq. (II-8) yields:

$$\xi^1 = (C + \frac{\dot{\epsilon}}{m} S) x^1 + \frac{\dot{\gamma}_1}{m} Sx^2$$

$$\xi^2 = \frac{\dot{\gamma}_2}{m} Sx^1 + (C - \frac{\dot{\epsilon}}{m} S) x^2 \tag{II-9}$$

$$\xi^3 = x^3$$

where,

$$m = \sqrt{\dot{\gamma}_1 \dot{\gamma}_2 + \dot{\epsilon}^2}$$

$$C = \cosh(ms)$$

$$S = \sinh(ms)$$

In the limit $\dot{\epsilon}$, $\dot{\gamma}_2 \longrightarrow 0$ Eq. (II-9) reduces to the proper SSF form, while for $\dot{\gamma}_1$, $\dot{\gamma}_2 \longrightarrow 0$ the motion approaches the planar elongation limit (Stevenson et al. 1975).

For the motion expressed by Eq. (II-9) the Cauchy-Green tensor will take the form:

$$C_{ij} = g_{kl} \frac{\partial \xi^k}{\partial x^i} \frac{\partial \xi^l}{\partial x^j}$$

$$= \begin{pmatrix} (C + \frac{\dot{\epsilon}}{m}S)^2 + (\frac{\dot{\gamma}_2}{m}S)^2 & (C + \frac{\dot{\epsilon}}{m}S)\frac{\dot{\gamma}_1}{m}S & 0 \\ & +(C - \frac{\dot{\epsilon}}{m}S)\frac{\dot{\gamma}_2}{m}S & \\ (C + \frac{\dot{\epsilon}}{m}S)\frac{\dot{\gamma}_1}{m}S & & \\ \quad +(C - \frac{\dot{\epsilon}}{m}S)\frac{\dot{\gamma}_2}{m}S & (\frac{\dot{\gamma}_1}{m}S)^2 + (C - \frac{\dot{\epsilon}}{m}S)^2 & 0 \\ & & \\ 0 & 0 & 1 \end{pmatrix} \quad \text{(II-10)}$$

(For the system considered the metric tensor g_{kl} is a unit tensor $\underset{\sim}{I}$.) Here too, when the proper limits are set $\underset{\sim}{C}$ reduces to its well known forms for SSF and for planar elongation (Middleman 1968).

In Eq. (II-10) C is the Cauchy-Green tensor (or the strain history) for the most general planar flow field.

The Finger strain tensor for this flow can be similarly obtained.

$$(C^{-1})_{ij} = g^{kl} \frac{\partial x^i}{\partial \xi^k} \frac{\partial x^j}{\partial \xi^l}.$$

$$= \begin{pmatrix} (C - \frac{\dot\epsilon}{m} S)^2 + (\frac{\dot\gamma_1}{m} S)^2 & -(C - \frac{\dot\epsilon}{m} S)\frac{\dot\gamma_2}{m} S & 0 \\[2ex] -(C - \frac{\dot\epsilon}{m} S)\frac{\dot\gamma_2}{m} S & -(C + \frac{\dot\epsilon}{m} S)\frac{\dot\gamma_1}{m} S & \\[2ex] -(C + \frac{\dot\epsilon}{m} S)\frac{\dot\gamma_1}{m} S & (\frac{\dot\gamma_2}{m} S)^2 + (C + \frac{\dot\epsilon}{m} S)^2 & 0 \\[2ex] 0 & 0 & 1 \end{pmatrix}$$

Another useful kinematic tensors are the Rivlin-Ericksen tensors, $\overset{(N)}{\underset{\sim}{A}}$. where,

$$\overset{(N)}{A}_{ij} = \left. \frac{\partial^N C_{ij}}{\partial s^N} \right|_{s=0} \tag{II-11}$$

For the flow considered here:

$$\overset{(1)}{\underset{\sim}{A}} = \underset{\approx}{\triangle}$$

and

$$\overset{(2)}{\underset{\sim}{A}} = 2 \begin{pmatrix} 2\dot\epsilon^2 + \dot\gamma_1 \dot\gamma_2 + \dot\gamma_2{}^2 & \dot\epsilon(\dot\gamma_1 - \dot\gamma_2) & 0 \\[2ex] \dot\epsilon(\dot\gamma_1 - \dot\gamma_2) & 2\dot\epsilon^2 + \dot\gamma_1\dot\gamma_2 + \dot\gamma_1{}^2 & 0 \\[2ex] 0 & 0 & 0 \end{pmatrix}$$

The kinematic tensors derived above provide a basis for further dynamic considerations.

II. 3   Dynamics

Now that some kinematic concepts have been put forth one can proceed in examining the dynamics in the general planar flow field, making use of

some crude constitutive models that are capable of predicting, at least qualitatively, the effect of the kinematic parameters on the stress field.

For viscoelastic fluids, the a-priori low levels of the extensional components ($\dot{\epsilon}/\dot{\gamma}_1 \ll 1$) in bounded coating flows may be irrelevant as to whether the flow can be approximated as SSF or not. Some viscoelastic constitutive models may weigh the extensional components much beyond their kinematic levels, as will be seen subsequently.

It is convenient to employ two simple rate models; the corotational Maxwell (CRM) and the codeformational Maxwell (CDM) equations.

Both models can be represented by the following rate expression:

$$\underset{\sim}{\tau} + t_R(\dot{\underset{\sim}{\tau}}) = \eta_o \underset{\sim}{\Delta} \tag{II-12}$$

t_R is a characteristic relaxation time, η_o is a viscosity parameter (or the zero-shear-rate viscosity), $\underset{\sim}{\tau}$ is the dynamic stress tensor and ($\dot{}$) is some operator that represents a convected time derivative that translates and deforms with a fluid particle.

For the CRM model,

$$(\dot{\tau}_{ij}) = \frac{D\tau_{ij}}{Dt} - \frac{1}{2}\omega_{jm}\tau_{mi} - \frac{1}{2}\omega_{im}\tau_{mj} \tag{II-13}$$

This is the corotational (or Jaumann) derivative. For the CDM model,

$$(\dot{\tau}_{ij}) = \frac{D\tau_{ij}}{Dt} - \tau_{kj}\frac{\partial u_i}{\partial x_k} - \tau_{ik}\frac{\partial u_j}{\partial x_k} \tag{II-14}$$

Eq. (II-14) defines the contravariant codeformational (or Oldroyd) derivative.

$\frac{D}{Dt}$ is the Stokes derivative.

In SSF, the CRM model is known to predict shear thinning viscosity with unrealistically low power-law exponent (-1) while the CDM model gives a constant viscosity in shear. The normal-stress coefficients Ψ_{12} and Ψ_{23} depend too strongly on shear rate in the case of the CRM model while they are constant in shear for the CDM model. In SEF the CRM model predicts constant elongational viscosity while the CDM model predicts a singularity in the elongational viscosity function, at $\dot{\in} = 1/2t_R$. The above is indicative of the limitations of these models, yet their qualitative nature is of some value in assessing the response of a viscoelastic fluid in complex flow fields.

For the planar flow field discussed in the previous section the following stress components are obtained for each of the models considered above.

<div align="center">CRM   CDM</div>

$$\tau_{12} = \frac{\eta_0(\dot{\gamma}_1 + \dot{\gamma}_2) - 2\eta_0 t_R \dot{\in}(\dot{\gamma}_1 - \dot{\gamma}_2)}{1 + t_R^2(\dot{\gamma}_1 - \dot{\gamma}_2)^2} \qquad \frac{\eta_0(\dot{\gamma}_1 + \dot{\gamma}_2) - 2 t_R \eta_0 \dot{\in}(\dot{\gamma}_1 - \dot{\gamma}_2)}{1 - 4t_R^2 \dot{\gamma}_1\dot{\gamma}_2 - 4t_R^2 \dot{\in}^2}$$

$$\tau_{11} - \tau_{22} = \frac{2\eta_0[2\dot{\in} + \dot{\gamma}_1^2 - \dot{\gamma}_2^2]}{1 + t_R^2(\dot{\gamma}_1 - \dot{\gamma}_2)^2} \qquad \frac{4\eta_0\dot{\in} + 2t_R[\dot{\gamma}_1 - \dot{\gamma}_2 + 2t_R(\dot{\gamma}_1 + \dot{\gamma}_2)]\tau_{12}}{(1 - 2t_R\dot{\in})(1 + 2t_R\dot{\in})}$$

$$\tau_{22} - \tau_{33} = \frac{-\eta_0 t_R(\dot{\gamma}_1^2 - \dot{\gamma}_2^2) - 2\eta_0\dot{\in}}{1 + t_R^2(\dot{\gamma}_1 - \dot{\gamma}_2)^2} \qquad \frac{-2\eta_0\dot{\in} - 2t_R\dot{\gamma}_1\tau_{12}}{(1 - 2t_R\dot{\in})}$$

It is noted that the CDM model predicts singularity in stress at $\dot{\in} = 1/2t_R$ and/or $\dot{\gamma}_1\dot{\gamma}_2 + \dot{\in}^2 = 1/4t_R^2$. Mathematically, the stresses will "blow up" at the singular points regardless of the relative magnitude of the kinematic parameters. In practice, the stresses may increase considerably under the given singular conditions and this will ultimately depend on the elasticity

of the fluid (through t_R) and on the absolute levels of the kinematic

parameters.

In a recently proposed scheme for classification of flow fields,

Tanner and Huilgol (1975) and Tanner (1976) devise some rather arbitrary

but nevertheless useful criteria for distinguishing between so-called "strong

flows" and "weak flows". Using Tanner's physical approach, linear dumb-

bells embedded in a viscoelastic medium will extend "indefinitely" under

"strong flow" conditions whereas in "weak flows" this will not happen.

"Strong flows" are, in effect, flows with dominant extensional components.

Tanner was able to show that for "strong flows",

$$\det \underset{\sim}{\mathcal{L}} > 0 \tag{II-15}$$

and,

$$\frac{27}{16} - \frac{3}{4} \, \text{tr} \underset{\sim}{\mathcal{L}}^2 + \det \underset{\sim}{\mathcal{L}} < 0 \tag{II-16}$$

where

$$\mathcal{L}_{ij} = \frac{\partial u^i}{\partial x^j} - \frac{1}{2} \delta_{ij} \, (t_R^{-1})$$

δ_{ij} is the Kroenecker delta.

For the general planar flow field,

$$\underset{\sim}{\mathcal{L}} = \begin{pmatrix} \dot{\epsilon} - 1/2t_R & \dot{\gamma}_1 & 0 \\ \dot{\gamma}_2 & -\dot{\epsilon} - 1/2t_R & 0 \\ 0 & 0 & -1/2t_R \end{pmatrix} \tag{II-17}$$

and consequently the criteria for "strong flow" are:

$$\dot{\epsilon}^2 + \dot{\gamma}_1 \dot{\gamma}_2 > 1/4 t_R^2 \tag{II-18}$$

and

$$\dot{\epsilon}^2 + \dot{\gamma}_1 \dot{\gamma}_2 < 1/t_R^2 \tag{II-19}$$

or,

$$4 > 4 t_R^2 \dot{\epsilon}^2 + 4 t_R^2 \dot{\gamma}_1 \dot{\gamma}_2 > 1 \tag{II-20}$$

As seen, the conditions for "strong flow" are compatible with the singularity conditions for the CDM model. This result is not surprising, inasmuch as the linear dumbbell considered by Tanner is, in fact, the molecular equivalent of the CDM model (Bird et al. 1977b). Tanner's conditions and the CDM singularity criteria define a range of kinematic behavior for which the general planar flow field will have dominant extensional components.

Can bounded coating flows be classified as "weak" or "strong" flows? Using Tanner's criterion (Eq. (II-20)), it is not impossible that bounded coating flows become "strong" even though $\dot{\epsilon}/\dot{\gamma}_1$, $\dot{\gamma}_2/\dot{\gamma}_1 \ll 1$. For very high deformation rates and high elasticity such flows can be within the "strong flow" regime. These flows, however, will be mostly "weak" since the absolute levels of $\dot{\epsilon}$ and $\dot{\gamma}_2$ are usually low as is implicit from the lubrication-like geometry.

Finally, it is instructive to examine the response of a viscoelastic fluid in the planar flow field using a more realistic constitutive equation. The Criminale-Ericksen-Fibley (CEF) equation, considered below, is

discussed in detail in IV.2. This equation has been recommended for use in the case of nearly viscometric and nearly steady flows. (Pipkin and Tanner 1972, Bird 1976). It is, nevertheless, useful to employ the CEF model for evaluating the effect of the various non-viscometric terms in the rate-of-deformation tensor on the dynamics.

The CEF equation (in a codeformational form) reads

$$\underset{\sim}{\tau} = \eta \underset{\sim}{\overset{(1)}{A}} + (\Psi_{12} + \Psi_{23}) \underset{\sim}{\overset{(1)^2}{A}} - \frac{1}{2} \Psi_{12} \underset{\sim}{\overset{(2)}{A}} \tag{II-21}$$

$\underset{\sim}{\overset{(i)}{A}}$, the Rivlin-Ericksen tensors, were evaluated in the previous section for the general planar flow field. η, Ψ_{12} and Ψ_{23} are the three viscometric functions. The various stress components for the planar flow field, as given by the CEF equation, are found to be:

$$\tau_{12} = \eta(\dot{\gamma}_1 + \dot{\gamma}_2) - \Psi_{12} \dot{\epsilon}(\dot{\gamma}_1 - \dot{\gamma}_2) \tag{II-22}$$

$$\tau_{11} - \tau_{22} = 4\dot{\epsilon}\eta + \Psi_{12}(\dot{\gamma}_1^2 - \dot{\gamma}_2^2) \tag{II-23}$$

and

$$\tau_{22} - \tau_{33} = -2\dot{\epsilon}\eta + \Psi_{12}(2\dot{\epsilon}^2 + \dot{\gamma}_1\dot{\gamma}_2 + \dot{\gamma}_2^2)$$
$$+ \Psi_{23}[4\dot{\epsilon}^2 + (\dot{\gamma}_1 + \dot{\gamma}_2)^2] \tag{II-24}$$

Now, if one imposes the kinematic condition for bounded coating flows, Eq. (II-2), square and cross terms of $\dot{\epsilon}$ and $\dot{\gamma}_2$ can be neglected and it follows that:

$$\tau_{12} = \eta\dot{\gamma}_1 + \eta\dot{\gamma}_2 - \Psi_{12}\dot{\epsilon}\dot{\gamma}_1 \tag{II-25}$$

$$\tau_{11} - \tau_{22} = \Psi_{12} \dot{\gamma}_1{}^2 + \underline{4 \, \dot{\epsilon} \, \eta} \qquad \text{(II-26)}$$

and

$$\tau_{22} - \tau_{33} = \Psi_{23} \dot{\gamma}_1{}^2 + \underline{\Psi_{12} \dot{\gamma}_1 \dot{\gamma}_2 + 2\Psi_{23} \dot{\gamma}_1 \dot{\gamma}_2 - 2\eta \dot{\epsilon}} \qquad \text{(II-27)}$$

The dashed-underlined terms represent, loosely, the first-order effect of the non-viscometric kinematic parameters on the dynamics in the system.

A definitive assessment of Eqs. (II-25) to (II-27) is not possible since, as was stated previously, the kinematics in planar flows are, generally, spatially inhomogeneous. That is, the relative magnitude of the various kinematic parameters is varying throughout the flow domain. This point can be illustrated by a qualitative examination of the sheet-and-roll system which is fully analyzed and discussed in VI.2. In this system, the bounding surfaces are moving in the same direction and at the same lateral speeds. The resulting velocity field in the fluid film has an axis of symmetry along which the velocity gradient vanishes identically. Thus, along this axis $\dot{\gamma}_1$, $\dot{\gamma}_2 = 0$ but $\dot{\epsilon} \neq 0$ and hence the condition given in Eq. (II-2) is indeed not homogeneously valid.

The transient nature of the flow field (in the Lagrangian frame) has not been considered as yet. This aspect of the kinematics is exceedingly important when dealing with viscoelastic fluids and it is briefly discussed in the following section.

II. 4 Transient (Relaxation) Effects – Deborah Number Considerations

Bounded coating flows and lubrication flows are flows with changing stretch histories (Huilgol 1975), i.e., when viewed from a frame attached to a fluid particle, the deformation field is rapidly changing in time. Provided the fluid is viscoelastic, the abruptly deformed particle may not be 'fast' enough to respond 'in phase' to the imposed strains which may, in turn, considerably affect the overall dynamics of the system.

In order to assess the effect of the transient kinematics on the response of the system it is necessary to consider the Deborah number (N_{De}). There is some controversy as to the exact mathematical definition of the Deborah number (Reiner 1964, Metzner et al. 1966, Marrucci and Astarita 1967, Huilgol 1975, Tanner 1976). Its physical meaning, however, is well accepted; it is the ratio of the fluid relaxation time to the duration time of an imposed deformation. For very abrupt deformations (high N_{De}) a viscoelastic fluid will respond in a nearly elastic manner while for long-lasting steady deformations (low N_{De}) the response will be more viscous-like.

In typical bounded coating flow systems the duration of an imposed deformation is $O(L/U)$ where U is a characteristic speed and L is a characteristic length. Thus, a characteristic Deborah number is given by

$$N_{De} = O(t_R \frac{U}{L})$$

(II-28)

For sufficiently high speeds N_{De} can attain high levels thus making the

problem essentially a "Deborah number problem" rather than a "Weissen-

berg number problem", i.e., the transient dynamics may practically over-

shadow the steady-state dynamics.

Many viscoelastic constitutive models predict substantial overshoots in

stress in response to fast step-up deformations (e.g., Bogue, Meissner,

Carreau, Spriggs and others) which was verified experimentally as well

(Leppard and Christiansen 1975). Hence, viscoelastic fluids when subject

to such deformations as found in coating flows may produce, at the time

of duration of the imposed strains, stresses which are much higher than

the expected steady-state stresses.

In order to account for such effects it is necessary, in principle, to

modify the planar flow equations (see II.2) by making the kinematic con-

stants functions of space. In the Lagrangian sense these constants will

rather be functions of time(s) and a solution of Eq. (II-8) will yield a

motion that is different from the one given in Eq. (II-9). This motion

should then be introduced into one of the constitutive models that are

instrumental in predicting transient viscoelastic response. The imprac-

ticallity of such an approach is obvious.

A more rational approach would be to consider a simple simulated

strain history, following a single particle trajectory, that qualitatively re-

presents the actual history in a lubrication-type system. This history can

then be used for calculating the transient stresses in the system by

employing an appropriate integral constitutive model, and see how they differ from the steady-state stresses. Such qualitative analysis is yet to be undertaken.

C H A P T E R III

VISCOELASTIC LUBRICATION FLOWS

III. 1 Hydrodynamic Lubrication - Brief Introduction

The classical theory of hydrodynamic lubrication is almost a century old. In 1886, Osborne Reynolds (Cameron 1966) published the first rigorous treatise of flow behavior in lubrication systems. In his work, Reynolds introduced a number of simplifying assumptions into the more general Navier-Stokes equations and transformed these relatively complex equations into a single partial differential equation. The simplifying assumptions that were introduced by Reynolds proved valid in most lubrication flow systems and consequently were given the collective title "the lubrication approximation".

The lubrication approximation can be posed in the following way (Pearson 1967):

Consider the system shown in Figure III-1. A viscous fluid is contained between two aribtrarily shaped boundaries

$$x^2 = B_1(x^1, x^3 , t)$$

and

$$x^2 = B_2(x^1, x^3 , t)$$

$$(III-1)$$

The functions B_1 and B_2 are smooth and well-behaved. The boundaries are separated by a thin fluid film of thickness $h(x^1, x^3, t)$ $(=B_1(x^1, x^3, t)-B_2(x^1, x^3, t))$
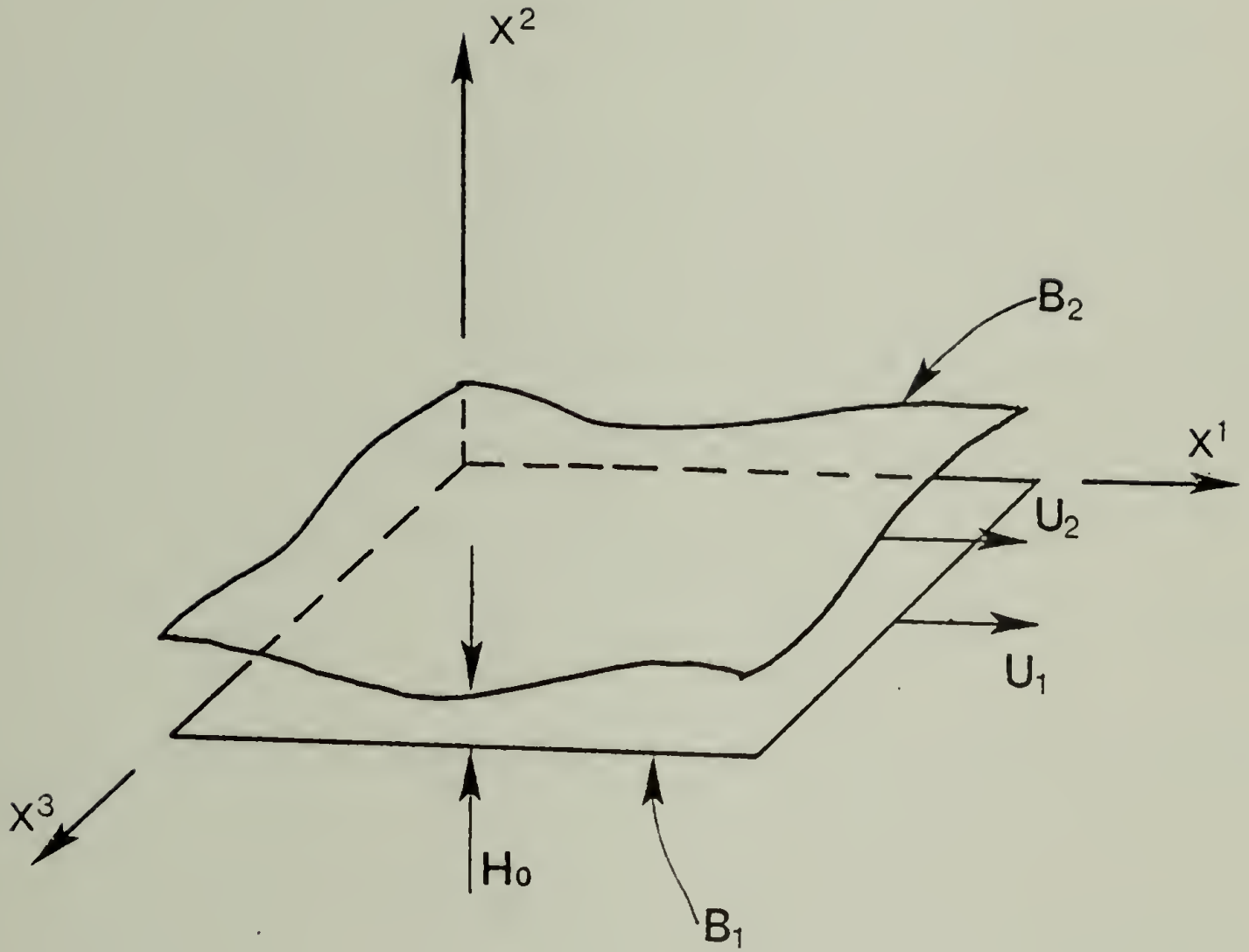
Figure III-1.   A characteristic lubrication geometry.

and are moving at lateral speeds of U_1 and U_2. For such a system the lubrication assumptions will be:

a. The fluid is Newtonian and incompressible.

b. The flow is laminar, isothermal and steady (in the Eulerian sense) with negligible body forces.

c. The characteristic length of the system (L) is much larger than any value of the function h. If one chooses some characteristic thickness, H_0 say, then $L/H_0 \gg 1$. This geometric statement leads to the physical assertion that velocity gradients across the film thickness are much larger than gradients along the primary flow direction, or

$$\frac{\partial}{\partial x^1} (\underset{\sim}{u}) \quad , \quad \frac{\partial}{\partial x^3} (\underset{\sim}{u}) \ll \frac{\partial}{\partial x_2} (\underset{\sim}{u}) \tag{III-2}$$

Also, the variation of the hydrostatic pressure will be only in the primary flow direction. This approximation is sometimes referred to as the "thin film approximation". The mathematical foundation of this approximation is presented in detail by Langlois (1964).

d. The curvature of the boundaries is negligible everywhere, i.e.,

$$\frac{\partial h}{\partial x^3} \quad , \quad \frac{\partial h}{\partial x^1} \ll 1$$

This implies that the surface velocities are nearly unidirectional and the boundaries are almost parallel.

Of the assumptions just outlined the last two are the most characteristic of the lubrication approximation and are widely extended to flows which

are not always identified as lubrication flows per-se.

The lubrication approximation is a very useful tool for solving the equations of motion in flow systems with geometric and kinematic features usually found in lubrication systems.

In many real systems, however, the lubrication approximation is partially invalid and consequently one has to relax some of the lubrication assumptions. A case in point is the extension of lubrication theory to non-Newtonian fluids. In the late 1950's macromolecular additives to lubricating oils were first introduced with the purpose of improving the thermal properties of the lubricants by increasing their Viscosity Index (i.e. reducing the dependence of viscosity on temperature) (Hutton 1973). This novel use of macromolecular solutions as lubricants required a re-vision of the theory of lubrication to account for the non-Newtonian rheological behavior of the fluids.

A complete solution of the viscoelastic lubrication problem, it was shown in Chapter II, is a formidable task. The lubrication approximation being essentially a kinematic statement may be irrelevant and misleading for viscoelastic fluids under high deformation rates. Hence, it is necessary to establish some reasonable constitutive approximation, in addition to the kinematic lubrication approximation, to make the problem mathematically tractable. Two leading approaches for dealing with viscoelastic lubrication flows have been advanced in the last decade; one is based on physical

considerations and the other on dimensional arguments. These approaches are briefly outlined in the next two sections and the subject is summarized in Section 4.

III. 2   Extensional Primary Field (EPF) Approximations

Most lubrication flows have kinematic extensional components which arise from finite variation of the velocity in the primary flow direction. These components are usually orders-of-magnitude smaller than the kinematic shear components (which is in accordance with the "thin film approximation" as stated above). The rate of deformation tensor for such flows will then take the form:

$$
\underset{\sim}{\triangle} = \begin{pmatrix} [\ 0\ ] & \triangle_{12} & 0 \\ \triangle_{21} & [\ 0\ ] & 0 \\ 0 & 0 & [\ 0\ ] \end{pmatrix} \tag{III-3}
$$

where the bracketted extensional terms are assumed to be negligible in comparison to the dominant shear components.

The role and importance of the extensional components, small as they are, needed a fundamental reexamination in view of some experimental evidence which pointed to the existence of very high normal stresses in elongational flows even under conditions of moderate extension rates (Metzner 1971). It is useful to consider this phenomenon in terms of the "Trouton ratio" which is defined as the ratio of the elongational viscosity to the shear viscosity,

$$N_{Tr} = \frac{\eta_{el}}{\eta_{sh}} = \frac{(\tau_{11} - \tau_{22})/\dot{\epsilon}}{\tau_{12}/\dot{\gamma}} \qquad \text{(III-4)}$$

This ratio is equal to 3.0 for Newtonian fluids but, as is discussed in detail by Metzner, there is ample evidence to indicate that this ratio can attain high values, of the order of 10^3, for finite values of extension rates ($\dot{\epsilon} \geq 1/2t_R$). Moreover, there are some constitutive models which support this observation as well (e.g., Bogue, WJFLMB, Lodge's rubber-like fluid and others (Pearson 1975)). This phenomenon, however, is not free from controversy and there are some experimental data and some constitutive models which do not exhibit such high stresses in elongational flows (Pearson 1975). It is the inherent difficulty in measuring the elongational viscosity of liquids which prevents current resolution of this matter.

If indeed a dramatic increase in the elongational viscosity is anticipated then the following approximation can be considered (for two-dimensional flows with moderate-to-high elongation rates)

$$\underset{\sim}{\tau} = \begin{pmatrix} \tau_{11} & [\ 0\ ] & 0 \\ [\ 0\ ] & \tau_{22} & 0 \\ 0 & 0 & \tau_{33} \end{pmatrix} \qquad \text{(III-5)}$$

Here, the shear components of the stress tensor are neglected and the dynamics of the flows are dominated by the normal stresses.

The ideas presented above were put forth by Metzner (1971, 1968) who termed the proposed approximations as "extensional primary field" (EPF) approximations. These approximations merely state that the relevant

rheological property for this class of flows is the elongational viscosity and that the purely viscous characteristics of the fluid are irrelevant for elongation rates that exceed $\dot{\epsilon} \cong 1/2t_R$.

III.3 Tanner's Approach – The Purely Viscous Approximation

An approach fundamentally different from the EPF approximations was proposed by Tanner (1960, 1962, 1968, Williams and Tanner 1970). His arguments are based on a straightforward order-of-magnitude analysis of the momentum equations for viscoelastic lubrication flows.

In the absence of inertia and body forces, the equations of motion in two dimensions and in cartesian coordinates reduce to,

$$\frac{\partial \tau_{11}}{\partial x^1} + \frac{\partial \tau_{12}}{\partial x^2} = \frac{\partial P}{\partial x^1} \qquad \text{(III-6)}$$

$$\frac{\partial \tau_{12}}{\partial x^1} + \frac{\partial \tau_{22}}{\partial x^2} = \frac{\partial P}{\partial x^2} \qquad \text{(III-7)}$$

Using the lubrication approximation, Eq. (III-7) can be further simplified to

$$\frac{\partial T_{22}}{\partial x^2} = 0 \qquad \text{(III-8)}$$

where $T_{22} = P - \tau_{22}$

and Eq. (III-6) is rearranged to

$$\frac{\partial (\tau_{11} - \tau_{22})}{\partial x^1} + \frac{\partial \tau_{12}}{\partial x^2} = \frac{\partial T_{22}}{\partial x^1} \qquad \text{(III-9)}$$

By defining the following dimensionless variables

$$\eta = \frac{x^2}{H_0}, \quad \xi = \frac{x^1}{L}$$

Eq. (III-9) can be rewritten as

$$\frac{\partial (\tau_{11} - \tau_{22})}{\partial \xi} + \frac{L}{H_0} \frac{\partial \tau_{12}}{\partial \eta} = \frac{\partial T_{22}}{\partial \xi} \qquad \text{(III-10)}$$

The central argument in Tanner's approach is based on the assertion that

the viscous term in Eq. (III-10) is much larger than the elastic term in

"true" lubrication systems (i.e., in systems where $L/H_0 \gg 1$).

The ratio of the two terms on the l.h.s. of Eq. (III-10) can be

written as

$$\frac{L}{H_0} \frac{\partial \tau_{12}/\partial \eta}{\partial (\tau_{11} - \tau_{22})/\partial \xi} = O \left[\left(\frac{L}{H_0}\right) \frac{1}{S_R} \right] \qquad \text{(III-11)}$$

In real systems, S_R (the "recoverable shear") is not usually larger than

10 (Middleman 1977) and the above ratio is indeed sufficiently large to

justify the elimination of the elastic term from Eq. (III-10). So,

$$\frac{\partial \tau_{12}}{\partial x^2} = \frac{\partial T_{22}}{\partial x^1} \qquad \text{(III-12)}$$

and since $\partial \tau_{22}/\partial x^1$ is much smaller than $\partial P/\partial x^1$, in accordance with

the lubrication approximation, one can write

$$\frac{\partial \tau_{12}}{\partial x^2} = \frac{dP}{dx^1} \qquad \text{(III-13)}$$

Eq. (III-13) states, in effect, that one needs to know only $\eta(\dot{\gamma})$, the shear

viscosity function, for even a viscoelastic fluid, in order to solve the equa-

tions of motion in lubrication systems. Tanner's approach can be challeng-

ed by arguing that S_R can attain high levels, comparable to L/H_0 under

conditions of high deformation rates. However, this approach seems

realistic, as a first approximation, within a wide range of deformation rates and it cannot be easily dismissed.

III.4 Summary

Tanner's and Metzner's approaches seem contradictory at first although both present valid supporting arguments. (If one accepts Metzner's notion of normal stress "blow-up" under conditions of finite deformation rates). It would be natural to reconcile this apparent contradiction by limiting each approach to a certain range of deformation-rates. This idea can be presented schematically as follows:

deformation rates	appropriate approximation to use
low ("weak flows")	Tanner's purely viscous approximation (η ($\dot{\gamma}$) needed)
moderate	a realistic constitutive model needed
high ("strong flows")	Metzner's EPF approximation ($\eta_{E\ell}(\dot{\gamma})$ needed)

Limits to the proposed deformation-rate ranges cannot be set a-priori and an extensive experimental program is needed in order to establish the range of applicability of any of the proposed approximations. It would be reasonable to assume that industrial coating processes operate at moderate-to-high deformation rates although operation at low deformation rates cannot be automatically excluded (since it much depends on the fluid through t_R). Interestingly, the phenomenon of stress "blow up" in elongation flows can be put to direct test by examining experimentally the applicability of the

"extensional primary field" approach. If such approach is found to be realistic then the phenomenon of stress "blow-up" seems acceptable and vice versa.

It was noted in Chapter II that bounded coating flows and thus lubrication flows can be "strong", in Tanner's sense, under conditions of extreme shear. It is not yet clear, however, whether "flow strength" necessarily implies that the dynamics in the system are going to be drastically affected as is suggested by Metzner. This question is of fundamental importance and it addresses itself to the constitutive nature of viscoelastic fluids.

Little has been said in the literature on the role of relaxation (transient) effects in viscoelastic lubrication flows. This is surprising in view of the arguments presented in Section II. 4. Only recently, it was suggested that transient effects may play a decisive role in lubrication flows (Harnoy 1976). These effects were introduced into the lubrication problem via a modified second-order model that allegedly "enables a separate parametric description of the stress relaxation process". This approach seems arbitrary and may not give a realistic representation of the actual dynamics. Consequently, further consideration of transient effects in lubrication flows is in order.

The few existing experimental studies on non-Newtonian lubrication flows show that polymeric lubricants are more effective than the equivalent

Newtonian lubricants (with viscosity equal to the zero-shear-rate viscosity of the non-Newtonian lubricants) (Cf: Walters 1973, Reiner et al. 1969). That is, the "load carrying capacity" in journal bearings with viscoelastic lubricants was shown to increase and the friction coefficient to decrease due to viscoelasticity. This observation is not compatible with Tanner's approach which predicts a decrease both in "load carrying capacity" and in friction coefficient due to the shear thinning character of the fluids. These experiments, however, are not sufficient and not satisfactory in the sense that they were performed in actual bearings where secondary effects such as non-isothermal conditions and the presence of cavitation could be easily overlooked (Tanner 1965). The question of the role of hydrodynamic elasticity in lubrication-type systems remains unresolved, and indeed may be resolved more readily through careful observation than intuition.

C H A P T E R IV

MODELING PHILOSOPHY

IV. 1 The Dynamic Equation

The complete set of momentum equations subject to the lubrication approximation reduces to a single equation, Eq. (III-9), which is rewritten here in the form

$$\underset{I}{\underbrace{\frac{\partial\left(\tau_{xx} - \tau_{yy}\right)}{\partial x}}} + \underset{II}{\underbrace{\frac{\partial\tau_{xy}}{\partial y}}} = \frac{\partial T_{yy}}{\partial x} \qquad (IV-1)$$

where x (previously x^1) is the primary flow direction, $y(x^2)$ is the shearing direction and $z(x^3)$ is the neutral axis.

One now faces the dilemma of what approach should be adopted in order to further simplify the dynamic equation and make it algebraically more tractable.. Specifically, which term on the l. h. s. of Eq. (IV-1), the elastic (I) or the viscous (II), should be retained for later calculations.

Two possible approximations have been cited and discussed in the preceding chapter, each relevant under a certain range ·of deformation rates. Tanner's purely viscous approximation was shown to be valid for relatively low deformation rates (weak flows) whereas the extensional primary field approximations due to Metzner are possibly useful at high deformation rates (strong flows). Even though no convincing experimental evidence is available at the present time to support either approach, the

purely viscous approximation seems to this author more appealing for
several reasons:

1. This approximation is certainly valid for weak lubrication flows
and it may well be valid for strong flows if the phenomenon of stress
"blow-up" is not manifested.

2. The current understanding of strong flows is poor, primarily due
to practical limitations in rheological characterization of viscoelastic fluids
under high deformation rates and especially under high elongation rates.

3. The simulated coating flows that have been tested experimentally
in this study were all weak flows.

These points provide a valid rationale for employing the purely
viscous approximation in the current study. When this approximation is
applied, Eq. (IV-1) assumes the following form

$$\frac{dP}{dx} = \frac{d}{dy} \left[\eta(II_\Delta) \frac{du}{dy} \right] \qquad (IV-2)$$

P, the hydrostatic pressure, and u, the x-component of the velocity vector,
are the unknown hydrodynamic functions to be determined through a solution
of Eq. (IV-2) subject to an appropriate set of boundary conditions. In
accordance with the "thin film approximation", P is strictly a function of
x whereas u is explicitly a function of y.

The only viscometric function needed for solving Eq. (IV-2) is $\eta(II_\Delta)$,
the shear viscosity function, which depends, in general, on the second
invariant of the rate-of-deformation tensor. Even though the elastic

characteristics of the fluid are not needed in the dynamic analysis (i.e.
solution of Eq. IV-2), they may be used for estimating the normal tract-
tions applied by the fluid on the solid boundaries of the system. One is
particularly interested in the total stress acting normally in the y direction.
Such a stress is given by

$$- T_{yy} = P - \tau_{yy} \qquad \qquad (IV-3)$$

P is evaluated from Eq. (IV-2) whereas τyy, the dynamic normal stress,
can be obtained from a second viscometric function, $\Psi_{12}(II_\Delta)$ - the first
normal stress coefficient. The viscometric functions η and Ψ_{12} can be
evaluated once an "appropriate" viscoelastic constitutive model has been
selected. Several such models are presented in the following section and
their limitations and merits are discussed in detail.

A regular perturbation scheme that is used in this study for solving
the dynamic equation is briefly outlined in Section 3. The boundary con-
ditions to be applied with Eq. (IV-2) are generally straightforward. The
only problem arises in the formulation of the dynamic boundary conditions
at the downstream end of the system where flow separation is taking place.
This question is briefly addressed in Section 4.

IV. 2   Constitutive Models

IV. 2. 2   <u>General</u>.   The task of selecting a "reasonable" constitutive
model for use in the dynamic analysis is complicated by virtue of the great
abundance of such models in the literature (see for example Bird 1976).

The goal of the selection process is to make the best compromise between algebraic tractability and physical realism, as it is usually the case that realistic models are mathematically difficult to apply in actual problems. It is, thus, useful to restrict our attention to the particular class of flows that is pertinent in the present study.

It has been stated in the previous section that the purely viscous approximation is reasonable for weak lubrication flows of viscoelastic fluids. This approximation can be restated in the following way. For low-to-moderate deformation rates, the flow in a lubrication-type system is nearly viscometric and nearly steady (in the Lagrangian sense). This is the kinematic counterpart of the purely viscous dynamic approximation and it permits a further restriction on the constitutive model to be selected.

For nearly steady shear flows one can apply constitutive models which are deriveable from the retarded-motion expansion (Bird et al. 1977a). Two such models, the second-order fluid model and the Criminale-Ericksen-Filbey (CEF) model, are considered subsequently. (The Newtonian fluid and the generalized Newtonian fluid are treated as special cases of these models.)

IV.2.2 The second-order fluid model. Modern polymer fluid rheology has been patterned, quite successfully, around the "simple fluid" concept. The simple fluid theory (Noll 1958, Coleman and Noll 1961) holds that the present state of the stress in any element of the fluid is a functional of

the rate-of-strain history of the element. If this functional is "sufficiently well-behaved" it can be expanded in Fréchet series (the equivalent of Taylor series for functionals) and depending on how slow and how slowly varying is the flow, the series can be truncated at a suitable term. The expansion of the rate-of-strain history about the present state, for flows in which the velocity gradient is slowly changing in time, is called the retarded-motion expansion (Bird et al. 1977a).

When only first- and second-order terms are retained, this expansion, in terms of the stress tensor, reduces to (Bird et al. 1977a)

$$\underset{\sim}{\tau} = \alpha_1 \underset{\sim}{\Delta} - \alpha_2 \frac{\mathcal{D}}{\mathcal{D}t} \underset{\sim}{\Delta} + \alpha_{11} \left(\underset{\sim}{\Delta} \cdot \underset{\sim}{\Delta} \right) \qquad\qquad \text{(IV-4)}$$

α_1, α_2 and α_{11} are constant material parameters and $\frac{\mathcal{D}}{\mathcal{D}t}$ is the corotational derivative defined in Eq. (II-13). A fluid obeying Eq. (IV-4), which is written in a corotational formalism, is called a second-order fluid. Simple examination of the viscometric properties of the second-order fluid shows that it has a constant viscosity (α_1) and constant normal-stress coefficients ($\Psi_{12} = 2\alpha_2$ and $\Psi_{23} = \alpha_{11} - \alpha_2$). Such behavior is clearly unrealistic and there is little evidence that fluids obeying the "second-order" equation exist at all. This model is, nevertheless, popular among fluid dynamicists for solving difficult viscoelastic flow problems. Its relative simplicity and its qualitative features which allow a "first-order" estimate of the effect of elasticity, are the main reasons for using the second-order fluid model.

The application of the second-order fluid model is especially simple

for flows which are creeping and planar (such as the flows considered in

this study) due to the Giesekus-Tanner theorem (Tanner 1966, Bird et al.

1977a). This theorem states that a second-order fluid and a corresponding

Newtonian fluid (a fluid with a viscosity equals to α_1) have the same

velocity fields in a given system provided that the flow is creeping and

planar and the velocity boundary conditions are identical in both cases.

A direct consequence of the Giesekus-Tanner theorem is the so-called

Giesekus-Tanner-Pipkin equation (Bird et al. 1977a) which reads

$$P = P^0 - \frac{\alpha_2}{\alpha_1} \frac{DP^0}{Dt} + (\alpha_{11} - \frac{1}{2}\alpha_2)\dot{\gamma}^2 \qquad (IV-5)$$

where P^0 is the pressure for a corresponding Newtonian fluid, $\frac{D}{Dt}$ is

the Stokes derivative and $\dot{\gamma} = \sqrt{\frac{1}{2} II_\Delta}$. Thus, the pressure and the velocity

fields for a second-order fluid in a creeping planar flow system can be

readily established once the Newtonian solution for the same boundary-

value problem is known. The Giesekus-Tanner theorem is used throughout

this study for evaluating the relevant hydrodynamic functions for a second-

order fluid in several coating systems.

The normal stress, τ_{yy}, for a second-order fluid in a (nearly) simple

shear flow is given by

$$\tau_{yy} = (\alpha_{11} - \alpha_2)\dot{\gamma}^2 \qquad (IV-6)$$

and, using Eq. (IV-5), the total stress, $-\tau_{yy}$, is

$$-T_{11} = P^0 - \frac{\alpha_2}{\alpha_1} \, u \, \frac{dP^0}{dx} + \frac{1}{2}\alpha_2 \, \dot{\gamma}^2 \qquad \text{(IV-7)}$$

This equation is used throughout for calculating the total normal traction exerted by a second-order fluid on the solid boundaries of the systems which are considered in this study.

To sum up, the second-order fluid model is useful for qualitative evaluation of first-order effects of hydrodynamic elasticity and it is readily applied in a dynamic analysis of creeping planar flows with the aid of the Giesekus-Tanner theorem. The obvious limitations of this model, however, should be recognized when judging its performance in quantitative terms.

A more elaborate and more realistic constitutive model is considered subsequently.

IV.2.3. <u>The Criminale-Ericksen-Filbey (CEF) equation.</u> A major limitation of the second-order fluid model is its inability to yield viscometric properties which are shear rate dependent. It turns out that this handicap can be corrected by a simple modification of the second-order equation. Replacing the constant coefficients in Eq. (IV-4) with scalar functions of II_Δ (the second invariant of the rate-of-deformation tensor) gives

$$\underset{\sim}{\tau} = \eta \underset{\sim}{\Delta} + (\tfrac{1}{2}\underset{-}{\psi}_{12} + \underset{\sim}{\psi}_{23})(\underset{\sim}{\Delta} \cdot \underset{\sim}{\Delta}) - \tfrac{1}{2}\underset{-}{\psi}_{12}\frac{\mathcal{D}}{\mathcal{D}t}\underset{\sim}{\Delta} \qquad \text{(IV-8)}$$

where η, $\underset{-}{\psi}_{12}$, and $\underset{-}{\psi}_{23}$, the three viscometric functions, are defined as

$$\eta = \frac{\tau_{xy}}{\dot{\gamma}} \tag{IV-9}$$

$$\Psi_{12} = \frac{\tau_{xx} - \tau_{yy}}{\dot{\gamma}^2} \tag{IV-10}$$

$$\Psi_{23} = \frac{\tau_{yy} - \tau_{zz}}{\dot{\gamma}^2} \tag{IV-11}$$

This equation (IV-8) was derived by Criminale et al. (1958) from more fundamental considerations and it was found especially useful for flows which are nearly viscometric and nearly steady (Pipkin and Tanner 1972, Bird 1976). Eq. (IV-8) is known as the Criminale-Ericksen-Filbey (CEF) equation and it has been used previously, in Chapter II, in the examination of planar flows. It can be easily verified that, in the limit of steady simple shear flow, the functions η, Ψ_{12} and Ψ_{23} have the meanings ascribed to them in Eqs. (IV-9) to (IV-11).

The viscometric functions are <u>not</u> specified by the CEF model. Rather, one is free to select these functions to fit any viscometric data. In the present study, two empirical expressions for $\eta(\dot{\gamma})$ and $\Psi_{12}(\dot{\gamma})$ have been chosen, (the third function is assumed vanishingly small). The selected viscosity function has the form

$$\eta = \frac{\eta_0}{1 + (|t_R \dot{\gamma}|)^{1-n}} \tag{IV-12}$$

η_0 is the zero-shear-rate viscosity, t_R is some characteristic time constant and n is a characteristic power-law exponent. The viscosity model, thus, contains three parameters which can be adjusted to fit reasonably well any

shear viscosity data. Eq. (IV-12) is similar to the Carreau viscosity

equation (Bird et al. 1974) which reads

$$\eta = \frac{\eta_o}{[1+(t_R \dot{\gamma})^2]^{(1-n)/2}}$$ (IV-13)

This form is also a useful empiricism but it is somewhat less convenient

to manipulate in a perturbation analysis that will be used throughout this

study (see next section).

Several researchers (Graessley and Segal 1969, Abdel-Khalik et al.

1974) have argued that the time constant appearing in Eqs. (IV-12) and (IV-

13) is related in some way to the viscoelastic nature of the fluid or, rather,

to its relaxation time. So, while viscoelasticity is not involved explicitly

in the dynamic analysis (Eq. IV-2), it is, nonetheless, associated with the

problem through the viscosity model.

A useful empiricism for the first normal-stress coefficient is

$$\underline{\Psi}_{12} = -\frac{1}{2} \frac{t_R}{\eta_o} [\eta(\mathrm{II}_\Delta)]^2$$ (IV-14)

This empirical expression will be used throughout this study for evaluating

the normal stresses generated by a CEF fluid.

The dynamic analysis with the second-order fluid was shown to be

greatly simplified through the use of the Giesekus-Tanner theorem. Such

simplification is not possible with the CEF equation. Substitution of the

empirical viscosity model into Eq. (IV-2) yields a non-linear ordinary

differential equation which cannot be solved by exact analytical methods.

Hence, one has to resort to some approximate techniques for solving Eq. (IV-2). One such technique is briefly outlined in the following section.

IV.3 Solution of the Non-Linear Dynamic Equation:
        A Perturbation Approach

The use of the empirical viscosity model, Eq. (IV-12), in the dynamic analysis introduces severe non-linearities into the dynamic equation. Such non-linearities can be handled quite effectively by standard (regular) perturbation methods.

For later arguments, it is convenient to make the problem dimensionless in the following way:

$$\varphi = \frac{u}{U}, \quad \xi = \frac{x}{L}, \quad \eta = \frac{y}{H}$$

and $$\tau = \frac{H^2 P}{\eta_o UL}$$

U is some characteristic velocity and L and H are characteristic dimensions of the system. In terms of these dimensionless variables, the equation of motion combined with the empirical viscosity model assumes the following form:

$$\dot{\tau} = \frac{d}{d\eta} \left[\frac{\frac{d\varphi}{d\eta}}{1 + N_e (|\frac{d\varphi}{d\eta}|)^{1-n}} \right] \tag{IV-15}$$

where $$N_e = (t_R \frac{U}{H})^{1-n}$$

$$= (W_S)^{1-n}$$

and Ws is the Weissenberg number. Also,

$$\dot{\pi} \equiv \frac{d\,\pi}{d\,\xi}$$

Eq. (IV-15) is a non-linear ordinary differential equation that contains a

single dynamic parameter, Ne. Ne is a viscoelastic characteristic of the

system and it would seem natural to use it as a perturbation parameter

in this problem.

Eq. (IV-15) can be integrated once with respect to η to give

$$(\dot{\pi}\eta+C)\,[1 + N_e\,(\,|\frac{d\,\varphi}{d\eta}|\,)^{1-n}] = \frac{d\,\varphi}{d\eta} \tag{IV-16}$$

$C = C(\xi)$ is a constant of integration. The perturbation analysis proceeds

in the following manner. All the dependent variables in Eq. (IV-16) ($\dot{\pi}$,

φ and C) are expanded in power series of Ne, in the usual perturbation

fashion (Van Dyke 1964),

$$f(N_e;\,x_i,\,n) = \sum_{j=0}^{\infty} f^j(x_i,\,n)\,N_e^{\,j} \tag{IV-17}$$

With the assumption that Ne << 1, the functions can be linearized as

$$f(N_e;\,x_i,\,n) = f^0(x_i,\,n)+N_e f^1(x_i,\,n) + O(N_e^{\,2}) \tag{IV-18}$$

f^0 , the zeroth-order function is the Newtonian solution and f^1, the first-

order function, is to be determined in the context of the perturbation

analysis. The standard procedure is to introduce the linearized expansions

back into Eq. (IV-16) and to compare terms of like orders in Ne. In

principle, one can proceed and extend this analysis to higher order terms in the expansions. However, the algebraic complexity involved makes it impractical.

It is important to note that the range of validity of the perturbation solution is quite limited, as in order for Ne to be much smaller than unity the deformation rates should be very small, of the order of 1 sec^{-1} say, for conventional viscoelastic fluids. Such deformation rates are much too low for common coating operations, or even for the simulated coating flows that have been studied experimentally in the present work. The value of this approximate solution lies in its ability to point to the direction of the effect of viscoelasticity, and specifically the effect of shear thinning, on the performance of the system relative to a Newtonian system. Thus, this solution is, in a sense, complementary to the analysis with a second-order fluid in which first-order effects of fluid elasticity are examined.

It is interesting to note that the power-law (Ostwald-de Waele) model is a special case of the empirical viscosity equation. The power-law model is written as

$$\eta = m'(\tfrac{1}{2} II_\Delta)^{(n-1)/2} \tag{IV-19}$$

where m' and n are constant parameters. For Ne >> 1, the empirical vis-cosity equation reduces to the power-law equation with $m' = \dfrac{\eta_0}{(t_R)^{1-n}}$. Thus, if a solution for a power-law fluid is available, it can be matched with the perturbation solution (for which Ne << 1) provided that the functions consid-ered are well-behaved.

In order for Eq. (IV-16) to be mathematically well posed it is necessary to consider an appropriate set of boundary conditions. Most of these conditions are standard and well accepted. The question of the boundary conditions at the separation region, however, is more involved and, hence, it is given a special consideration in the next section.

IV.4   The Separation Boundary Conditions

The boundary conditions imposed on the pressure field at the upstream end of a lubrication converging-diverging system are not of great concern since they are, usually, not associated with free surfaces (in the case of a flooded inlet). The pressure is taken to be zero (ambient) at a distance far upstream from the nip (position of minimum separation), or it can assume some arbitrary value if a finite pressure is imposed on the system at the inlet zone.

A more difficult problem is the question of the boundary conditions at the downstream end, i.e., at the point where the liquid film separates or cavitates and it gives way to a flow system bounded by free surfaces. The complexity of this problem stems from the fact that the location and shape of the free meniscus at separation are a-priori unknown and, hence, the role of surface-tension forces in the dynamics of the separation region is difficult to assess. The exact form of the boundary conditions is expected to have a strong effect on the dynamics in the bounded flow regime and it will, certainly, have an appreciable effect on the thickness of the fluid film

deposited on the moving surface(s) (Taylor 1974 a, b). Consequently, this problem has been the subject of numerous analyses and investigations and it dates back to Reynolds' classical treatise on the journal-bearing problem (Cameron 1966).

It has been noted, by Taylor (1963) (see also Birkhoff 1964), that free boundaries in partial lubrication can arise from two physically different causes. In converging-diverging flow systems, where sub-ambient pressures can be generated in the diverging section, it is possible that a gas which is dissolved in the fluid will be emitted from solution as the pressure falls to the saturation pressure of the gas in the liquid. The cavitation formed in this way has been refereed to by Taylor as internal cavitation. This kind of cavitation was found to develop in heavily loaded systems (high dynamic pressures) (Banks and Mill 1954). In lightly loaded systems, the cavitation is formed through physical splitting or separation of the liquid film, caused by external forces. This type of cavitation is, thus, termed separation cavitation. As will be shown, each of these mechanisms is associated with a certain set of boundary conditions. (Floberg (1965) has argued that both types of cavitation are essentially a single physical phenomenon that is man-ifested differently under different loads.)

Reynolds, in his journal-bearing analysis, has proposed the following boundary conditions (Cameron 1966):

$$\left.\frac{dP}{dx}\right|_{x_1} = 0 \ , \quad \left.P\right|_{x_1} = P_{cavity} \tag{IV-20}$$

where x_1 is the position of film separation. The cavity pressure (P_{cavity}) is usually taken to be ambient and surface-tension forces are neglected. (Note that since the position of film separation, x_1, is not known, two separate boundary conditions are associated with the separation region.) The above conditions have been applied successfully in a variety of lubrication systems and are most common today in hydrodynamic lubrication analyses (Pinkus and Sternlicht 1961, Cameron 1966). Reynolds introduced these conditions without a firm physical basis. The Reynolds' conditions were given a physical justification by Swift (1932) and separately by Stieber (Cf: Taylor 1963, Birkhoff 1964). Swift derived this condition as a stability condition for a bearing free to seek a position of stable equilibrium (and not as a condition for flow through a space of fixed dimensions). Stieber, on the other hand, derived it as a condition for flow continuity. Even though the arguments presented by Swift and Stieber are both dubious (Taylor 1974a, Savage 1977a), these conditions are known today as the Swift-Stieber (SS) conditions. Taylor (1963) first noted that the SS conditions are applicable to systems which are heavily loaded, i.e., when the cavitation is formed via an internal cavitation mechanism.

It was observed that, when the system is lightly loaded, sub-ambient pressures develop in the diverging section of the system (Floberg 1965, 1968; Cf: Taylor 1974 a, b). Such negative pressures cannot be accommodated by the SS conditions. This failure of the SS conditions have motivated a search

for a new set of boundary conditions for lightly loaded systems (i.e., for separation cavitation).

Hopkins (1957) seems to be the first to use separation conditions in a lubrication-type system. His conditions, applied to a sheet-and-roll system with both surfaces in motion, are kinematic in nature and are based on the intuitive notion that separation will occur at the first stagnation point downstream from the nip. That is,

$$u \Big|_{x_1} = 0 \quad , \quad \frac{du}{dy}\Big|_{x_1} = 0 \tag{IV-21}$$

Similar conditions have been mentioned previously by Prandtl (Cf: Birkhoff and Hays 1963). Thus, these conditions are called the Prandtl-Hopkins (PH) separation conditions. Birkhoff and Hays (1963) have noted that the PH conditions correspond to the position of "incipient counterflow", i.e., separation occurs at a point where there is reverse flow in the divergent space if the system is fully immersed. The PH conditions can clearly account for subambient pressures in the divergent section of the system and they were found in reasonable agreement with observation (see VI.5). For coating systems, where the dynamic loads are somewhat lower than in typical lubrication systems and the solid boundaries are usually rigid, the PH conditions seem adequate and convenient for practical application. If the systems are heavily loaded, then the SS conditions would be more appropriate.

$$\beta = \frac{H_\infty}{H_1}$$

A major drawback of the PH conditions is their inability to accommodate backflow or circulation patterns in the flow system just upstream from the separation meniscus. Such flow patterns were observed by several investigators for lightly loaded systems (Myers et al. 1959, Pitts and Greiller 1961, Cf: Savage 1977a). Also a numerical calculation of the flow field in the separation zone, by Williamson (1972), clearly demonstrates the (possible) existence of eddies behind the meniscus.

A condition for separation has been formulated by Floberg (1965, 1968, Taylor 1974b) and it was found in good agreement with experimental data. This condition, however, was derived for lubrication systems in which striations (or streamers) are prevalent at separation and it is mathematically cumbersome to apply in practical situations.

A more rigorous approach to this complex problem has been pursued by Coyne and Elrod (1969, 1970). They solved the complete free surface problem of the rupture of a lubricating film due to sliding of a flat rigid surface parallel to a stationary one (see Figure IV-1). Their solution gives the shape of the free surface at the separation region as a function of three dimensionless numbers representing surface tension, gravity and inertia forces acting on the fluid in the separation region. The shape of the free surface can be expressed in terms of two independent functions

$$\beta = \frac{H_\infty}{H_1} \qquad \text{(IV-22)}$$

and
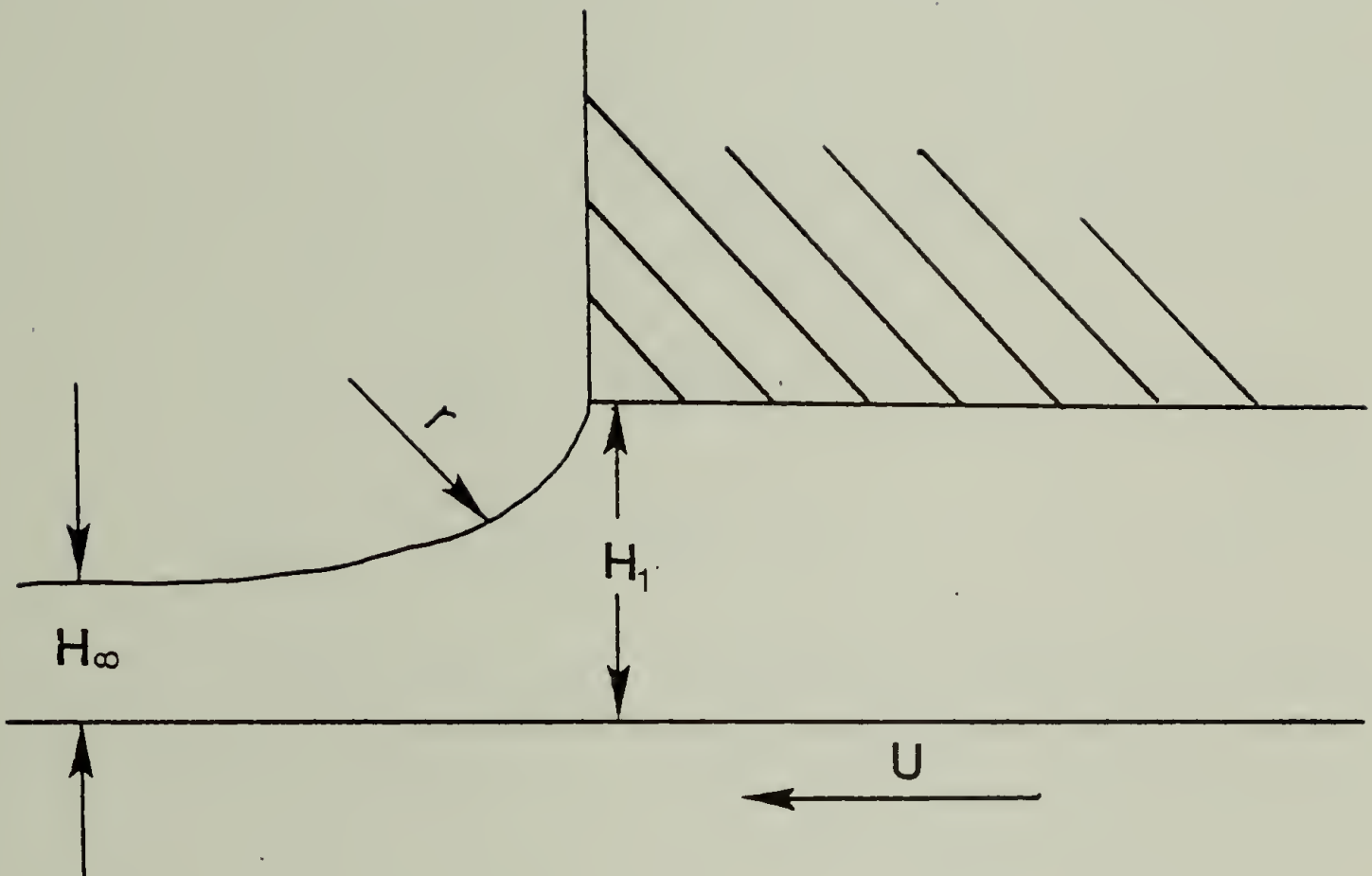
Figure IV-1. Coyne and Elrod's separation geometry.

$$\mathcal{X} = \frac{r}{H_1} \tag{IV-23}$$

where H is the thickness of the film deposited on the moving surface (far downstream from the point of separation), H_1 is the height of the film at separation and r is the radius of curvature of the meniscus at separation. β and $\mathcal{X}$ are, independently, functions of all the dimensionless parameters involved in this calculation. Coyne and Elrod proposed to use these functions in the formulation of general boundary conditions for Reynolds' equation. These conditions take the form:

$$P\Big|_{x1} = - \frac{\gamma}{\mathcal{X}H_1} + \Delta P$$

$$\frac{dP}{dx}\Big|_{x1} = \frac{6\mu U}{H_1^2} (1-2\beta) \tag{IV-24}$$

γ is the surface tension and ΔP is a correction to the pressure associated with the transition region (and it is usually negligible). The first condition is a simple force balance whereas the second condition is based on the assumption that the pressure gradient at separation should match identically the gradient calculated for the bounded regime using Reynolds' equation.

The CE conditions are not completely satisfactory inasmuch as they are based on some assumptions that were not given sufficient justification. One such assumption regards the velocity distribution perpendicular to the free surface to have a quadratic form. Also, in their analysis, Coyne and Elrod do not discuss the dynamics near the contact-line (liquid-air-solid contact). Rather, they fix the contact angle (the tangent to the curvature

of the free surface near the solid boundary) at some value and regard it as an independent parameter of the system (this point is discussed in more detail in V.5). Finally, they argue that their conditions are applicable to the case when both surfaces are in motion even though this is not obvious from their analysis. Despite these drawbacks, the CE conditions are regarded superior to the other separation conditions that are currently availalbe (Taylor 1974a, Savage 1977a) and they provide a firm basis for most of the observed phenomena in the neighborhood of the separation region (Namely, sub-ambient pressures and backflow patterns). The CE conditions are also well reproduced experimentally.

In practice, it is usually more convenient to employ the PH conditions especially when the fluids concerned are non-Newtonian (such as in the current study). It will be shown, in VI.3, that the PH conditions are, in fact, indistinguishable from the more rigorous CE conditions except at very low capillary numbers ($N_{Ca} = \mu U/\tau$). At this range of capillary numbers the CE conditions themselves are not adequate (Savage 1977a). This, together with some experimental data (VI.5) will confirm the claim that the PH conditions represent reasonably well the physical situation at the separation region.

CHAPTER V

BLADE COATING

V. 1   Introduction

Blade coaters are common means for applying a thin coating layer in a controlled manner onto a moving web. Such coaters are used in a variety of configurations for coating high viscosity materials and are found primarily in the paper and textile industries (Booth 1968). Figure V-1 shows a schematic diagram of a blade coating system. The blade is a solid surface oriented at some angle relative to the moving web. The coating material is 'dragged' by the web through the system and it emerges at the blade tip in the form of a uniform coating layer.

It is immediately apparent that two geometrical factors are of utmost importance in the design of a blade coater. The first is the blade angle, i. e., the angle which the stationary blade forms with the moving web. This geometrical factor is bound to have a strong effect on the flow field in the converging space under the blade and hence it is likely to have some influence on the resulting coating thickness. Blade angles can vary from zero ("slot coaters") to ninety degrees ("knife coaters") depending upon the specific application of the coater. The second design consideration is the rigidity of the blade. Under high hydrodynamic loading the blade can bend
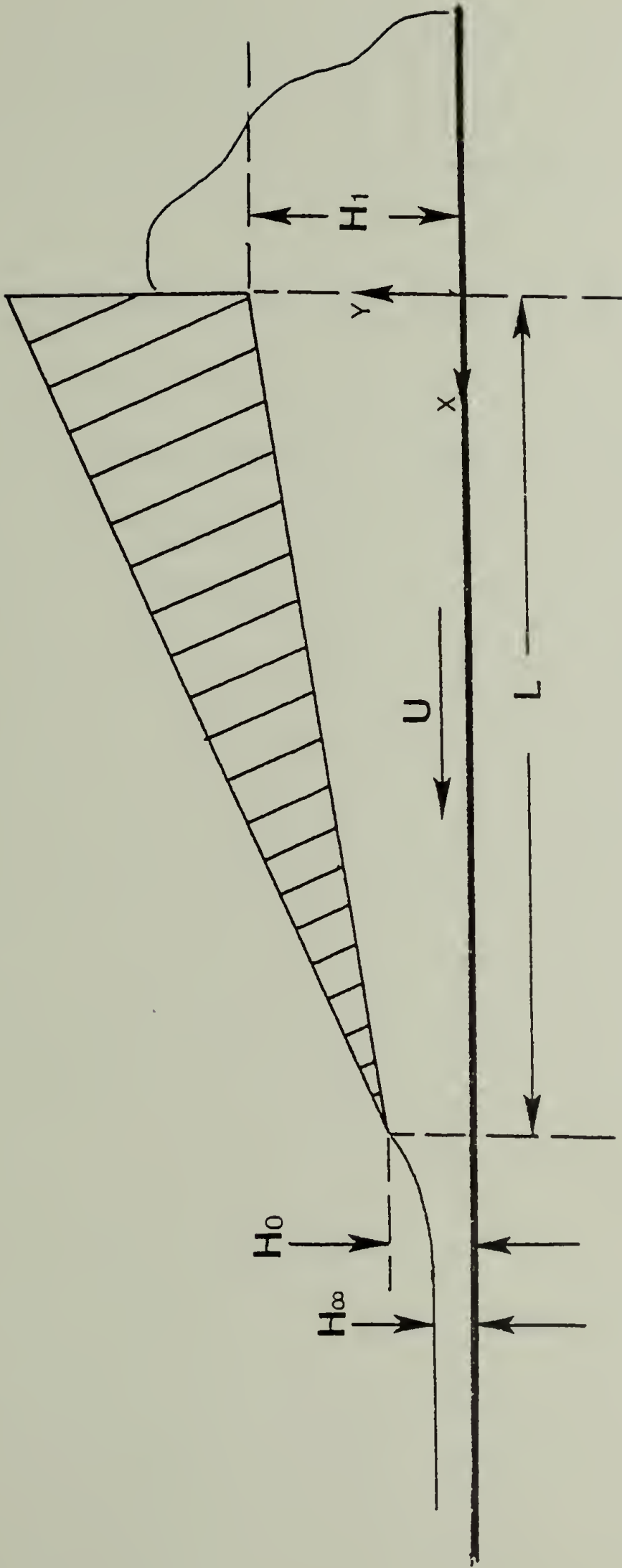
Figure V-1. A schematic of a blade coating system.

and deform thereby altering considerably the thickness of the ensuing coating (Middleman 1977). The degree to which this happens depends on the elasticity of the blade and the rheological properties of the coating fluid.

In the limit of small blade angles and narrow flow spaces the blade coater is essentially a slider bearing which is a fundamental configuration in lubrication hydrodynamics. Detailed hydrodynamic analyses for the slider bearing and for a host of variations thereof can be found in the classical lubrication literature (e.g., Pinkus and Sternlicht 1961, Cameron 1966). Much less, in comparison, has been published on the hydrodynamics of blade coaters. Most of the studies of the blade coating problem that have been reported in the literature are concerned with situations encountered in specific processes. (Windle and Beazley 1967, 1968; Bliesner 1971; Modrak 1973; Canard 1974). In these studies, the actual dynamics are complicated by such effects as blade deflection, web deflection, fluid viscoelasticity and solvent loss which are considered collectively. This approach is practical but narrow in scope as it does not permit a definitive assessment of each of these effects separately.

A theoretical study of the effect of viscoelasticity on the performance of a blade coater was reported by Greener and Middleman (1974). In their analysis, the blade was considered rigid and flat and the blade angle was assumed sufficiently small that the lubrication approximation can be used.

This analysis is laid out, in part, in the following section. The flexible blade problem was analyzed by Middleman (1977) who discusses also some aspects of the effect of viscoelasticity.

The problem of a rigid planar blade tilted at a small angle relative to a flat web is analyzed in the following section. The analysis is carried out for two viscoelastic constitutive models using the lubrication approximation. (The Newtonian lubrication solution is presented without derivation.) In Section 3, a simple experiment with a rigid small-angled blade is described and the results are presented and discussed in Section 4. The role of surface tension in the formulation of the dynamic boundary conditions at the blade tip is considered briefly in Section 5.

V.2 The Rigid Planar Blade Coater - Lubrication Analyses

V.2.1 General. The blade coater shown in Figure V-1 is considered hereafter with the additional stipulations that the system is infinitely wide (no z dependence) and that the blade angle is 'small', or

$$\frac{H_1-H_0}{L} \ll 1 \quad \text{and} \quad \frac{H_0}{L} \ll 1 \tag{V-1}$$

The implication of this constraint is that the lubrication approximation is applicable. The practical meaning of the term 'small' will be commented on at a later stage.

The coating thickness, H_∞, is not, in general, equal to the tip separation (H_0) but is rather a function of the dynamics in the converging

flow space.   It is the goal of this analysis to relate geometric character-istics of the system and some rheological properties of the fluid to the thickness of the coating deposited on the web.   An additional performance variable that may be of interest is the total loading on the blade which results from the dynamics of the flow field under the blade.   This variable is also evaluated in the analyses to follow.

The analysis is carried out for two constitutive models, the second-order fluid model and the CEF model, with the intention of gaining some insight as to the effect of certain viscoelastic parameters on the perform-ance of the system.

It is convenient now to introduce the following dimensionless variables:

$$\xi = \frac{x}{L} \;, \quad \eta = \frac{y}{H_0}, \quad \varphi = \frac{u}{U}$$

and

$$\pi = \frac{P H_0}{\eta_a U L}$$

where

$$\eta_a = \begin{cases} \mu \text{ for a Newtonian fluid} \\ \alpha_1 \text{ for a second-order fluid} \\ \eta_o \text{ for a CEF fluid} \end{cases} \qquad (V\text{-}2)$$

And the boundary conditions for the system considered herein can be written as

(a) $\varphi = 1$ @ $\eta = 0$

(b) $\varphi = 0$ @ $\eta = \sigma(\xi)$

(c) $\pi = 0$ @ $\xi = 0$ (V-3)

(d) $\pi = 0$ @ $\xi = 1$

Eqs. (V-3a, b) are the no-slip conditions where $\sigma(\xi)$ represents the position of the blade surface and it is given by

$$\sigma = K + (1-K)\xi \qquad (V-4)$$

where

$$K \equiv \frac{H_1}{H_0}$$

Eqs. (V-3c, d) state that the hydrodynamic pressures at the leading edge ($\xi = 1$) and the trailing edge ($\xi = 0$) of the blade are zero (or ambient). This statement is not exactly correct as regards the blade tip, where finite (negative) curvature of the fluid-air interface will introduce some contribution of the surface tension to the dynamics of the separation region. In many practical cases, however, this contribution is negligible and Eq. (V-3d) is a valid approximation. The effect of surface tension is briefly addressed in V.5.

The solution of the blade coating (or, equivalently, the slider bearing) problem for a Newtonian fluid is available in texts on hydrodynamic lubrication (e.g., Pinkus and Sternlicht 1961). Inasmuch as this solution is used later in the analyses for the viscoelastic fluids, the important results for the Newtonian case are presented below. A straightforward lubrication

analysis of the planar rigid blade coating problem yields the following

Newtonian functions:

$$\varphi = 1 - \frac{\dot{\pi}\sigma^2 + 2}{2\sigma}\eta + \frac{1}{2}\dot{\pi}\eta^2 \tag{V-5}$$

$$\dot{\pi} = 12\frac{0.5\sigma - \lambda}{\sigma^3} \tag{V-6}$$

$$\pi = \frac{6(K-1)\,\xi\,(1-\xi)}{(K+1)\,\sigma^2} \tag{V-7}$$

and,

$$\lambda = \frac{K}{K+1} \tag{V-8}$$

where $\quad \dot{\pi} \equiv \dfrac{d\,\pi}{d\,\xi}$

and λ, the dimensionless coating thickness (and the dimensionless flow rate) is defined by

$$\lambda \equiv \frac{H_\infty}{H_0}$$

Inspection of Eq. (V-7) reveals that the pressure function, $\pi(\xi)$, has a maximum within the interval [0, 1] and the position and magnitude of this maximum are strictly dependent on the geometric parameter K. Likewise, the dimensionless coating thickness, λ, is solely a function of the geometry (K) and it lies in the range $0.5 \le \lambda \le 1.0$. It is important to keep in mind that these results are valid only for small blade angles in which case the flow field is nearly unidirectional.

The Newtonian results are used subsequently in the analyses for a second-order fluid and a CEF fluid.

V.2.2 <u>The second-order fluid.</u> The second-order fluid model has been discussed in detail in IV.2. As has been noted, this model is especially useful in examining first-order effects of viscoelasticity (and specifically elasticity) that arise under conditions of low deformation rates. This model is now applied in the analysis for a rigid planar blade coater.

Inasmuch as the flow field under the blade is creeping and planar, one can make use of the Giesekus-Tanner theorem (see IV.2) in the calculation of the hydrodynamic functions for the second-order fluid. It can be immediately stated that the coating thickness (or the flow-rate) for a second-order fluid in a given blade coating system will be identical to that for a corresponding Newtonian fluid since, as given by the Giesekus-Tanner theorem, the velocity fields of both fluids are identical. Thus, the problem essentially reduces to determining the pressure (or the total stress) distribution under the blade. This task is also made simpler through the use of the Giesekus-Tanner-Pipkin equation (see IV.2). This equation, in a dimensionless form, reads:

$$\pi = \pi^0 - S_R \ (\frac{H_0}{L}) \ \varphi \ \dot{\pi}^0 \tag{V-9}$$

where
$$S_R = \frac{\alpha_2}{\alpha_1} \frac{U}{H_0}$$

and π^0 is the pressure function for a corresponding Newtonian fluid. The total stress $-T_{yy}$ $(=P - \tau_{yy})$ can now be written in a dimensionless form using Eq. (IV-7),
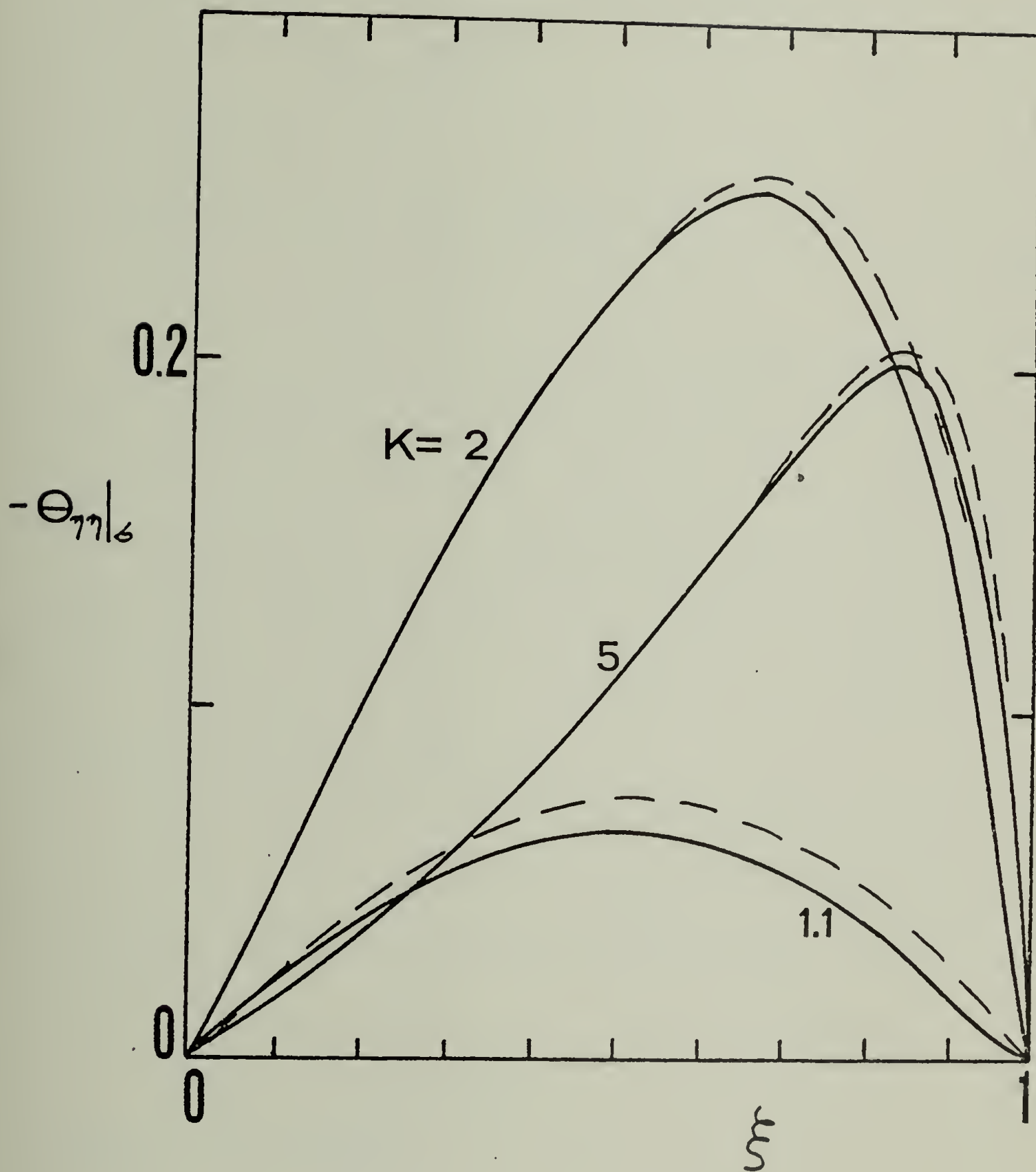
Figure V-2. Total (normal) stress distributions for a second-order fluid in a rigid planar blade coater ($H_0/2L = 0.01$). Solid curves: $S_R = 0$; Dashed curves: $S_R = 1$.

$$-\Theta_{\eta\eta} = \ddot{\pi}^0 - S_R \left(\frac{H_0}{L}\right) \varphi \dot{\pi}^0 + \frac{1}{2} S_R \left(\frac{H_0}{L}\right) \left(\frac{d\varphi}{d\eta}\right)^2 \tag{V-10}$$

where

$$\Theta_{\eta\eta} = \frac{T_{yy} H_0^2}{\alpha, UL}$$

and it follows that

$$-\Theta_{\eta\eta}\Big|_{\varsigma} = \ddot{\pi}^0 + \frac{1}{2} S_R \left(\frac{H_0}{L}\right) \left(\frac{\dot{\pi}^0 \varsigma^2 - 2}{2\varsigma}\right)^2 \tag{V-11}$$

In Eq. (V-11) the total stress is evaluated at the blade surface. Total stress distributions for several values of K are shown in Figure V-2. In this figure stress distributions for a Newtonian fluid are compared to corresponding distributions for a second-order fluid with $S_R = 1.$, taking $\frac{H_0}{2L} = 0.01$. As seen, the effect of viscoelasticity, as expressed by S_R, is to increase the total stress. This effect is likely to be small in true lubrication systems where $\frac{H_0}{2L} \ll 1$.

A direct consequence of this result is that the blade loading (or the load carrying capacity) generated by a second-order fluid will be higher than the loading generated by a corresponding Newtonian fluid. The blade loading can be calculated as follows:

$$\Phi = \int_0^1 -\Theta_{\eta\eta}\Big|_{\varsigma} d\xi \tag{V-12}$$

where

$$\Phi \equiv \frac{H_0^2 F}{\alpha, UL^2}$$

and F is the actual loading per unit width.. Using Eq. (V-11) one finds that

$$\Phi = \Phi^0 (K) + \frac{1}{2} S_R \left(\frac{H_0}{L}\right) \Phi^1 (K) \tag{V-13}$$

where $\qquad \bar{\Phi}^{\circ}(K) = \dfrac{6}{(1-K)^2} \left(\ln K - 2 \, \dfrac{K-1}{K+1} \right).$

and

$$\bar{\Phi}'(K) = \dfrac{4}{K(K-1)(K+1)^2} \, [K^3 - 2K^2 + 2K - 1]$$

The variation of $\bar{\Phi}$ with K for several values of S_R is shown in Figure V-3 (with $\dfrac{H_0}{2L} = 0.01$). As expected, the blade loading for a second-order fluid is higher than the loading for a corresponding Newtonian fluid.

V.2.3 $\underline{\text{The CEF fluid.}}$ The CEF model is now applied in the analysis for the rigid planar blade coater. This model has been presented and discussed in Chapter IV and it is used here as a means for examining first-order effects of shear thinning. It was shown that the CEF model is essentially represented by two empirical viscometric functions, $\eta\,(\dot{\gamma})$ and $\Psi_{12}(\dot{\gamma})$, which are given in IV.2. Only the viscosity function, in accordance with the purely viscous approximation, is used explicitly in the dynamic analysis. The first normal stress coefficient is used subsequently in the evaluation of the total normal traction.

The analysis begins with Eq. (IV-16) which is rewritten here in the form:

$$(\dot{\tilde{\tau}}\eta + C) \left[1 + N_e \left(\left| \dfrac{d\varphi}{d\eta} \right| \right)^{1-n}\right] = \dfrac{d\,\varphi}{d\,\eta} \qquad\qquad\text{(V-14)}$$

As stated in IV.3 Eq. (V-14) is a non-linear ordinary differential equation and it does not have a closed form solution. An approximate solution is thus sought via a perturbation scheme. The viscoelastic parameter Ne is
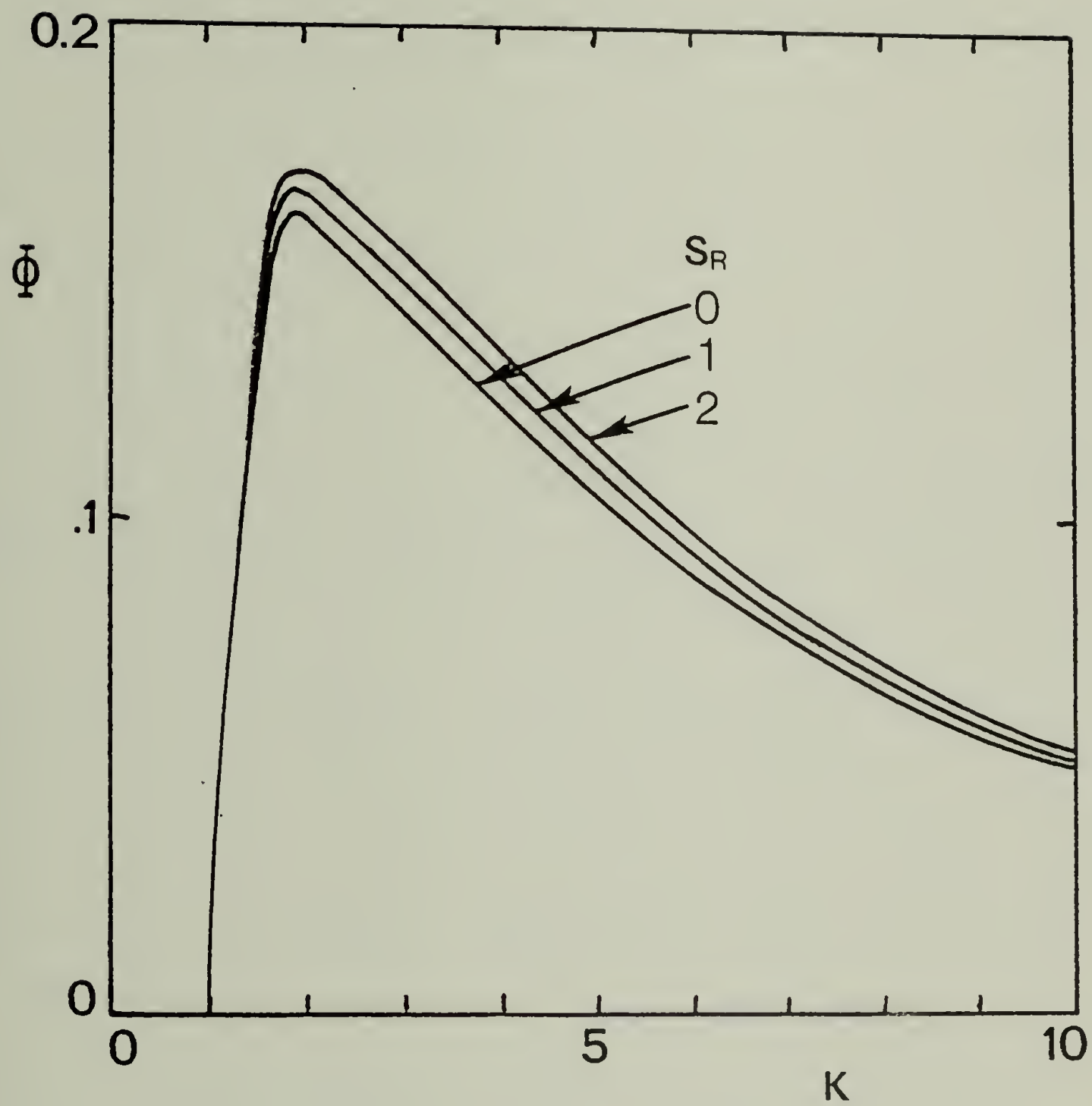
Figure V-3. Blade loading vs. K for a second-order fluid in a rigid planar blade coater ($H_0/2L = 0.01$).

chosen as a perturbation parameter and the various hydrodynamic functions are expanded in the form

$$\varphi = \varphi^0 + N_e \varphi^1 + O(N_e^2) \tag{V-15}$$

$$\dot{\mathcal{R}} = \dot{\mathcal{R}}^0 + N_e \dot{\mathcal{R}}^1 + O(N_e^2) \tag{V-16}$$

$$C = C^0 + N_e C^1 + O(N_e^2) \tag{V-17}$$

and

$$\lambda = \lambda^0 + N_e \lambda^1 + O(N_e^2) \tag{V-18}$$

The zeroth-order terms are the already known Newtonian functions whereas the first-order functions are to be determined in the course of this analysis. Higher order terms are assumed to be negligible for the limiting case $N_e \ll 1$ considered herein. Thus, this analysis seeks to estimate "first-order effects" of viscoelasticity (or rather, shear thinning) on the performance of the system. The expanded functions are introduced back into Eq. (V-14) and the solution proceeds in the usual perturbation fashion (see IV.3). In the course of the algebraic manipulation one is faced with the necessity to integrate functions that include an absolute-value operator; this difficulty makes the derivation considerably lengthier. Such problem arises for velocity fields that do not possess a plane of symmetry. To overcome this difficulty one has to investigate the velocity field throughout the flow domain and divide it (the domain) into zones according to the general shape of the local velocity profile. The solution is carried out separately for each zone

with the condition that the hydrodynamic functions are continuous across the zone boundaries. In the present analysis, the following functions are used for dividing the flow domain

$$X = \frac{\mathcal{S}\dot{\mathcal{R}}^0}{2} - \frac{1}{\mathcal{S}} \tag{V-19}$$

$$Y = \frac{\mathcal{S}\dot{\mathcal{R}}^0}{2} + \frac{1}{\mathcal{S}} \tag{V-20}$$

and three zones are identified. Inasmuch as the analysis itself is quite lengthy the important results are presented below without derivation and the details are given in Appendix C. The final results are as follows. In zone A (Y > 0, X < 0),

$$\dot{\mathcal{R}}_A^1 = -12\frac{\lambda^1}{\mathcal{S}^3} \quad \frac{6}{\mathcal{S}^2 p \, \dot{\mathcal{R}}^0}[(-X)^p + Y^p]$$
$$- \frac{12}{\mathcal{S}^3 \dot{\mathcal{R}}^{02} p(p+1)}[(-X)^{p+1} - Y^{p+1}] \tag{V-21}$$

and

$$\varphi_A^1 = \dot{\mathcal{R}}_A^1 \frac{\eta^2}{2} - \frac{\eta}{\mathcal{S}}[\dot{\mathcal{R}}_A^1 \frac{\mathcal{S}^2}{2} + \frac{(-X)^p - Y^p}{p \, \dot{\mathcal{R}}^0}]$$
$$+ \frac{1}{p\dot{\mathcal{R}}^0}(Y - \dot{\mathcal{R}}^0 \eta)^p - \frac{Y^p}{p\dot{\mathcal{R}}^0} \tag{V-22}$$

In Zone B (X > 0, Y > 0),

$$\dot{\mathcal{R}}_B^1 = -12\frac{\lambda^1}{\mathcal{S}^3} - \frac{6}{\mathcal{S}^2 p\dot{\mathcal{R}}^0}[X^p + Y^p]$$

$$+ \frac{12}{\mathcal{S}^3 \dot{\mathcal{R}}^{02}\, p(p+1)}[X^{p+1} + Y^{p+1}] \tag{V-23}$$

For case B1 ($d\varphi^\circ/d\eta < 0$),

$$\varphi^1_{BI} = \dot{\pi}^1_B \frac{\eta^2}{2} - \frac{\eta}{\varsigma}[\dot{\pi}^1_B \frac{\varsigma^2}{2} + \frac{X^p + Y^p}{p\dot{\pi}^0}]$$

$$+ \frac{1}{p\dot{\pi}^0}(Y - \dot{\pi}^0\eta)^p - \frac{1}{p\dot{\pi}^0} Y^p \tag{V-24}$$

and for case B2 ($d\varphi^\circ/d\eta > 0$),

$$\varphi^1_{B2} = \dot{\pi}^1_B \frac{\eta^2}{2} - \frac{\eta}{\varsigma}[\dot{\pi}^1_B \frac{\varsigma^2}{2} + \frac{X^p - Y^p}{p\dot{\pi}^0}]$$

$$+ \frac{1}{p\dot{\pi}^0}(\dot{\pi}^0\eta - Y)^p - \frac{1}{p\dot{\pi}^0} Y^p$$

$$\tag{V-25}$$

In Zone C ($X < 0$, $Y < 0$),

$$\dot{\pi}^1_C = - 12\frac{\lambda^1}{\varsigma^3} - \frac{6}{\varsigma^2 p\dot{\pi}^0}[(-X)^p + (-Y)^p]$$

$$- \frac{12}{\varsigma^3\dot{\pi}^{02}p(p+1)}[(-X)^{p+1} + (-Y)^{p+1}] \tag{V-26}$$

For case C1 ($d\varphi^\circ/d\eta > 0$)

$$\varphi^1_{C1} = \dot{\pi}^1_C \frac{\eta^2}{2} - \frac{\eta}{\varsigma}[\dot{\pi}^1_C \frac{\varsigma^2}{2} + \frac{(-X)^p - (-Y)^p}{p\dot{\pi}^0}]$$

$$+ \frac{1}{p\dot{\pi}^0}(\dot{\pi}^0\eta - Y)^p - \frac{1}{p\dot{\pi}^0}(-Y)^p \tag{V-27}$$

and for case C2 $(d\varphi^{\circ}/d\eta < 0)$,

$$\varphi^1_{C2} = \dot{\pi}^1_C \frac{\eta^2}{2} - \frac{\eta}{6} \left[\dot{\pi}^1_C \frac{\varsigma^2}{2} + \frac{(-X)^p - (-Y)^p}{p \dot{\pi}^0}\right]$$

$$+ \frac{1}{p\dot{\pi}^0}(Y - \dot{\pi}\eta)^p - \frac{1}{p\dot{\pi}^0}(-Y)^p$$

(V-28)

where,

$$\lambda^1 = \int_0^{\varsigma} \varphi^1 d\eta$$

and $\qquad p = 3-n$

λ^1, the first-order coating thickness function is still unknown and thus none of the functions given above can be evaluated explicitly at this stage. λ^1 can be calculated by specifying

$$\pi^0(1, \lambda) + N_e\pi^1(1, \lambda) = 0$$

(V-29)

where

$$\pi^{\circ}(1, \lambda) = \frac{6}{K}\left(1 - \lambda\frac{1+K}{K}\right)$$

(V-30)

and λ is given by Eq. (V-18). It follows from Eq. (V-29) (by equating first-order terms) that

$$\lambda^1 = \frac{K^2}{6(1+K)}\pi^1(1)$$

(V-31)

Since λ^1 appears in all the expressions for π^1, this equation must be solved simultaneously with the equation(s) for $\dot{\pi}^1$. A solution for

$\lambda^1 = \lambda^1(K, n)$ worked out by successive approximations, is presented in

Figure V-4. The fact that λ^1 is a positive function implies that the coating thickness will increase for a viscoelastic fluid (Ne > 0) relative to a corresponding Newtonian fluid. This increase depends both on the geometry (K) and on the rheological characteristics of the fluid (Ne, n).

Once λ^1 is known, total stress distributions can be evaluated using Eqs. (V-21), (V-23) and (V-26). The total stress function evaluated at the blade surface is given by

$$-\Theta_{\eta}\Big|_{\sigma} = \mathcal{R}^0 + Ne\mathcal{R}^1 + \frac{1}{2} Ne^{\frac{1}{1-n}} \ (\frac{H_0}{L}) \ \frac{(\dot{\mathcal{R}}^0\sigma^2-2)^2}{4\sigma^2} \qquad (V-32)$$

where use has been made of Eqs. (IV-14) and (V-5) in deriving the dashed-underlined normal stress term. This term is evidently negligible in comparison to the other terms in Eq. (V-32) since it is of order higher than one in Ne (as n < 1) and, in addition, it contains the geometrical factor $\frac{H_0}{L}$ which is much smaller than unity in the context of a lubrication analysis. It is, thus, justified to neglect this term in the calculation of the total stress distribution which essentially reduces to the pressure distribution. Pressure distributions for several rheological parameters are presented in Figure V-5 for the case K=5. These results show that a viscoelastic fluid will produce pressures that are lower than those produced by a corresponding Newtonian fluid (a Newtonian fluid with a viscosity equal to the zero-shear-rate viscosity of the viscoelastic fluid). The effect of the power-law index is contrary to the expected; the closer it is to one
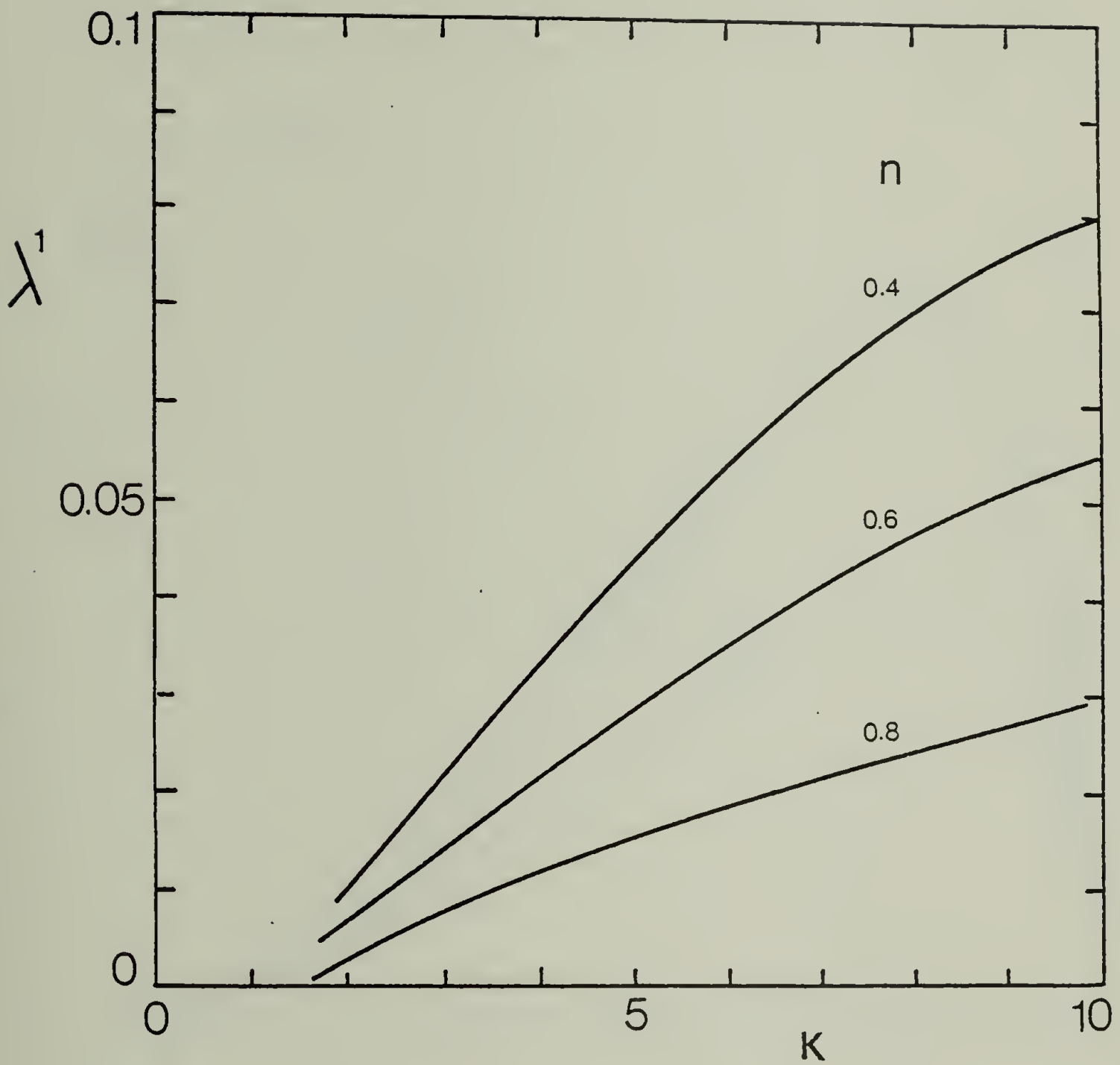
Figure V-4. λ^1 vs. K.   Perturbation analysis result for a CEF fluid in a rigid planar blade coater.
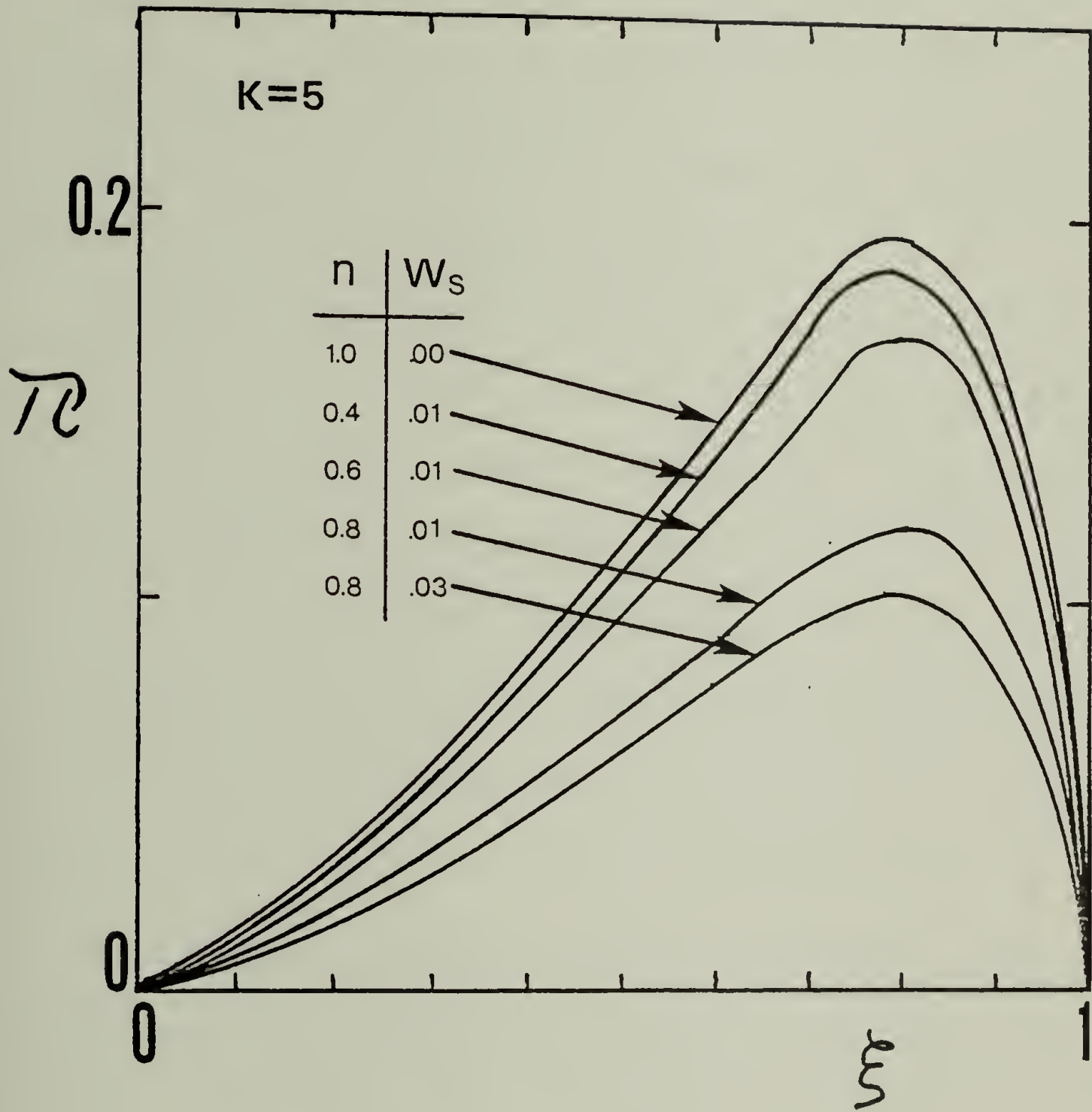
Figure V-5. Pressure distributions for a CEF fluid in a rigid planar blade coater.

the more pronounced is the effect of viscoelasticity. This "paradox" is apparently an artifact of the viscosity model as according to this model a viscoelastic fluid with a high power-law index will depart from the Newtonian viscosity plateau at much lower shear rates than a fluid with a lower n. Thus, at the lower range of shear rates, pertinent to this analysis, the former fluid will be on the average less viscous.

From the given pressure distributions one can evaluate the blade loading using Eq. (V-12). Since the contribution of the normal stress term to the total normal traction was shown to be insignificant, it is expected that the loading generated by a viscoelastic, shear thinning fluid will be less than the loading for a corresponding Newtonian fluid. The fractional reduction in blade loading as a function of K is shown in Figure V-6 for several material parameters. ($\underline{\phi}^{0}$ is the loading for a corresponding Newtonain fluid.)

V.2.4 <u>Discussion.</u> First-order effects of hydrodynamic elasticity and shear thinning on the performance of a rigid planar blade coater have been examined through the analyses with a second-order fluid model and a CEF model. It was shown that the effect of elasticity as manifested by the performance of a second-order fluid, is to increase the total normal traction acting on the blade. This effect is likely to be small for 'true' lubrication systems and it is bound to be suppressed by purely viscous effects in accordance with Tanners' purely viscous approximation. The coating
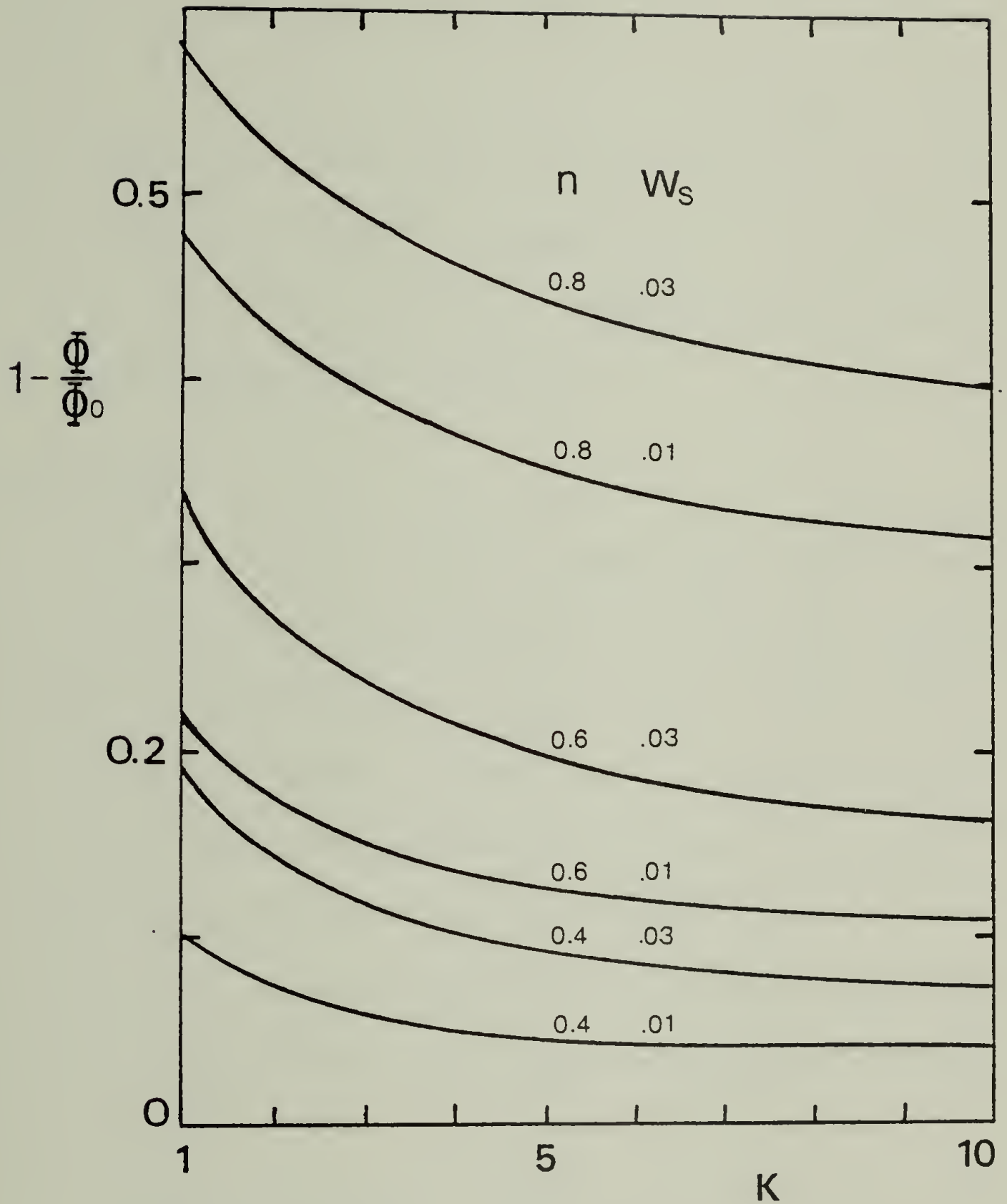
Figure V-6. The fractional reduction in blade loading of a CEF fluid (relative to a Newtonian fluid) in a rigid planar blade coater.

thickness, however, is unaffected by elasticity (to a first order).

The first-order effect of shear thinning, as given in the solution for the CEF fluid, is to reduce the pressure distribution relative to a corresponding Newtonian fluid. The opposing (positive) contribution of the normal stresses was shown to be negligible in comparison to the shear thinning effect, in 'true' lubrication systems. The coating thickness, however, was shown to increase slightly with viscoelasticity.

V. 3   Experimental

V. 3. 1   Scope.   A simple planar rigid blade coating system was constructed to simulate actual coating operations. The system was designed to allow variation of the blade angle in the range 0°-5° and, equivalently, the geometric parameter K could be adjusted at any value within the interval [0, 6.3]. Several fluids, both Newtonian and viscoelastic, were tested. The coating thickness, the only performance variable considered, was measured by a direct contact technique and the results were related to the geometry of the system (K) and to the viscous and rheological properties of the fluids examined.

V. 3. 2   Experimental system.   A scheme of the experimental set-up along with a general view of the system are shown in Figure V-7. The "blade" is a rigid piece of acrylic plastic (7.8 cm long, 8.1 cm wide) which can be set at different angles and clearances with respect to the moving web. It is attached to the main body of the system by a pair of screws

Figure V-7.   The experimental blade coating system.   (a)   General view
of the system. , (b)   A schematic of the experimental set-up.

1.   The blade (an acrylic wedge)
2.   Take-up roll
3.   Constant speed DC motor
4.   Micrometer-driven needle
5.   A travelling microscope
6.   Rotating guides
7.   Film (web) reservoir
8.   Aluminum plate
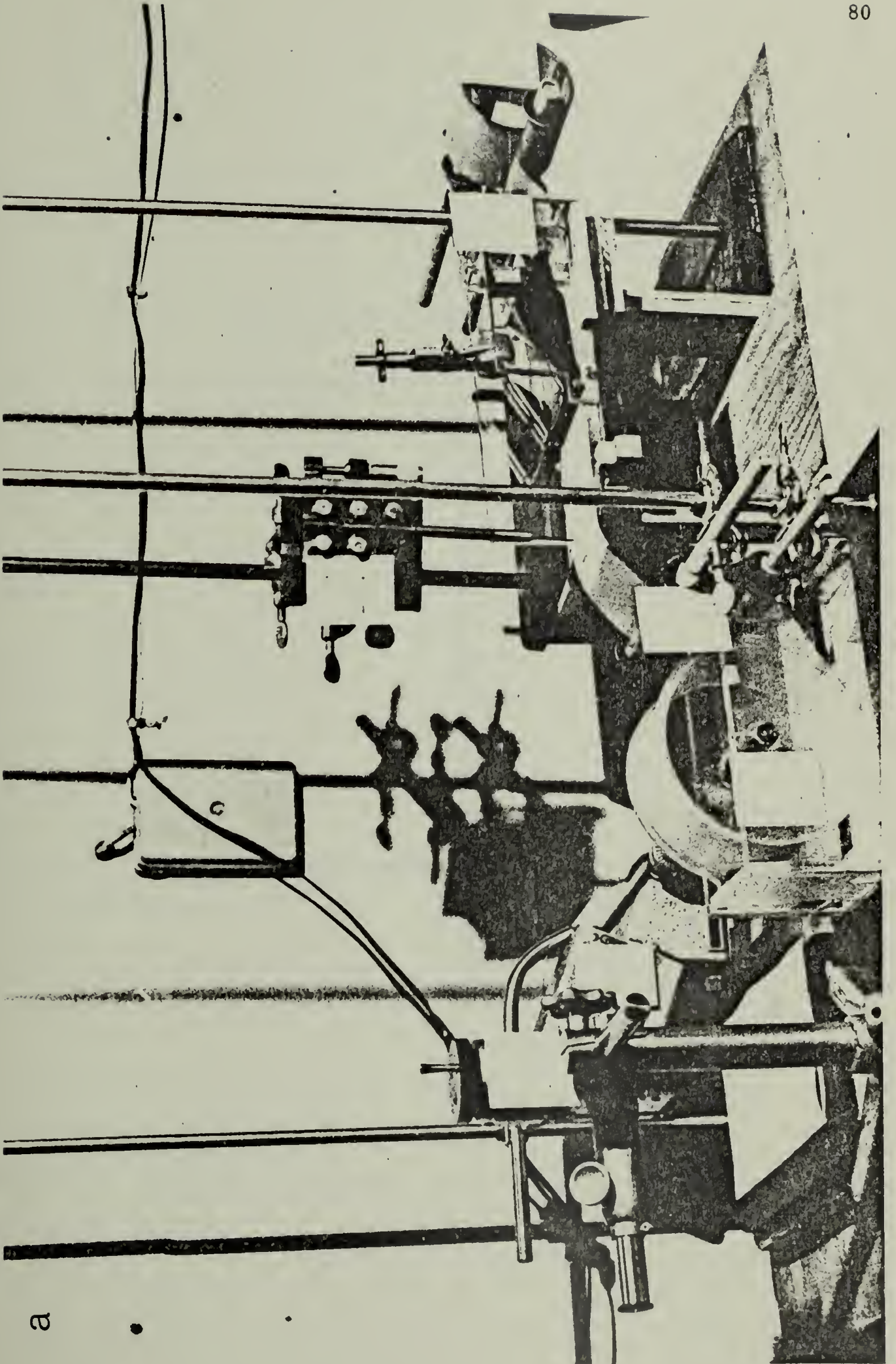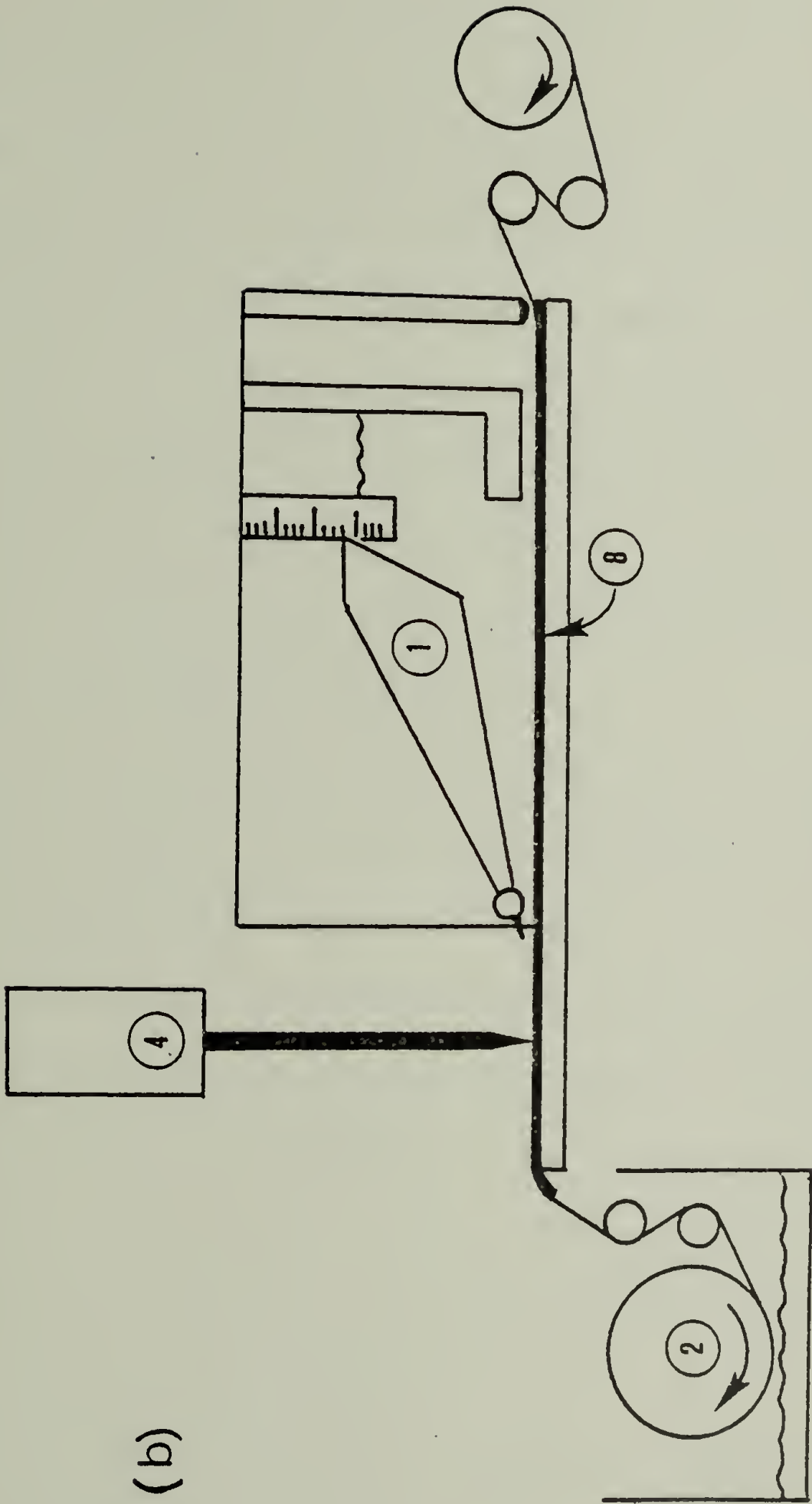
(b)

that permit changing continuously the angular position of the blade. A

smooth aluminum plate (26 cm long, 8.1 cm wide), that serves as a rigid

planar lathe, is glued permanently to the main body underneath the blade.

The space between the blade and the plate was carefully adjusted to be

uniform in the neutral (z) direction. An arbitrary, pre-calibrated scale

was used for determining the angular position of the blade and the pertinent

geometric parameters of the system. Table V-1 lists the geometric para-

meters for the positions used throughout this experiment. In order to

reduce as much as possible various entry effects the blade was tapered (at

$\sim 45^{\circ}$) and smoothed at the entrace zone.

The web itself is a flexible clear plastic (ICI, Melinex 'O' flim,

$7^{+}_{-}0.5$ mils thick, 8 cm wide) and it passes through a series of rigid and

moving guides within and outside the system. The guides were constructed

to insure that the web would travel "flat" on the aluminum plate.

The web was driven through the system by a constant speed motor

(Inframo-Wayne Model RXR1-64). After passing through a pair of circular

guides the web was wound up onto a take-up roll (14.7 cm in diameter).

This roll was positioned in an acrylic box that served as a drainage for

the coating fluid after leaving the system.

The coating thickness was measured by a direct contact method using

a long micrometer-driven needle that was positioned above the aluminum

plate and in front of the blade tip. The contact of the needle with the

coated layer was observed through a travelling microscope.

Table V-1

The Experimental Blade Coating System:
Geometric Parameters for Five Blade Positions

Position	H_0[1] [cm]	H_1[2] [cm]	K	Blade Angle
K-10	0.165	0.210	1.29 ± 0.08	$2 1'$
K-13	0.148	0.430	2.92 ± 0.02	$2^{o}6'$
K-15	0.138	0.590	4.27 ± 0.01	$3^{o}13'$
K-16	0.135	0.680	5.02 ± 0.01	$4^{o}0'$
K-18	0.129	0.810	6.29 ± 0.01	$5^{o}1'$

[1] ± 0.003

[2] ± 0.020

V.3.3 <u>Materials.</u> Two viscous Newtonian fluids and three viscoelastic fluids were tested in the present experiment. Some pertinent information regarding these fluids is given in Table V-2.

The viscosities of the Newtonian fluids were measured with an Epprecht-Rheomat 15 viscometer (a co-axial cylinder mode) at the average room temperature at which the corresponding runs were conducted. The viscometric properties of the viscoelastic fluids, being less temperature sensitive, were measured at 25.0° C using a Rheometrics Mechanical Spectrometer (a cone and plate mode). The viscometric functions, $\eta(\dot{\gamma})$ and $\Psi_{12}(\dot{\gamma})$, are shown in Figures V-8 and V-9 for the shear-rate range of interest. The corresponding viscometric data are listed in Appendix B.

The viscoelastic fluids are aqueous solutions of polyacrylamide (Polyhall) (H - X) and carboxymethylcellulose (CMC-X). The recoverable shear, S_R, given in Table V-2 is a viscoelastic parameter that represents the ratio of the (elastic) normal stresses to the (viscous) shear stresses at a given shear-rate. It is defined as

$$S_R = \frac{\tau_{xx} - \tau_{yy}}{2\tau_{xy}}$$

$$= \frac{\Psi_{12}}{2\eta}\dot{\gamma}$$

In Table V-2, S_R is evaluated at $\dot{\gamma} = 50$ sec^{-1} which is an approximate nominal shear rate for the experimental system studied. (It was nearly constant for all the runs.)

Table V-2

The Blade Coating Experiment:
List of Materials

Fluid	Symbol	μ(or η_0)[4] [poise]	$S_R 50$
Glycerin[1](G)	○	9.3	0
Karo Syrup[1](KS)	⬤	38.2	0
H-1 [2]	△	320	3.2
H-1.5 [2]	▽	820	3.6
CMC-2.5 [3]	☐	47	0.6

[1]For more information see Table VI-4.

[2]H-X = aqueous solution of polyhall 295 (Stein, Hall and Co. Inc), X% by wt.

[3]CMC-X = aqueous solution of CMC7M (Hercules, Inc.), X% by wt.

[4]Viscosities measured at room temperature for the corresponding runs.
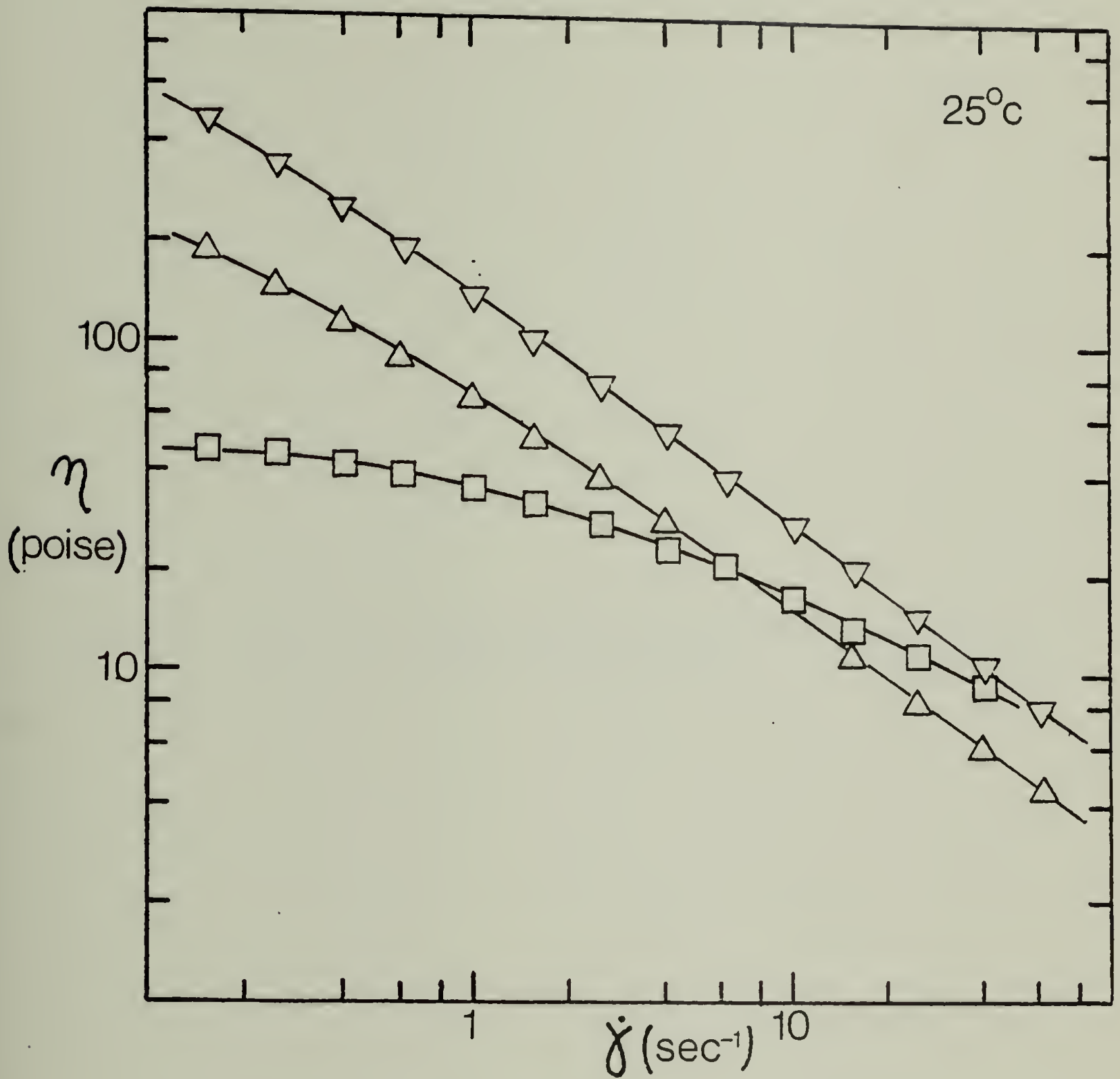
Figure V-8. The shear viscosity functions for the viscoelastic fluids used in the blade coating experiment. (Key in Table V-2.)

Figure V-9. The first normal-stress coefficients for the viscoelastic fluids used in the blade coating experiment (Key in Table V-2).
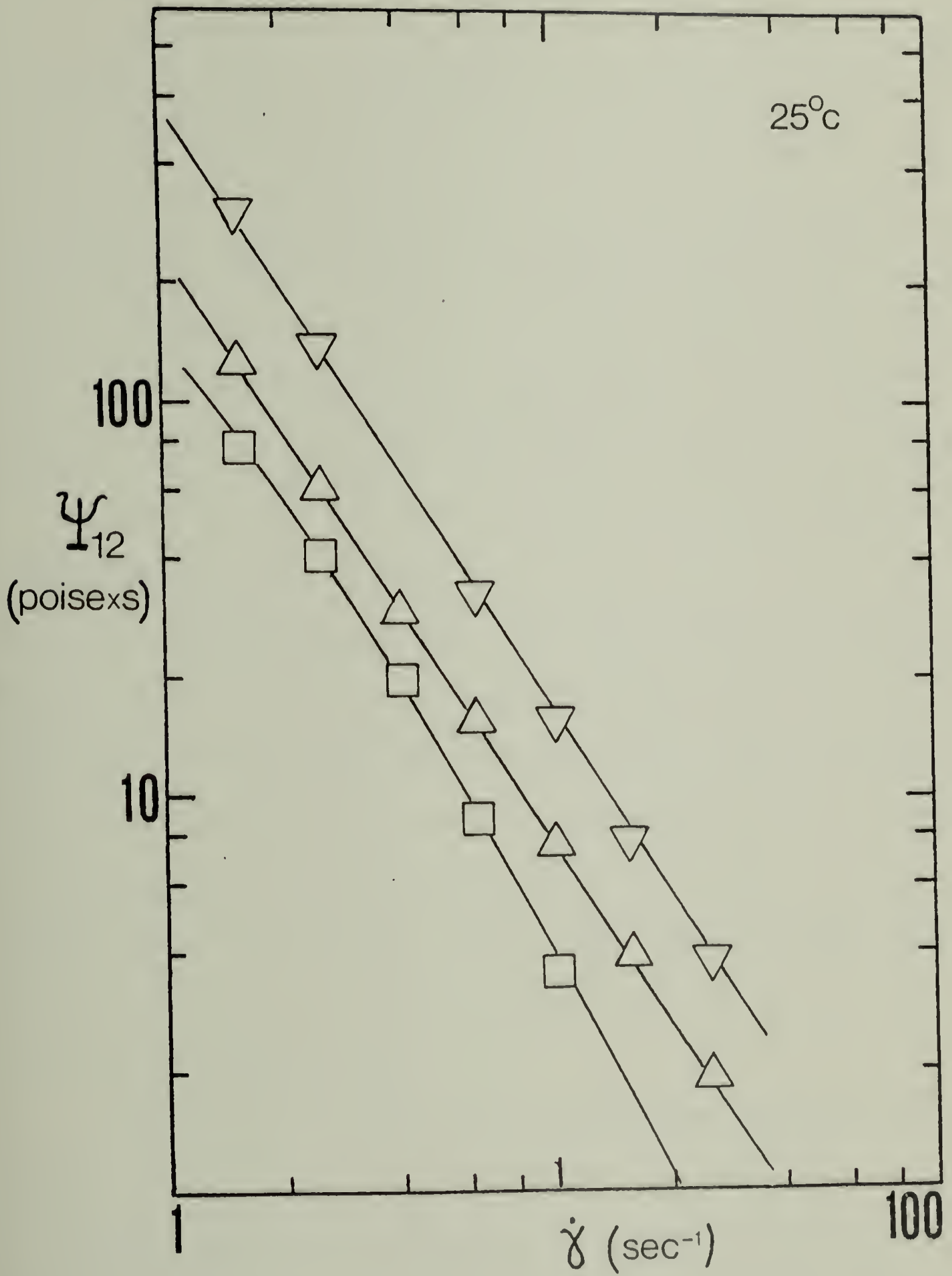
The Polyhall solutions were prepared by first preslurrying the polymer in acetone (1:5 by wt.) and then adding a specified amount of tap water with a simultaneous vigorous mixing (using a zig-zag shaped impeller) for several hours. The acetone was added to assist in the mixing stage by preventing the formation of lumps. It was also found that the presence of acetone repressed bacterial growth in the solution. The preparation of the CMC solution was essentially similar except that acetone was not added. Instead, the polymer powder was poured quickly into the vortex of a stirred cool tap water and then it was mixed vigorously by a high speed zig-zag shaped impeller for several hours.

V. 3. 4 Experimental procedure. The angular position of the blade was adjusted using the calibrated position scale on the main body. The system was loaded with the web film taking great care that it would stay tight and flat on the aluminum plate during its motion through the system. To insure a smooth motion of the web, the various guides were carefully alligned and adjusted prior to the actual run. Then, the rear part of the system, just behind the blade, was filled with the coating fluid and the web was set in motion at a pre-calibrated speed.

The thickness of the coating layer deposited on the moving web was measured in the following manner. The needle was carefully driven by the micrometer toward the coated surface until a contact was observed (through the travelling microscope) and the needle position was recorded. After the

entire fluid volume was driven out through the system, the needle was

advanced further toward the bare aluminum plate until it touched the plate.

The thickness was then determined from the difference between the two

"contact" positions of the needle. To insure statistically meaningful read-

ings, each run was repeated about eight times when at each time the needle

was positioned at random at different spots above the coated area. All the

measurements were taken at points sufficiently removed from the blade tip

where the curvature of the fluid-air interface was apparently zero. Also,

in order to avoid significant pressures at the entrance zone (due to hydro-

static head) the readings were taken when the fluid head in the reservoir

was sufficiently low (2-3cm).

This procedure was not without pitfalls. Viscous drag (fluid slipping

under the web) and irregular motion of the web due to misallignment and

nonuniformity of the film (web) itself were the severest problems encountered

throughout this experiment. The thickness measuring technique, however,

proved simple, convenient and reliable to within ± 2 mils in coating thickness.

V.4 Experimental Results and Discussion

A graphical representation of the final results is given in Figures V-10

and V-11. The corresponding data are listed in Appendix A. The variation

of λ, the dimensionless coating thickness, with the geometrical parameter

K is shown in Figure V-10. It is seen that the data for the Newtonian

fluids (Glycerin and Karo Syrup) fall close to the Newtonian lubrication
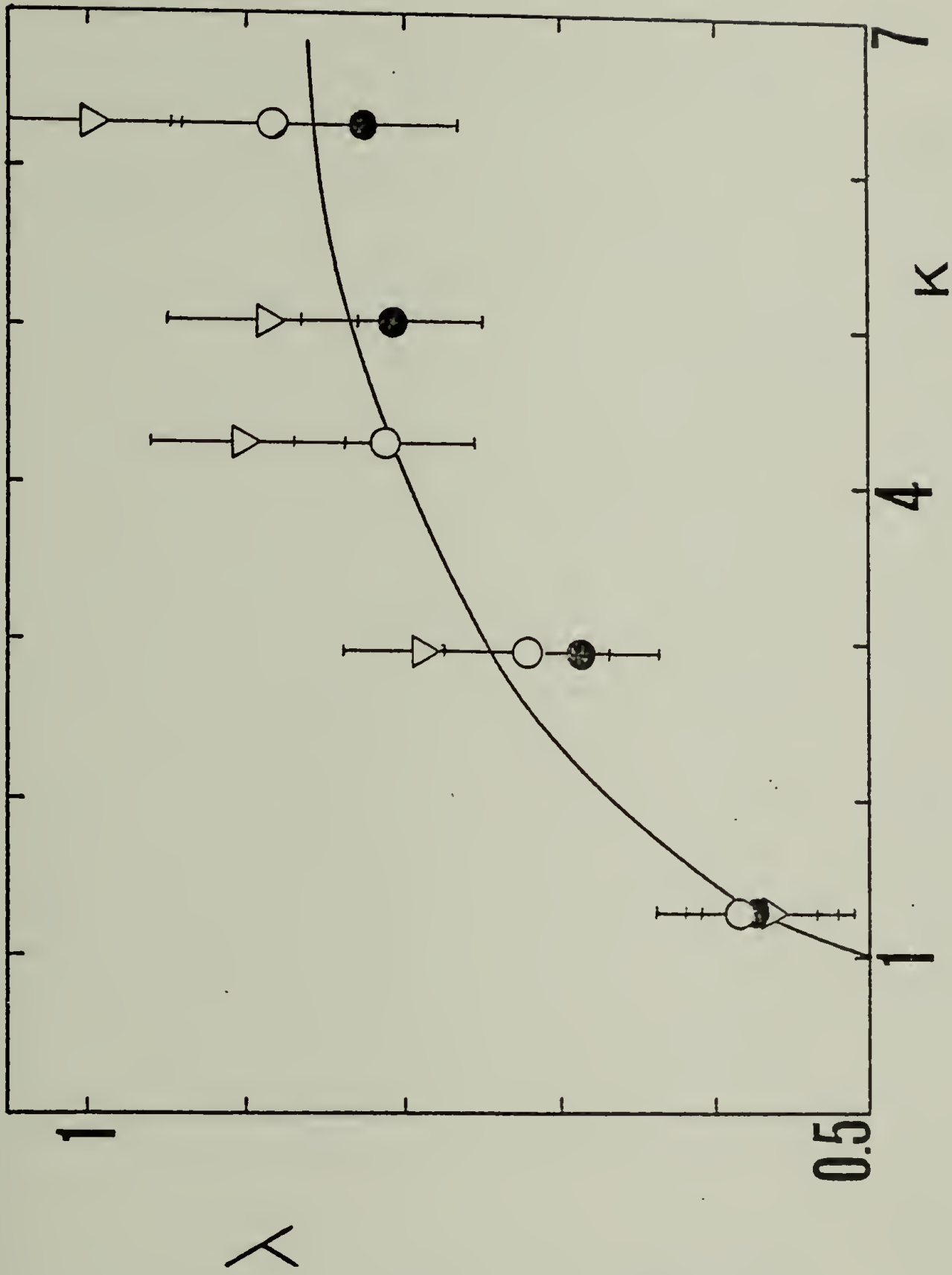
Figure V-10. Coating thickness vs. K. Experimental data are compared to the Newtonian lubrication solution for a rigid planar blade coater (the solid curve). U = 9.3 cm/sec. (Key in Table V-2).
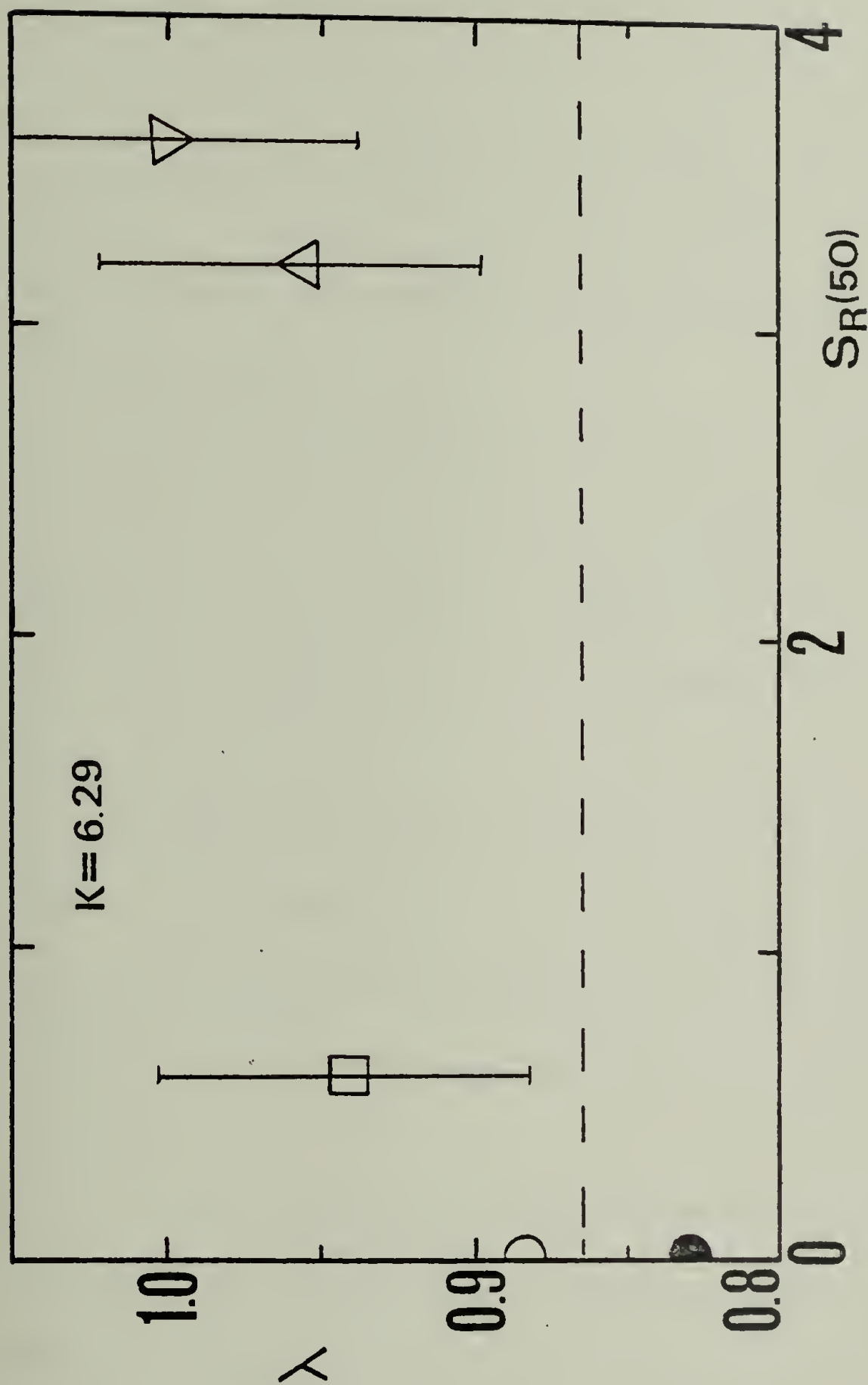
Figure V-11. Coating thickness vs. recoverable shear. Experimental data for the blade coating experiment. U = 9.3 cm/sec. (Key in Table V-2).

solution (within experimental error). The experimental points for H-1.5, the most elastic solution studied, do fall consistently above the Newtonian data in accordance with the predictions of the viscoelastic (CEF) analysis. However, owing to the large experimental error ($\sim 7\%$) the observed difference is not statistically meaningful. This error originates from irregularities in the motion of the web and some uncertainties in the measurement of H_1, H_0 and H_∞.

The effect of viscoelasticity is better demonstrated in Figure V-11. In this figure λ is correlated with the recoverable shear (at K=6.29). The recoverable shear is evaluated at a nominal shear rate of 50 sec^{-1}. This value represents shear rates at the neighboorhood of the blade tip, i.e.,

$$\dot{\gamma}_N = U/H_0.$$

Although the experimental uncertainity does not permit any quantitative conclusions as regards the effect of viscoelasticity (or S_R) on λ, it is apparent that viscoelasticity tends to increase (though mildly) the coating thickness. Similar trend was predicted by the perturbation analysis for the CEF fluid.

In order to assess the various experimental data and especially the observed $\lambda(K)$ for the Newtonian fluids, it is pertinent to address the following question: "To what extent is the lubrication approximation valid for the experimental system studied?" This question should be divided into two: 1) Is the flow field in the experimental system planar and z-independent and 2) How good is the approximation of a unidirectional flow? It is

expected that the velocity field be weakly z-dependent in the immediate vicinity of the side walls where the no-slip condition is met. In general, the effect of the side walls would be to retard the flow and to slightly reduce the flow rate in comparison to the z-independent case. However, owing to the small fraction of the area of the side walls ($\sim 3\%$) it is reasonable to assume that their overall effect on the flow field would be marginal. In addition, since no side leakage is allowed in this system the flow can be safely assumed planar.

The assessment of the effect of the y-component of the velocity on the overall system dynamics is more difficult. Such assessment can be done via a complete solution of the full planar flow case for the geometry of the experimental system. A numerical solution for a slider-bearing with an angle of $5^{\circ}43'$ (and K=7.0) has been carried out using a Finite Element method. The solution scheme is presented in detail in Appendix D. The numerically calculated pressure distribution for the (two-dimensional) slider bearing problem is presented in Figure V-12 and compared to the Newtonian lubrication solution. The difference between the "numerical" and the "analytical" distributions for the geometry considered is apparently small and one can conclude that the lubrication approximation is valid for blade angles of $5^{\circ}43'$ and less. Inasmuch as blade angles in this experimental study were smaller than $5^{\circ}43'$ (and K<7.0), then the unidirectional flow approximation for this experiment is justified. The effect of the angle on the applicability of the lubrication approximation is addressed by Pinkus and

Figure V-12.   The approximate pressure distribution (the solid curve),
                calculated through the lubrication approximation, is
                compared to the FEM calculations ($\triangle$) for a blade
                coating system with K = 7.0 and a blade angle of $5^{o}43'$.
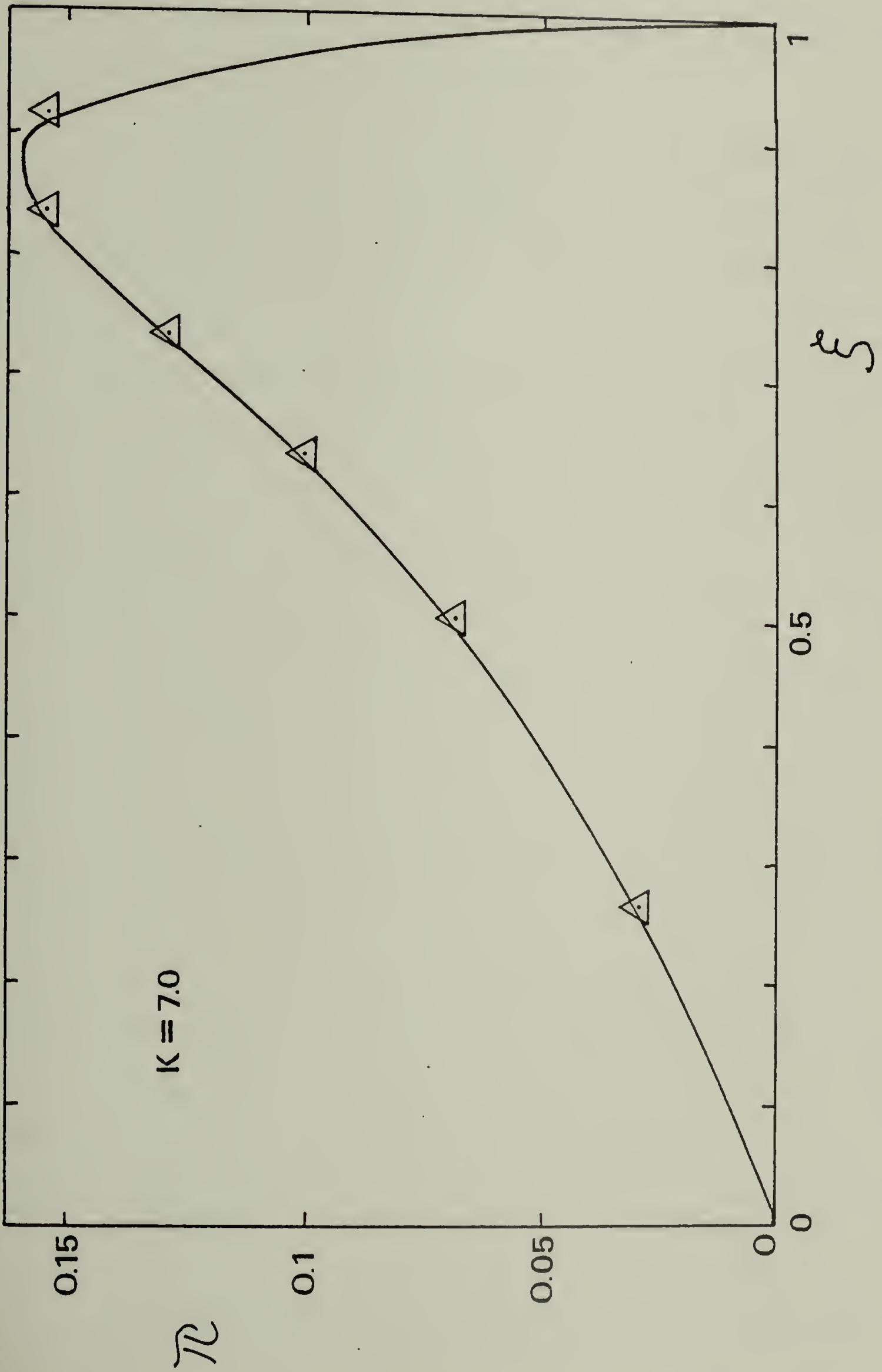
Sternlicht (1961) and by Middleman (1977) who conclude that the lubrication approximation is "reasonable" for non-parallelism of up to 30°.

In this experimental study, inertial effects were apparently insignificant as the Reynolds number, $N_{Re} = \frac{\rho U H_L^2}{\eta L}$, did not exceed unity for all the experimental runs. (On the effect of inertia in slider bearings, see Pinkus and Sternlicht 1961).

Additional approximations that deserve a critical consideration are the dynamic boundary conditions for the pressure function. It was stated, in Section 2, that the pressure is zero (or ambient) at the leading and trailing edges of the blade. At the entrance zone the flow is converging through a wide-angled ($\sim 45^\circ$) contraction into the narrow flow space under the blade. This may give rise to some finite pressures at $\xi = 0$. A finite hydrostatic head at the fluid reservoir may also contribute to a finite pressure at the entrance zone. It is expected, however, that these contributions be small since the measurements throughout this experiment were taken when the fluid head at the reservoir was low. It was noted previously that the pressure boundary condition at the leading edge of the blade ($\xi = 1$) may be, somehow, influenced by the surface tension of the fluid due to the negative curvature of the liquid-air interface in the vicinity of the blade tip. While, in the experiments conducted the effect of surface tension is very likely negligible $(\frac{\eta U}{\gamma} \gtrsim 1.5)$, it is expected that under conditions of light dynamic loading (low ηU) the surface tension will have a controlling effect on the dynamics in the separation zone and hence on the thickness of the coating

layer deposited on the moving web. This point is briefly addressed in the following section.

V.5 Some Comments on the Effect of Surface Tension in Blade Coating

So far the role of surface tension was ignored in the formulation of the dynamic boundary conditions at the blade tip ($\xi = 1$). This is justified so long as the dimensionless group $\frac{\eta U}{\sigma}$ (the capillary number) is large, i.e., when the dynamics in the separation region are dominated by viscous forces. When the blade is lightly loaded (the dynamic pressures generated under the blade are small) it is necessary to consider surface tension forces acting in the concave separation region and to have a closer look at the mechanism of film separation.

A similar problem, the rupture of a lubricating film due to sliding of a flat surface parallel to a stationary one, was considered by Coyne and Elrod (1969, 1970). This work was discussed in some detail in IV.4. One important result of Coyne and Elrods' theory is the functional dependence of the thickness (of the coating deposited on the moving slider) on the capillary number. It can be argued that the problem of parallel surfaces is actually indistinguishable from the rigid blade problem in the limit of light loading (i.e., when the dynamic pressure gradients in the bounded regime are very small). Consequently, the results of Coyne and Elrod can be readily extended to the case of a lightly loaded blade. These results are replotted in Figure V-13 and they show that coating thickness decreases as surface
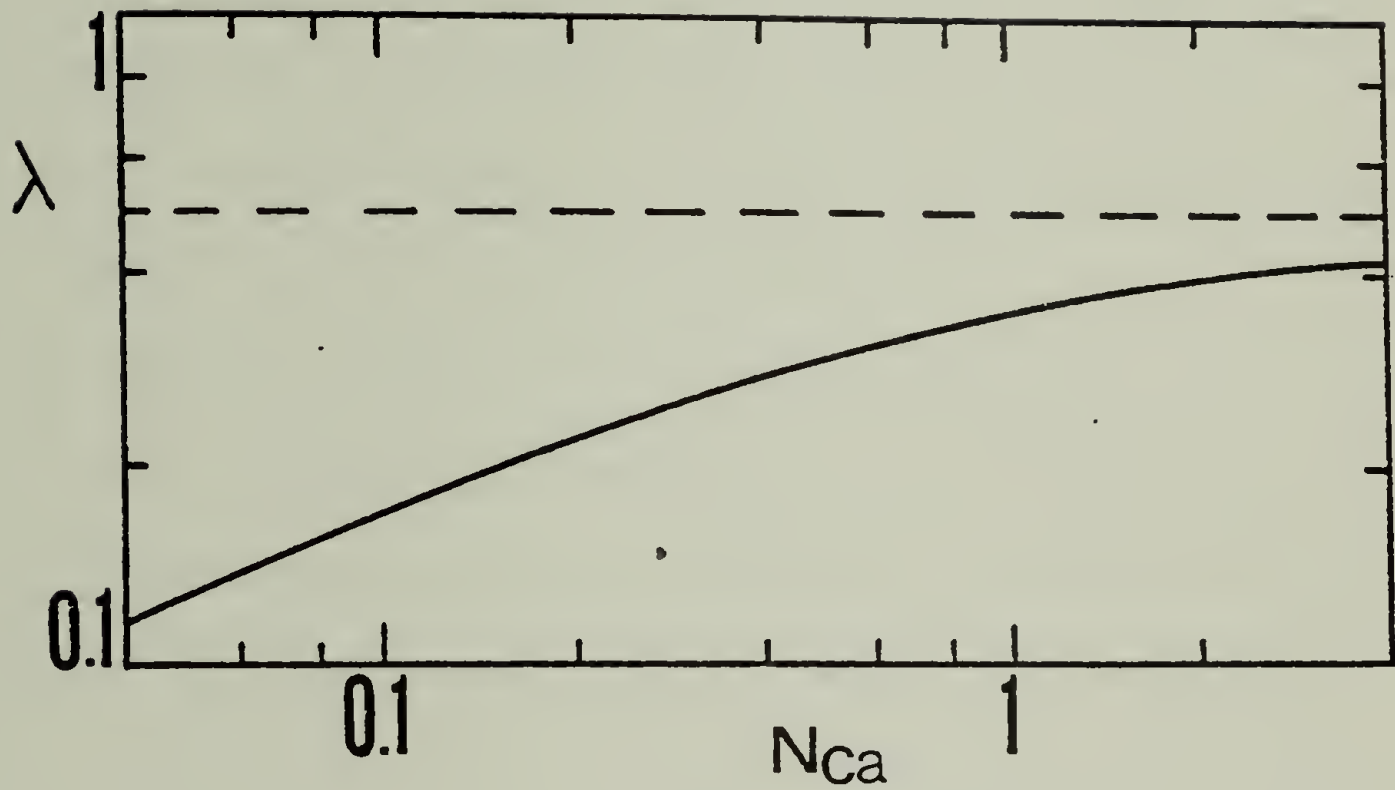
Figure V-13.   Coating thickness vs. the capillary number for a slot
               coater (K = 1.0).   The solid curve is extracted from
               Coyne and Elrod's (1969, 1970) theory.   The dashed
               line represents the asymptote for high capillary
               numbers.

tension increases ; From considerations of conservation of mass such reduction in coating thickness (or flow rate) must be a result of backflow in the bounded regime. Thus, for the lightly loaded case, in the limit of high surface tension, λ is a function of the capillary number and perhaps the gravity and Reynolds numbers as opposed to the heavily loaded case in which λ depends on K (i.e., blade geometry) alone.

More recently, Ruschak (1974) has given a lengthy account of the free surface problem encountered in slot coating, which is similar to the problem considered by Coyne and Elrod. With the aid of regular and singular perturbation techniques, Ruschak solved the complete set of momentum equations combined with the usual kinematic and traction boundary conditions on the free surface. The limiting cases considered by Ruschak are those of low web speed and high surface tension (i.e., low capillary numbers). An a-priori statement in his analysis is that H_∞ (the coating thickness far downstream from the exit point) is half the slot height or, equivalently, that the velocity gradient far upstream in the bounded regime is linear, and no backflow is allowed (even when surface tension goes to infinity!). An important consequence of this statement is that the coating thickness is always independent of the capillary number and the effect of surface tension is strictly to alter the shape of the free surface in the neighborhood of the separation region. For small web speeds (first-order about the stationary case) in the limit of high surface tension, the surface curvature downstream from the contact line (solid-liquid-air contact) is uniformly small and the

flow is nearly rectilinear. At large distances from the slot the flow profile transforms from parabolic to plug and the film height reduces asymptotically to half the slot height.

This result is seemingly in sharp contrast with Coyne and Elrods' results which do not exclude backflow for high values of surface tension. Their theory is backed by some experimental data (separation in lubrication converging-diverging spaces and the motion of a bubble in a tube) but it remains to be seen whether these data are pertinent to the slot coating case. One flaw in Coyne and Elrods' development is that they avoid a rigorous treatment of the contact line where the dynamics are not well defined. They, rather, fix the contact angle (the tangent of the curvature of the liquid-air interface near the solid surface) at some level thereby making it an independent parameter of the system rather than a function of the capillary number and the other dynamic parameters considered. Such arbitrary constraint is <u>not</u> imposed by Ruschak who discusses, though not conclusively, some aspects of the local behavior at the contact line.

A more complete solution of the difficult free surface problem in blade coaters or slot coaters is yet to be devised. Such theoretical study must be accompanied by a careful experimental investigation of the shape of the free surface and the velocity field in the separation region.

C H A P T E R VI

ROLL COATING

VI. 1 Introduction

The application of rollers for the deposition of uniform liquid films onto moving or stationary webs is a common industrial operation. It is especially wide-spread in the photographic, printing and paper-pulp industries where coating-thickness specifications are often very strict. Schematic diagrams of some typical roll coating processes are shown in Figure VI-1. Such "rolling geometries" are commonplace in lubrication engineering and the fundamental hydrodynamic analyses for these systems are available in texts on hydrodynamic lubrication (e.g., Pinkus and Sternlicht 1961, Cameron 1966).

Calendering is an important operation that resembles roll coating. This operation differs from roll coating principally in the way by which the fluid separates downstream from the nip (the position where the rigid surfaces are at closest approach). While in calendering the fluid "leaves off" without wetting the rotating rollers, in roll coating the fluid splits and adheres onto each of the moving surfaces. The nature of flow separation, which must have a considerable effect on the dynamics in the bounded regime, will ultimately depend upon the rheology and adhesion characteristics
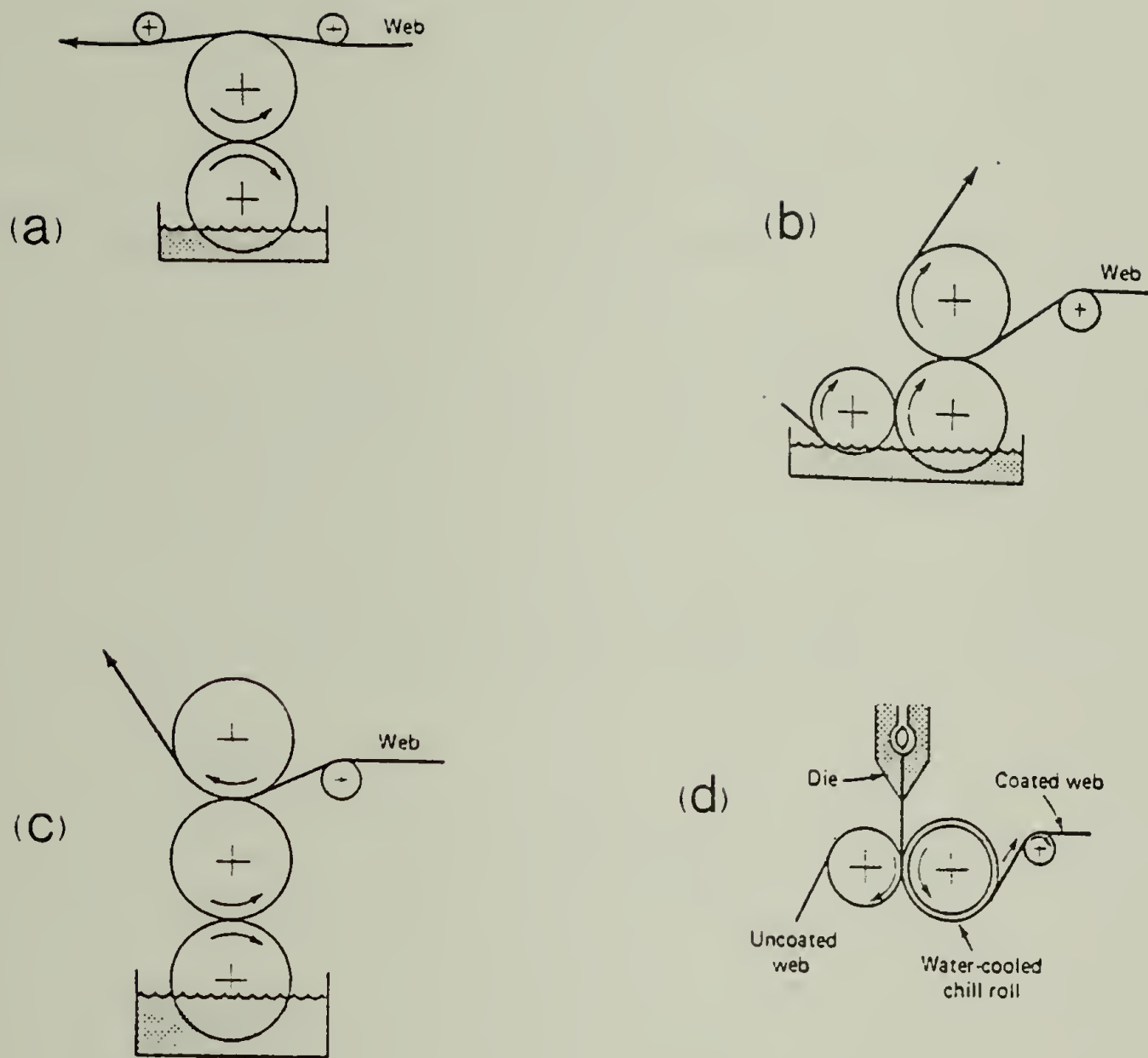
Figure VI-1.   Schematic diagrams of typical roll-coating processes.
(After Middleman 1977): (a) Kiss coater, (b) reverse-
roll coater, (c) forward-roll coater, (d) extrusion
coater.

of the fluid. High viscosity materials and softened plastics are likely to be calendered, whereas low viscosity liquids will be more commonly roll-coated (Middleman 1977). This distinction constitutes a loose, but practical definition of roll coating. Even though calendering and roll coating have equal footing in industry, calendering has received far greater attention in the literature. (See for example, McKelvey 1962 and Middleman 1977.) This discriminatory approach stems, possibly, from the relative difficulty in handling the separation boundary conditions in roll coating. Indeed, the question of these boundary conditions has not yet been fully resolved (see IV. 4), although some approximations have been proposed and applied with relative success.

The lubrication problem of flow between counter-rotating rollers fully immersed in a viscous fluid was first considered by Martin in 1916 (Cf: Banks and Mill 1954) and later by Gatcombe (1945). The full film lubrication analysis was employed by Banks and Mill (1954) to study the problem of cavitation in the diverging section of the two-roll system. Tanner (1960) analyzed the full-film lubrication of rolling elements for a corotational Maxwell fluid. His approximate solution predicts that a viscoelastic fluid will generate lower pressures than a corresponding Newtonian fluid.

A first attempt to consider the problem of flow separation was made by Hopkins (1957). He examined the case of a fluid film driven by a roller and a flat sheet, splitting at some point downstream from the nip. As the

position of film separation is <u>a-priori</u> unknown, Hopkins was compelled to consider an additional boundary condition. He assumed that film separation would take place at the first stagnation point from the nip. This simple condition was discussed in IV.4 and it is known as the Prandtl-Hopkins separation condition. As will be seen later, this condition, despite its simplicity, is useful and valid for systems where surface tension effects are comparatively unimportant.

Several phenomenological studies of flow separation and cavitation in a roll nip, using photographic techniques, were conducted by Myers and coworkers (Miller and Myers 1958, Myers et al. 1959, Myers and Hoffman 1961, Hoffman and Myers 1962). Their observations indicate that backflow patterns can be formed in the vicinity of the separation meniscus for sufficiently low speeds (low capillary numbers). At high speeds bubbles started to form in the low pressure region which is indicative of the onset of internal cavitation (see IV.4).

Pitts and Greiller (1961) examined, both theoretically and experimentally, the flow induced by counter-rotating rollers partially immersed in a viscous fluid. Their analysis involved an approximate solution of the biharmonic equation combined with the full traction boundary conditions on the free surface at separation. The shape of the separation meniscus was assumed to be parabolic. Pitts and Greiller's predictions for the position of the separation point were in satisfactory agreement with their experimental data.

Some observations on the splitting of a water film between rotating rollers were reported by Hintermaier and White (1965). They measured the heights of films issuing from the nip region and found them generally proportional to the nip separation. In a more recent study, Williamson (1972) analyzed the problem of the tearing of an adhesive layer between flexible tapes passed between cylindrical guides. This problem is hydrodynamically similar to the problem considered by Pitts and Greiller as it involves the splitting of a viscous fluid film between counter-rotating rollers. Williamson solved numerically the biharmonic equation for the separation region taking the shape of the separation interface to be expressible by a sixth order polynomial. His calculations exhibit circulation patterns behind the separation meniscus, which are similar to those observed by Pitts and Greiller.

An analysis of the sheet-and-roll system was carried out by Greener and Middleman (1974). They applied the Prandtl-Hopkins conditions combined with a plausible approximation for the geometry of the interface at separation. This simplification made it possible to consider, at least approximately, non-Newtonian and surface tension effects. Inasmuch as this analysis is presented (with some corrections) in Section 2, further comment is reserved for later.

Lubrication analyses for the sheet-and-roll system, are developed in detail in Section 2 with a concurrent discussion of the approximate separation

model used. These analyses are carried out for three constitutive models; the purely viscous power-law model, the second-order fluid model and the CEF model. In Section 3, the power-law sheet-and-roll analysis is extended to the system of partially immersed counter-rotating rollers. Also in this section, the effect of gravity is given some consideration and the approximate separation model is critically assessed. Experiments designed to test the theoretical models are described in Section 4 and the experimental results are reported and discussed in Section 5. Finally, in Section 6, some experimental observations on reverse roll coating are presented along with a simplified theory. This chapter is strictly concerned with the (hydrodynamically) stable roll coating problem. As flow instabilities are known to impose severe restrictions on the application of roll coating devices, this problem will be given a full consideration in Chapter VIII.

VI.2. The Sheet-and-Roll System: Lubrication Analyses

VI.2.1 <u>General.</u> The essentials of a typical sheet-and-roll system are given in Figure VI-2. As shown, the fluid is driven out of a large reservoir behind the roll by the concerted motion of the web and the roll. The fluid emerging from the front-end splits onto the moving surfaces such that a uniform coating layer is formed on each surface. This model specifies that both surfaces move at the same lateral speeds. This requirement is arbitrary as it is not always encountered in practice. However, for convenience, the additional factor of non-equal speeds is not considered
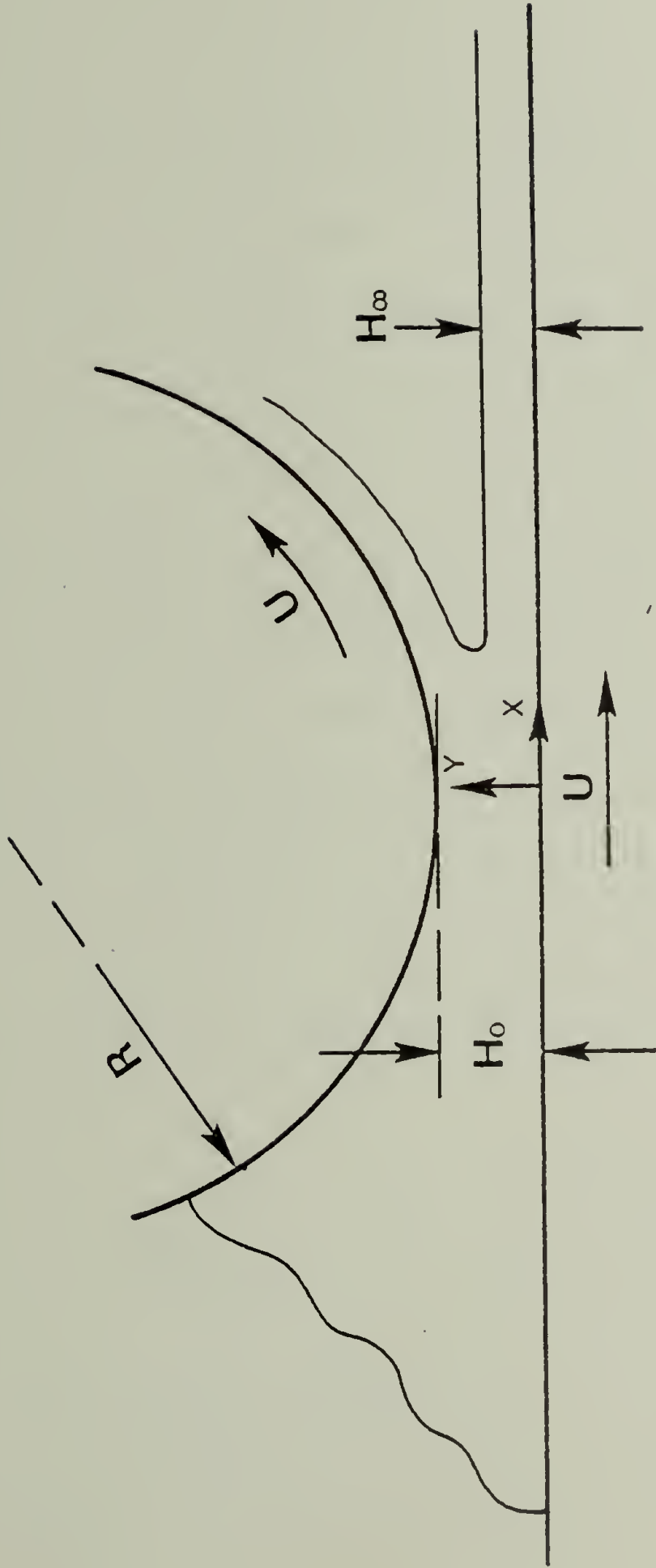
Figure VI-2. The sheet-and-roll system. A schematic diagram.

and a brief comment to that effect is made in VI. 2. 5.

The sheet-and-roll system, being a prototype of many industrial roll coating devices is analyzed in full in this section. This analysis is intended to provide some useful relations between the design and operation parameters of the system and some performance variables such as the coating thickness and the pressure distribution. The effect of the rheology of the fluid is given a special consideration as three rheological models are examined: the power-law fluid (of which the Newtonian fluid is considered a special case), the second-order fluid and the CEF fluid. The corresponding constitutive equations were discussed in Chapter IV. As before, the lubrication approximation is utilized and it leads to a considerable simplification of the equations of motion. In essence, the planar mixed flow is replaced by a unidirectional shear flow. (The lubrication thin film approximation is applicable so long as $H_0/R \ll 1$ and end effects are negligible.) Eq. (IV-2) is thus the starting point.

It is convenient, for later operations, to make the problem dimensionless by defining

$$\xi = \frac{x}{(RH_0)^{1/2}} \quad , \quad \eta = \frac{y}{H_0} \quad , \quad \varphi = \frac{u}{U}$$

and

$$\mathcal{R} = \frac{P}{\eta_a \frac{U}{H_0}} \left(\frac{H_0}{R} \right)^{1/2}$$

where

$$\eta_a = \begin{cases} K \cdot (\frac{U}{H_0})^{n-1} & \text{for the p.l. fluid} \\ \alpha, & \text{for second-order fluid} \\ \eta_o & \text{for CEF fluid} \end{cases} \qquad (VI-1)$$

The boundary conditions for the sheet-and-roll system, in terms of these dimensionless variables, are as follows

(a) $\varphi = 1$ @ $\eta = 0$

(b) $\varphi = 1$ @ $\eta = \sigma(\xi)$

(b^1) (or d φ/d$\eta = 0$ @ $\eta = 1/2 \, \sigma(\xi)$)

(c) $\varphi = 0$ @ $\eta = 1/2 \, \sigma_1$

(d) $\pi = 0$ @ $\xi = -\infty$

(e) $\pi = N_S/(r/H_0)$ @ $\xi = \xi_1$

$$(VI-2)$$

Eqs. (VI-2a, b) are the 'no-slip' conditions where $\sigma(\xi)$ is a function representing the position of the roll surface. It is most commonly approximated by

$$\sigma = 1 + 1/2 \, \xi^2 \qquad (VI-3)$$

This "parabolic" approximation is valid for $H_0/R \ll 1$. Eq. (VI-2b^1) is a statement of symmetry of the velocity profile about the midplane ($\eta = 1/2\sigma$) and it is equivalent to Eq. (VI-2b). The Prandtl-Hopkins separation condition is expressed by Eq. (IV-2c) and it will be used for determining the yet unknown position of film separation ($\xi = \xi_1$). This condition deserves a comment as to its applicability and relevance.

In actual lubrication systems the relative position of the rolling boundaries (H_0) is entirely controlled by the dynamics, i.e., the solid boundaries are free to adjust their position in response to the pressures developed in the system. In addition, the pressures generated are often high to withstand the usually high loads in typical lubrication systems. Under such conditions, the purely dynamic Swift-Stieber conditions are applicable. (The question of the downstream-end boundary conditions in rolling elements has been discussed at length in IV.4; see also Swift 1932, Birkhoff and Hays 1963, Taylor 1963 and Cameron 1966). In contrast, the rolling boundaries in coating systems are usually rigid (fully or partially) so that the coating thickness can be more effectively controlled. As a consequence, it is expected that a separation cavitation (rather than internal cavitation) mechanism will prevail in the separation region and a proper separation condition is needed to reflect this. The Prandtl-Hopkins separation condition used herein has not been borne out by a rigorous theory or an empirical study. It, rather, constitutes a simple, reasonable postulate. It is known today that this condition fails to represent the separation region for systems in which surface tension is important (i.e., where the capillary number is small). For such systems the actual separation takes place further downstream from the first stagnation point (Myers et al. 1959, Pitts and Greiller 1961, Williamson 1972, Savage 1977a). It will be shown in Section 3 that this condition is, nonetheless, comparable

to the more rigorous Coyne and Elrod conditions (Coyne and Elrod 1970) over a wide range of capillary numbers. The rationale for using the Prandtl-Hopkins condition in this analysis, aside from its simplicity, is that it can be readily extended to non-Newtonian fluids unlike, say, the Coyne and Elrod conditions.

Cases of heavy loading (high pressures) are not uncommon in roll coating as it is known that the pressures generated in some systems can be sufficiently high to bend the roll (the "roll bowing" effect) and to alter considerably the nip geometry. For such heavily loaded systems it is more appropriate to consider the Swift-Stieber conditions. The effect of the boundary conditions on the performance of the system will be briefly addressed in VI.2.5.

Eqs. (VI-2d, e) are the dynamic boundary conditions for the pressure function. Eq. (VI-2d) states that the inlet is "flooded", i.e., the pressure is ambient far upstream from the nip and Eq. (VI-2e) is a simple force balance at the point where the film splits ($\xi = \xi_1$). The pressure at this point is balanced by the surface tension force, which is finite and negative since the curvature of the separation meniscus is negative. The parameter N_S appearing in Eq. (VI-2e) is defined as

$$N_S = \frac{\gamma}{\eta_a U} \left(\frac{H_0}{R}\right)^{(1/2)}$$

(VI-4)

N_S is a surface tension parameter and it can be looked at as a modified (inverse) capillary number. r is the radius of curvature of the free surface at $\zeta = \zeta_1$. Since the geometry of the free surface is not known, some approximate model for the film-splitting region is needed. Figure VI-3 depicts the approximate separation geometry considered herein; the free surface at separation is assumed to be semicircular. This model is somewhat crude, but, as will be shown later, it does a fair job (together with the Prandtl-Hopkins condition) as compared to more sophisticated models. The inherent assumption involved in this approximation is that $_1$ is sufficiently small so that the rigid surfaces can be taken as being nearly parallel. Consequently,

$$2r + 2H_\infty = H_1$$

or

$$2\left(\frac{r}{H_0}\right) + \lambda = \frac{H_1}{H_0} = \zeta_1 \tag{VI-5}$$

where

$$\lambda \equiv \frac{2H_\infty}{H_0}$$

λ is a dimensionless coating thickness. Eq. (VI-5) together with the boundary conditions will be utilized in the analysis that follows.
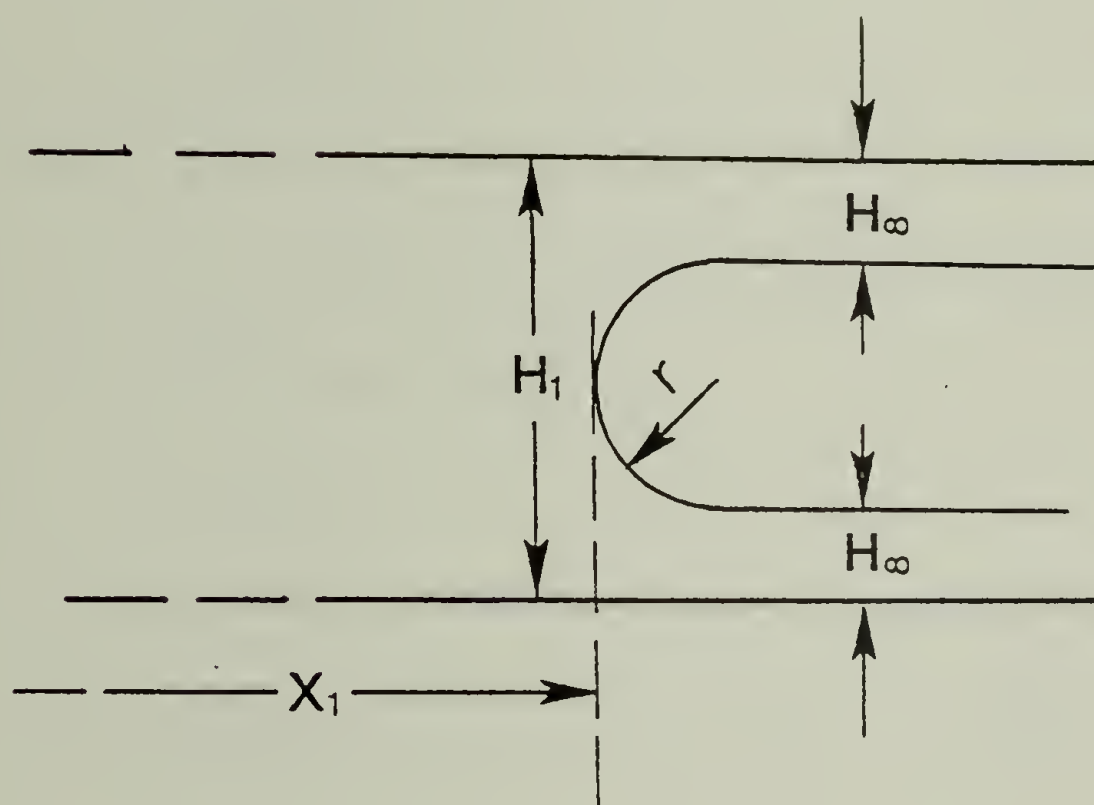
Figure VI-3.   An approximate model for the film-splitting geometry in the sheet-and-roll system.

VI. 2. 2 <u>The power-law fluid.</u> For a power-law fluid Eq. (IV-2) becomes

$$O = -\frac{dP}{dx} + K \frac{d}{dy} \left[\left| \frac{du}{dy} \right|^{n-1} \frac{du}{dy} \right] \qquad \text{(VI-6)}$$

or, in dimensionless form,

$$O = -\dot{\mathcal{R}} + \frac{d}{d\eta} \left[\left| \frac{d\varphi}{d\eta} \right|^{n-1} \frac{d\varphi}{d\eta} \right] \qquad \text{(VI-7)}$$

where

$$\dot{\mathcal{R}} \equiv \frac{d\,\mathcal{R}}{d\,\xi}$$

As the pressure gradient is constant across the film (i.e. $\dot{\mathcal{R}} \neq \dot{\mathcal{R}}(\eta)$)

Eq. (VI-7) can be integrated twice with respect to η to give,

$$\varphi = \frac{\dot{\mathcal{R}}^{q-1}}{q} \left[|\eta - \xi|^{q} - \left(\frac{\xi}{2} \right)^{q} \right] + 1 \qquad \text{(VI-8)}$$

where $q = \frac{1}{n} + 1.$

In deriving Eq. (VI-8) use has been made of conditions (VI-2a, b). Since there are two unknowns in Eq. (VI-7) (φ, $\mathcal{R}$), an additional equation is needed. This additional equation is provided by the statement of conservation of mass,

$$\lambda = 2 \int_{\xi/2}^{\xi} \varphi \; d\eta \qquad \text{(VI-9)}$$

(Note that, aside from being a dimensionless coating thickness, λ is also a dimensionless flow-rate)

λ is a hitherto unknown quantity but it will be treated hereafter as a

constant parameter. A combination of Eqs. (VI-8) and (VI-9) gives the

following expression for the pressure-gradient,

$$\dot{\pi} = 2(2q + 2)^n \ \frac{|\varsigma - \lambda|^{n-1} (\varsigma - \lambda)}{\varsigma^{1+2n}} \tag{VI-10}$$

This expression can be introduced back into Eq. (VI-8). With the more

explicit expression for φ at hand, condition (VI-2c) is applied and it

follows that

$$\varsigma_1 = \frac{1 + 2n}{n} \lambda \tag{VI-11}$$

or, using Eq. (VI-5),

$$\int_1 = [2 \ (\frac{1 + 2n}{n} \lambda - 1)]^{1/2} \tag{VI-12}$$

r/H_0 can now be evaluated by combining Eqs. (VI-5) and (VI-11),

$$\frac{r}{H_0} = \frac{1 + n}{2n} \lambda \tag{VI-13}$$

Substitution of Eq. (VI-13) into condition (VI-2e) yields

$$\lambda (\frac{1+n}{2n}) \ \dot{\pi}_1 = - N_S$$

or,

$$\lambda (\frac{1+n}{2}) \int_{-\infty}^{f_1} \dot{\pi} d\int = - N_S \tag{VI-14}$$

Eq. (VI-14) is an integral equation for λ with N_S as a parameter. This

equation was solved for N_S ($N_S = N_S(\lambda)$) by specifying λ (since it is

explicit in N_S). The integration of $\dot{\pi}$ was performed numerically via the

trapezoidal rule. The solution is presented in Figure VI-4 in the form of

λ vs. N_S curves for several values of n. The variation of λ with n in

the limit of zero surface-tension ($N_S \rightarrow 0$) is given in Figure VI-5. It is

apparent from Figures VI-4 and VI-5 that both surface tension (as expressed

by N_S) and non-Newtonian character (as expressed by 1-n), act to increase

(modestly) the coating thickness. In practice, the parameter N_S will vary

in the range [0, 1] (since $H_0/R \ll 1$ and $\dfrac{\tau}{\eta_a U} = 0(1)$ or less). Within

this range the dependence of or N_S is very weak, and it is practically

inobservable. In addition, in view of the approximations made concerning

the separation region, the theory should not be expected to hold for $N_S > 1.0$,

where surface tension forces start to dominate.

Once the values of λ have been determined it is a simple matter to

evaluate the pressure distributions; the appropriate values of λ ($\lambda(n, N_S)$)

are introduced into Eq. (VI-10) which is then integrated numerically. Pres-

sure distributions for several values of n, in the limit of vanishing surface

tension ($N_S \rightarrow 0$), are plotted in Figure VI-6. The results indicate that the

non-Newtonian distributions are "sharper" in comparison to the corresponding

Newtonian distribution (i.e., $|\tau_N| \leq |\tau_{p.e.}|$). (A corresponding Newtonian

fluid is a fluid with a constant viscosity equal to the apparent viscosity of

the power-law fluid evaluated at a nominal shear-rate of U/H_0).

An important performance variable is the total force acting on the

roll. This force originates from the pressure field generated in the fluid,

and in some instances it can be sufficiently high to bend the roll and to
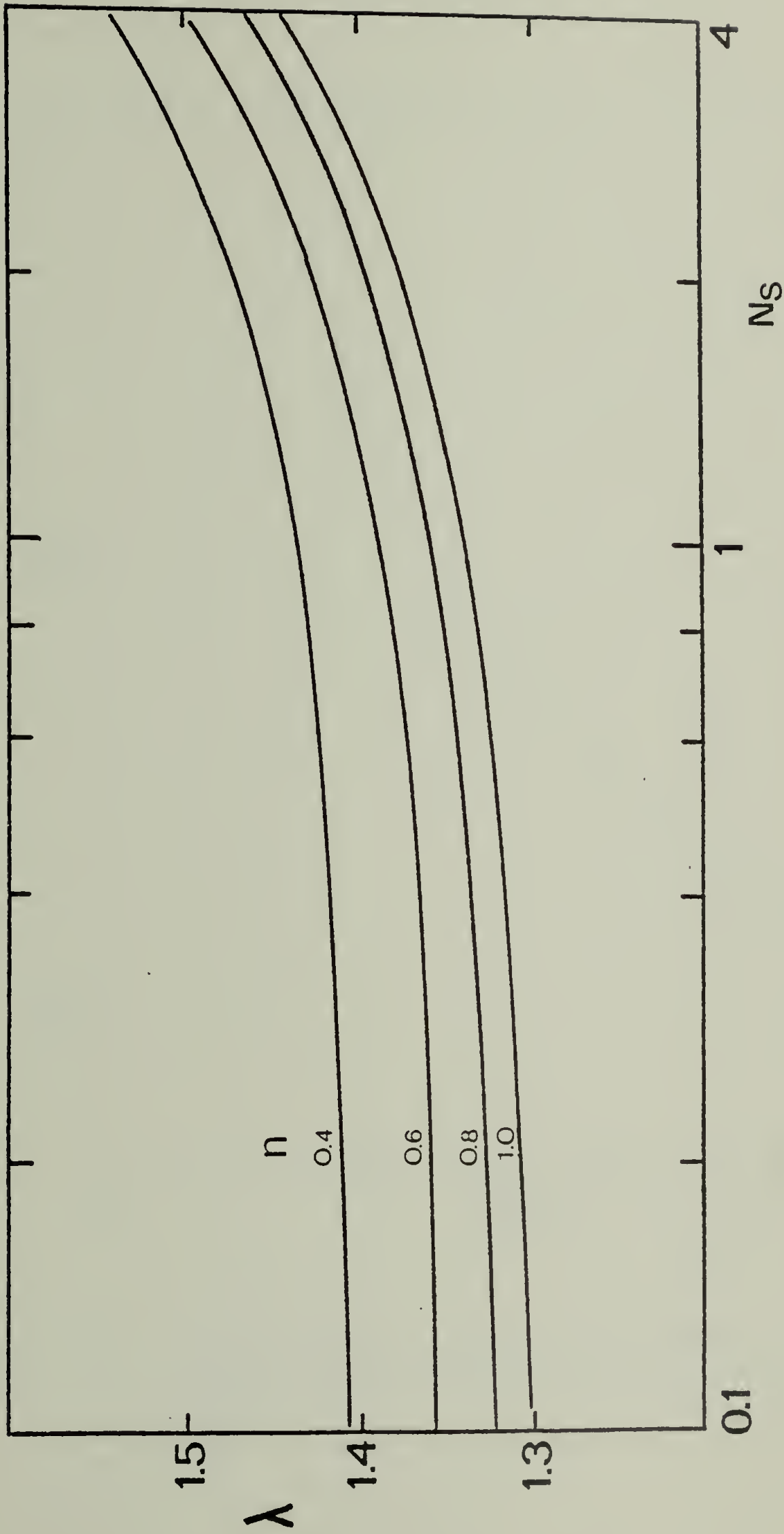
Figure VI-4. Coating thickness vs. surface-tension parameter. Analytical results for a power-law fluid in the sheet-and-roll system.
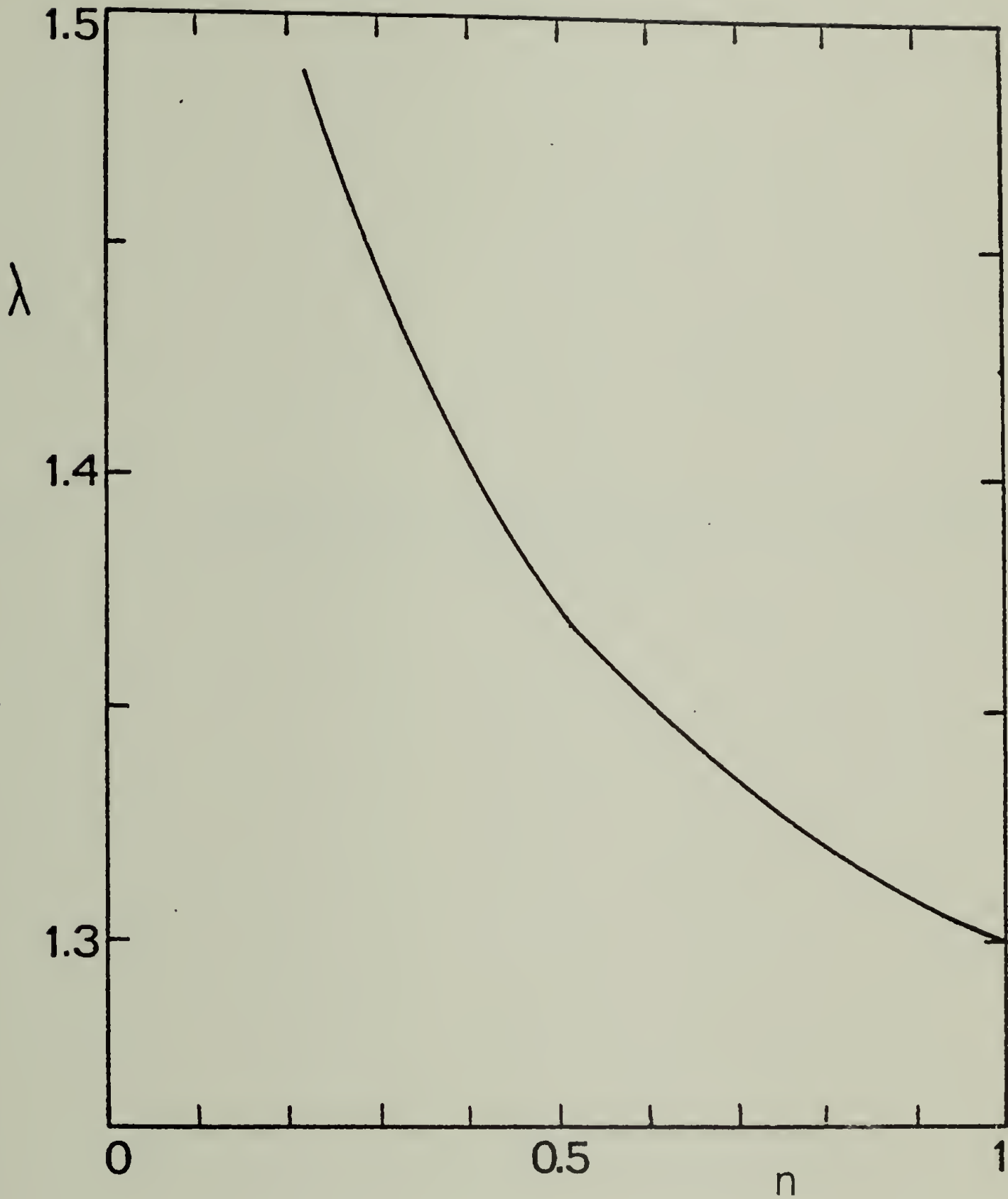
Figure VI-5.   Coating-thickness vs. the power-law index.   Analytical
                curve for a power-law fluid in the sheet-and-roll system
                ($N_S \longrightarrow 0$).

Figure VI-6.   Analytical pressure distributions for a power-law fluid in the sheet-and-roll system ($N_S \rightarrow 0$).
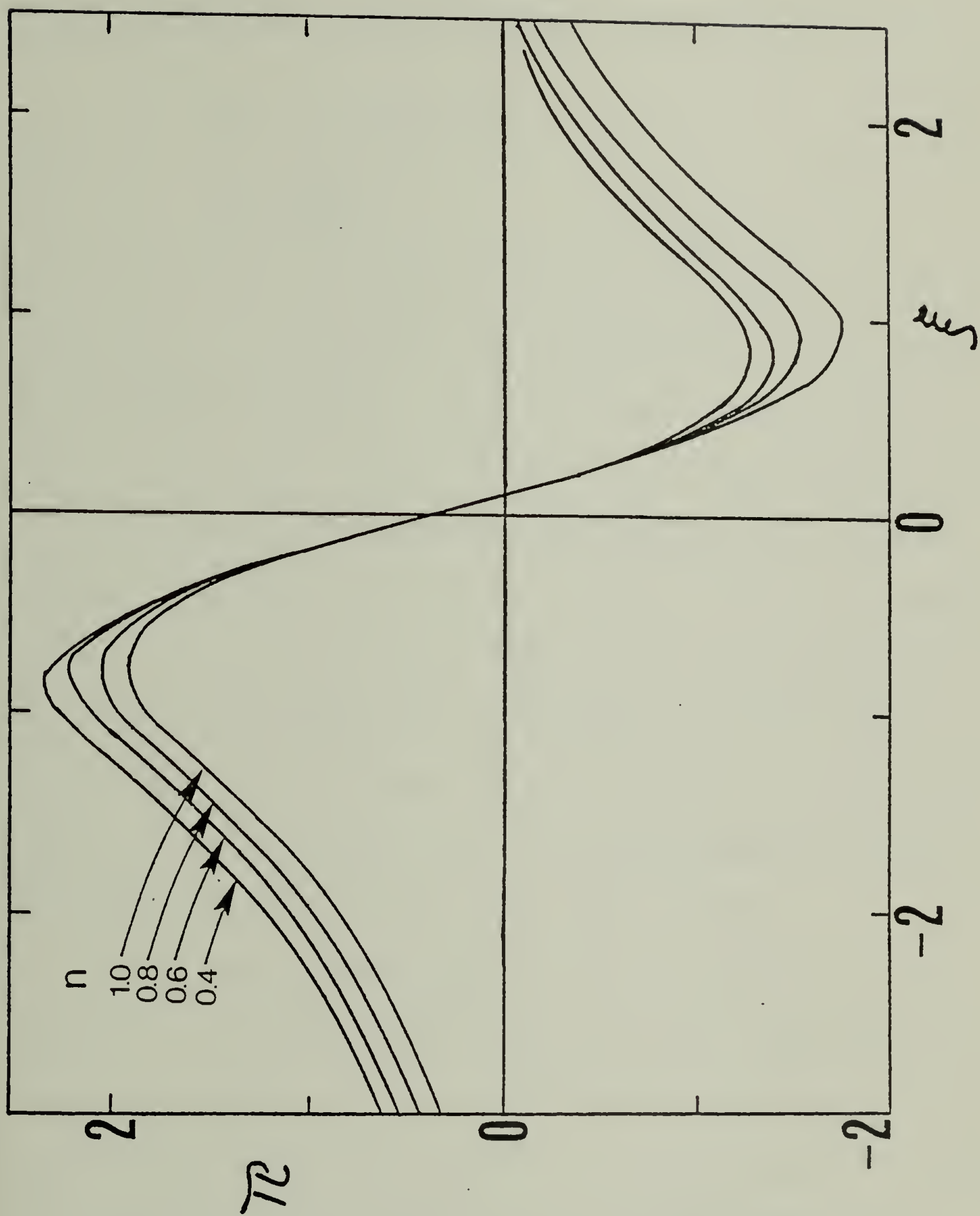
alter the nip geometry. The roll-separating force is calculated as follows:

$$\bar{\phi} = \int_{-\infty}^{\xi_1} - \Theta_{\eta\eta}\big|_{6} \, d\xi \qquad (VI-15)$$

where

$$\bar{\phi} \equiv \frac{F H_0^2}{\eta_a U}$$

and F is the actual roll-separating force per unit width. (The term roll-separating force is equivalent to "load carrying-capacity" commonly used in the lubrication literature.) $- \Theta_{\eta\eta}$ is the dimensionless form of the total stress $-T_{yy}$ ($=p - \tau_{yy}$). In the purely viscous case $- \Theta_{\eta\eta} = \pi$, and Eq. (VI-15) can be evaluated for the power-law fluid, using Eq. (VI-10). The calculation of $\bar{\phi} = \bar{\phi}$ (n) was carried out via a numerical double-integration of $\dot{\pi}(\xi)$. The results are shown in Figure VI-7 for the limiting case, $N_S \rightarrow 0$. This figure shows that a non-Newtonian fluid will exert higher force on the roll than a corresponding Newtonian fluid. It is important to keep the basis of comparison in mind: the corresponding Newtonian fluid "corresponds" in viscosity at the nominal shear rate U/H_0.

VI.2.3 <u>The second-order fluid.</u> The limitations and merits of the second-order fluid model have been discussed in IV.2. This model is now applied in the analysis of the sheet-and-roll system with the aim of examining first-order effects of viscoelasticity on the performance of the system.

It has been pointed out that the second-order fluid differs from a corresponding Newtonian fluid only dynamically (provided that the flow is creeping and planar). Since the velocity fields for both fluids are identical
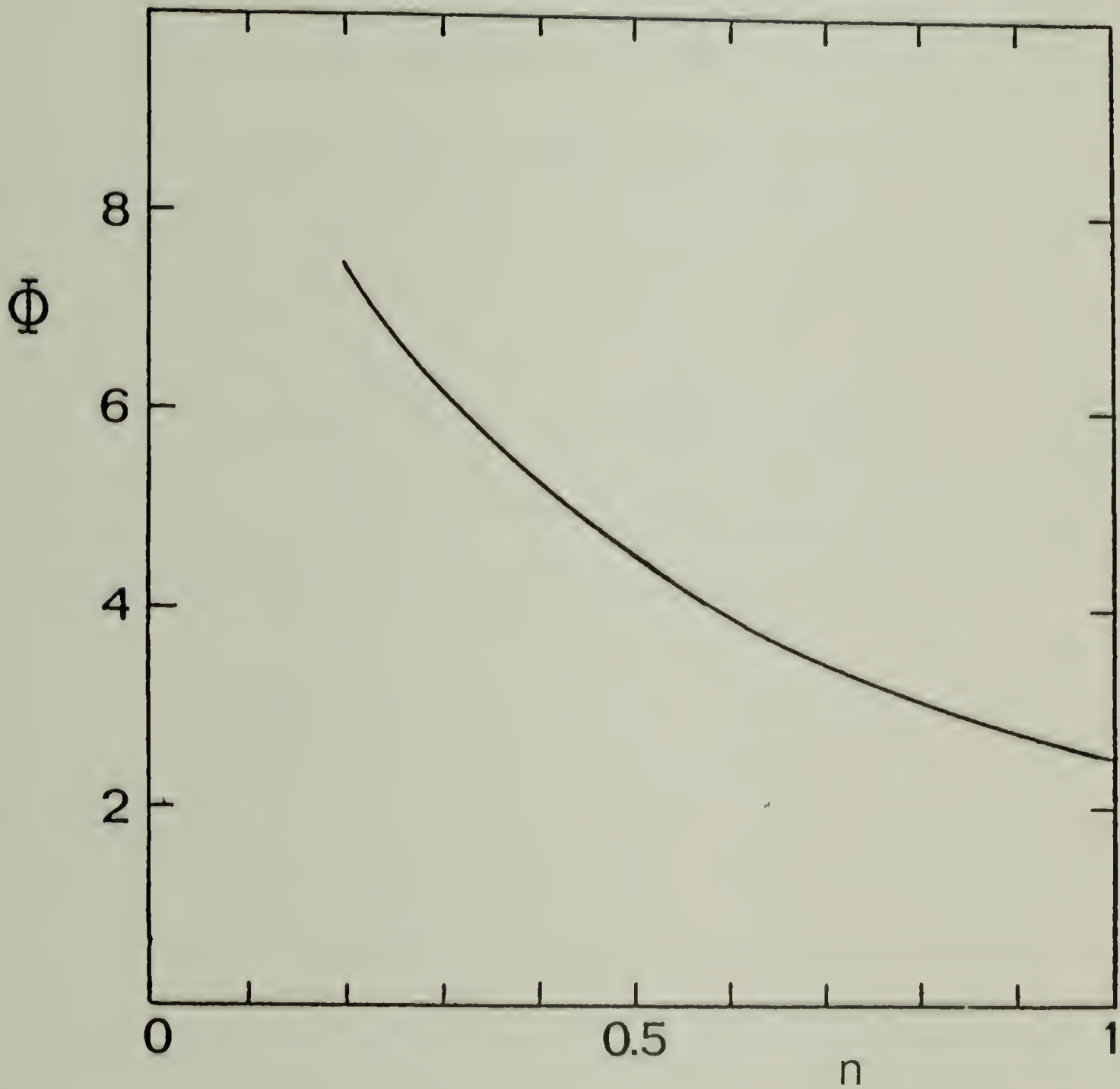
Figure VI-7. The roll-separating force vs. the power law index for a power-law fluid in the sheet-and-roll system ($N_S \rightarrow 0$).

for the same boundary-value problem, it is to be expected that the coating thickness, which is essentially a kinematic quantity, will be identical for both fluids as well. Thus, the problem narrows down to determining the pressure distribution for the second-order fluid in the system. Inasmuch as the second-order fluid is a viscoelastic fluid it is appropriate to consider the total stress distribution $(-\Theta_{\eta\eta})$ rather than the hydrodynamic pressure distribution (π). With the aid of the Giesekus-Tanner theorem (see VI.2) one can write,

$$- \Theta_{\eta\eta} = \pi^0 - S_R \left(\frac{H_0}{R}\right)^{1/2} \varphi\,\pi^0 + \frac{1}{2} S_R \left(\frac{H_0}{R}\right)^{1/2} \left(\frac{d\varphi^0}{d\eta}\right)^2 \tag{VI-16}$$

where π^0 is the pressure function for a corresponding Newtonian fluid $(\mu = \alpha_1)$ and S_R, the recoverable shear, is defined as

$$S_R = \frac{\alpha_2}{\alpha_1}\left(\frac{U}{H_0}\right)$$

$\Theta_{\eta\eta}$ is defined by

$$\Theta_{\eta\eta} = \frac{T_{\eta\eta}}{\alpha_1\left(\frac{U}{H_0}\right)}\left(\frac{H_0}{R}\right)^{1/2}$$

Eq. (VI-16) is the dimensionless form of Eq. (IV-7). With expressions for $\dot{\pi}^0$ and φ taken from the preceding purely-viscous analysis (for the case $n = 1$), Eq. (VI-16) takes the form

$$- \Theta_{\eta\eta}\big|_s = \pi^0 + S_R \left(\frac{H_0}{R}\right)^{1/2} \dot{\pi}^0 \left[\frac{1}{8}\,\dot{\pi}^0\,\sigma^2 - 1\right] \tag{VI-17}$$

Figure VI-8.   Total (normal) stress distributions for a second-order fluid
in the sheet-and-roll system (H_0/R = 0.01, $N_S \to 0$).
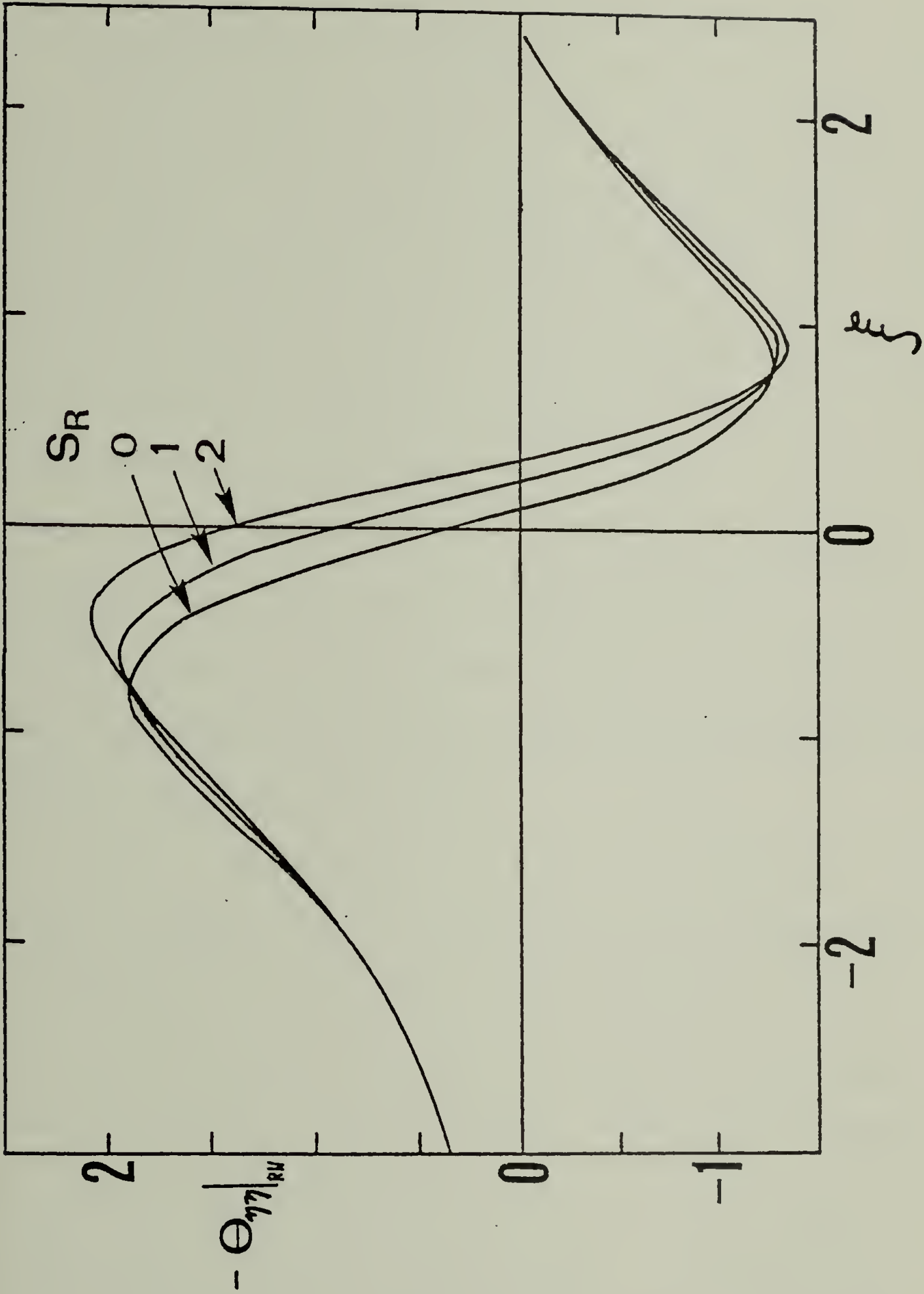
$\Theta_{\eta\eta}$ in Eq. (VI-17) is evaluated at the roll surface ($\eta = \le$).

Inspection of Eq. (VI-17) reveals that the total stress distribution will reduce identically to the Newtonian pressure distribution in the limit $S_R \to 0$ and/or $H_0/R \to 0$. This result is essentially in accordance with Tanner's purely viscous approximation for viscoelastic lubrication flows. In order to consider finite elastic effects it is necessary to assign a finite value to H_0/R. Figure VI-8 shows stress distributions as given by Eq. (VI-17) for several values of S_R taking $H_0/R = 0.01$. Apparently, the effect of viscoelasticity is to shift the stress function upward in the neighborhood of the nip region. This "shift upward" will increase the total force exerted on the roll. Indeed, as shown in Figure VI-9, the roll-separating force is a linearly increasing function of fluid viscoelasticity (as expressed by S_R). $\oint$ was evaluated using Eq. (VI-15).

VI.2.4 <u>The CEF fluid.</u> The second-order fluid is limited in its ability to predict the effect of viscoelasticity on the coating thickness or, for that matter, on the kinematics of flow in the bounded regime. It is, thus, useful to consider a slightly more elaborate and more realistic constitutive model such as the CEF equation. This equation was discussed in IV.2, and it is essentially represented by two empirical viscometric functions, $\eta(\dot{\gamma})$ and $\Psi_{12}(\dot{\gamma})$ (as given in Eqs. (IV-12) and (IV-14)). Only $\eta(\dot{\gamma})$ is used explicitly in the analysis in compliance with the purely viscous approximation; $\Psi_{12}(\ )$ enters the analysis in the evaluation of the total
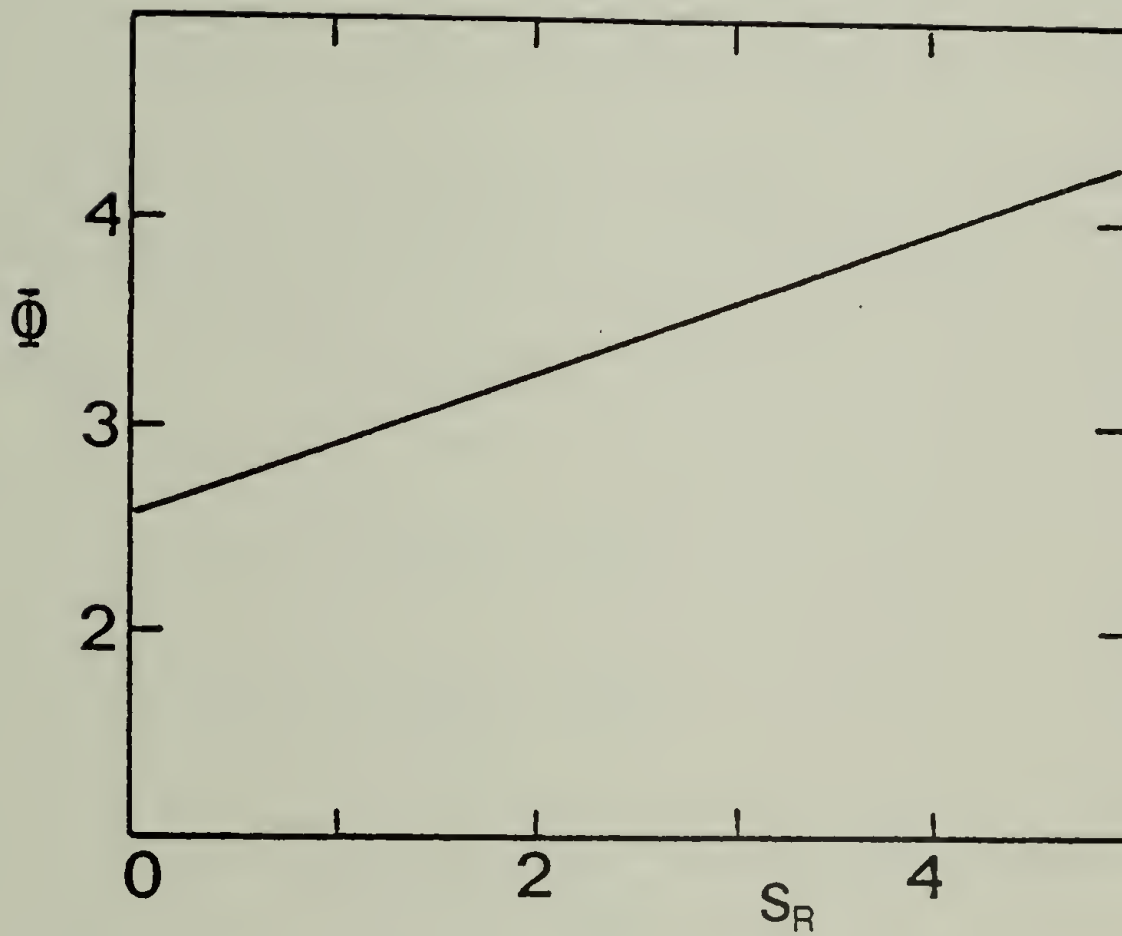
Figure VI-9.   The roll-separating force vs. the recoverable shear for a second-order fluid in the sheet-and-roll system ($H_0/R = 0.01$, $N_S \rightarrow 0$).

stress, $-T_{yy}$. Inasmuch as the empirical viscosity equation introduces severe non-linearities into the equation of motion, an approximate analytical solution, with the aid of regular perturbation techniques is worked out in a manner as outlined in IV. 3.

The analysis begins with Eq. (IV-15). This equation is integrated once with respect to η, to give

$$\frac{d\varphi}{d\eta} = \dot{\pi}(\eta - \delta/2)\left\{1 + N_e\left[\left(|\frac{d\varphi}{d\eta}|\right)^{1-n}\right]\right\}$$

(VI-18)

where use has been made of the symmetry of the velocity profile about the mid-plane (Eq. VI-2b'). (It is noted that the symmetry condition considerably simplifies the present analysis, compared to the corresponding blade coating analysis, as there is no need to account for the absolute-value operator.) The functions appearing in Eq. (VI-18) are expanded in the form,

$$\varphi = \varphi^0 + N_e\varphi^1 + O(N_e^2)$$

(VI-19)

$$\dot{\pi} = \dot{\pi}^0 + N_e\dot{\pi}^1 + O(N_e^2)$$

(VI-20)

and also

$$\lambda = \lambda^0 + N_e\lambda^1 + O(N_e^2)$$

(VI-21)

The viscoelastic perturbation parameter, Ne (as defined in Eq. IV-15) is assumed to be sufficiently small that the expansions can be truncated beyond the first-order terms. Thus, this procedure seeks to estimate the first-order effect of viscoelasticity, as expressed by Ne, in relation to the

zeroth-order (Newtonian) case. After the truncated functions are introduced

into Eq. (VI-18) and terms of order higher than 1 are eliminated, the

following equation is obtained,

$$\frac{d\varphi}{d\eta} = \dot{\pi}^0 (\eta - \varsigma/2) + N_e \dot{\pi}^1 (\eta - \varsigma/2)$$
$$+ N_e [|\dot{\pi}^0 (\eta - \varsigma/2)|]^{1-n} [\dot{\pi}^0 (\eta - \varsigma/2)]$$

(VI-22)

Eq. (VI-22) is integrated once again with respect to η, taking $\varphi = \varphi^0 = 1$ @

$\eta = \varsigma$, and it is found that

$$\varphi = \varphi^0 + N_e \left\{ \dot{\pi}^1 \frac{(\eta - \varsigma/2)^2 - (\varsigma/2)^2}{2} \right.$$

$$\left. + \dot{\pi}^0 |\dot{\pi}^0|^{1-n} \frac{(\eta - \varsigma/2)^{3-n} - (\varsigma/2)^{3-n}}{(3-n)} \right\}$$

(VI-23)

The mass balance, as given by Eq. (VI-9), is applied by integrating Eq.

(VI-23), and after some rearrangements, the following expression for the

pressure-gradient is obtained:

$$\dot{\pi} = \dot{\pi}^0 - 12 \frac{\lambda - \lambda^0}{\varsigma^3} - 3 N_e \dot{\pi}^0 |\dot{\pi}^0|^{1-n} \frac{(\varsigma/2)^{1-n}}{4-n}$$

(VI-24)

It is expected that surface-tension will play a minor role in the actual

dynamics, as in the purely-viscous case. Thus, this analysis is strictly

concerned with the asymptotic case of vanishing surface-tension ($N_S = 0$).

For that case,

$$\tau(\xi_1) = 0 \tag{VI-25}$$

This boundary condition, together with Eq. (VI-24) gives

$$\lambda = \frac{B(\xi_1)}{A(\xi_1)} - \frac{N_e}{2^{3-n}(4-n)A(\xi_1)} \int_{-\infty}^{\xi_1} (\dot{\tau}^0 \, |\dot{\tau}^0| \,^{1-n}) \, \varsigma^{1-n} \, d\xi \tag{VI-26}$$

where,

$$A(\xi_1) \equiv \int_{-\infty}^{\xi_1} \frac{d\xi}{\varsigma^3} \quad \text{and} \quad B(\xi_1) = \int_{-\infty}^{\xi_1} \frac{d\xi}{\varsigma^2}.$$

With little loss of generality ξ_1 is evaluated using Eq. (VI-12). Thus,

$$\xi_1 = \sqrt{6\lambda - 2}$$

Eq. (VI-26) was solved for λ via successive approximations that required no more than three iterations. The variation of λ with the Weissenberg number $(W_S = Ut_R/H_0)$, for several values of the power-law index, is shown in Table VI-1. This result indicates that the first-order effect of viscoelasticity is to slightly increase the coating thickness relative to the Newtonian case, with n rather than W_S dominating this trend.

Now that $\lambda = \lambda(W_S, n)$ has been evaluated it is possible to calculate the total stress distributions. The hydrodynamic pressure distribution is obtained through integration of Eq. (VI-23) and the dynamic normal-stress is evaluated using Eq. (IV-14). It follows that

$$-\left.\Theta_{\eta\eta}(\xi)\right|_\varsigma = \int_{-\infty}^{\xi} \dot{\tau} \, d\xi + \frac{1}{8} N_e^{\frac{1}{1-n}} \left(\frac{H_0}{R}\right)^{1/2} \dot{\tau}^{0\,2} \varsigma^2 \tag{VI-27}$$

Table VI-1

Coating Thickness of a CEF Fluid in Roll Coating:
Perturbation Analysis Results[1]

$W_S(= Ut_R/H_0)$	n	$N_e(= W_S{}^{1-n})$	λ
0.005	0.4	0.0416	1.30
"	0.6	0.120	1.30
"	0.8	0.346	1.31
0.010	0.4	0.0631	1.30
"	0.6	0.158	1.31
"	0.8	0.398	1.31
0.015	0.4	0.0805	1.30
"	0.6	0.186	1.31
"	0.8	0.432	1.31
0.020	0.4	0.0956	1.31
"	0.6	0.209	1.31
"	0.8	0.457	1.31

[1]For the case $N_S \rightarrow 0$.

Note that the normal-stress term in Eq. (VI-27) is of order higher than 1

in Ne as n is usually in the range [0, 1]. Also, this term contains the

factor $(H_0/R)^{1/2}$ which is much smaller than unity for actual lubrication

systems. Therefore, it is expected that the contribution of the normal-

stress term to the total stress will be negligible. This assertion is

supported by the results presented in Figure VI-10. This figure shows

stress distributions for several rheological parameters. It is evident that

the shear thinning (purely viscous) characteristics dominate for the range

of parameters considered, as no significant "shift upward" for the viscoe-

lastic stress distributions was obtained (quite unlike the results for the

second-order fluid model). Rather, the viscoelastic distributions "flatten"

(i.e., $\left| \pi_{VE} \right| < \left| \pi_N \right|$) as is expected for fluids that are shear-thinning.

Quite paradoxically, the closer the power-law index is to 1 the more pro-

nounced is the deviation from the Newtonian result. As in the correspond-

ing blade coating analysis, this result is an artifact of the viscosity model,

as this model holds that a fluid with a higher power-law index will depart

from the Newtonian "viscosity plateau" at much lower shear rates than a

corresponding fluid with a lower power-law index. In Figure VI-11 the

roll-separating force is plotted against the Weissenberg number. Expectedly,

ϕ is a decreasing function of WS.

It should be reiterated that the results that have been presented for the

CEF model hold only within the scope of the perturbation solution. That is,

Figure VI-10.   Total (normal) stress distributions for a CEF fluid in the sheet-and-roll system ($H_0/R = 0.01$, $N_S \rightarrow 0$).

| n	W_S
0.8	0.03
0.8	0.01
0.6	0.01
0.4	0.01
1.0	0.00
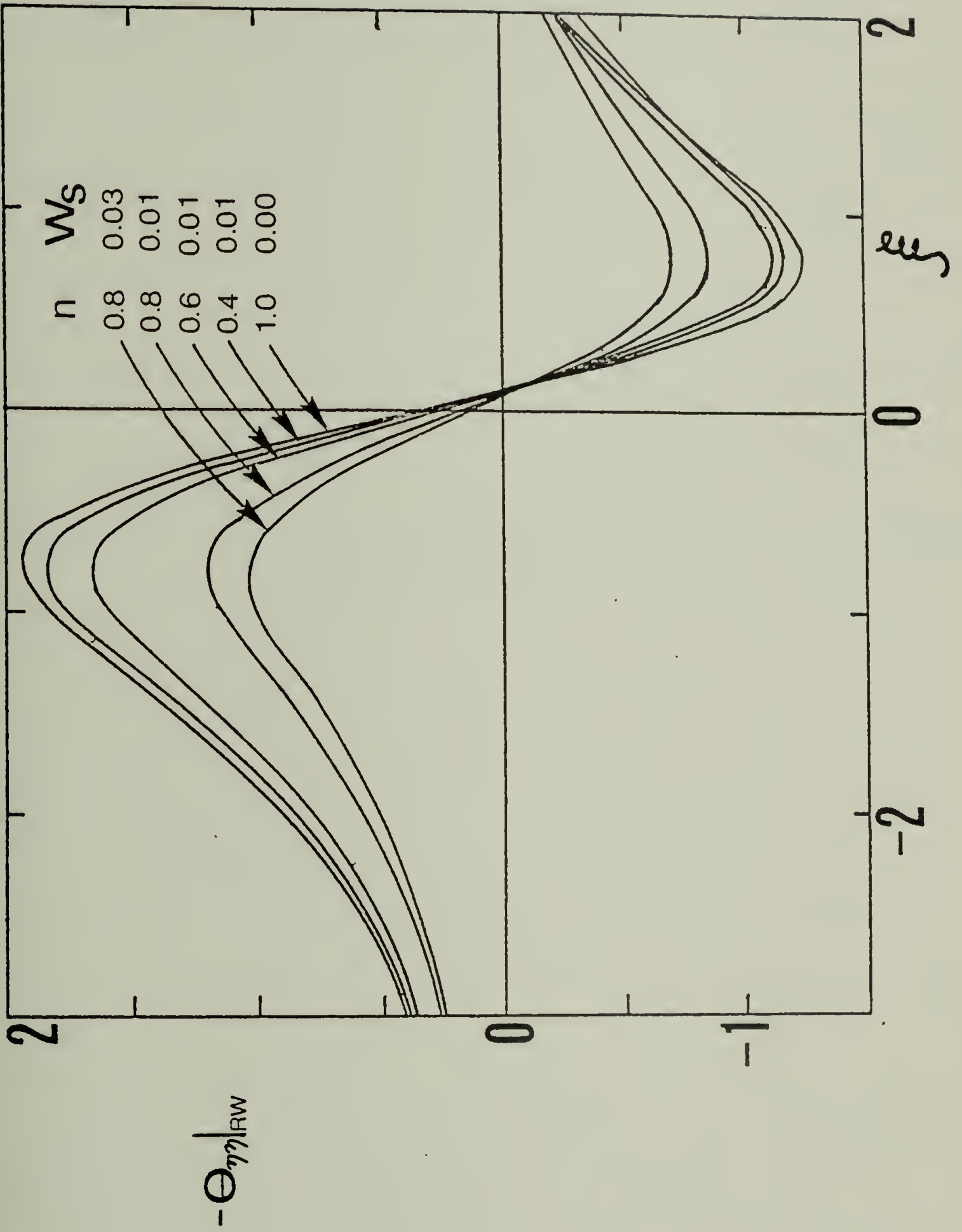
Figure VI-11. The roll-separating force vs. the Weissenberg number for a CEF fluid in the sheet-and-roll system ($N_S \rightarrow 0$).
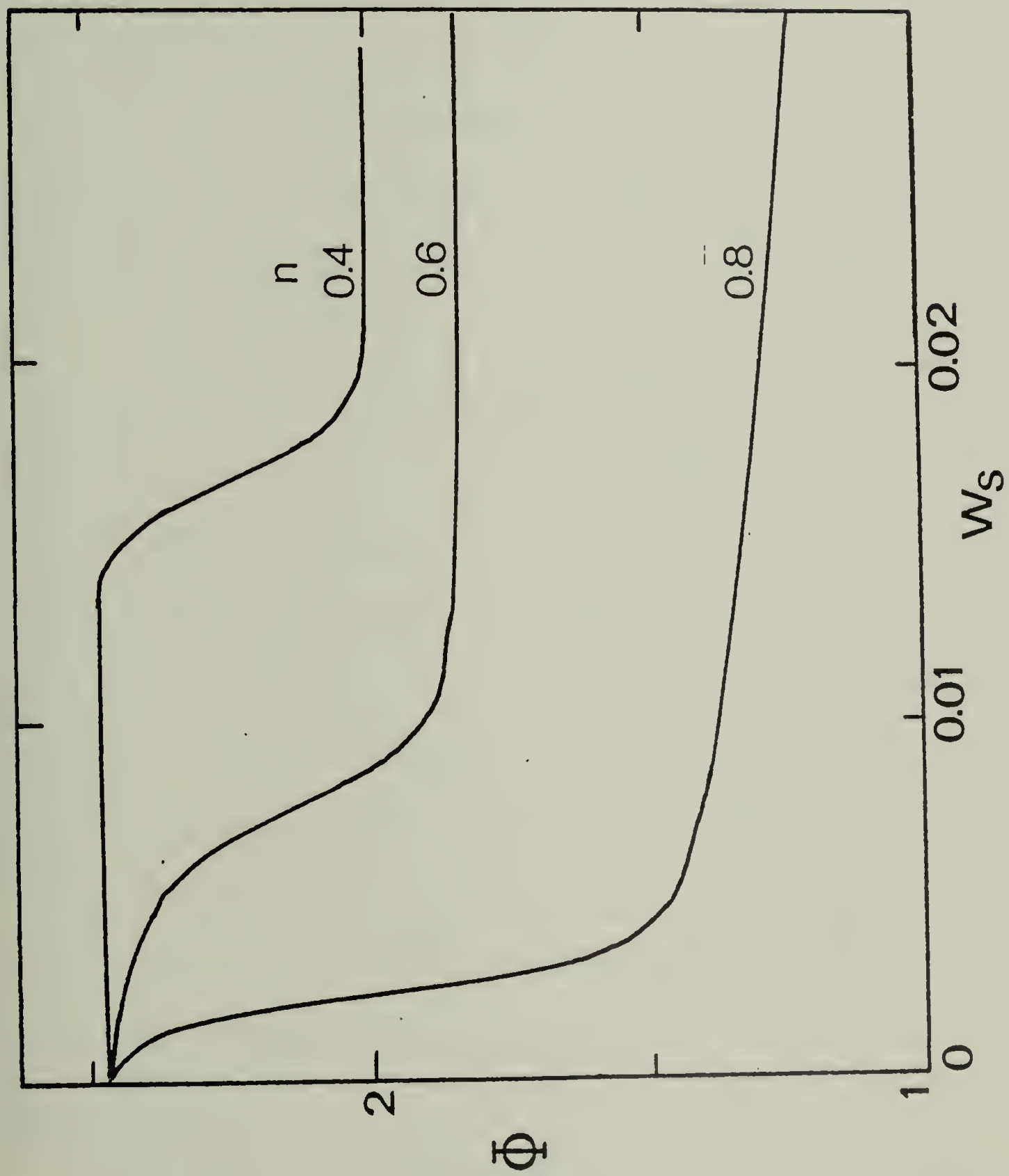
the various model results apply to systems in which Ne (or W_S) is much smaller than unity.

VI. 2.5 <u>Discussion.</u> The sheet-and-roll model considered in this section involves two major assertions that have not, as yet, been accounted for. The first specifies that the speeds of the moving surfaces are equal and the second regards the system to be lightly-loaded. As these statements do not conform with reality in some instances, brief comments to that effect are made below prior to assessing the various analytical results.

It is a simple matter to show that the pressure gradient and hence all the dynamic variables will vary marginally and only by a numerical factor in response to a change in the speed ratio. Taylor (1974a) carried out an analysis for the equivalent lubrication problem of a cylinder-plane configuration using also the Prandtl-Hopkins conditions. He found that λ will go from 1.30 to 1.26 and the maximum dimensionless pressure will vary in the range 1.92-2.05 by changing the speed ratio from 1 to 0 (or ∞). (In the case of non-equal speeds λ denotes the dimensionless flow-rate rather than the dimensionless coating thickness.) The actual film thicknesses will be proportional to the speeds of the corresponding surfaces. It is conceivable that the speed ratio will have a similar effect in the case of a non-Newtonian fluid.

The assumption of light-loading made in the analysis is usually applicable especially when the system dimensions are fixed and the dynamic

pressures are low. However, it is not uncommon to confront situations where very high loads are generated. For such cases, the Prandtl-Hopkins conditions should be replaced by the Swift-Stieber conditions (see IV.4). Application of the Swift-Stieber conditions in the sheet-and-roll case yields $\lambda = 1.226$ and $\mathcal{R}_{max} = 2.15$, as compared to $\lambda = 1.30$ and $\mathcal{R}_{max} = 1.92$ in the lightly-loaded case (for $N_S \rightarrow 0$). Also, the pressure distribution in the heavily-loaded case will not have a sub-ambient (negative) loop and consequently the roll-separating force for this case will be considerably higher. It is expected, however, that high dynamic pressures as found in heavily-loaded systems will be accompanied by surface instabilities (see Chapter VIII) and hence such limiting situations should be avoided if a smooth coating is desired.

Three constitutive models have been considered in the foregoing analyses, each providing some insight as to the importance and effect of certain fluid parameters. The purely viscous power-law theory predicts generally an increase in coating thickness for non-Newtonian fluids. An increase in coating thickness, though considerably milder, is also a result of the CEF analysis. From the nature of the perturbation solution, the results for the CEF fluid are expected to be relevant only in a region where the fluid slightly departs from Newtonian behavior (i.e., under small deformation rates). It has been noted that the empirical viscosity equation used in the CEF model will approach a power law equation in the limit

Ne >> 1. Thus, practically, two asymptotic limits of the empirical viscosity equation have been considered, Ne >> 1 and Ne << 1. In reality, non-Newtonian systems will fall within these extremes and hence the performance of such systems can be estimated from a qualitative matching of the asymptotic results (provided that $\lambda(Ne)$ is a well-behaved function). As both asymptotic solutions show a similar effect on λ, it is expected that λ will fall somewhere between the power-law result and the CEF result. In any case, λ will always be higher than the Newtonian value. How far removed λ is from the Newtonian limit will ultimately depend upon the magnitude of Ne. This effect on λ, which is expected to be small, is strictly a consequence of shear-thinning behavior. The second-order fluid, being elastic and Newtonian in shear, will be indistinguishable from a corresponding Newtonian fluid in terms of the coating thickness.

A similar matching of the pressure distributions for the CEF fluid and the power-law fluid is not possible since the pressure functions in each case are made dimensionless in a different way; the power-law pressure is reduced using a viscosity evaluated at a nominal shear rate of U/H_0. The pressure function for the CEF fluid is made dimensionless using the zero-shear-rate viscosity (η_0). However, the general conclusions reached for the coating thickness function apply here as well. It is implicit from the purely viscous approximation that elastic (Weissenberg number) effects should not count in systems with lubrication-type geometry. The theoretical

results, which are based on the purely viscous approximation, seem to comply with this assertion; it was shown that the total stress distribution in the CEF case is dominated by shear-thinning effects. In the case of the second-order fluid the only non-Newtonian contribution comes from the elastic term. This contribution manifests itself by the "shifting upward" of the stress distribution in the vicinity of the nip region which results in an increase in the roll-separating force. This effect, again, will be small in the limit of small H_0/R and it will be most likely dominated by purely viscous effects.

VI. 3 Partially Immersed Counter-Rotating Rollers

VI. 3. 1 The system. A schematic diagram of the system of partially immersed counter-rotating rollers along with a definition scheme for the geometry of the nip region are given in Figure VI-12. As pictured, the flow is induced by the rotation of the rollers; the fluid is driven out of the bath through the narrow gap between the rollers up to a point where it splits evenly into two films that travel around and return back to the bath. Such a system, although not directly applicable as a coating device, simulates hydrodynamically many actual coating operations. Its resemblance to the system considered in Section 2 is self-evident. The primary motivation for studying this system pertains to the fact that it can be conveniently investigated experimentally as it allows a continuous coating operation which requires relatively small amounts of fluid. Indeed, the system of
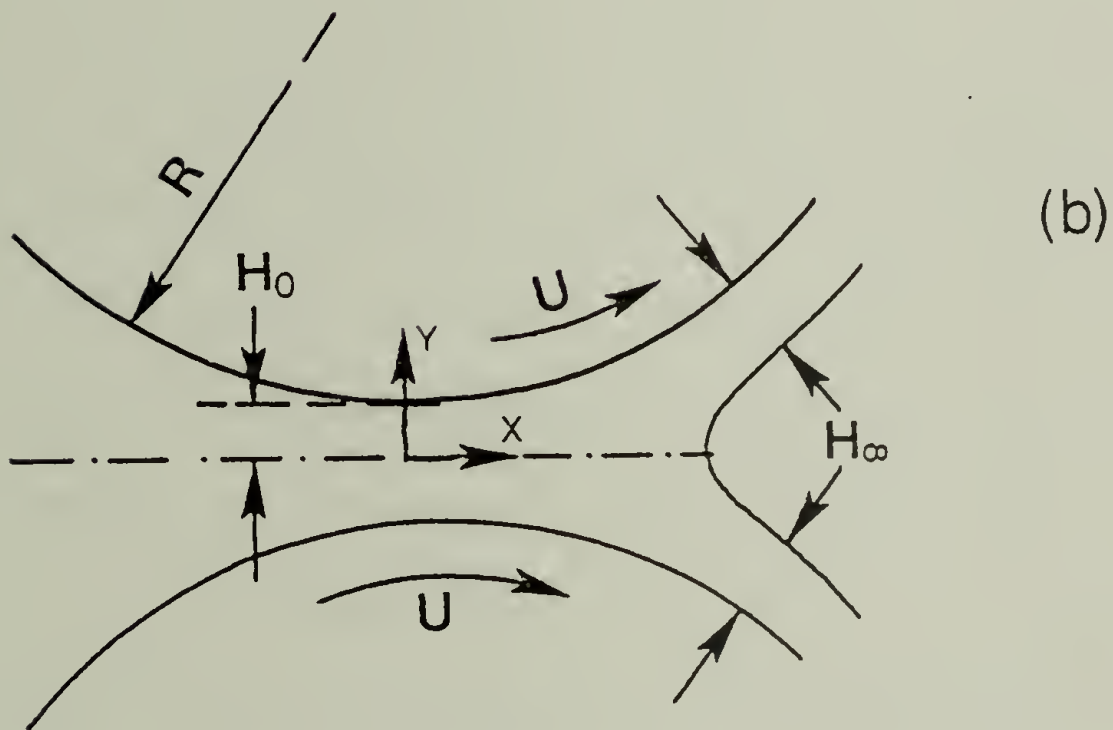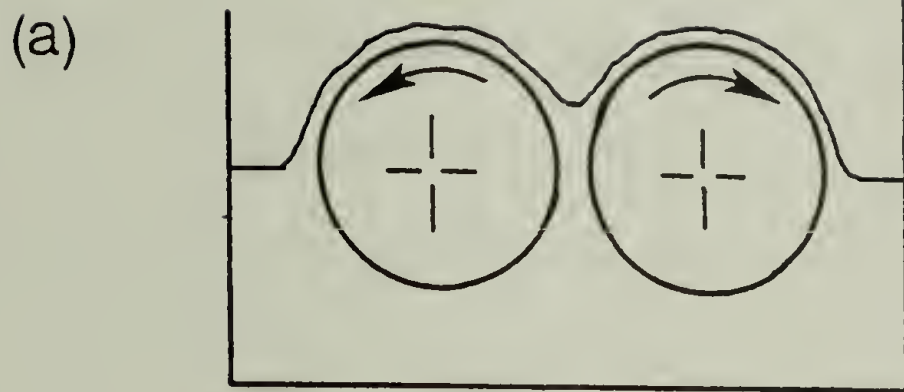
Figure VI-12. A schematic diagram of the system of half-immersed counter-rotating rollers (a) and a definition scheme for the nip region (b).

counter-rotating rollers has been the subject of several studies both theoretical and experimental, and it was also selected for an experimental study of roll coating in this work (see Sections 4 and 5).

A particularly thorough examination of this problem was made by Pitts and Greiller (1961). They applied the lubrication approximation to the bounded flow regime and made some assumptions concerning the separation region. Specifically, they approximated the shape of the separation meniscus with a parabola which is characterized by a latus rectum of unknown length. This length was determined by requiring that the lubrication solution will satisfy the traction boundary conditions on the free surface near the axis of symmetry. They ended up with expressions that give the position of the separation point as a function of the capillary number. Experimental data that were reported by Pitts and Greiller seem to agree with their theoretical predictions. Their attempt to measure the coating thickness was less successful and not conclusive; they report values for λ in the range 1.26-1.38 ($\pm 10\%$). Pitts and Greiller made also some observations on flow patterns in the domain between the rotating rollers and have detected two areas of circulatory flow behind the meniscus which could not be accounted for by their approximate theory. Williamson (1972) in a later study of a related problem solved numerically the biharmonic equation coupled with the traction boundary conditions along the free surface. He expressed the position of the meniscus by a sixth order polynomial with

unknown coefficients. Williamson's solution shows circular flow patterns just upstream from the separation meniscus in conformity with Pitts and Greiller's observations. As this analysis required the specification of the flow-rate through the nip it could not be directly compared to Pitts and Greiller's work where the flow-rate was part of the solution.

The system of counter-rotating rollers was used by several researchers to study the problem of flow instability in roll coating. However, this subject will be discussed separately in Chapter VIII where the question of stability is considered.

VI.3.2 A lubrication analysis. Aside from small geometric differences, the system of counter-rotating rollers is essentially identical to the sheet-and-roll system considered in the previous section. As the analysis for this system follows closely the sheet-and-roll analysis it is not given explicitly in this section. Rather, the important results are presented and discussed. Only the purely viscous power-law model is considered here. The analytical results for the second-order fluid and the CEF fluid, obtained in the preceding section, are expected to apply qualitatively to the present system by virtue of its hydrodynamic similarity to the sheet-and-roll system.

The dimensionless variables are defined as before (Note that H_0, in this case, denotes half the nip separation!). Also, the boundary conditions and the separation model are identical to those used in the sheet-and-roll analysis (Eqs. VI-2, 3, 4) with the only exception that the axis of symmetry

(or the mid-plane) is along $\eta = 0$ (rather than $\eta = 1/2\,\zeta$). A rationale for using the Prandtl-Hopkins condition is given at the end of this section.

The final results for the system of counter-rotating rollers are as follows:

$$\dot{\mathcal{R}} = (q+1)^n \frac{\left(\left|\zeta-\lambda\right|\right)^{n-1}(\zeta-\lambda)}{\zeta^{1+2n}} \qquad \text{(VI-28)}$$

$$= \frac{\left|\dot{\mathcal{R}}\right|^{q-1}}{q}(\eta^q - \zeta^q) + 1 \qquad \text{(VI-29)}$$

and the integral equation for λ is

$$\lambda \left(\frac{1+n}{n}\right) \int_{-\infty}^{\zeta_1} \dot{\mathcal{R}}\, d\zeta = -N_S \qquad \text{(VI-30)}$$

where

$$\lambda \equiv \frac{H\infty}{H_0}$$

and ζ_1 is evaluated as before (Eq. VI-12). A solution of Eq. (VI-30) for two values of the power-law index is presented in Figure VI-13 in the form of λ vs. N_S curves. A comparison of the above expressions to the corresponding expressions for the sheet-and-roll system reveals that the hydrodynamic variables for both systems are functionally similar and they differ only by a numerical constant (which depends upon n). Thus, virtually all the conclusions made concerning the power-law results for the sheet-and-roll system apply to the present system as well.
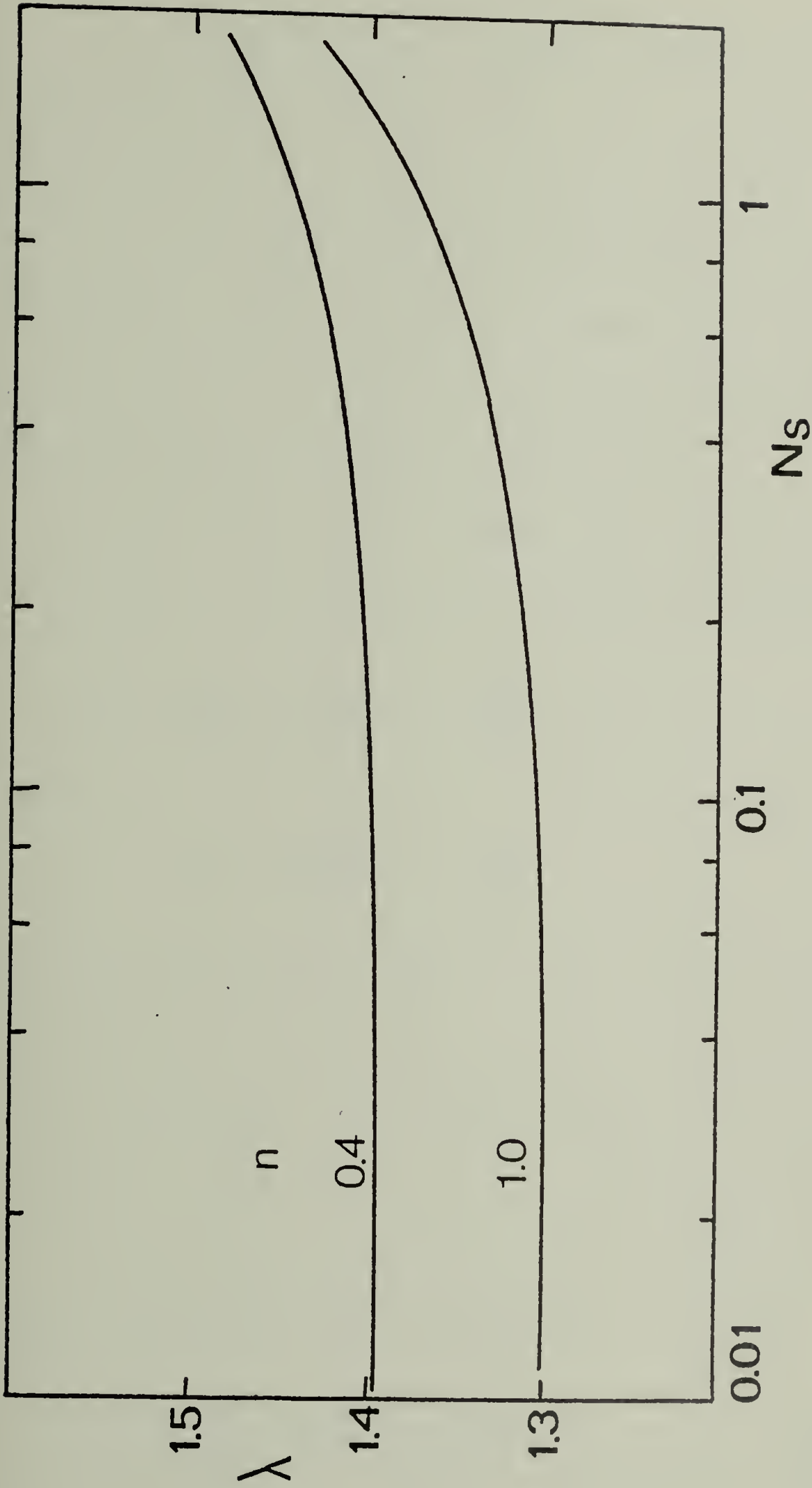
Figure VI-13. Coating thickness vs. the surface-tension parameter. Analytical curves for a power-law fluid in the system of half-immersed counter-rotating rollers.

VI.3.3 <u>Gravity effects.</u> The effect of gravity is usually marginal in typical roll coating operations. Under certain operating conditions, though uncommon, gravity forces may be comparable to the usually dominant viscous forces and their effect on the performance of the system may be considerable. Indeed, a regime where gravity effects start to dominate was encountered in the course of the experimental work of the present study, and thus this problem is briefly considered below.

In the system of counter-rotating rollers the gravity field acts in the - x direction. Hence, the equation of motion takes the form

$$\dot{\mathcal{R}} = \frac{d}{d\eta}\left[\left(\left|\frac{d\varphi}{d\eta}\right|\right)^{n-1}\frac{d\varphi}{d\eta}\right] - N_g \tag{VI-31}$$

where

$$N_g = \frac{\rho g H_0^2}{\eta_a U} = \frac{N_{Re}}{N_{Fr}}$$

N_g, the gravity number, reflects the ratio of gravity forces to viscous forces and it is sometimes taken as the ratio of the Reynolds number (N_{Re}) to the Froude number (N_{Fr}). (Bird et al. 1960). Since N_g is a constant parameter it is possible to replace by $\dot{\mathcal{R}}' = \dot{\mathcal{R}} + N_g$ in Eq. (VI-31) and the lubrication analysis essentially follows the gravity-less analysis. Finally, the following integral equation for λ is obtained,

$$(q+1)^n \int_{-\xi_0}^{\xi_1} \frac{|(\xi-\lambda)|^{n-1}(\xi-\lambda)}{\xi^{1+2n}}\,d\xi - N_g(\xi_1 - \xi_0) = -\frac{N_S}{q\lambda} \tag{VI-32}$$

or,

$$Ng = \frac{\mathcal{R}_1 + \dfrac{N_S}{q\lambda}}{\int_1 - \int_0}$$

(VI-33)

where $\int_0$ is a position far upstream that corresponds to zero gravity (it is the actual $-\infty$) and $\mathcal{R}_1$ is the pressure at $\int = \int_1$ as calculated via Eq. (VI-28). λ is now dependent upon two dynamic parameters, N_S and Ng; both parameters will have to be considered in the limit of small viscous forces. A solution of Eq. (VI-33) is presented in Figures VI-14 and VI-15 in the form of λ vs. Ng curves with N_S as a parameter. $\int_0$ was set arbitrarily at $\int = -5$. Figures VI-14 and VI-15 clearly show that the effect of gravity is to reduce the coating thickness as opposed to surface tension. Both effects will be important and competetive in the limit of small viscous forces.

VI.3.4 <u>A critical assessment of the Prandtl-Hopkins (PH) separation conditions.</u> The question of the separation boundary conditions for converging-diverging lubrication systems has been discussed at length in Chapter IV. It was noted there that the PH conditions are not completely satisfactory as they cannot account for circulation patterns just upstream from the separation meniscus that were observed in some cases (Pitts and Greiller 1961, Myers et al. 1959, Savage 1977a). This condition was, nevertheless, employed in the foregoing roll coating analyses on the basis of the assertion that it is a valid approximation of the actual situation in the separation region. It now remains to be determined under what conditions
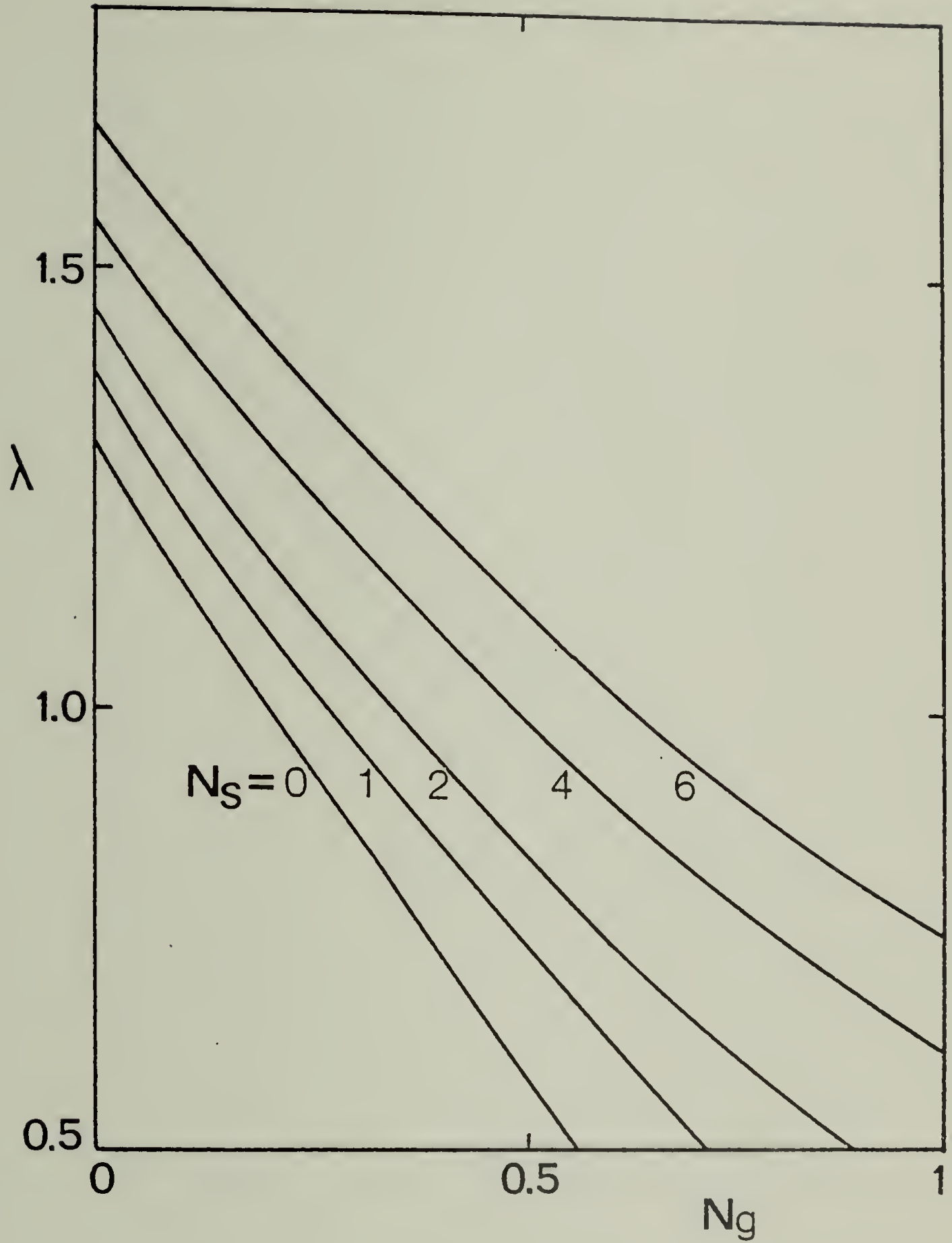
Figure VI-14. Coating thickness vs. the gravity number for a Newtonian
fluid in a system of half-immersed counter-rotating rollers.
($\mathcal{F}_0 = -5$).
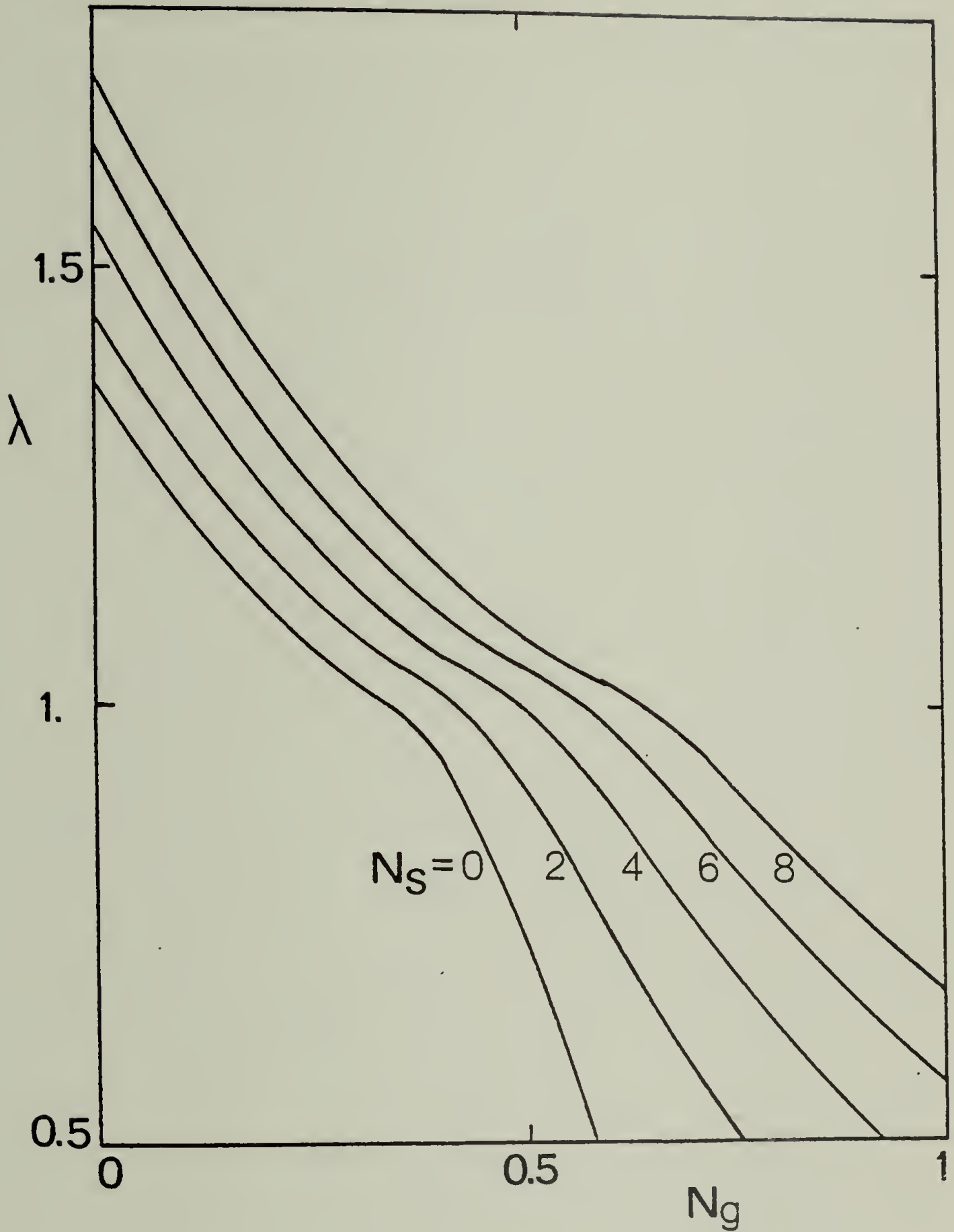
Figure VI-15. Coating thickness vs. the gravity number for a power-law (n=0.4) fluid in a system of half-immersed counter-rotating rollers. ($\int_0 = -5$).

(if any) this approximation is indeed valid. The range of validity of the

PH conditions is determined via a comparison of these conditions to the

more rigorous Coyne and Elrod (CE) conditions (Coyne and Elrod 1969,

1970) which were discussed in Chapter IV. The CE conditions were de-

rived from a solution of the complete Navier-Stokes equations combined

with the full traction boundary conditions on the separation meniscus.

Despite some minor flaws, these conditions are the best available to date

as they conform well with experimental observations, especially for mod-

erate-to-high capillary numbers ($N_{Ca} = \mu U / \delta$). The CE conditions can be

easily applied to the system of counter-rotating rollers to yield a λ vs. N_S

curve. A detailed derivation of the relationship $\lambda = \lambda(N_S)$ for the CE case

is given in Appendix E. The result is shown in Figure VI-16 along with

the theoretical curve for the approximate separation model (i.e., the PH

condition with a semicircular separation geometry) that was used in the

roll coating analyses. The agreement is remarkably good in the range

$N_S \doteq 0-1.0$ as was anticipated. The two curves start to diverge at $N_S = 1.0$

where the CE model predicts more moderate increase in coating thickness.

(The scatter in the CE model results is due to the approximate nature of

the solution technique used.) Whether the CE model itself is applicable

for low capillary numbers (i.e., high values of N_S) is not yet clear.

Savage (1977a) points out that the CE conditions fail in the limit of small

capillary numbers and it remains to be seen how real systems behave in
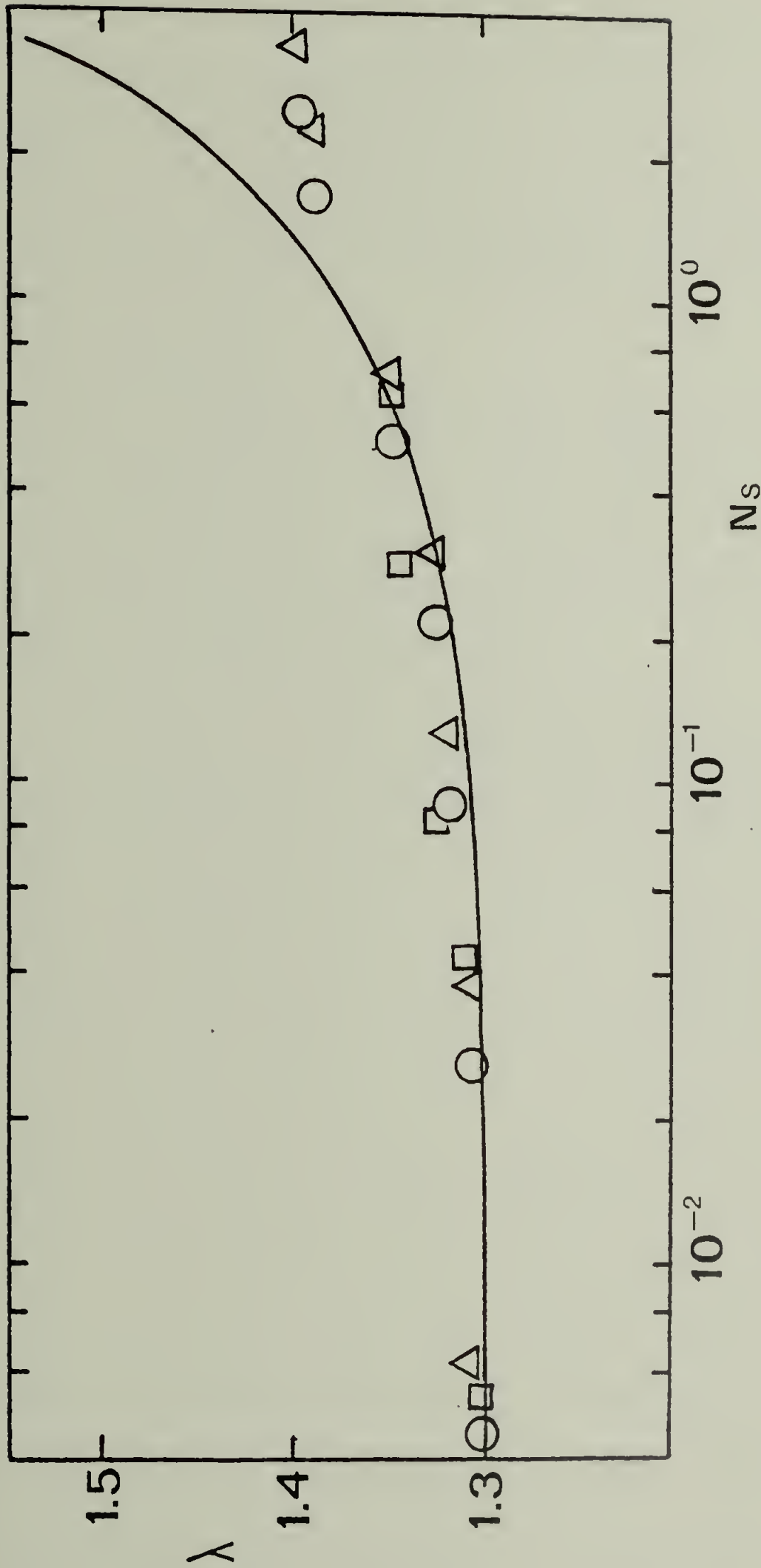
Figure VI-16. Coating thickness vs. the surface-tension parameter for a system of half-immersed counter-rotating rollers. A comparison between the result for the approximate separation model (the solid curve) to the calculations made on the basis of the Coyne and Elrod theory ($H_0/R = 0.005$ ($\bigcirc$), 0.01 ($\triangle$), 0.05 ($\square$)).

this limit. where reliable experimental data are not easily accessible.

Since the parameter N_S does not exceed unity in typical roll coating operations then, in a practical sense, the approximate separation model that was employed throughout is representative of the actual separation dynamics.

VI.4 Experimental

VI.4.1 <u>Scope.</u> An experimental study of roll coating was carried out and it is detailed in this section. This study was designed specifically to test the effect of fluid rheology and system geometry on the coating thickness observed under stable coating operation.

The system of partially immersed counter-rotating rollers was selected for this investigation as it simulates hydrodynamically many typical roll coating systems and it allows a continuous and steady coating operation requiring relatively small amounts of fluid. Both Newtonian and viscoelastic fluids were tested over a wide range of rheological behavior.

The coating experiments were severly hindered by the onset of surface irregularities and air-entrainment phenomena at high speeds. At low speeds, the dynamics were practically governed by gravity forces thereby limiting the effective range of experimental testing. This part of the experimental program is exclusively concerned with stable (uniform) coating, both in the gravity-free and the gravity-controlled regimes. An extension of this study to the unstable flow regime is made in Chapter VIII.

VI.4.2 <u>Experimental system.</u> A general view of the experimental system is shown in Figure VI-17. A schematic diagram of the system is depicted in Figure VI-18 and its various dimensions are listed in Table VI-2. The system consists of a square acrylic box and a pair of steel rollers. The box serves as a container for the test fluid and a holding frame for the rollers. Each roller, together with a 3/8 in. dia. steel shaft and a pair of tight-fitted sealed ball-bearings, is a removeable and exchangeable unit. A pair of round slots on two opposite walls of the box were designed to house the bearings and to keep the roller axes at a fixed distance apart. The rollers are mounted by carefully fitting the bearings into the corresponding slots in the box and tightening them by standard set screws.

Two pairs of rollers were machined at two different diameters and they were turned around centers to an accuracy of ± 0.0005 in. for concentricity. All four rollers were paired into three different sets: two sets of roller-pairs at equal diameters each and a third set of two rollers at two different diameters. Since the distance between the roller axes was fixed (at 2.000 in.), each set corresponds to a different nip separation $(2H_0)$. The relevant geometric parameters for these alternative combinations are listed in Table VI-3. As seen, this simple arrangement made it possible to vary the parameter H_0/R nearly threefold. The system was checked for parallelism which was found to be ± 0.0015 in. for all the roller sets.

Figure VI-17.   A general view of the experimental roll coating system.

CONSTANT SPEED AND TORQUE CONTROL UNIT

SERVODYNE
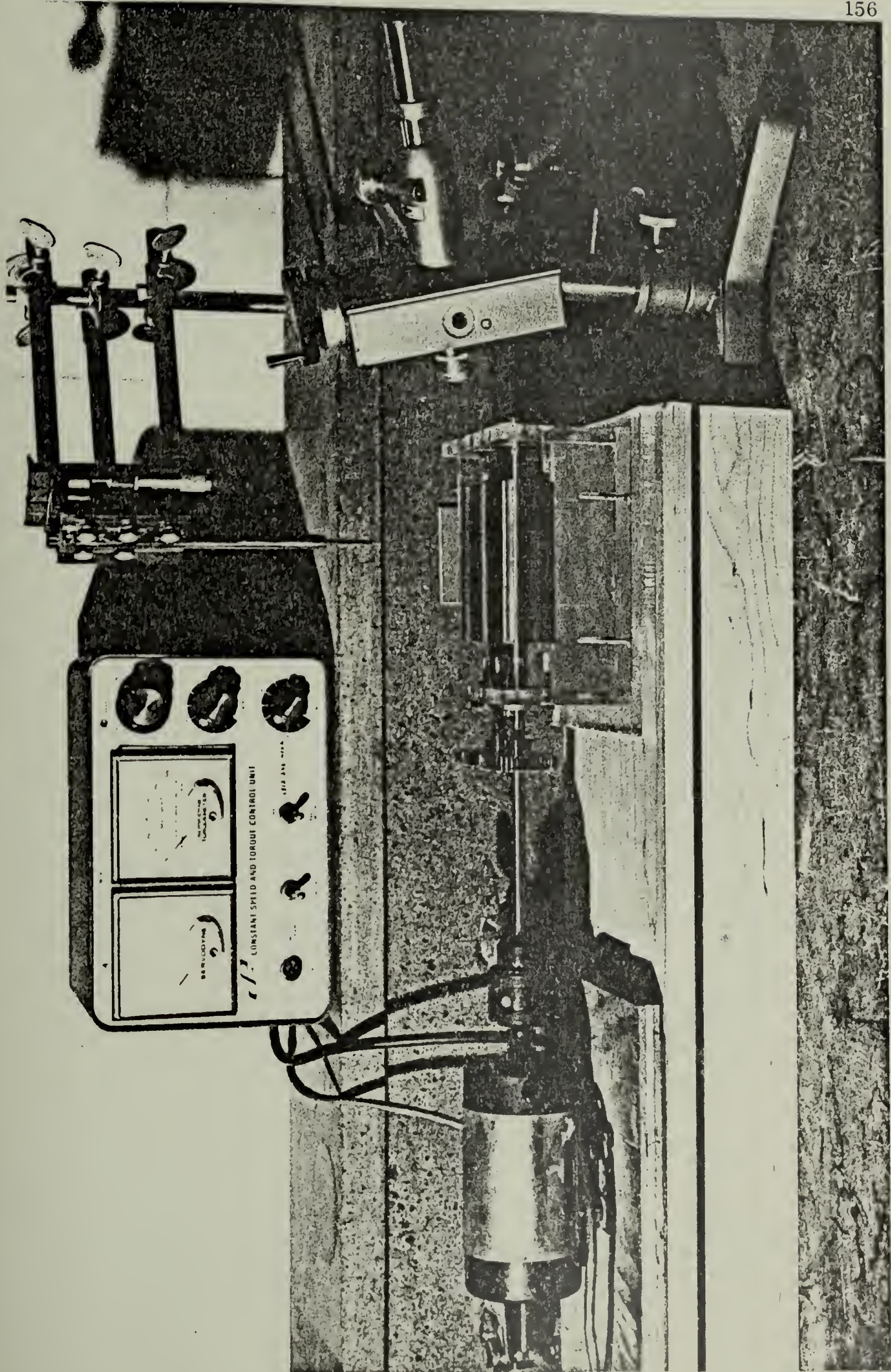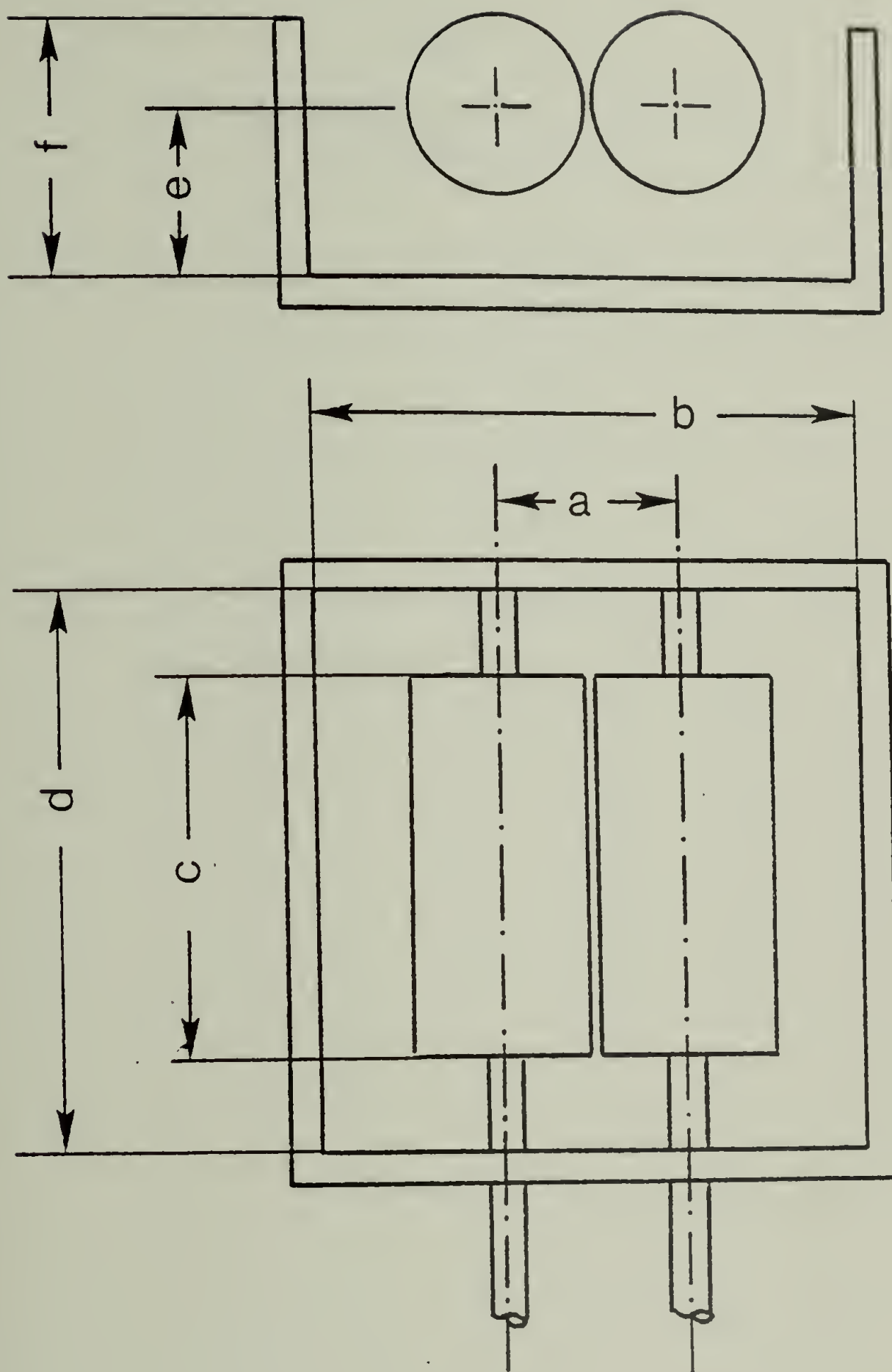
Figure VI-18.   A diagram of the experimental system of half-immersed
counter-rotating rollers.

Table VI-2

Physical Dimensions of the Experimental
Roll Coating System

L^1	[cm]
a	5.08
b	15.3
c	10.2
d	15.2
e	5.1
f	6.5

[1]See Figure VI-18

Table VI-3

The Experimental Roll Coating System:
Geometric Parameters for Alternative Combinations

Set #	$2H_0$[1] [cm]	H_0/R
1	0.152	0.0306
2	0.065	0.0129
3	0.114	0.0228

[1] ± 0.005

In order to coordinate the motion of the roller-pairs the shafts were coupled by a pair of equal size spur gears (P.I.C. cat. no. G79-48; P.D. 2.000 in., O.D. 2.083 in.). These gears, guaranteed equal rotational speeds for both rollers. The peripheral speeds for sets 1 and 2, were equal as well since the diameters of the rollers for each pair were identical. For set 3 the peripheral speeds differed by 1-2% due to the small variance in the roller diameters. This small difference, however, was ignored and the speed ratio for set 3, as for sets 1 and 2, was taken to be equal to unity. The system was driven by a constant speed DC motor that was connected to a Cole-Parmer speed and torque control unit. The actual speed scale in the unit was checked and recalibrated.

As in the blade coating experiment, coating thickness was measured by a physical contact technique. A detailed account of this technique, is given in V.3.

VI.4.3 <u>Materials.</u> A series of Newtonian and viscoelastic fluids with widely varying physical and rheological properties were tested in this experiment. Table VI-4 lists all the fluids examined, their physical properties, their sources and their codes. The rheological properties of the fluids are given separately; inasmuch as the Newtonian viscosity is a strong function of temperature this property was measured individually for each run at or about the corresponding (room) temperature and it is reported in Appendix A together with the coating data. Generally, the Newtonian viscosities in

Table VI-4

The Roll Coating Experiment:
List of Materials

Fluid[1]	Symbols[9]			ρ [g/cc]	γ [dynes/cm][10]
Glycerin(G)[2] Ⓝ	△	▲	△	1.26	63
Karo Syrup[3] (KS) Ⓝ	▽	▼	▽	1.38	75
GW-0.95[4] Ⓝ	⊞	■	☐	1.25	64
GW-0.90[4] Ⓝ	◐	●	○	1.24	65
GW-0.75[4] Ⓝ	⬡	⬢	⬡	1.20	67
Motor-Oil[5] (MO) Ⓝ	◈	◆	◇	0.88	35
GWS-0.90[6] Ⓝ	⊕	⬤	⊖	1.24	28
H-0.15[7] Ⓟ	▽	▼	▽	1.00	76
H-0.25[7] Ⓟ	◐	●	○	1.00	76
H-0.35[7] Ⓟ	⊞	■	☐	1.00	75
H-0.5[7] Ⓟ	△	▲	△	1.00	75
HS-0.75[7] Ⓟ	◈	◆	◇	1.00	74
HS-0.35[8] Ⓟ	⊞	■	⊟	1.00	27
HS-0.5[8] Ⓟ	△	▲	△	1.00	27

[1] Ⓝ = Newtonian, Ⓟ = Viscoelastic

[2] Source: Fisher Scientific Co.

[3] Commercial brand. Source: CPC Corp.

Table VI-4 Con't

4 GW-X = Glycerin-water solution, 100X% Glycerin by volume.

5 A mix of commerical brands "Golden Shell" and "Shell 100-X multigrade".

6 GWS-X = Glycerin-water solution, 100X% Glycerin by volume + 0.4% by wt. of sodium oleate (a surfactant)

7 H-X = Aqueous solution of Polyhall 295 (Stein, Hall and Co., Inc.), X% by wt.

8 HS-X = Aqueous solution of Polyhall 295, X% by wt. + 0.4% by wt. of sodium oleate (a surfactant).

9 Left column of symbols is for $H_0/R = 0.0306$, right column - $H_0/R = 0.0129$ and central column - $H_0/R = 0.0228$.

10 ± 2 dymes/cm

this experiment varied from 0.5 to 30. poise. The viscometric functions, $\eta(\dot{\gamma})$ and $\Psi_{12}(\dot{\gamma})$, for the viscoelastic fluids are shown in Figures VI-19 and VI-20 and the corresponding viscometric data are listed in Appendix B. (The addition of a surfactant, in the cases specified in Table VI-4, was found to have negligible effect on the rheological behavior of the corresponding fluids.)

The densities of all the fluids were measured by a standard picnometer at room temperature. Two techniques were employed for measuring the surface tension: the drop-weight method and the pendant-drop method. These and other methods are discussed extensively in two excellent review articles by Padday (1969) and Gaines (1972). Both methods are based on the properties of an equilibrium drop.

The drop-weight method is based on the relation between the surface tension and the weight of an equilibrium drop. The surface tension was measured by weighing a specified number of drops issuing from a known capillary. The flow rate was maintained small (so that true equilibrium conditions are met) and constant by means of a syringe pump (Harvard Scientific Co., Series 900). The surface tension was then calculated from available tabulated correlations (Padday 1969). For viscoelastic fluids the pendant-drop method was found better suited. This method is based on a relation between the surface tension and the shape of an equilibrium drop. The shape of an equilibrium bubble attached to the tip of a capillary was
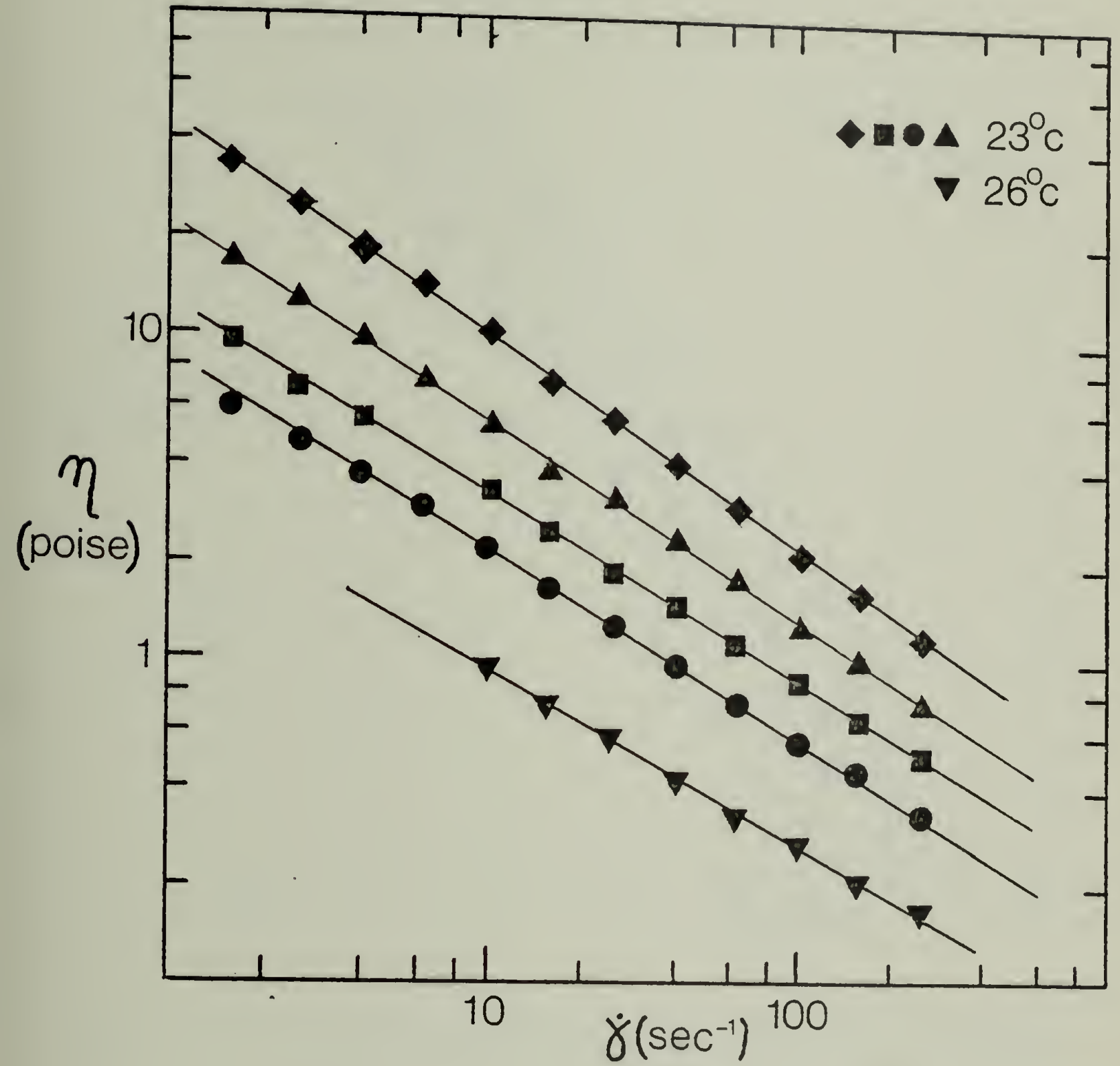
Figure VI-19.   The shear viscosity functions for the viscoelastic fluids used in the roll coating experiment (Key in Table VI-4).
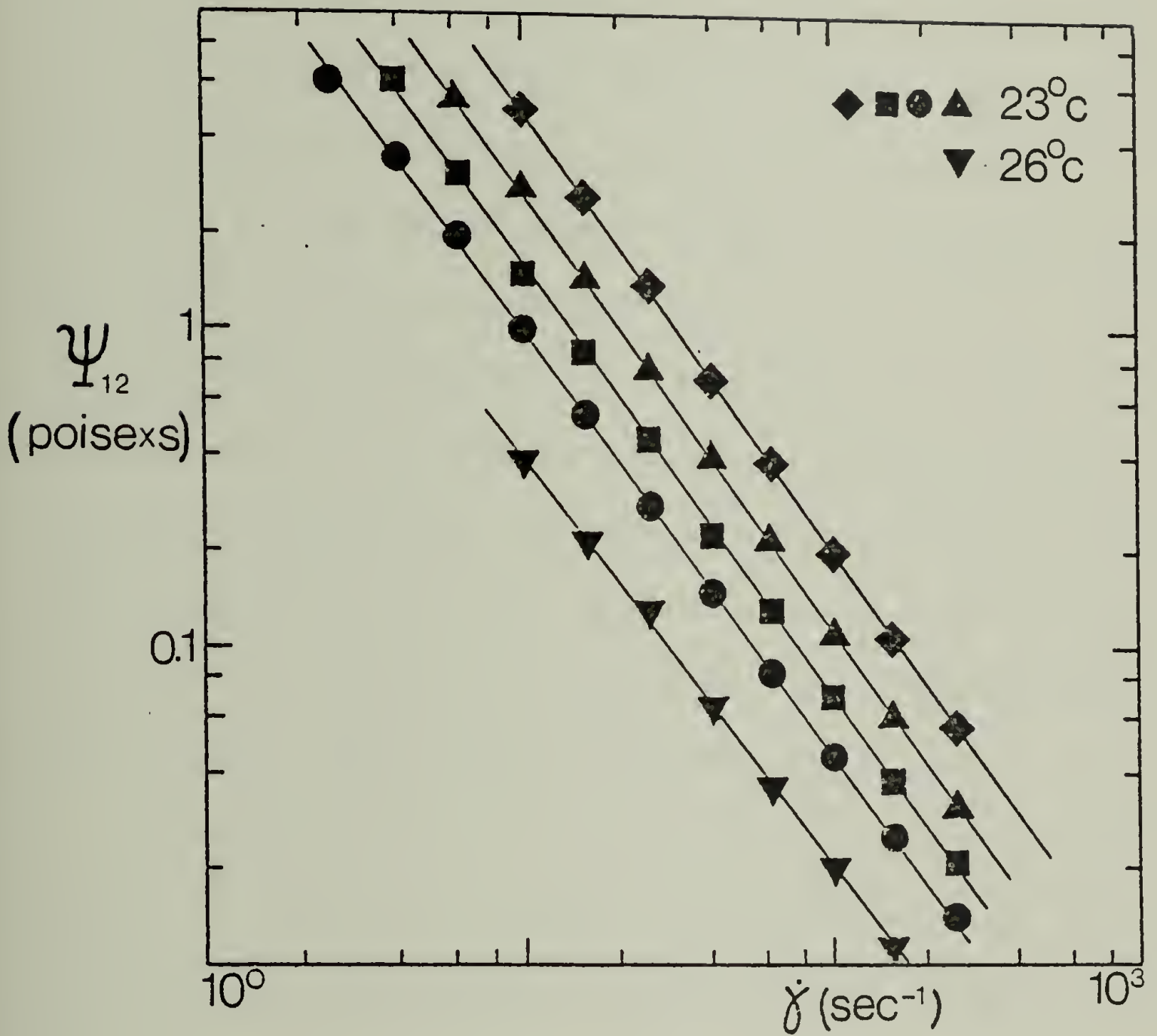
Figure VI-20.　The first normal-stress coefficients for the viscoelastic fluids used in the roll coating experiment (Key in Table VI-4).

determined photographically. (SLR 35 mm. Nikon F2 Photomic camera, Mikro Nikkor - P Auto 1:3.5 lens and red filter. Film: Kodak Tri-X 400 ASA). The appropriate shape factors were extracted from the photographs and used for calculating the surface tension through a given correlation (see Pearson 1975, Roe et al. 1967). In both cases the results were found reproducible within 2 dynes/cm.

The Newtonian viscosities were measured by an Epprecht (R-15) rheometer which is essentially a coaxial cylinder viscometer, and the viscometric functions of the viscoelastic fluids were measured by a Rheometrics Mechanical Spectrometer using a cone-and-plate mode. The first normal stress coefficients were corrected for errors originating from finite inertial effects. This correction is discussed in Appendix B.

The aqueous polyacrylamide solutions were prepared in the following manner. A 0.025% by wt. of sodium azide was dissolved in cool tap water (10°-15^oc). The water was then poured into a beaker containing a specified amount of the polymer with a simultaneous stirring using a magnetic stirrer. After ~15 minutes the magnetic stirrer was replaced by a high speed zig-zag shaped impeller and the solution was mixed thoroughly for about two hours. After the solution became clear and no lumps were visible it was stored for at least two days prior to being used. The addition of sodium azide was found effective in preventing bacterial growth and a resulting degradation of the polymer.

VI. 4. 4 <u>Procedure.</u> The acrylic box was filled with the test fluid up
to the level of the axes of the roller pair. The rollers were then set in
motion at a specified rotational speed and the coating thickness (on one
roller) was measured using the physical contact method following a proced-
ure outlined in V. 3. The measurement was taken at the center of the roller
to avoid errors due to end effects. (Apparent end effects were visible only
within a narrow margin off the roller ends.) The testing speed was in-
creased gradually, in small intervals, from zero up to a point where sur-
face instabilities or air entrainment effects were first seen. All the runs
were carried out at room temperature ($24 \pm 3^{\circ}c$).

The data corresponding to the gravity-dominated regime were singled
out by an apparent dependence of the coating thickness on the rotational
speed. In the gravity-free regime the coating thickness was insensitive to
the rotational speed in accordance with the prediction of the lubrication
analysis.

VI. 5 Experimental Results and Discussion

The experimental results are presented graphically in Figures VI-21
to VI-25; the corresponding data are listed in Appendix A. Figure VI-21
shows the observed variation of the coating thickness with the parameter
N_S for Newtonian systems in the gravity-free regime. This result is com-
pared to the theoretical prediction (Figure VI-13, $n=1.0$) represented by
the solid line. The weak theoretical dependence of λ on N_S could not be
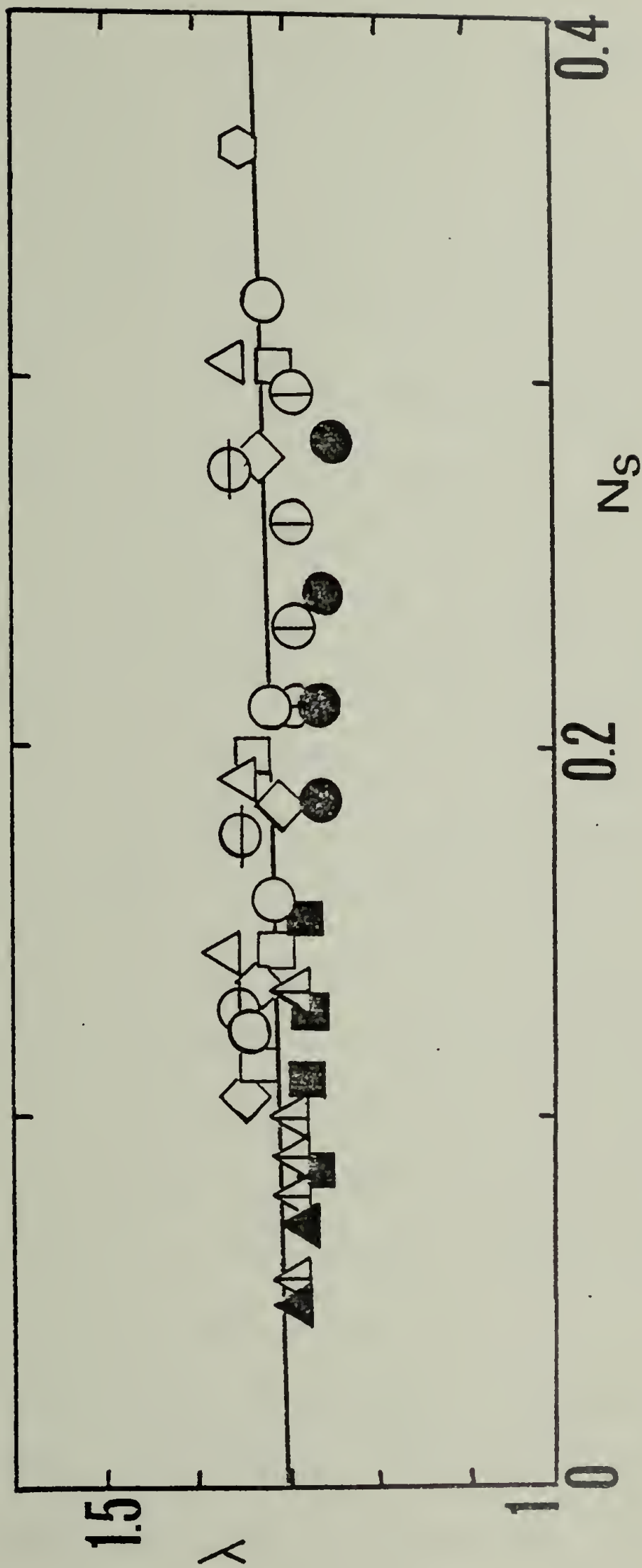
Figure VI-21.   Coating thickness vs. the surface-tension parameter.   Experimental data for Newtonian fluids in the gravity-free regime are compared to the lubrication solution (the solid line).   Key in Table VI-4.

ascertained by this experiment because of the experimental error

($\delta \lambda$ max $\cong$ 0.08) which exceeds the expected variation. Otherwise, the

agreement is satisfactory; the experimental results confirm that the coating

thickness is practically independent of the parameter N_S (for $0.05 < N_S < 0.5$)

and that λ averages around the asymptotic theoretical value of 1.30. The

limits on N_S were imposed by the onset of hydrodynamic instabilities (for

$N_S < 0.05$) and by gravity effects (for $N_S > 0.5$).

Figure VI-22 shows some data in the transition region from gravity-

dominated to gravity-free coating. This "transition" was found to take

place at Ng $\cong$ 0.1. For Ng lower than this "critical" value the coating

thickness was nearly independent of Ng. At higher Ng's the coating

thickness was a strong function of Ng, which is expected for systems that

are gravity-controlled. Coating thickness data for gravity-dominated New-

tonian systems are shown in Figure VI-23. The experimental data follow

a trend that is in accordance with the theoretical results (the solid lines).

Inasmuch as the experimental values of N_S are in the range [0, 4], the

experimental results fall consistently between the theoretical curves for

N_S = 0.0 and N_S = 4.0. The theoretical curves in Figure VI-23 were

calculated taking $\mathcal{f}_0 = -5.0$ (see Eq. VI-33).

The viscoelastic data were somewhat limited in comparison to the

Newtonian data. It was found that the viscoelastic systems were consider-

ably less stable than the Newtonian systems under comparable conditions.

Figure VI-22. Coating thickness vs. the gravity number. Experimental data for Newtonian fluids in the transition from gravity-free to gravity-controlled regime. (Key in Table VI-4.)
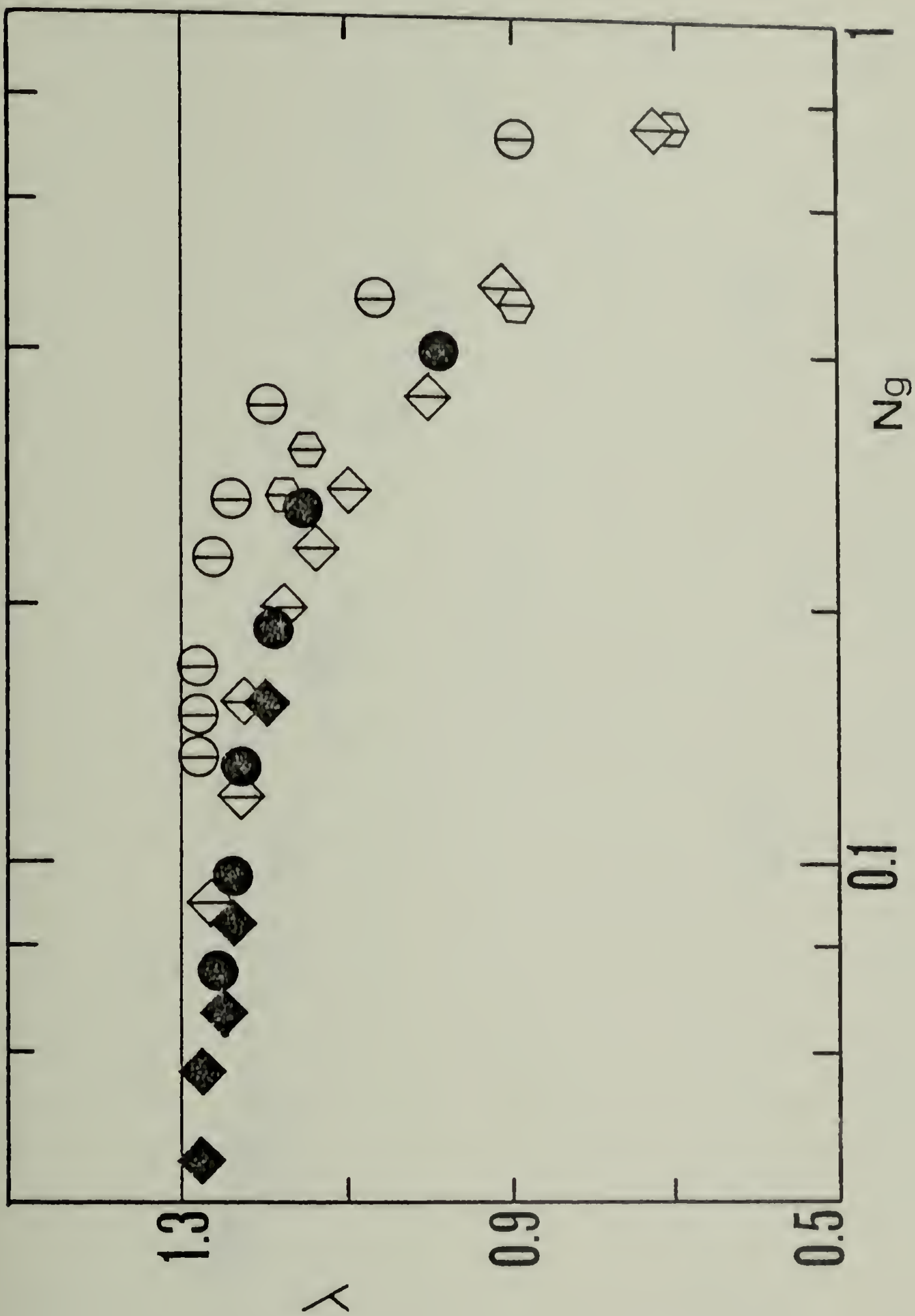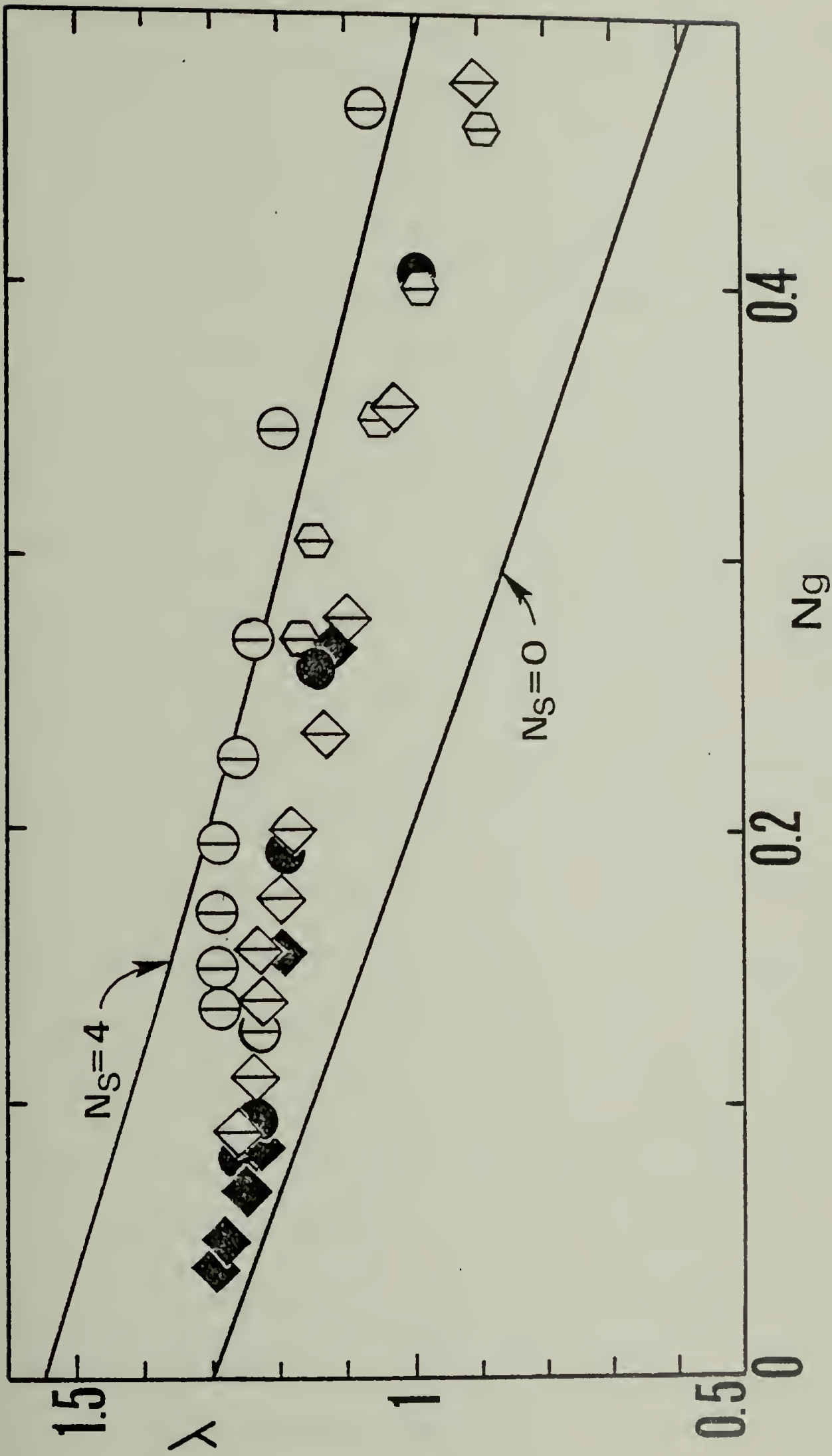
Figure VI-23. Coating thickness vs. the gravity number. Experimental data for Newtonian fluids in the gravity-controlled regime are compared to the lubrication solution (the solid lines). (Key in Table VI-4.)

This was manifested by the appearance of surface irregularities at such low speeds where gravity effects were still overriding. Thus, it was not possible to obtain stable gravity-free coating with the viscoelastic fluids. Figure VI-24 shows the variation of λ with N_S; the experimental values are compared to the purely viscous power-law theory for n = 0.4. (All the viscoelastic solutions are essentially power-law fluids, within the shear-rate range of interest, with n $\doteq$ 0.34-0.41.) A substantial discrepancy between theory and experiment is evident. Further, the coating thickness does not seem to correlate with the parameter N_S. A far better correlation is presented in Figure VI-25. Here, λ is plotted against Ng and a clear trend emerges consistent (qualitatively) with the gravity-controlled theory for a power-law fluid. The experimental error, in this case, is quite large (up to 15% in coating thickness) and thus a good quantitative fit between these data and the theory is not expected. In addition, as in the Newtonian case, the theoretical curves in Figure VI-25 were calculated taking f_0 = -5. As was pointed out in VI.3.4 this choice of f_0 is arbitrary and it could account for the small difference between the theoretical results and the data. Despite this, it is reasonable to state that gravity effects are possibly the major cause for the low level of coating thickness observed.

Only few experimental studies have been reported in which coating thickness was measured in a roll coating operation. Pitts and Greiller (1961) report on coating thickness measurements conducted in a system of
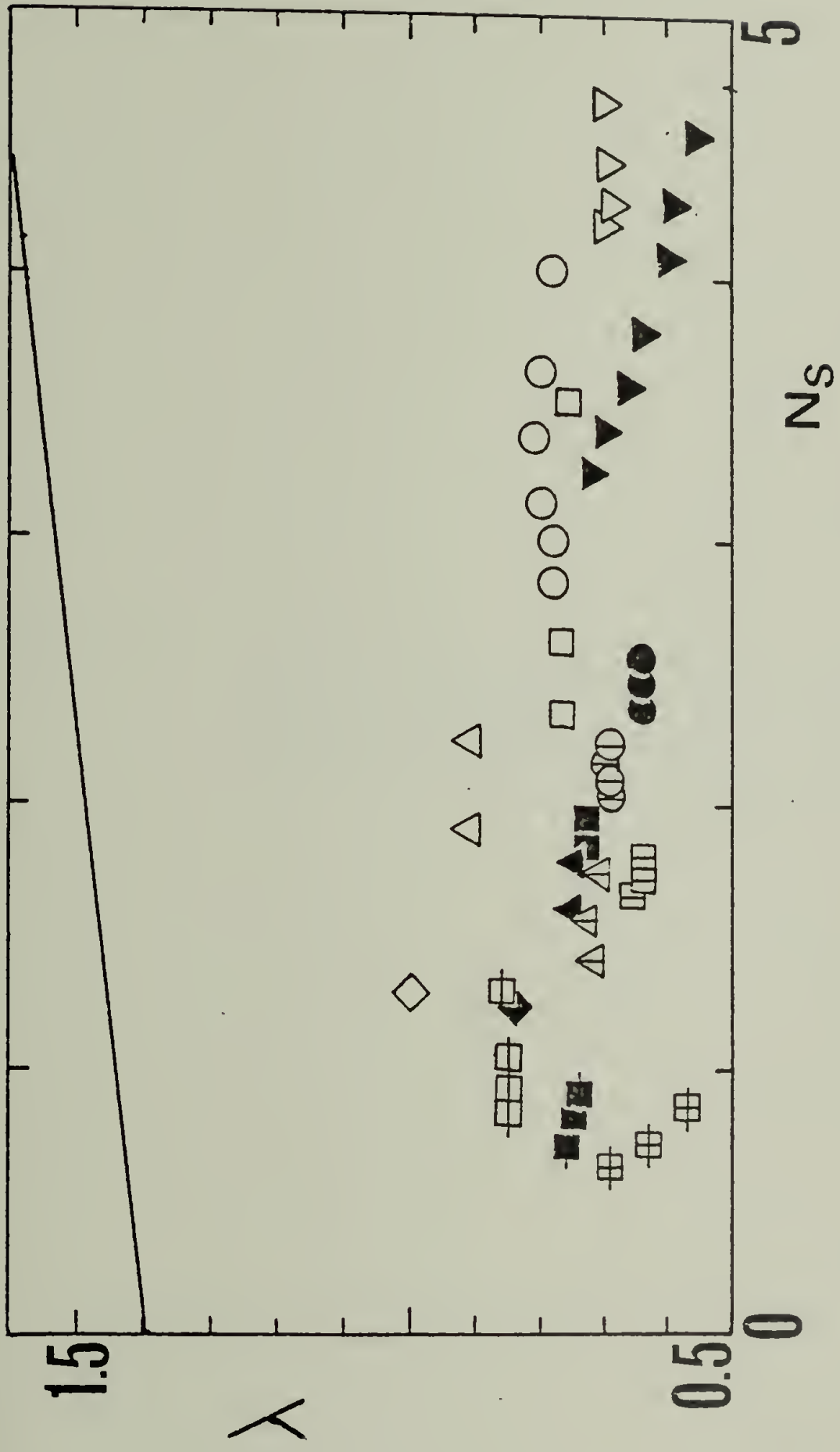
Figure VI-24. Coating thickness vs. the surface-tension parameter. Experimental data for viscoelastic fluids compared to the lubrication solution for a power-law fluid (n = 0.4) in the gravity-free regime. (Key in Table VI-4.)

Figure VI-25.   Coating thickness vs. the gravity number.   Experimental
data for viscoelastic fluids are compared to the lubrication
solution for a power-law fluid (n = 0.4) in the gravity-
controlled regime.   (Key in Table VI-4.)
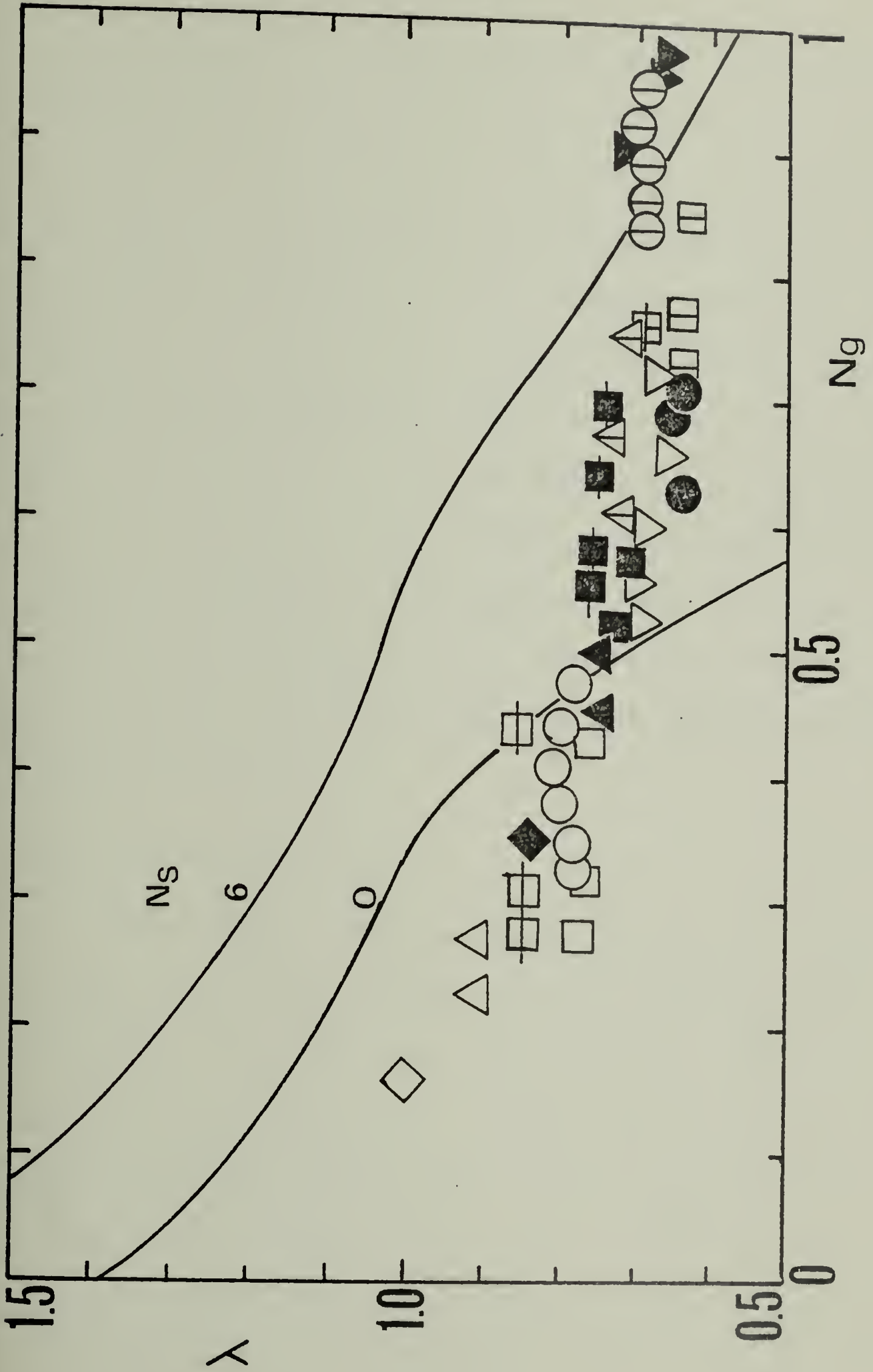
counter-rotating rollers, similar to the one considered in this study. Their observed λ's are in the range 1.26-1.38, which is consistent with the data of the present work. However, a critical assessment of Pitts and Greiller's work cannot be made inasmuch as the corresponding values of N_g and N_S were not given. Hintermaier and White (1965) have also conducted coating thickness measurements (of water films) on counter-rotating rollers. Their values seem quite sparse and they fall in the range 1.34-1.68. Here, as in Pitts and Greiller's work, no account was made of gravity and surface tension effects. However, a sample calculation using their data shows that N_g was smaller than 0.1 but N_S was as high as 0.8 in some cases. In both studies the fluids investigated were Newtonian and the film thickness was measured by the fairly unreliable technique of collecting and weighing the total throughputs.

VI.6 Reverse-Roll Coating

VI.6.1 <u>General</u>. One of the principal limitations of a forward (regular) roll coating device is its susceptibility to flow instabilities. Such instabilities are manifested by the appearance of coating surface irregularities at moderate-to-high speeds. In Chapter VIII it is shown and argued that this undesireable phenomenon cannot be easily eliminated unless the speed is reduced to uneconomically low levels. One way that was found effective in assuring a smooth coating was to reverse the direction of rotation of the roll relative to the web. Such operation is called reverse-roll coating.

Owing to its ability to yield smooth and well controlled coatings at high throughputs, the reverse-roll coater is one of the most versatile and common coaters in use (Booth 1968).

A scheme of a reverse-roll coating system is depicted in Figure VI-26. It is noted that the reverse roll is precoated prior to entering the metering (or application) zone. This feature is bound to have some effect on the final web coating and, indeed, the question of the relation between the thickness of the precoated layer to the thickness of the final web coating is central in the design and operation of reverse-roll coaters. This question is addressed below through a simple lubrication analysis of a reverse-roll coating system.

VI.6.2 <u>Newtonian lubrication analysis</u>. Attention is focused on the system of co-rotating rollers which is shown in Figure VI-26. It is anticipated that the two-dimensional character of the flow becomes strong far from the nip, near the liquid-air meniscus. At this range the lubrication approximation is probably not valid. However, in the neighborhood of the nip the lubrication character of the flow is expected to be preserved. In the following analysis, the lubrication approximation is used for characterizing the flow in the nip region. This is supplemented by a simple mass balance that provides qualitative but useful performance relations for the system.

Clearly, the present analysis differs from the analysis given in VI.3.3 (for the system of counter-rotating rollers) only in the form of the kinematic boundary conditions. These conditions for the present system are:
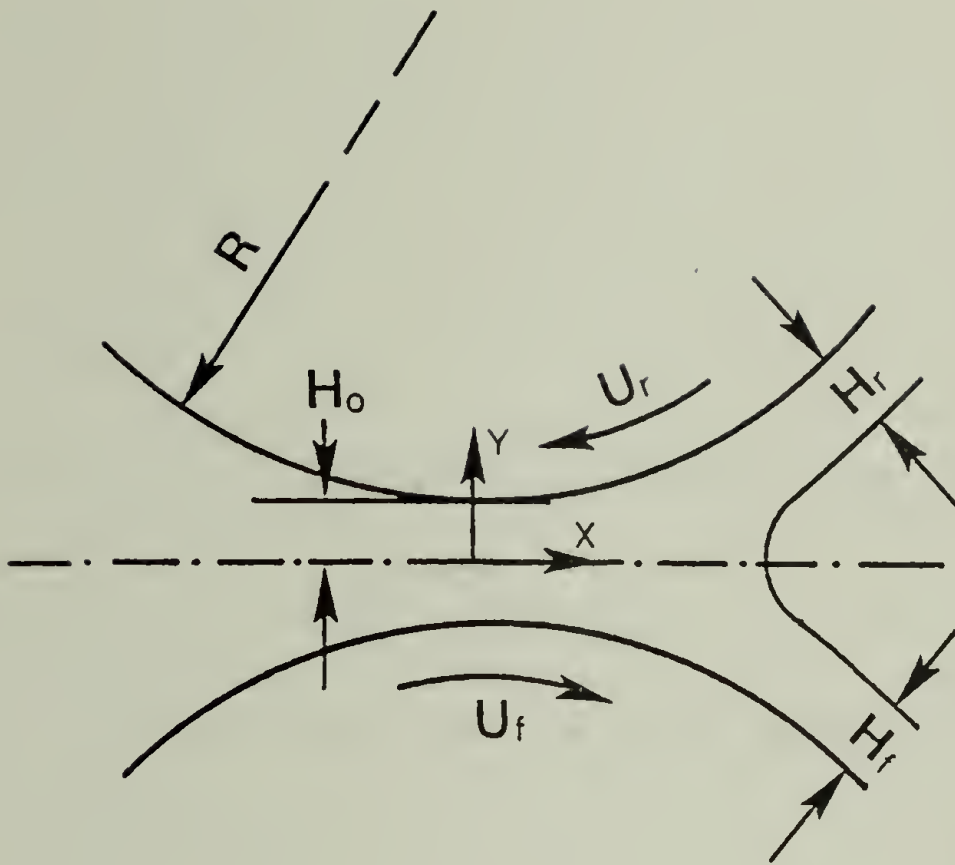
Figure VI-26.   A definition scheme for a reverse-roll coating system.

(a) $\quad \varphi = 1 \quad$ @ $\quad \eta = -\zeta$

and

<div align="right">(VI-34)</div>

(b) $\quad \varphi = -k \quad$ @ $\quad \eta = +\zeta$

where $\quad k = \dfrac{U_r}{U_f}$

and $\quad \varphi = \dfrac{u}{U_f}$

The equation of motion, combined with the above conditions, gives

$$\varphi = \frac{\dot{\pi}}{2}(\eta^2 - \zeta^2) - \frac{1+k}{2}\frac{\eta}{\zeta} + \frac{1-k}{2}$$

<div align="right">(VI-35)</div>

and a reduced flow-rate through the nip can be calculated as

$$\lambda = \frac{1}{2}\int_{-\zeta}^{+\zeta}\varphi \, d\eta$$

$$= -\frac{1}{3}\dot{\pi}\zeta^3 + \left(\frac{1-k}{2}\right)\zeta$$

<div align="right">(VI-36)</div>

(Note that λ, in this case, is a dimensionless flow-rate through the nip

and not a dimensionless coating thickness). It follows that

$$\dot{\pi} = \frac{3}{2}\frac{(1-k)\zeta - 2\lambda}{\zeta^3}$$

<div align="right">(VI-37)</div>

Eqs. (VI-35) and (VI-37) can be used for evaluating the position of the first

stagnation point (denoted by a subscript s) along the symmetry plane ($\eta = 0$).

Introducing Eq. (VI-37) into Eq. (VI-35) and taking $\varphi = 0$ and $\eta = 0$,

one finds

$$\zeta_s(1-k) = 6\,\lambda$$

<div align="right">(VI-38)</div>

This equation specifies the position of the first stagnation point along the

symmetry axis downstream from the nip.

In addition, a total mass balance for the system can be written in the form

$$U_f H_f = U_r H_r + 2 \lambda H_0 U_f \tag{VI-39}$$

This can be reduced to

$$\nu = k + 2\lambda \left(\frac{H_0}{H_r}\right) \tag{VI-40}$$

where $\quad \nu \equiv \dfrac{H_f}{H_r}$

Even though the problem has not been completely solved at this stage, and λ still remains unknown, some speculations can be made concerning the dependence of H_f on U_f, and H_r, using Eqs. (VI-38) and (VI-40). It is useful to examine three general cases:

i. When $k = 1$ λ is zero (according to Eq. VI-38) and consequently,

$$\nu = 1.0 \text{ for all } \frac{H_0}{H_r} \tag{VI-41}$$

ii. When $k < 1$, λ is positive and

$$\nu = k + 2|\lambda| \frac{H_0}{H_r} \tag{VI-42}$$

Thus $\lim\limits_{H_0/H_r \to 0} \nu = k \ (<1.0)$

and for $H_0/H_r > 0$, $\nu > k$

iii. When $k > 1$, λ is negative and,

$$\nu = k - 2|\lambda| \frac{H_0}{H_r} \tag{VI-43}$$

Thus $\lim\limits_{H_0/H_r \to 0} \nu = k \ (>1.0)$

and for $H_0/H_r > 0$, $\nu < k$
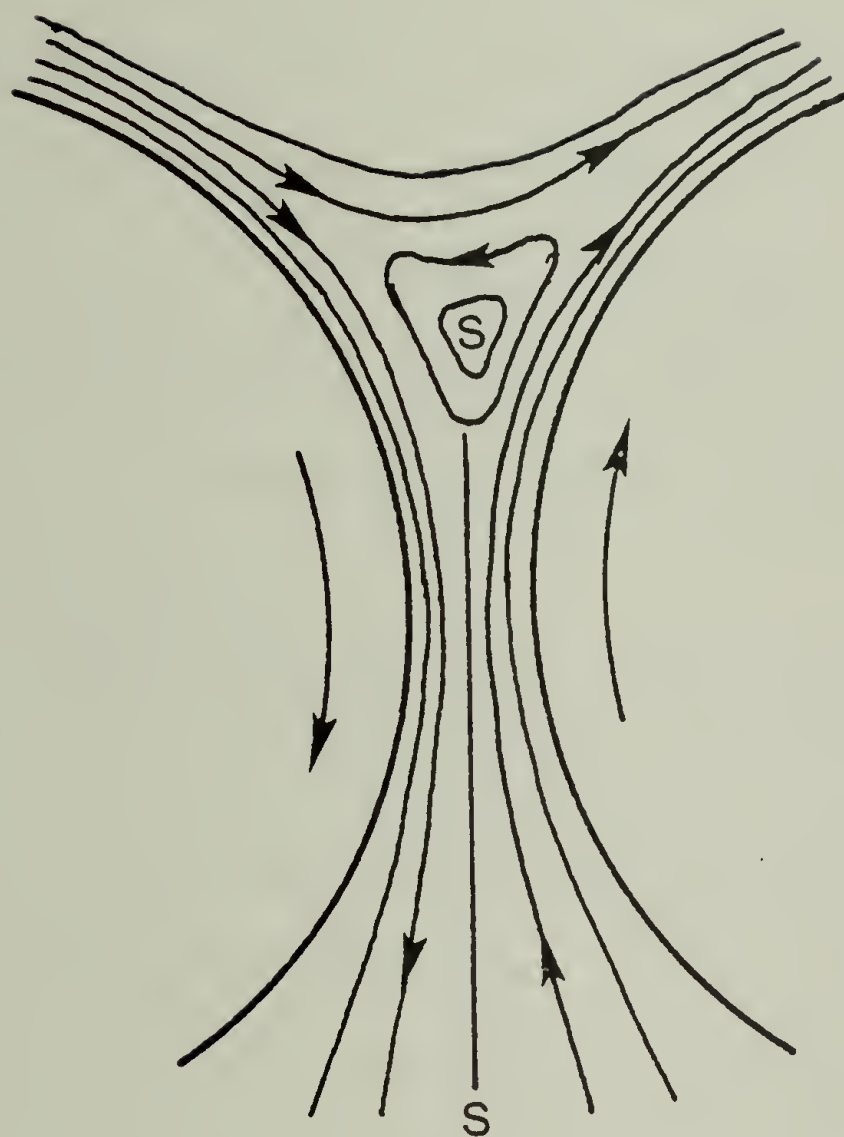
Figure VI-27.   A qualitative stream-line pattern for the system of
co-rotating rollers.

These are the general relationships between ν (or H_f) and κ. For a quantitative evaluation of H_f it is necessary to determine λ which is the only unspecified quantity in Eq. (VI-40). From Eq. (VI-38) it is expected that λ is solely a function of κ. The functional dependence of λ on κ can be determined through observation using Eqs. (VI-38) or (VI-40).

Before passing on to an experimental examination of the various model results it is useful to present a qualitative stream-line pattern for the system at hand. This pattern, shown in Figure VI-27, is directly deducible from the foregoing analysis.

VI. 6. 3 <u>Experimental observations</u>. An experimental investigation of reverse-roll coating aimed at studying the general relationships between ν, κ and H_0/H_r was carried out and it is reported below.

The experimental system described in VI.4.2 was employed in this study and it required only a slight modification; the driving mechanism (a pair of coupled gears) was replaced by a set of geared pulleys and a positive drive belt so that the roller pair could co-rotate (rather than counter-rotate) and thereby simulate a reverse-roll coating operation. Two sets of pulleys were used; a pair of identical pulleys which guaranteed equal speeds for both rollers ($\kappa = 1.0$) and a pair of non-equal pulleys which gave κ values of 0.57 and 1.75 (no slip geared pulleys, P. I. C. cat. nos. FEI-32 and FEI-56; positive drive belt, P. I. C. cat. no. FA-128).

The experimental procedure is similar to the procedure outlined in VI.4.4 with the exception that the coating thickness was measured on both the forward and the reverse rolls so that ν could be determined. Two Newtonian fluids were examined: Glycerin and GW-0.90 (see Table VI-4). Each was tested at three speed ratios (K = 0.57, 1.00, 1.75) with the nip separation ($2H_0$) set at 0.065 cm. (set 2 in Table VI-3). In addition, Glycerin was tested at three different nip separations (sets 1, 2 and 3) with K = 1.00. The precoated film on the reverse roll was formed by free withdrawal of fluid from the bath.

The final experimental results are listed in Appendix A. These data are reduced to ν vs. H_0/H_r plots presented in Figures VI-28 and VI-29. Figure VI-28 shows data for both fluids at constant geometry ($2H_0$ = 0.065 cm) and three speed ratios. The general trends that are displayed by the data are in accord with Eqs. (VI-41) through (VI-43): ν decreases with H_0/H_r for K > 1, ν increases for K < 1., and ν is indepedent of H_0/H_r for K = 1.0. Data for Glycerin at K = 1 for three different nip separations are given in Figure VI-29. This figure clearly slows that ν is independent of the nip geometry and that H_f is equal to H_r for the case K = 1.

λ values were extracted from the data for both fluids for the cases K = 0.57 and K = 1.75. These values were evaluated using Eq. (VI-40) and were found nearly constant (with respect to changes in speed) for each K. The average values of λ are plotted in Figure VI-30 against K.

Figure VI-28.   Coating thickness ratio vs. H_0/H_r.   Experimental data for Newtonian fluids in a system of half-immersed co-rotating rollers.   (Glycerin: $\triangle$ - k = 1.0, $\triangle$ - k = 1.75, $\triangle$ - k = 0.57; GW-0.90: $\bigcirc$ - k = 1.0, $\ominus$ - k = 1.75, $\oplus$ - k = 0.57).   The solid line is a theoretical result for k = 1.0.
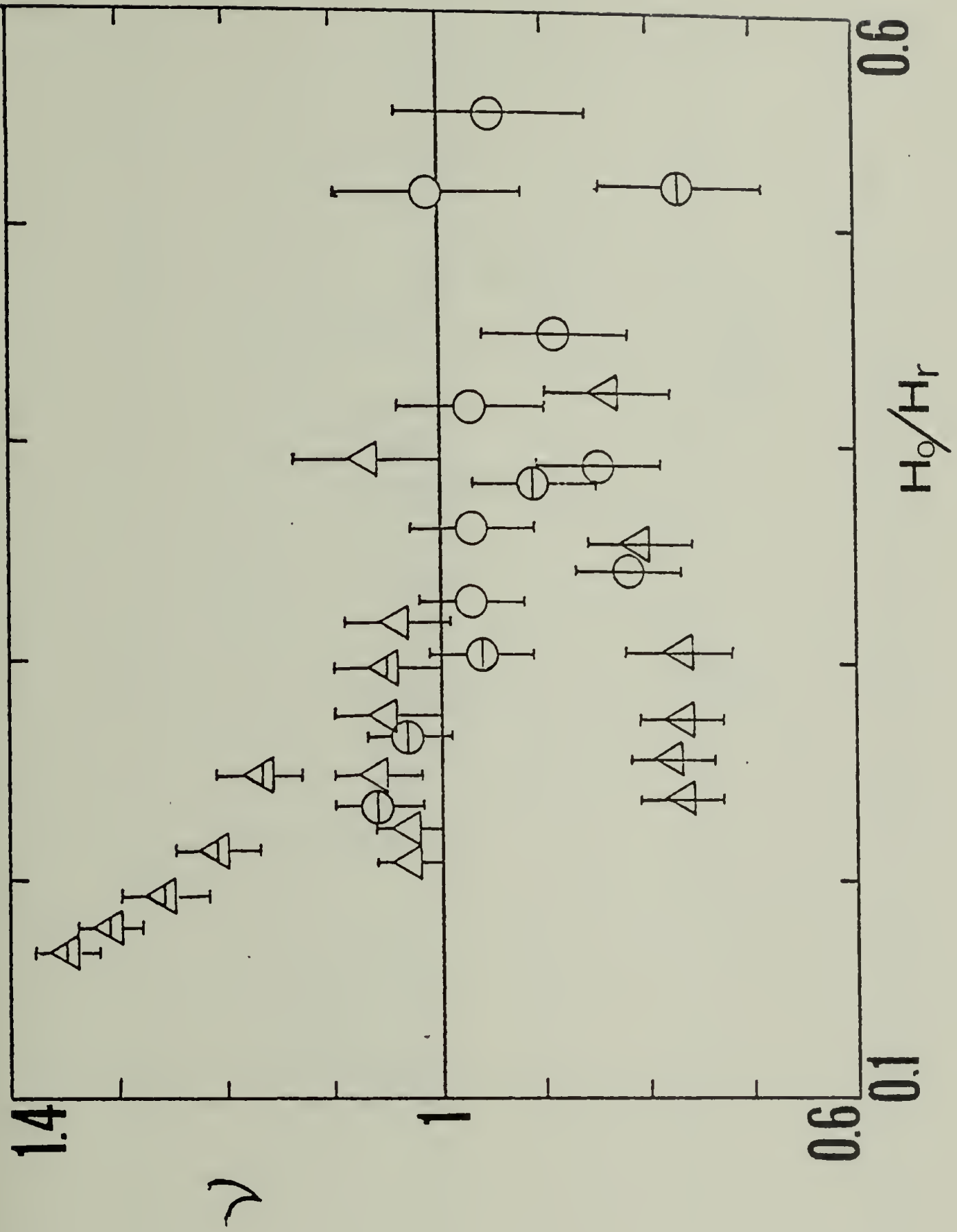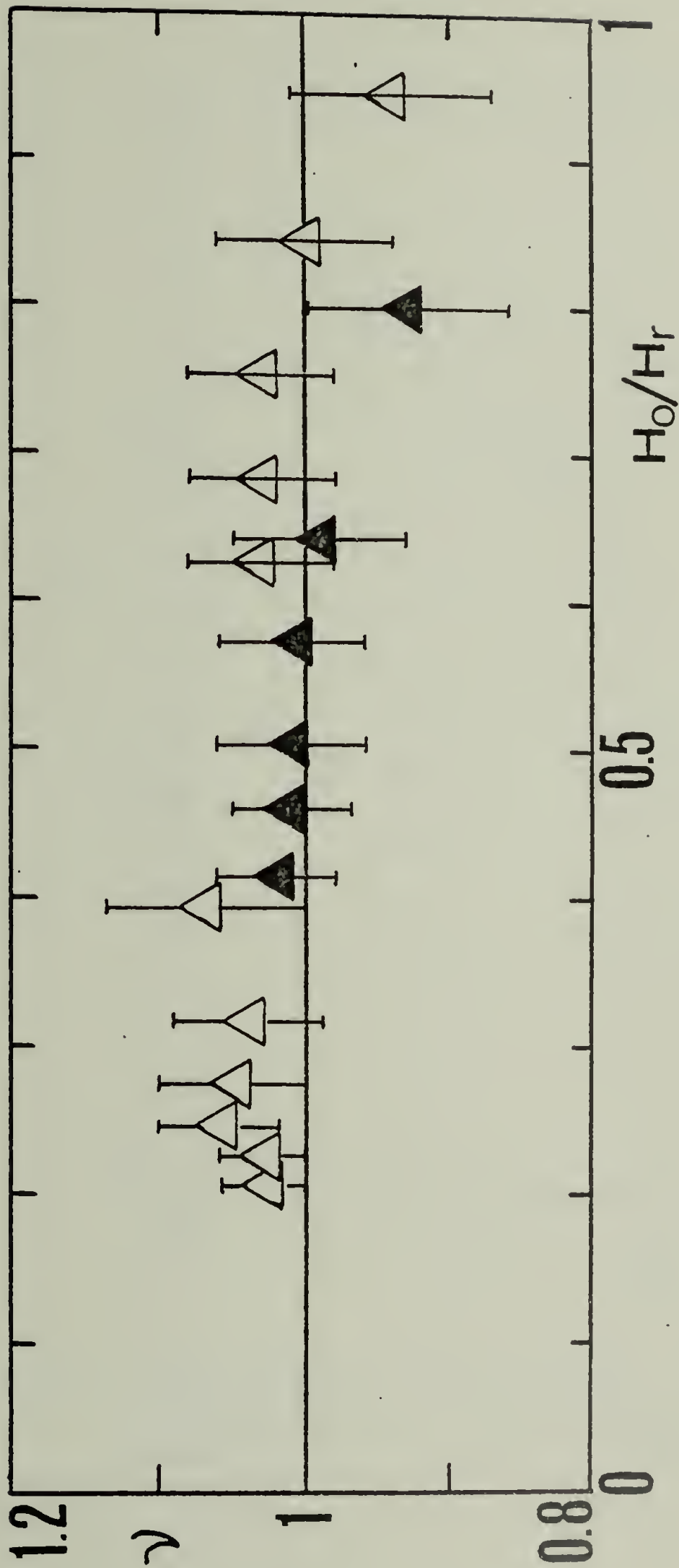
Figure VI-29. Coating thickness ratio vs. H_0/H_r. Experimental data for Newtonian fluids in a system of half-immersed co-rotating rollers. ($\mathcal{K} = 1.0$). (Key in Table VI-4.)
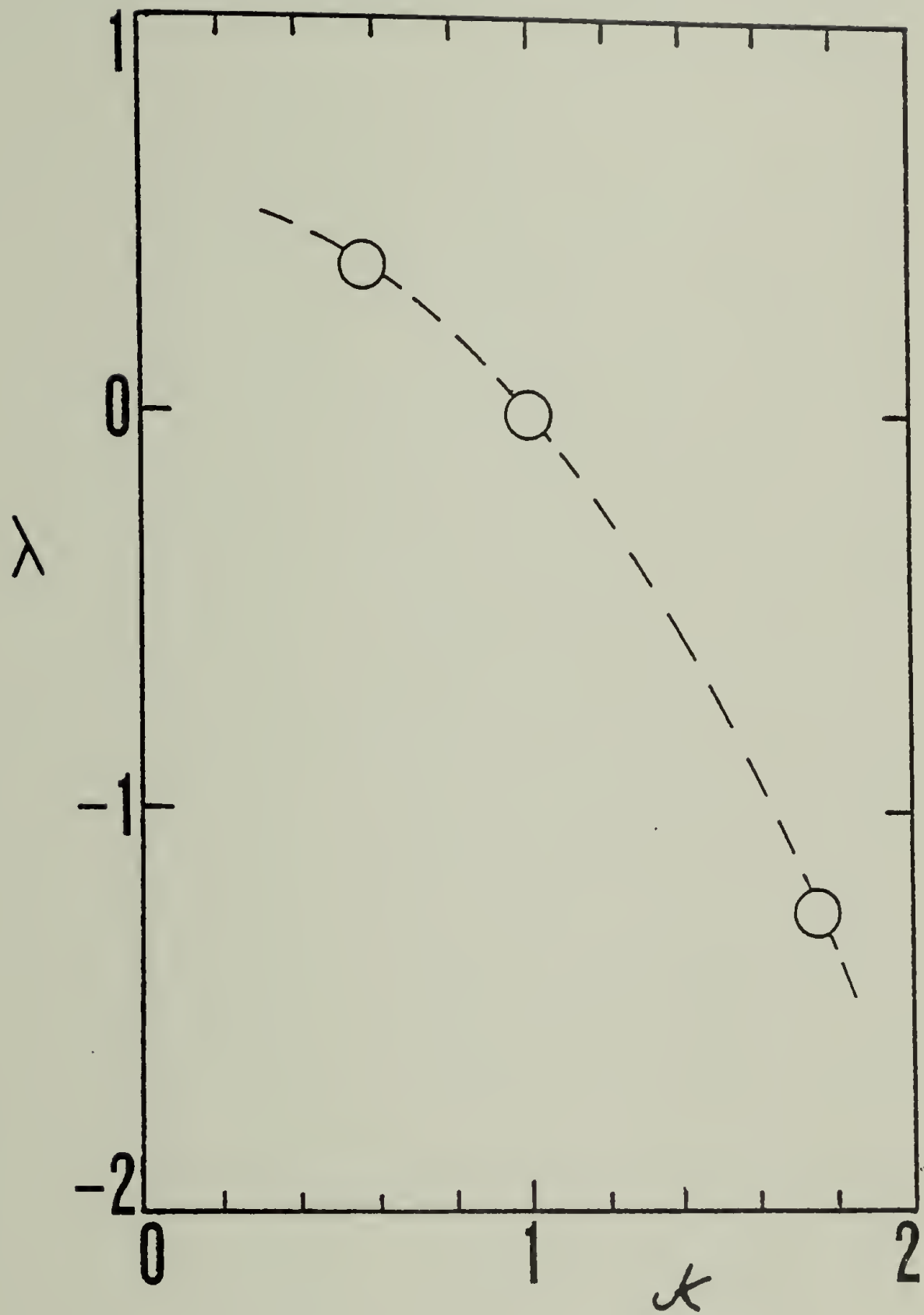
Figure VI-30. "Nip flow-rate" vs. the speed ratio. Experimental data for Newtonian fluids in a system of half-immersed co-rotating rollers.

λ (1) = 0 is a theoretical result that has been confirmed experimentally.

CHAPTER VII

ROLL COATING DYNAMICS:
THE SUBMERGED-ROLL SYSTEM

VII. 1   Introduction

An attempt to elucidate the dynamic behavior of fluids in roll coating,

through a study of a model system, is reported in this chapter.

An experimental study of the dynamics in roll coating is hampered by

the inherent difficulty in measuring pressures in narrow flow spaces.   Such

experimental undertaking can be made somewhat easier by replacing an

actual roll coating system with a dynamic prototype, the submerged-roll

system.

A schematic of the submerged-roll system is presented in Figure

VII-1.   This system consists of an infinitely long roll and a stationary,

infinitely wide, wall that is situated parallel to the roll axis at a relatively

short distance, $H_0(<<R)$, from the roll surface.   The system is fully im-

mersed in a "sea" of fluid and a motion in the fluid is induced by the

rotation of the roll.   Both the wall and the roll are rigid and their relative

position is unaffected by the flow field.   Attention is focused on the con-

verging-diverging flow space in the vicinity of the nip.   Clearly, this

system does not fall in the general category of coating flows according to

the definition given in Chapter II.   The submerged-roll system   is,
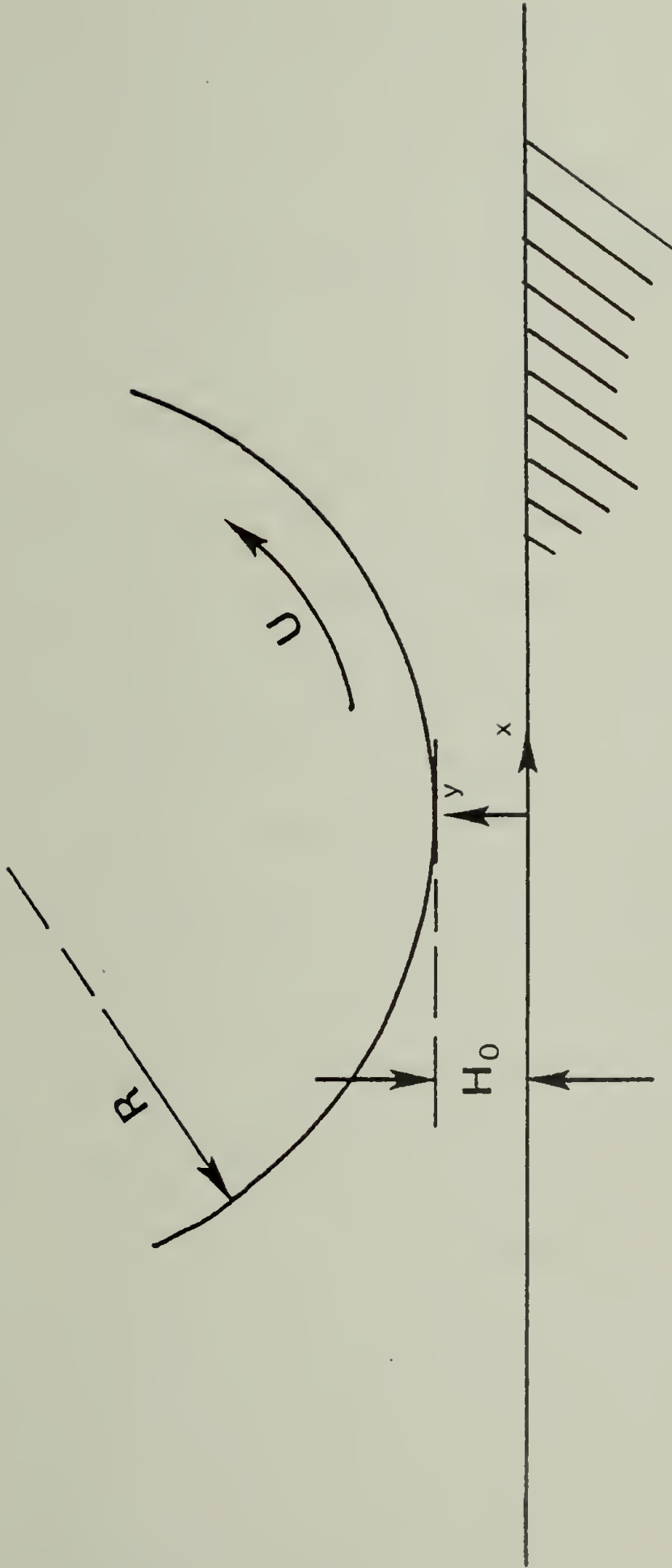
Figure VII-1.   A schematic of the submerged-roll system;   geometry of the nip region.

however, dynamically similar to a (forward) roll coating system and it is thus used here to simulate the dynamic response in roll coating.

It will be seen that the Newtonian pressure distribution for the sub-merged-roll system is an odd function of the x coordinate, i.e., the load-carrying capacity for the system is identically zero. This dynamic property makes this system unattractive in the lubrication sense. For sufficiently high pressures, however, a cavitation is likely to develop at the negative pressure zone (Banks and Mill 1954, Taylor 1963), thus altering radically the dynamics of the system. To avoid the additional complexity involved in the presence of cavitation, this study is exclusively concerned with the non-cavitating case which is prevalent under conditions of light loading (low deformation rates).

As this study is essentially an extension of the roll coating chapter (VI) some of the early reports concerning the submerged-roll problem have been cited in VI.1. Few studies on the system of a lubricated cylinder lightly loaded against a stationary plane have been reported. Floberg (1964, 1965, 1968), in an attempt to elucidate the origin of striations (or streamers) arising in a variety of lubricating rolling elements, conducted a series of experiments in which pressure distributions were measured. In the system considered by Floberg, the downstream end was not flooded. Rather, a separation cavitation, accompanied by striations, was taking place in the lubricating film. Floberg's observations, nevertheless, lend

themselves to the various analytical pressure distributions presented in

Chapter VI; the general features of the observed pressure function are in

agreement with the theoretical results of Chapter VI. In a later publication,

Taylor (1974b) discusses Floberg's work by comparing the experimental

pressure distributions to those predicted by the Coyne and Elrod theory

(see IV. 4). The agreement was found satisfactory even though the Coyne

and Elrod theory was derived for a striation-free case. Is this agreement

accidental, or is it that the presence of striations has little effect on the

boundary conditions? As pointed out by Taylor, this question is yet to be

answered. In any case, Coyne and Elrods' theory has proved useful and

practically valid. It is pertinent to note that the Coyne and Elrod condition

was found generally compatible with the separation model used in Chapter

VI (see VI. 3. 4). Thus, Floberg's observations indirectly validate the

theoretical pressure distributions presented in Chapter VI for the Newtonian

case. One still lacks, however, sufficient information regarding the response

of viscoelastic fluids in the system.

An experimental study of the submerged-roll system was undertaken

with an attempt to investigate the behavior of both Newtonian and viscoelastic

fluids in the converging-diverging flow space. Lubrication analyses for the

submerged-roll system are presented in Section 2. These analyses are

carried out for two constitutive models: The second-order fluid model and

the CEF model. (Results for the Newtonian case are given without

derivation.) In Section 3, an experimental study of the system is reported and the experimental results are presented and discussed in Section 4.

VII. 2 The Submerged-Roll System: Lubrication Analyses

VII. 2. 1 <u>General</u>. The geometric resemblance of the submerged-roll system to the sheet-and-roll system discussed in VI. 2, permits dimensionless variables for this system to be defined in a similar way,

$$\xi = \frac{x}{(RH_0)^{1/2}} \quad , \quad \eta = \frac{y}{H_0} \quad , \quad \varphi = \frac{u}{U}$$

and

$$= \frac{PH_0^{3/2}}{\eta_a UR^{1/2}}$$

where η_a has been defined in Eq. (VI-1). For the <u>non-cavitating</u> case one can write the following boundary conditions,

(a) $\varphi = 1$ @ $\eta = \varsigma$

(b) $\varphi = 0$ @ $\eta = 0$ (VII-1)

(c), (d) $\pi = 0$ @ $\xi = \pm \infty$

where ς, the position of the roll surface, is given by Eq. (VI-3). Eqs. (VII-1a, b) are the 'no-slip' conditions and Eqs. (VII-1c, d) state that the pressure vanishes at points far upstream and far downstream from the nip.

Note that in the absence of flow separation the number of boundary conditions is reduced by one. Since no actual coating is taking place in this system, the only performance variable that is considered in the analyses to follow is the pressure (or the total stress in the case of a viscoelastic fluid).

The Newtonian lubrication analysis for this system is straightforward and hence the important results are presented below without derivation. Two integrations of Eq. (IV-2) and application of the boundary conditions, Eq. (VII-1), together with a mass balance, yield the following results:

$$\pi = \frac{8\,\xi}{(2+\xi^2)^2} \tag{VII-2}$$

$$\varphi = \frac{3\sigma-4}{\sigma^3}\eta^2 - \frac{2(\sigma-2)}{\sigma^2}\eta \tag{VII-3}$$

and,

$$\lambda = \frac{Q}{UH_0} = \frac{2}{3} \tag{VII-4}$$

where Q is the volumetric flow-rate per unit width. As was noted previously, the pressure function is indeed antisymmetric with respect to the origin ($\xi = 0$). This situation will prevail only in the absence of cavitation. Also, from inspection of the velocity profile, φ, it is apparent that it does not possess an axis of symmetry as in the sheet-and-roll case. It will be seen that this fact will introduce some difficulties in the perturbation solution for the CEF model. The results for the Newtonian case are subsequently used in the analyses for the second-order fluid and the CEF fluid.

VII. 2. 2 <u>The second-order fluid.</u> The Newtonian results presented above are now modified to account for first order effects of viscoelasticity using the second-order fluid model. As before, the Giesekus-Tanner-Pipkin equation is used and it is rewritten here in a dimensionless form

as an expression for the total stress,

$$-\Theta_{\eta\eta} = \mathcal{T}^0 - S_R \left(\frac{H_0}{R}\right)^{1/2} \varphi^\circ \dot{\mathcal{T}}^0 + \frac{1}{2} S_R \left(\frac{H_0}{R}\right)^{1/2} \left(\frac{d\varphi}{d\eta}\right)^2 \qquad \text{(VII-5)}$$

where $S_R = \dfrac{\alpha_2}{\alpha_1} \dfrac{U}{H_0}$

This expression, evaluated at the plane wall $(\eta=0)$, reads

$$-\Theta_{\eta\eta}\Big|_{pw} = \mathcal{T}^0 + \frac{1}{2} S_R \left(\frac{H_0}{R}\right)^{1/2} \left(\frac{d\varphi}{d\eta}\right)^2\Big|_{\eta=0} \qquad \text{(VII-6)}$$

$$= \mathcal{T}^0 + 2 S_R \left(\frac{H_0}{R}\right)^{1/2} \left(\frac{\xi-2}{\xi^4}\right)^2$$

Stress distributions as given by Eq. (VII-6) are presented in Figure VII-2 for several values of the parameter S_R, taking $\dfrac{H_0}{R} = 0.01$. The familiar "shift upward" of the distribution in the neighborhood of the nip is displayed by the results. This shift is expected to give rise to a finite force on the wall (or the roll). Integration of Eq. (VII-6) with respect to ξ gives

$$\Phi_{pw} = 2.22 \left(\frac{H_0}{R}\right)^{1/2} S_R \qquad \text{(VII-7)}$$

where Φ has been defined in Eq. (VI-15). Thus, Φ_{pw}, the total separating force acting on the wall, is finite and linear in S_R for a viscoelastic second-order fluid. The magnitude of this force, however, will be small compared to unity in the limit $\dfrac{H_0}{R} \ll 1$ that is pertinent to this analysis.

Figure VII-2.   Total (normal) stress distributions for a second-order fluid in a submerged-roll system ($H_0/R = 0.01$).
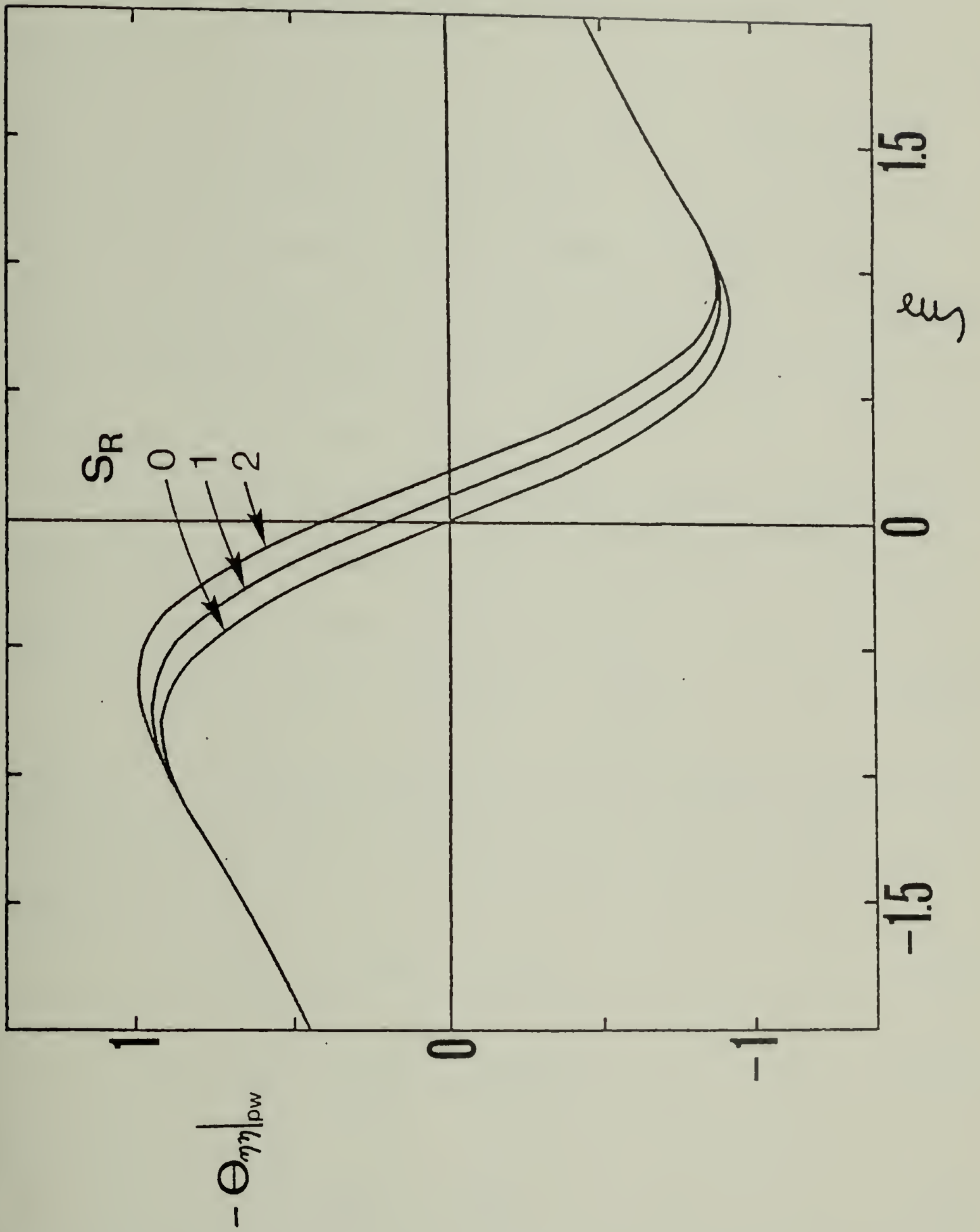
VII.2.3 **The CEF fluid.** The CEF model is now applied in the analysis for the submerged-roll system. This analysis is, in a way, complimentary to the preceding analysis as it regards, in addition to elastic effects, first-order effects of shear-thinning. As has been noted in IV.2 the CEF model is essentially represented by two empirical viscometric functions, $\eta(\dot{\gamma})$ and $\Psi_{12}(\dot{\gamma})$. Both functions are given in IV.2. While $\eta(\dot{\gamma})$ is used directly in the dynamic analysis, $\Psi_{12}(\dot{\gamma})$ is considered only in the calculation of the total stress distribution.

In a familiar fashion by now, the dynamic equation is solved using a regular perturbation method, as it cannot be subject to an exact analytical solution. The analysis begins with the equation

$$(\dot{\mathcal{K}}\eta + C)\ [1\ +\ N_e\ (|\frac{d\varphi}{d\eta}|)^{1-n}]\ =\ \frac{d\varphi}{d\eta} \tag{VII-8}$$

where Ne, the viscoelastic parameter (see IV.2) is selected as a perturbation parameter, as before, all the unknown functions are expanded in the form

$$\varphi\ =\ \varphi^0\ +\ N_e\varphi^1\ +\ O(N_e^2) \tag{VII-9}$$

$$\dot{\mathcal{K}}\ =\ \dot{\mathcal{K}}^0\ +\ N_e\dot{\mathcal{K}}^1\ +\ O(N_e^2) \tag{VII-10}$$

and

$$C\ =\ C^0\ +\ NeC^1\ +\ O(N_e^2) \tag{VII-11}$$

The expanded functions are introduced back into Eq. (VII-8) and the solution proceeds in the usual perturbation scheme (see IV.3). This problem is

somewhat hampered by the fact that the Newtonian velocity profile does not possess an axis of symmetry. In the course of solution one is faced with integrands that contain an absolute-value operator applied to the velocity-gradient function, and analytical integrations cannot be performed unless the velocity function is investigated throughout the entire flow domain. Similar difficulties were faced in the CEF analysis for the blade coating system. To overcome this problem one needs to divide the flow domain into zones which are defined by the general shape of the velocity profile. All the unknown functions are derived for each zone separately with the condition that they are continuous across the zone boundaries.

The resulting derivation is quite lengthy and it is presented in detail in Appendix C. The final results are given below.

For Zone A $(\sigma<2)$ where $\frac{d\varphi^0}{d\eta}$ is always positive,

$$\varphi_A^1 = \dot{\pi}_A^1 \frac{\eta^2}{2} + (\frac{(-X)^p - Y^p}{\sigma\,\dot{\pi}^0 p} - \frac{\dot{\pi}_A^1 \sigma}{2})\,\eta$$

$$+ \frac{(\dot{\pi}^0\eta - X)^p - X^p}{\dot{\pi}^0 p} \tag{VII-12}$$

and

$$\dot{\pi}_A^1 = -\lambda^1 \frac{12}{\sigma^3} - \frac{6((-X)^p + Y^p)}{\sigma^2 \dot{\pi}^0 p}$$

$$- \frac{12((-X)^{p+1} - Y^{p+1})}{p(p+1)\sigma^3 \dot{\pi}^{02}} \tag{VII-13}$$

For Zone B ($\mathfrak{S} > 2$) where $\frac{d\varphi^0}{d\eta}$ is either positive or negative

$$\dot{\mathcal{R}}_B^1 = -\lambda^1 \frac{12}{\mathfrak{S}^3} \frac{6\,[(+X)^p + Y^p]}{\mathfrak{S}^2 \dot{\mathcal{R}}^0 \, p}$$

$$+ \, 12 \frac{[(+X)^p + (Y)^{p+1}]}{p\,(p+1)\,\mathfrak{S}^3 \, \dot{\mathcal{R}}^{02}}$$

(VII-14)

For $\frac{d\varphi^0}{d\eta} < 0$ (case B1),

$$\varphi_{B1}^1 = \dot{\mathcal{R}}_B^1 \frac{\eta^2}{2} + \left[\frac{(+X)^p - Y^p}{\mathcal{R}^0 p\,\mathfrak{S}} - \frac{\dot{\mathcal{R}}_B^1 \mathfrak{S}}{2}\right]\eta$$

$$+ \, \frac{(-\dot{\mathcal{R}}^0\,\eta + X)^p - (+X)^p}{\dot{\mathcal{R}}^0 p}$$

(VII-15)

and for $\frac{d\varphi^0}{d\eta} > 0$ (case B2),

$$\varphi_{B2}^1 = \dot{\mathcal{R}}_B^1 \frac{\eta^2}{2} + \left[\frac{(+X)^p - Y^p}{\mathcal{R}\,p\,\mathfrak{S}} - \frac{\dot{\mathcal{R}}_B^1 \mathfrak{S}}{2}\right]$$

$$+ \, \frac{(\dot{\mathcal{R}}^0\eta - X)^p - (+X)^p}{\dot{\mathcal{R}}^0 p}$$

(VII-16)

where $\qquad p \equiv 3-n$

$$X \equiv -\frac{1}{\mathfrak{S}} + \frac{1}{2}\dot{\mathcal{R}}^0\mathfrak{S}$$

$$Y \equiv \frac{1}{\mathfrak{S}} + \frac{1}{2}\dot{\mathcal{R}}^0\mathfrak{S}$$

and

$$\lambda^1 = \begin{cases} \displaystyle\int_0^{\mathfrak{S}} \varphi_A^1 \, d\eta & \text{in Zone A} \\[3mm] \displaystyle\int_0^{\eta_E} \varphi_{B1}^1 \, d\eta + \int_{\eta_E}^{\mathfrak{S}} \varphi_{B2}^1 \, d\eta & \text{in Zone B} \end{cases}$$

η_E is the position of the extrenum of the velocity profile at ξ.

$\lambda^1 = \lambda^1(n)$ is determined by specifying $\pi^1(0) = 0$ (as one would expect the pressure function to remain antisymmetric with respect to the origin for fluids that are shear-thinning).

With $\lambda^1(n)$ on hand, it is possible to calculate the total stress distributions for the system using Eqs. (VII-13) and (VII-14). The total stress function evaluated at the plane surface is

$$-\Theta_{\eta\eta}\Big|_{pw} = \pi^0 + N_e \int_{-\infty}^{\xi} \dot\pi^1 \, d\xi + \frac{1}{2} N_e^{\frac{1}{1-n}} \left(\frac{H_0}{R}\right)^{1/2} \frac{4(\zeta-2)^2}{\zeta^2} \tag{VII-17}$$

where the normal stress, Z_{yy}, has been evaluated using Eqs. (IV-14) and (VII-3). Evidently, the dashed-underlined normal stress term in Eq. (VII-17) is much smaller than the other terms (see Eq. (VI-27) for similar considerations). Thus, this term is neglected in the calculation of the total stress distributions. These distributions are presented in Figure VII-3 for several values of the parameter $W_s (=Ne^{1/(1-n)})$. Since the resulting distributions are odd functions of ξ only the positive branch is shown.

The results obtained are consistent with the results for the corresponding sheet-and-roll analysis (VI.2.4). That is, the non-Newtonian distributions are "flatter" in comparison to the corresponding Newtonian distribution. Also, the effect is more pronounced for fluids with a higher power-law index. This "paradox" has been rationalized both in V.2.3 and in VI.2.4 and it was shown to be an artifact of the viscosity model. The general result of this calculation, namely $|\pi_{ve}| \leq |\pi_N|$, is nothing but surprising as one
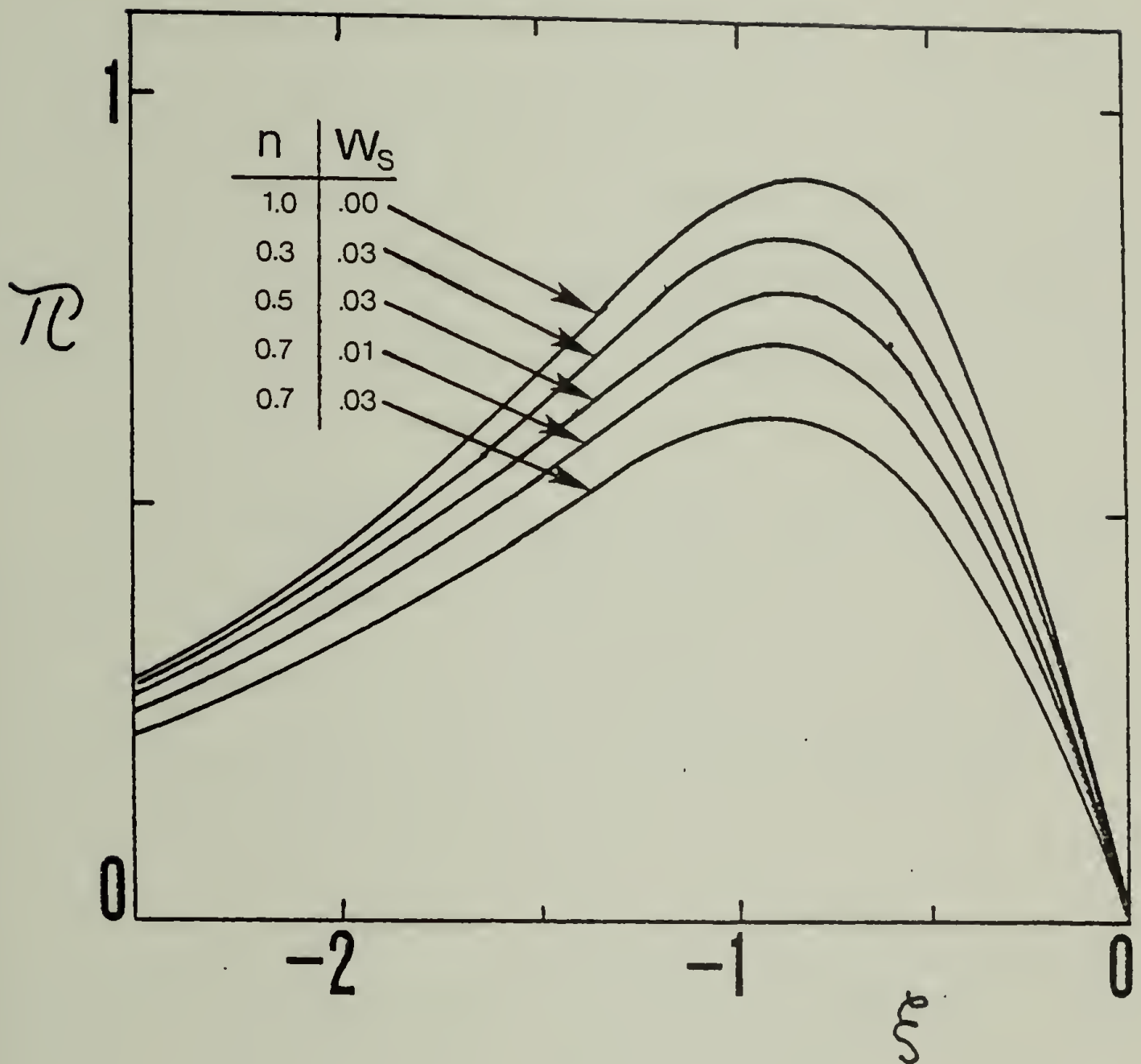
Figure VII-3. Total (normal) stress distributions for a CEF fluid in a submerged-roll system.

would expect a purely viscous shear-thinning fluid to generate, on the average, lower pressures than a Newtonian fluid with a viscosity equal to the zero-shear-rate viscosity of the viscoelastic fluid. Also, as expected, the contribution of the normal-stress term to the total-stress distribution was found insignificant (see VI. 2. 4-5). This term, however, will be the only one to contribute to a finite, though small, roll separating force. By inspection, the total force acting on the plane wall is given by Eq. (VII-7) with W_s replacing S_R.

VII. 2. 4 <u>Discussion.</u> All the theoretical results presented in this section give some credence to the claim that the submerged-roll system is dynamically similar to the roll coating system; similar trends were found for the second-order fluid model and for the CEF model in both systems. These trends have been discussed in VI. 2. 5.

The equivalent problem of a full-film, non-cavitating journal-bearing was analyzed by Davies and Walters (1973) using an Oldroyd-type constitutive model. (This model is not particularly realistic but its qualitative features are quite satisfactory:) They present total-stress distributions that agree qualitatively with the results of the present work. Specifically, they found that: 1) The Newtonian distribution is an odd function of the primary flow (x_1) coordinate, 2) Shear-thinning effects tend to "flatten" the distribution, and 3) elastic effects tend to "shift" the distribution "upward" in the vicinity of the nip. It now remains to be seen how well these results are reproduced in practice.

VII. 3   Experimental

VII. 3. 1   <u>Scope</u>.   An experimental study was undertaken aimed at testing the various theoretical results for the submerged-roll system.   In this study, pressure distributions were measured in the vicinity of the nip using a U-tube manometer.   The runs were conducted at room temperature and measurements were taken for several rotational speeds of the roll. Two fluids were tested: a viscous Newtonian fluid and a highly viscoelastic fluid.   The error involved in the use of a manometer for measuring pressures generated by a viscoelastic fluid, the "hole-pressure error", was approximately corrected via a given correlation.

VII. 3. 2   <u>Experimental system.</u>   The experimental submerged-roll system was designed so as to enable a study of the dynamics under cavitation-free conditions.   The dimensions of the system were thus dictated by the anticipated low level of the pressures and by the size and sensitivity of the pressure sensing device to be used in this experiment.   The essentials of the experimental system are given in Figure VII-4.   The system consists of a smoothed steel roll (38.2 cm. long, 21.40 cm. in diameter) that is positioned vertically in a large acrylic tank (41.1 x 41.9 x 49.3 cm.).   The roll is firmly attached to a rigid holding frame and its rotation is accommodated by two ball bearings; a regular sealed bearing on top and a sealed thrust bearing at the bottom.   The thrust bearing is attached permanently to the bottom part of the frame whereas the upper bearing is
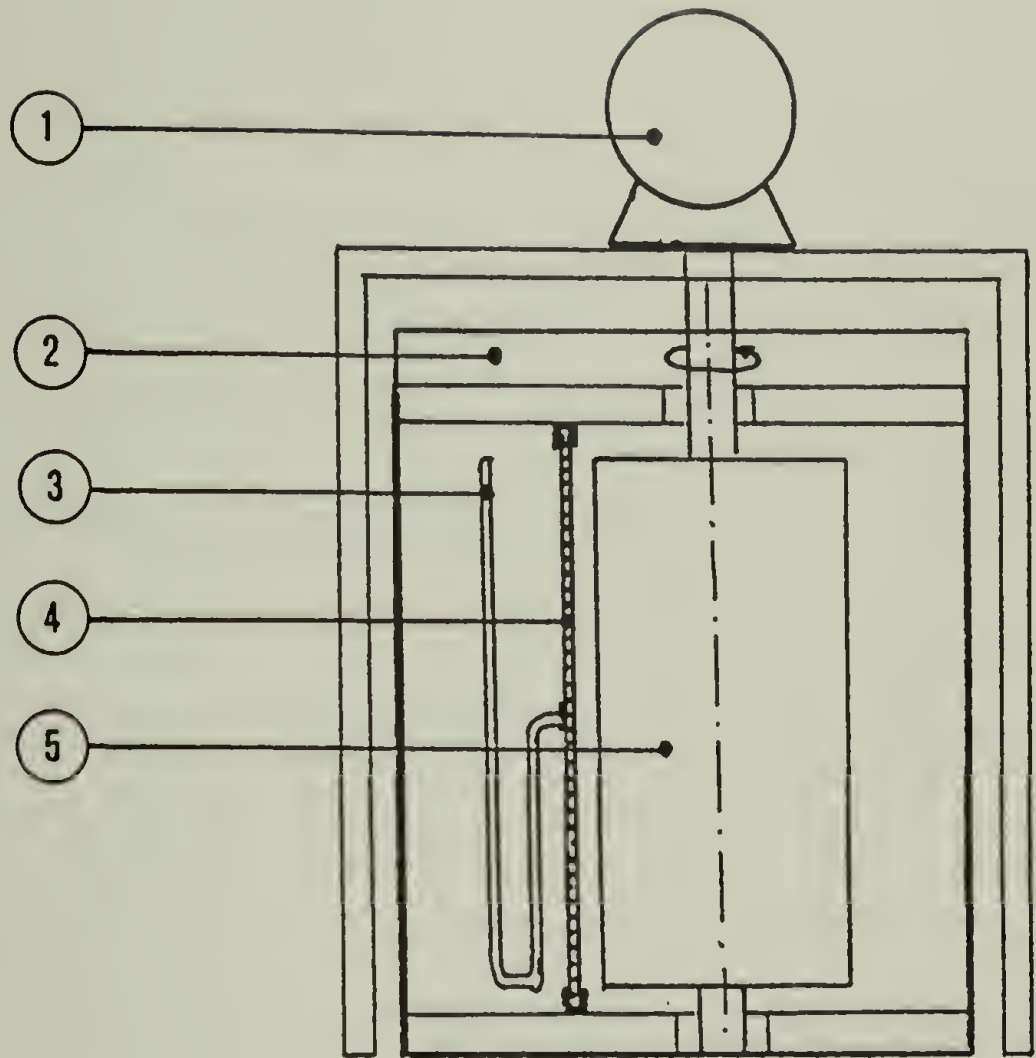
Figure VII-4. A scheme of the experimental submerged-roll system.
1. DC constant-speed motor. 2. An acrylic container.
3. U-tube manometer. 4. An acrylic plate (side view).
5. Steel roll.

tight-fitted on the roll shaft. The roll was turned around centers to an accuracy of ± 0.001 in. for concentricity.

A flat acrylic board (3/8 in. thick, 44.3 cm. long and 30.1 cm. wide) is positioned vertically in the tank, parallel to the roll axis. This board serves as a pressure-sensitive rigid wall and it is attached to the frame through a pair of aluminum channels (one at the bottom and one on top). The horizontal position of the board can be adjusted by sliding it along the channels, and its distance from the roll surface can be set by moving the channels; both channels are attached to the frame in a way that permits changing their distance from the roll.

A U-tube manometer was used for measuring pressures. The manometer is attached to the board at the center and by sliding the board along the channels pressure readings could be taken at different horizontal positions on the mid-plane (away from the roll edges).

The roll was driven by a 3HP DC motor through a vertical face mounted speed reducer (Boston Gear; 18300-B Baldor 3HP DC face mounted motor; F-231 SPV Boston vertical face mounted optimount speed reducer). The driving system was positioned on a firm stand above the submerged-roll system and a standard coupling was used for connecting the roll shaft to the driving shaft. The speed of the motor was controlled by an electronic speed control unit (Boston Gear, VE-300 Boston 3HP Ratiotral motor control). The arbitrary speed scale on the unit was calibrated before each run.

VII. 3. 3 <u>Materials and Experimental Procedure</u>. Experiments were conducted with two fluids; Karo Syrup (KS), a Newtonian fluid, and an aqueous solution of polyacrylamide (Polyhall), 1% by wt. nominal (H-1) which is a viscoelastic fluid. Some physical properties of these materials and other pertinent information are given in Table V[-4. The viscosity of the Karo Syrup, being strongly temperature dependent, was measured at the temperature recorded for the corresponding experiment, using an Epprecht Rheomat 15. This temperature was noted to be constant within the time span of the experiment. The viscometric properties of the viscoelastic solution (H-1) were measured using a rheometrics mechanical spectrometer and they are given in Figure VII-5. The corresponding data are presented in a tabular form in Appendix B. Some degradation of the polymeric species was detected at an early stage of the "viscoelastic" run and it was manifested by a reduction in both the shear viscosity and the first normal-stress coefficient. These properties stabilized after the initial stage and they remained nearly constant throughout most of the run. The data in Figure VII-5 represent the sample after the initial degradation.

The experimental procedure was as follows. The system was carefully assembled with special attention given to the distance and allignment of the acrylic board relative to the roll. With the aid of thin spacers, a uniform gap between the roll and the board was set and it was then measured by a proper set of feeler gauges. The board was also carefully alligned at a plane tangential to the roll surface to insure uniformity of the

209
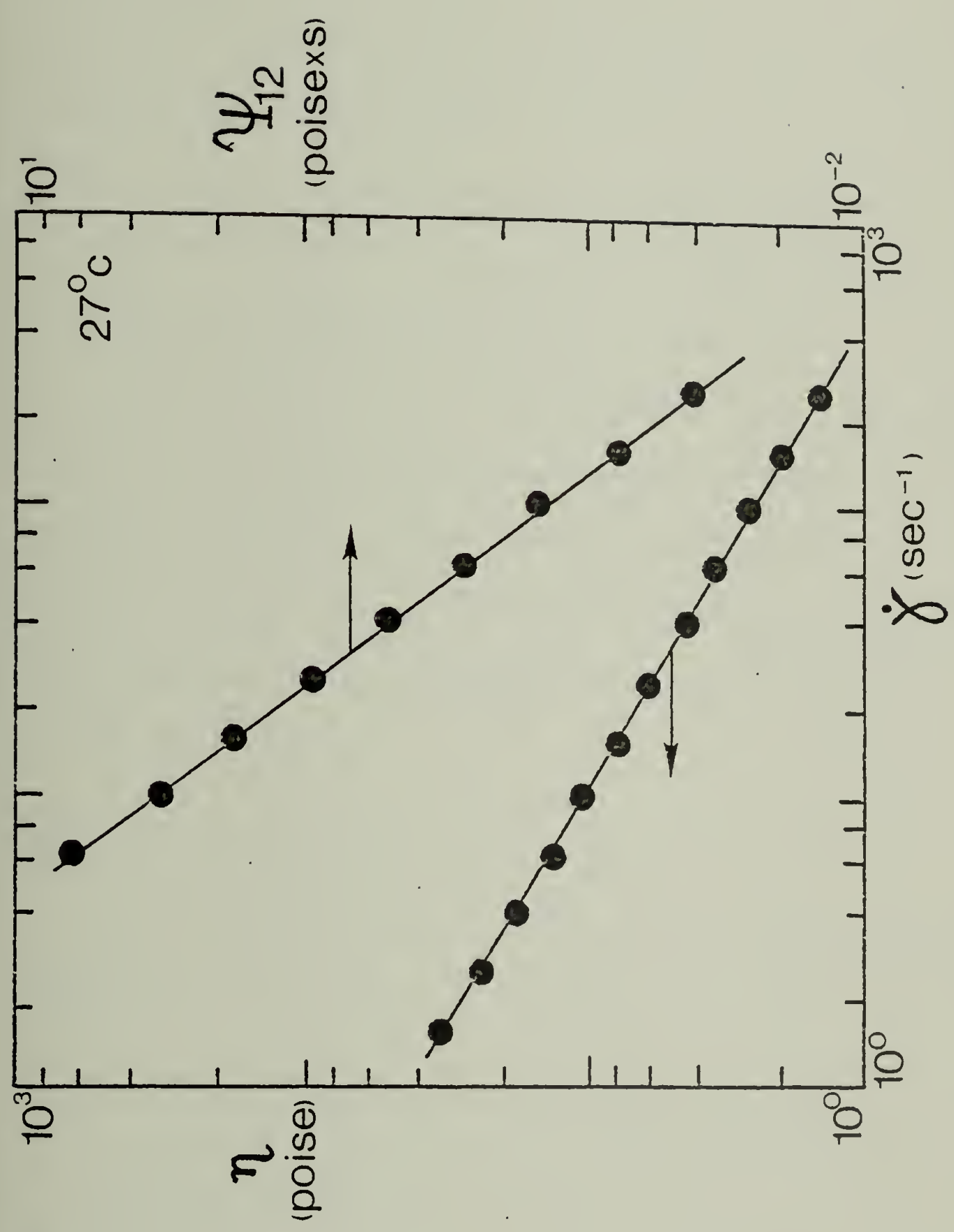
Figure VII-5. The viscometric functions for solution H-1 used in the submerged-roll experiment.

converging-diverging space. After the system was assembled it was filled with the test fluid such that the entire cylinder-plane system be fully immersed. In the "viscoelastic" run the solution was prepared directly in the acrylic tank. The total capacity of the system was nearly fifteen gallons. Pressure readings were taken at several positions of the pressure tap relative to the nip. By sliding the acrylic board along the channels, the pressure tap could be stationed at any position within an interval of 5 cms. on both sides of the nip. The measurements were repeated for several rotational speeds which were maintained sufficiently low to avoid the onset of cavitation. As the viscosities of the test fluids were relatively high, the response of the manometer to a step change in pressure was fairly slow: few minutes for the Karo Syrup and up to an hour (!) for the viscoelastic solution.

VII.4 Experimental Results and Discussion

The experimental pressure distributions are presented graphically in Figures VII-6 through VII-8. The relevant data and the pertinent information are given in Appendix A. The pressures observed in the "Newtonian" run are presented in Figure VII-6 in a properly reduced form where they are compared to the Newtonian lubrication solution (the solid line) and to a numerical solution of the full planar flow problem (the dashed line). Each data point in this figure represents an average of four pressure readings taken at four rotational speeds (24.4, 45.4, 67.4, 87.6 rpm). All four
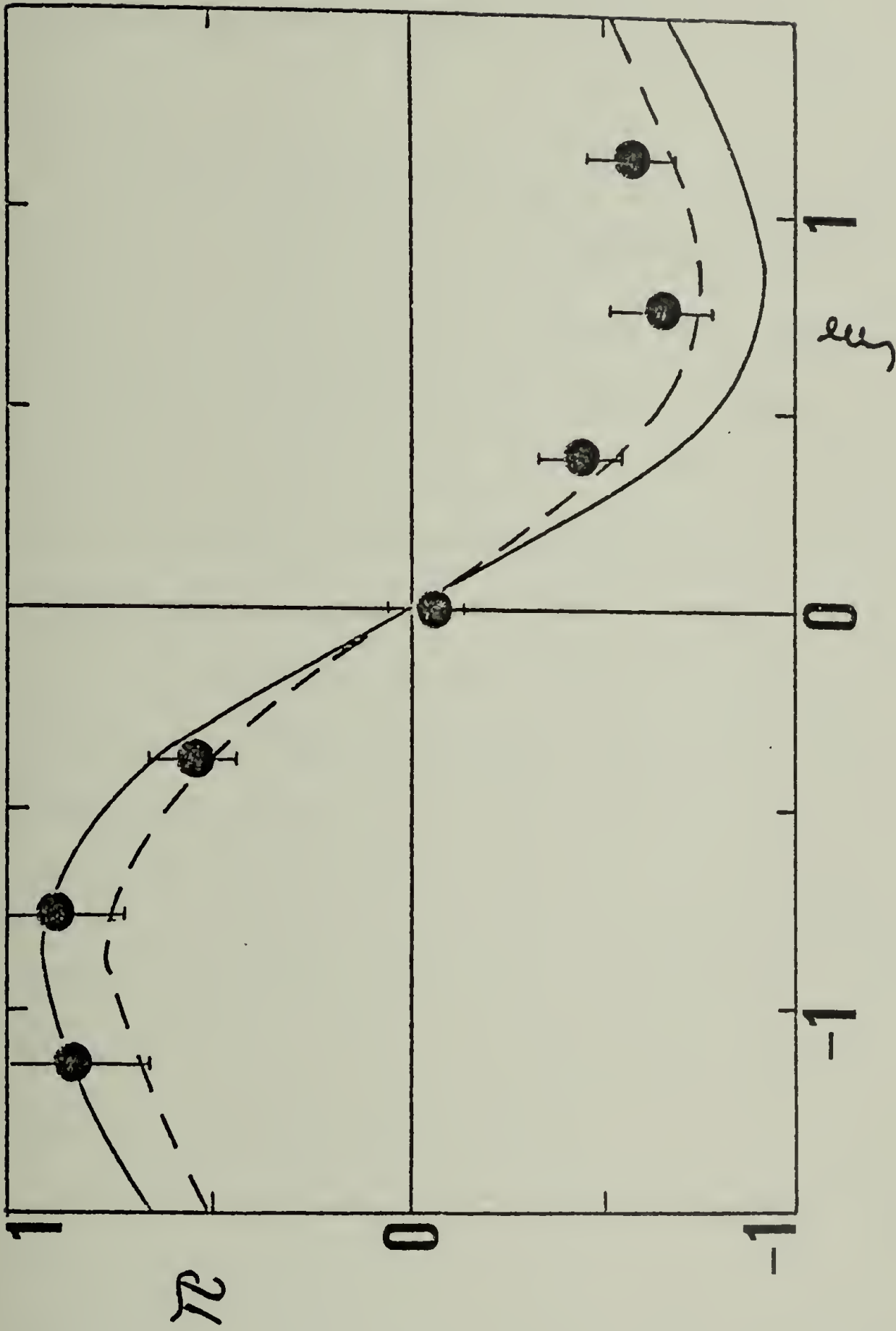
Figure VII-6. Experimental pressure distribution for Karo Syrup (27.8°c) in the submerged-roll system. The data are compared to the Newtonian lubrication solution (the solid curve) and to a numerical solution by FEM (the dashed curve).

readings gave consistently nearly the same values for the reduced pressure (within the experimental uncertainty) at all seven positions where readings were taken.

It is safe to assume that for a roll with length-to-diameter ratio of ~ 1.8 as in the present system the two-dimensional character of the flow is preserved and the contribution of end effects to the measured pressures is marginal (see Pinkus and Sternlicht 1961). However, the relatively large H_0/R in this run ($H_0 = 0.64$ cm., $R = 10.70$ cm.) raised some doubts about the validity of the lubrication solution for this particular geometry. To verify this, the full planar creeping flow problem was solved numerically by a Finite Element scheme that is detailed in Appendix D. The numerically calculated pressure distribution is presented in Figure VII-6. One important result of this "more exact" solution is that the level of the pressure is somewhat reduced in comparison to the approximate lubrication solution. The velocity field, however, was found nearly unaffected by this "geometry effect". Within the experimental uncertainity, the Newtonian data seem to validate the numerical result.

It was more difficult to assess the experimental data for the viscoelastic fluid. One handicap involved in the use of manometers for measuring "pressures" (or total normal tractions) generated by viscoelastic fluids, is the so-called "hole-pressure error". This error arises from the presence of a cavity adjacent to the flow field and it is directly related to the

rheological properties of the fluid (Pipkin and Tanner 1972, Novotny and

Eckert 1973, Higashitani and Lodge 1975). The "hole-pressure error" is

usually negative and its magnitude can be estimated from a well accepted

correlation (Higashitani and Lodge 1975) that reads:

$$\text{Perror} \cong -0.2\ (\tau_{xx} - \tau_{yy}) \qquad\qquad (\text{VII-18})$$

This correlation has proved valid for polymer solutions at low Reynolds

numbers. Thus, in order to have an estimate of the "hole-pressure error"

one has to have sufficient information as regards the first normal stress

difference at the position where the pressure reading is taken. $\tau_{xx} - \tau_{yy}$

can be evaluated from the available viscometric data once the local shear-

rate is known. In the present work, the local shear-rates were estimated

by making the crude but not unreasonable assumption that the flow field is

controllable; that is, the velocity field for a viscoelastic fluid is the same

as for a Newtonian fluid. While this assumption is identically correct for

a viscoelastic second order-fluid, it is less good for the viscoelastic fluid

that was studied in this experiment. In any case, this assumption admits

the evaluation of the shear-rate using the Newtonian lubrication solution,

and thus the first normal stress difference can be calculated at any position

in the vicinity of the nip.

Pressure readings, in this run, were taken for two speeds (53.1,

89.2 rpm) at seven positions relative to the nip. Also, the nip separation

for this run was set at $H_0 = 0.19$ cm. (i.e., $\frac{H_0}{R} = 0.0178$). Thus, it is

Figure VII-7. Experimental total (normal) stress distribution for H-1 in the submerged-roll system at two rotational speeds: 59.47 cm/sec. (O) and 99.92 cm/sec. (□). Full symbols represent the data corrected for the pressure-hole error.
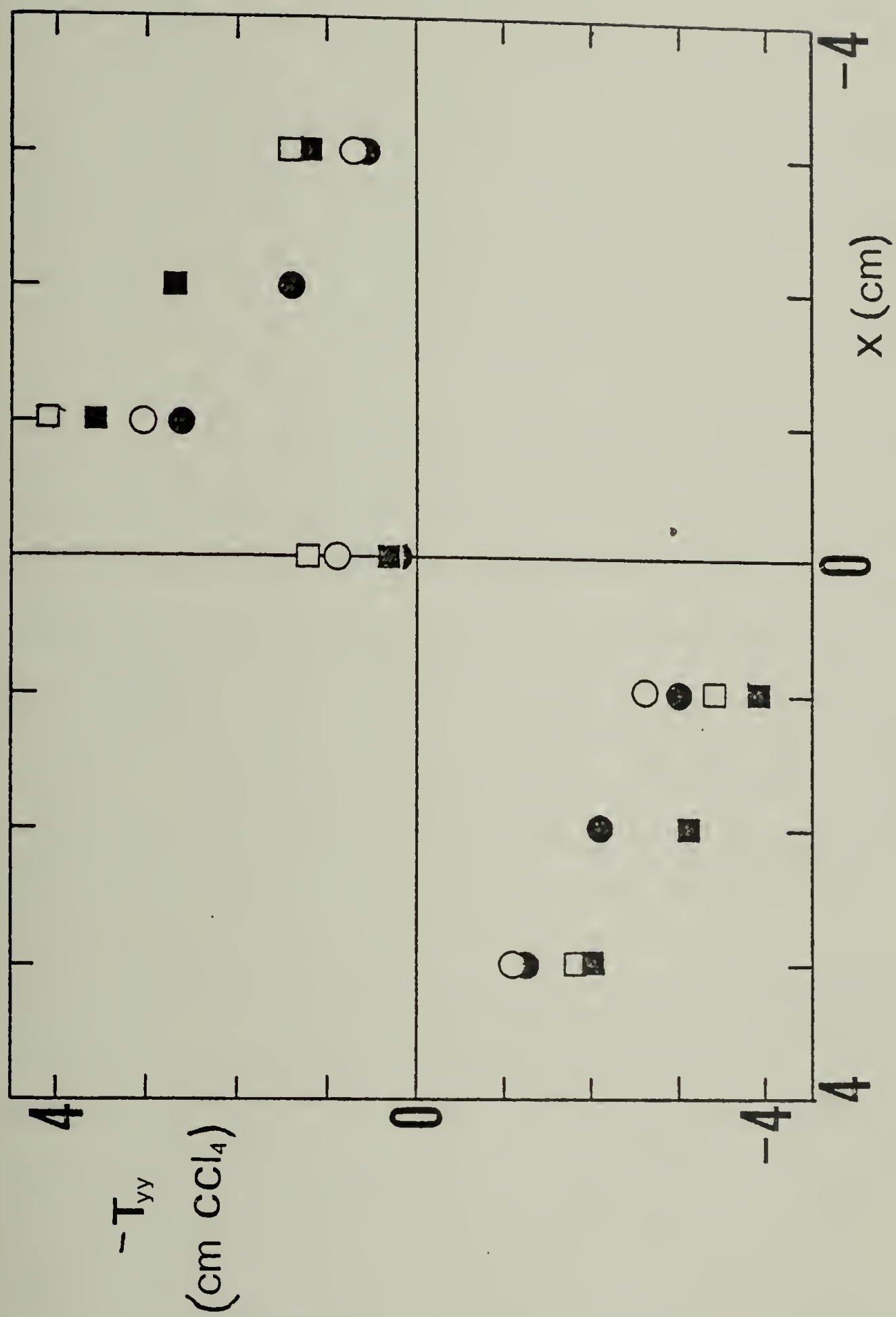
expected that the Newtonian lubrication solution for this geometry will be much closer to the "exact solution" than in the preceding run. The results are displayed in Figure VII-7 together with the corrections for the "pressure-hole error". The corrected pressures are then presented in a reduced form in Figure VII-8 where

$$\Theta_{\gamma\gamma} \equiv \frac{T_{\gamma\gamma} \; H_o^{3/2}}{\eta_a \; U \; R^{1/2}}$$

and η_a, the apparent viscosity, is evaluated at a nominal shear-rate of $(\frac{U}{H_0})$. According to this representation $\left| \frac{\pi_N}{\pi_{ve}} \right| < 1$. However, if the pressure is made dimensionless using the (estimated) zero-shear-rate viscosity (as in the perturbation analysis for the CEF fluid) then it is found that $\left| \frac{\pi_N}{\pi_{ve}} \right| > 1$ which is consistent with the result obtained in the CEF analysis. Furthermore, in conformity with the CEF solution, the experimental stress function appears to be antisymmetric with respect to the position of the nip ($\xi = 0$).

A more critical assessment of the data is not possible, as no 'exact' solution for a viscoelastic fluid is available at the present time. It can be concluded, however, that the experimental total-stress distributions conform qualitatively with the approximate analytical distributions for the CEF fluid. In addition, elastic effects are apparently suppressed by purely viscous effects as no "shift upward" of the total stress at the nip ($\xi = 0$) is observed within the experimental uncertainty.
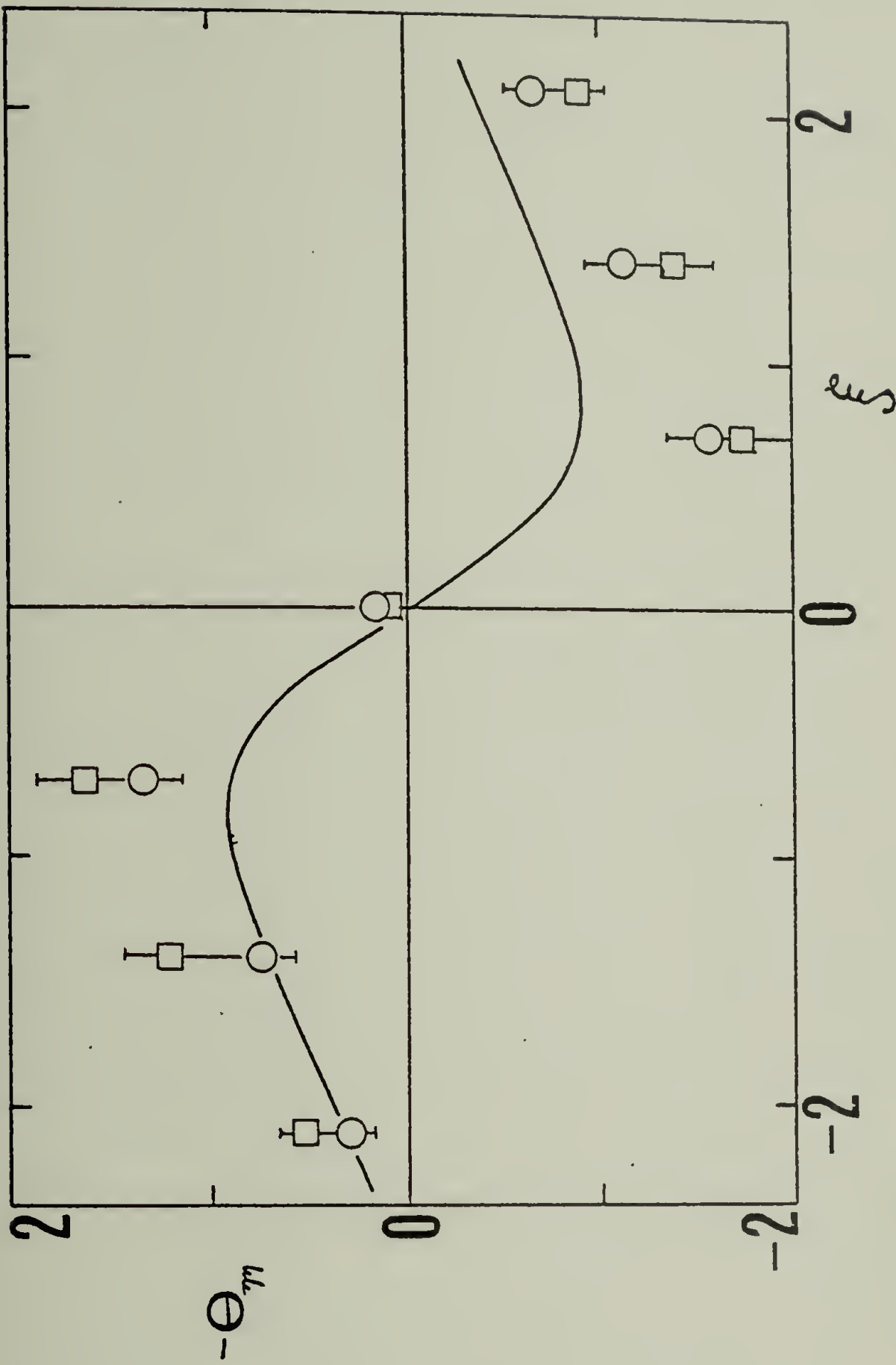
Figure VII-8. The corrected (reduced) total stress distribution for H-1 in the submerged-roll system. The experimental data are for two rotational speeds: 59.47 cm/sec. (O) and 99.92 cm/sec. (□). The solid curve is the Newtonian lubrication solution.

Inertia effects in this experiment were insignificant as the "nip"

Reynolds numbers, in both runs were small. (N_{Re} was less than 5 in the

'Newtonian' run and it was less than 20 in the 'viscoelastic' run.)

CHAPTER VIII

INSTABILITIES IN COATING FLOWS:
THE RIBBING PHENOMENON

VIII. 1 Background

In the roll coating analysis (VI. 2) the flow was assumed planar and hydrodynamically stable for the entire range of variation of the parameter N_S. It is, however, well established that unstable flow will ensue under some conditions. This will inherently restrict the effective range of stable coating and it is thus of interest to understand the nature and the mechanism of the instability encountered in coating flows. A brief survey of experimental and theoretical studies concerning this instability is presented in this section.

It is a common observation that when thick paint is applied onto a smooth surface by means of a soft brush thin ribs (or crests) appear on the coated surface running in the direction of brushing. A similar phenomemon is observed on coatings deposited by rolling contacts (such as journal bearings, cylinder-plane configurations and counter-rotating rollers) where evenly spaced ribs appear on the moving surfaces. A photograph portraying the "ribbing instability" is shown in Figure VIII-1. In this photograph, the ribbed coating is issuing from the nip region of a sheet-and-roll system, with the sheet and the roll moving in the same direction and at the same lateral speeds.

Figure VIII-1.   A pictorial view of the ribbing instability in a sheet-and-roll system.
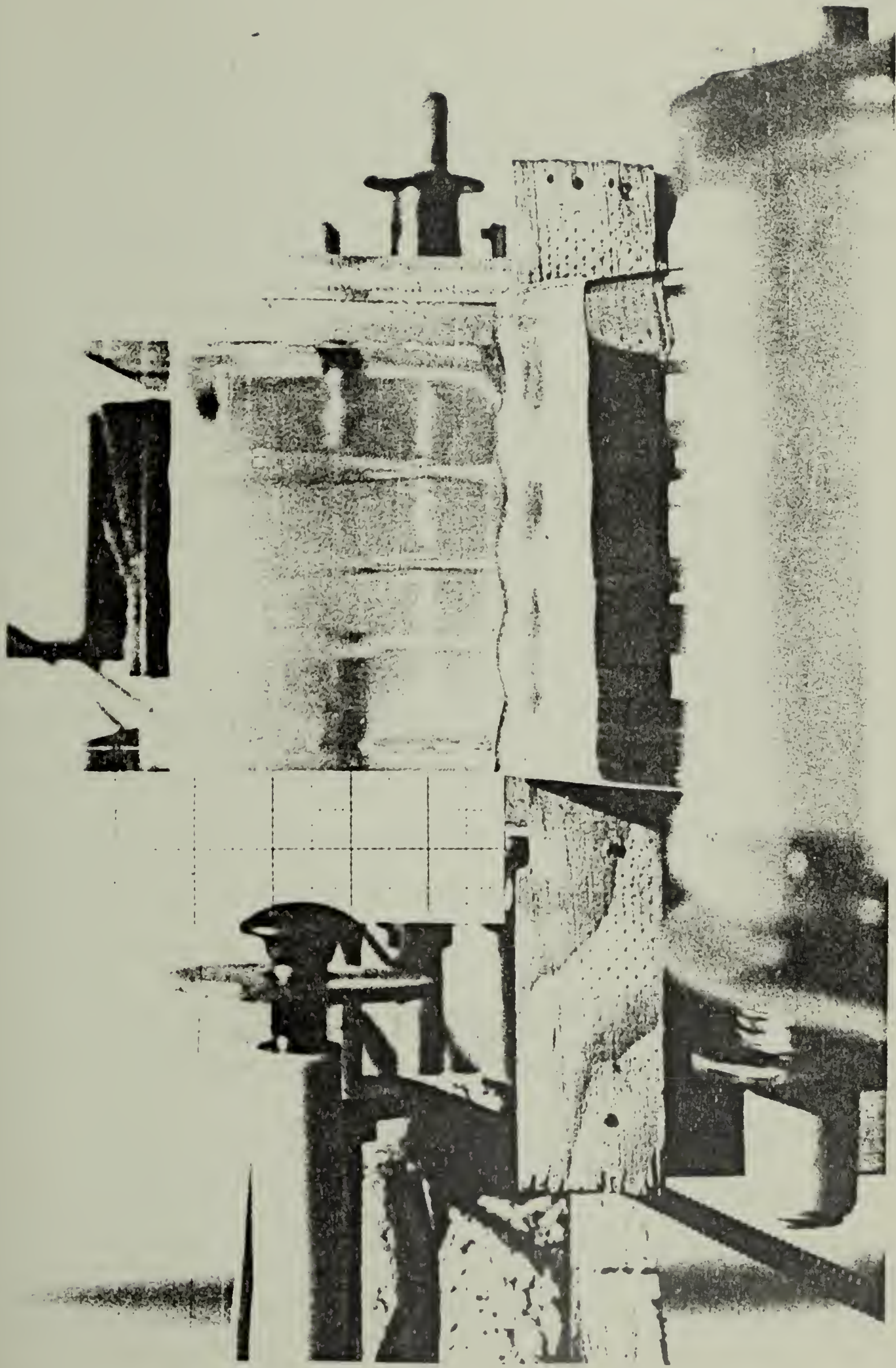
The first documented reference to the ribbing phenomenon was made in 1937 (Cf: Mill and South 1967) and it has since attracted considerable 'industrial' attention due to its obvious technological implications (especially in the photographic, painting and printing industries). Pearson (1960) cites some early industrial reports concerning the ribbing instability. This important problem has received relatively little attention in the open literature, however. The few analyses and experimental studies to date have dealt almost exclusively with Newtonian fluids and the results obtained so far are not conclusive as to the exact physical origin of the ribbing instability.

Pearson (1960) appears to be the first to undertake a theoretical study of this complex problem. By means of a linear stability analysis applied to the wide-angled wedge (v shaped) spreader, Pearson was able to show that the dimensionless group $\mu \bar{U}/\gamma$ (the capillary number) is central to the ribbing phenomenon. Lacking a suitable set of boundary conditions for the separation region, Pearson made some crude assumptions regarding these conditions. He was, nevertheless, able to obtain an expression relating the wave number of the nonuniform coating to the capillary number, which agreed favorably with some of his experimental data, especially for high $\mu U/\gamma$. Pearson's theory, however, did not yield an explicit stability criterion.

An important contribution to the understanding of this problem was made by Pitts and Greiller (1961). They investigated the system of counterrotating rollers and were able to devise a stability criterion that qualitatively

agreed with their experimental data. As was noted earlier (VI.3.1), Pitts and Greiller used an approximate theory for determining the shape and position of the separation meniscus. This allowed them to improve somewhat the basic ideas put forth by Pearson.

Their stability theory consists of two parts. First, they attempt to derive a criterion based on some plausible physical statements regarding the dynamics of the separation region. This "physical analysis" yields

$$N_{Ca1}^{*} \cong 10 \tag{VIII-1}$$

where

$$N_{Ca1} \equiv \frac{U\mu}{\sigma} \frac{R}{H_0}$$

and the superscript * means "evaluated at the onset of ribbing". (Note that H_0 is half the gap thickness.) Then they carry out a more exact linear stability analysis, which gives

$$N_{Ca1}^{*} \cong 28 \tag{VIII-2}$$

This is a slight improvement over the previous result as their experimental value for N_{Ca1}^{*} was $62(\pm 15)$. Pitts and Greiller attributed this apparent discrepancy to the crudeness of both their theory and their experimental technique.

A more refined experimental study of this phenomenon was reported by Mill and South (1967). They used pairs of counter-rotating rollers with equal and non-equal radii and arrived at the following stability criterion, based solely on their experimental observations:

$$N_{Ca2}^{*} \cong 10.3 \tag{VIII-3}$$

where

$$N_{Ca2} \equiv \frac{U\mu}{\tau} \left(\frac{R}{2H_0}\right)^{3/4}$$

This result is seemingly not in accord with Pitts and Greiller's criterion.

A more recent account of this problem was given by Savage (1977a). In his analysis Savage made use of the same physical criterion originally proposed by Pitts and Greiller. But, unlike Pitts and Greiller, Savage combined this criterion with the rigorous Coyne and Elrod condition (see IV.4) for the separation region. This resulted in a marginal stability line that gives the variation of the critical capillary number (N_{Ca}^{*}) with the geometric parameter H_0/R. The functional dependence of N_{Ca}^{*} on H_0/R is quite complex and it cannot be cast in the form of a single critical number as in the aforementioned cases. Savage presented few experimental points for a cylinder-plane system that agree well with his predictions. It is regretable, however, that very little was said about the experimental procedure used.

In a companion paper, Savage (1977b) carried out a linear stability analysis which, again combined with the Coyne and Elrod condition, gives a relation between the wave number, the capillary number and the geometry. His solution exhibited a bifurcation point which implies mathematical (and possibly physical) non-uniqueness.

All that has been said so far applies exclusively to Newtonian fluids. The ribbing phenomenon extended to viscoelastic fluids was given very little attention in the literature. Sone et al. (1963) report on some experiments in which viscoelastic fluids (irradiated silicone oils) exhibit ribbed patterns in roll-milling with the relaxation time having generally an enhancing effect. Ribbed patterns produced with viscoelastic fluids were also reported by Eckert and Novotny (1973). These patterns, however, were observed for viscoelastic fluids (aqueous solutions of Polyox) issuing from a narrow (and uniform) channel where the fluids were subject to a Poiseuille-type flow. This case is evidently different from the cases discussed above and it may well correspond to an altogether different phenomenon.

A more critical assessment of the various Newtonian stability criteria together with additional data for Newtonian fluids are presented in the following section. Then, in Section 3, experiments with viscoelastic fluids are described and discussed in detail. The strong destabilizing effect of viscoelasticity that was observed experimentally is rationalized in the context of a physical stability analysis that is developed in Section 4.

VIII. 2 Some Observations on the Newtonian Ribbing Instability

The onset of ribbing and the nature of the instability for Newtonian fluids were investigated and are reported in this section. The experiments conducted were limited in scope as they were aimed at providing a comparative basis for the more extensive study on the stability of viscoelastic fluids

in roll coating which is reported in the following section. These experiments, nevertheless, cover a wide range of fluid properties, and the results obtained are compared with earlier studies on the ribbing phenomenon.

The experimental system used for this investigation is identical to the one employed in the study of stable roll coating and it is described in detail in VI.4. The system of counter-rotating rollers was selected for this study as it enables a relatively simple and reliable measurement of the critical speed, and it allows a direct comparison with the experimental data of Pitts and Greiller (1961) and Mill and South (1967).

The experimental procedure is as follows. A fresh sample of fluid was placed in the square acrylic box filling it up to the level of the axes of the steel rollers. The rollers were then set in motion and their speed was gradually increased until ripples were first seen on the concave inter-face between the rollers. This process was repeated many times to insure consistent observation. It was, nonetheless, difficult to determine the speed at which ribbing first appeared with sufficient accuracy, and the sizable experimental error reflects this uncertainty. In a second experiment, photographs of the wavy surfaces were taken (with a 35 mm SLR Nikon F2 camera and Kodak Tri-X film). These photographs were used for deter-mining the variation of the wavelength of the perturbed coating with speed. All the experiments were carried out at room temperature $(24 \pm 3^{\circ}c)$. The temperature was recorded and the viscosities of the test fluids were

measured at the temperature of the corresponding experiment.

Table VIII-1 lists the various fluids used, their respective properties and the averaged critical speeds observed. The results are presented graphically in Figure VIII-2 where the modified capillary number, N_{Ca1}^*, is plotted against the "nip" Reynolds number ($N_{Re} = \rho H_0 U / \mu$). The resulting correlation suggests that N_{Ca1}^*, proposed originally by Pitts and Greiller (1961), is indeed adequate for characterizing the Newtonian ribbing instability, at least for the range of capillary numbers encountered, as this number is nearly constant for a wide range of variation of the Reynolds number. In all the cases considered, gravity and inertia effects were evidently unimportant, as $N_{Re}^* < 1.0$ and $N_g^* < 0.01$ for all the fluids studied. The quantitative agreement of the data with Pitts and Greiller's work is somewhat less satisfactory. As was noted in Section 1 the experimental value for N_{Ca1}^* obtained by Pitts and Greiller was $62(\pm 15)$. This number is low compared to $93(\pm 20)$ obtained in this work. The experimental difficulty involved in determining the exact critical speed may well explain this gap. Mill and South's (1967) data, recalculated in terms of N_{Ca1}^*, give $N_{Ca1}^* = 70-110$ (for their combination "B"). This range agrees more favorably with the results of this work. On the other hand, the empirical criterion suggested by Mill and South, namely $N_{Ca2}^* = 10.3$, is not nearly in as good agreement with our observation of $N_{Ca2}^* = 19.1 \pm 4$. On the basis of the present work it is not possible to determine which of the two criteria,

Table VIII-1

The Newtonian Ribbing Phenomenon:
Observed Critical Speeds

Fluid[1]	μ[2] [poise]	H_0/R	$U*$[3] [rpm]
Glycerin (G)	10.5	0.0129	26 ± 3
Karo Syrup (KS)	28.5	0.0228	21 ± 3
GW-0.90	2.30	0.0129	146 ± 15
GW-0.95	5.01	0.0129	56 ± 5
Motor-Oil (MO)	1.44	0.0129	110 ± 10
GWS-0.90	2.50	0.0129	49 ± 5

[1] More complete information for the fluids listed is given in Table VI-4.

[2] Viscosities measured at the room temperature for the corresponding runs.

[3] Errors represent standard deviation for repetitive trials.
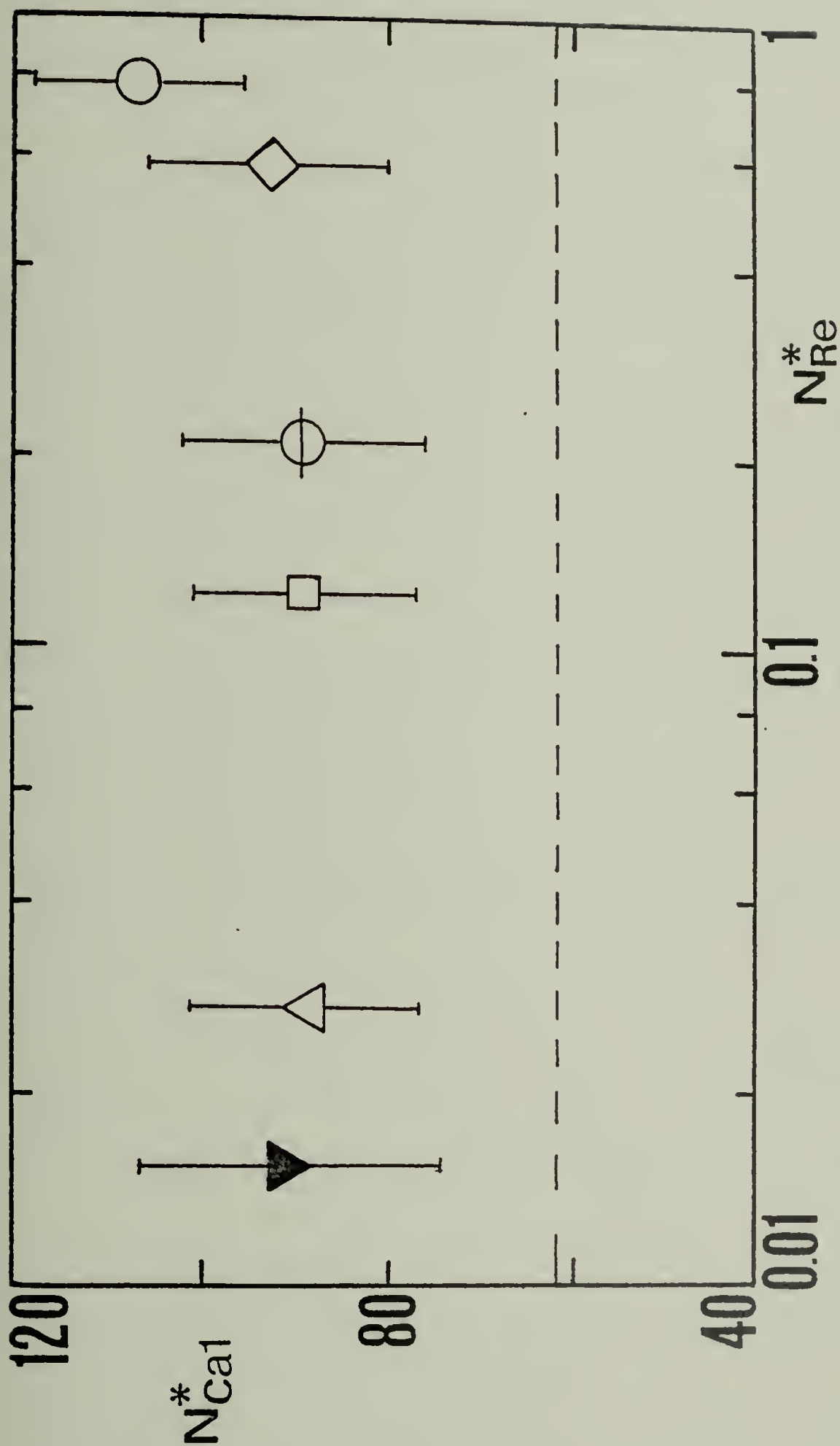
Figure VIII-2.   The critical modified capillary number vs. the "nip" Reynolds number.   Experimental data for Newtonian fluids in the system of half-immersed counter-rotating rollers. The dashed-line is Pitts and Greiller's (1961) experimental result.   (Key in Table VI-4.)

N_{Ca1}^* or N_{Ca2}^*, is more appropriate inasmuch as the variation of the parameter H_0/R is quite limited and the experimental uncertainty involved in measuring the critical speed is considerable.

The various criteria can be most conveniently cast in the form of limiting stability curves of log (N_{Ca}^*) vs. log (H_0/R). Such a representation allows to examine Savage's criterion in relation to the other available stability conditions, both theoretical and empirical. In his analysis, Savage derives a stability criterion for a cylinder-plane configuration (rotating cylinder-stationary plane). He also gives the relevant equations for the system of counter-rotating rollers without explicitly deriving the dependence of H_0/R on N_{Ca}^*. The necessary calculation was carried out (see Appendix E) and the result for counter-rotating rollers is presented in Figure VIII-3 along with the theoretical and empirical criteria of Pitts and Greiller and Mill and South. Close examination of this figure reveals that the slopes of the empirical curves seem to conform locally with Savage's theory. Yet, the various empirical results fall well within the envelope formed by Savage's criterion. The significant numerical difference between the experimental data and Savage's theory does not necessarily repudiate this theory. Savage maintains that his condition is necessary but not sufficient for ribbing to arise. Moreover, he shows that a bifurcation point exists beyond which the solution to the equations considered is non-unique. Only one branch of the double-valued solution, Savage claims, is physically
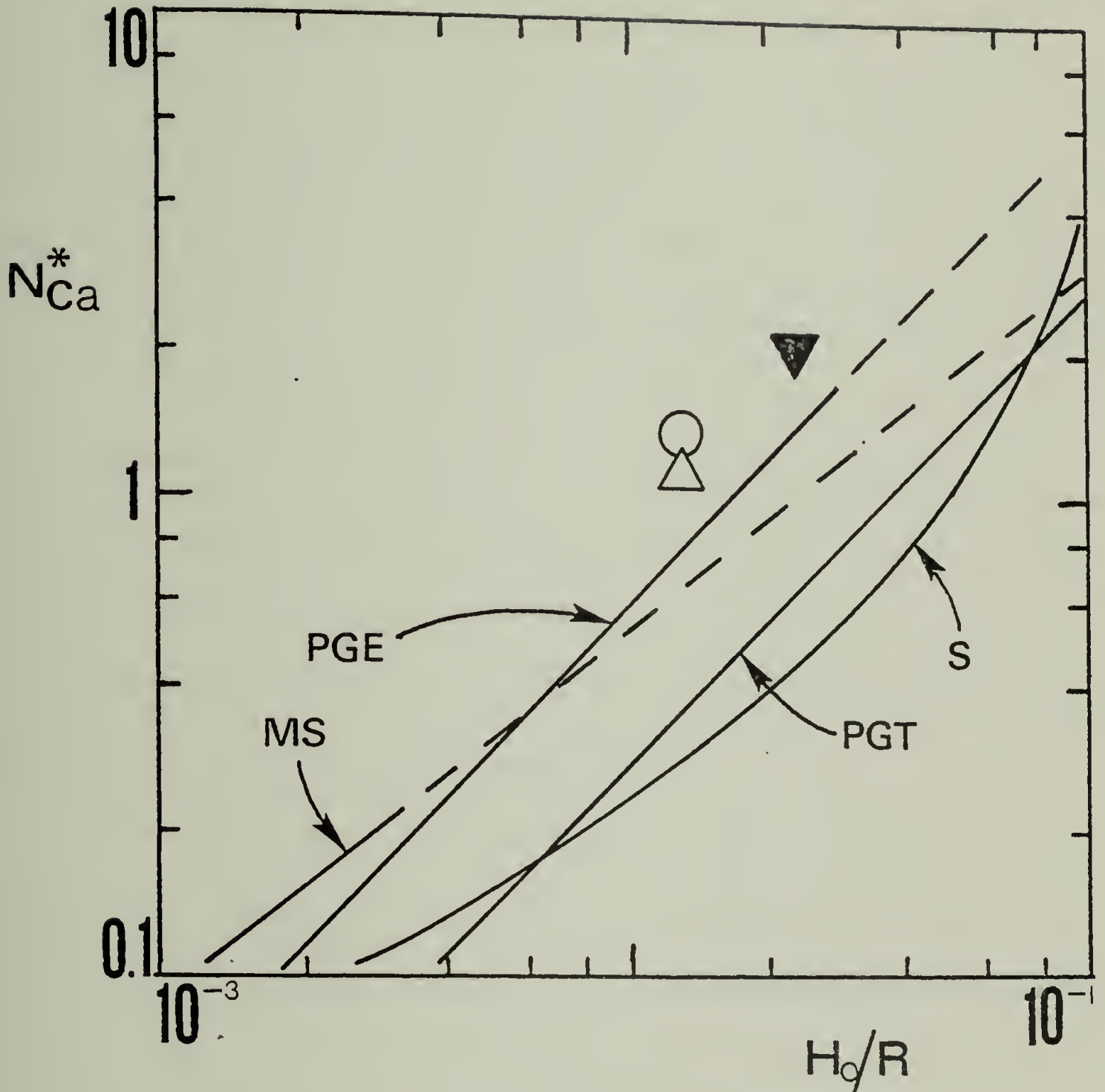
Figure VIII-3. The critical capillary number vs. H_0/R. Experimental data of the present work (Key in Table VI-4) are compared to the modified Savage (1977a) theory (S), Pitts and Greiller's (1961) theory (PGT), Pitts and Greiller's experimental result (PGE) and Mill and South's (1967) experimental result (MS). The dashed lines are extrapolations of empirical curves.

admissible as the total energy for this branch is minimized. This latter

argument may suggest that his stability criterion is, in fact, a global

(universal) criterion rather than a neutral stability limit (Riley 1975). This

implies that the domain "below" the stability curve in Figure VIII-3 will be

globally stable whereas the domain "above" the curve will be conditionally

(asymptotically) stable. It is to be expected that the neutral stability curve

beyond which instability is guaranteed will lie somewhere above Savage's

global stability curve and perhaps much closer to the experimental data.

Further theoretical studies are needed in order to devise the more useful

neutral stability condition for this problem. Likewise, more data need to

be gathered over a wider range of H_0/R's in order to have a more complete

picture of the Newtonian ribbing phenomenon.

Some photographs showing the ribbing instability (for Glycerin) at

various roller speeds are presented in Figure VIII-4. A common feature

to all the fluids tested is the insensitivity of the wavelength of the unstable

coating to roller speed. It was observed, in fact, that the wavelength

decreases from infinity, at the onset, to some asymptotic value, W_0, at a

speed $\sim 10\%$ higher than the critical speed. This observation is compatible

with a similar observation made by Mill and South (1967) for much lower

H_0/R's.

Wavelength measurements were made for three Newtonian fluids:

Glycerin, Karo Syrup and GWS-0.90. In analyzing the corresponding

Figure VIII-4. Photographs of the Newtonian ribbing instability.
a. Glycerin, 20 rpm, set #2.
b. Glycerin, 100 rpm, set #2.
c. Glycerin, 150 rpm, set #2.
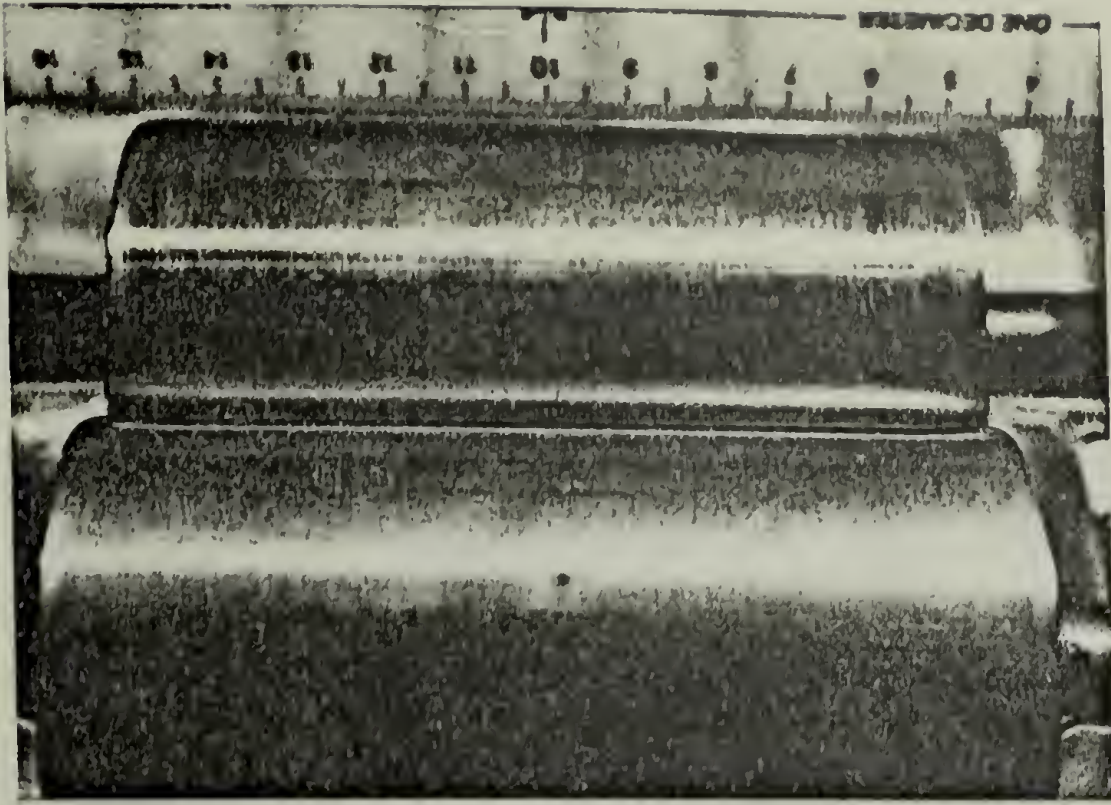
a
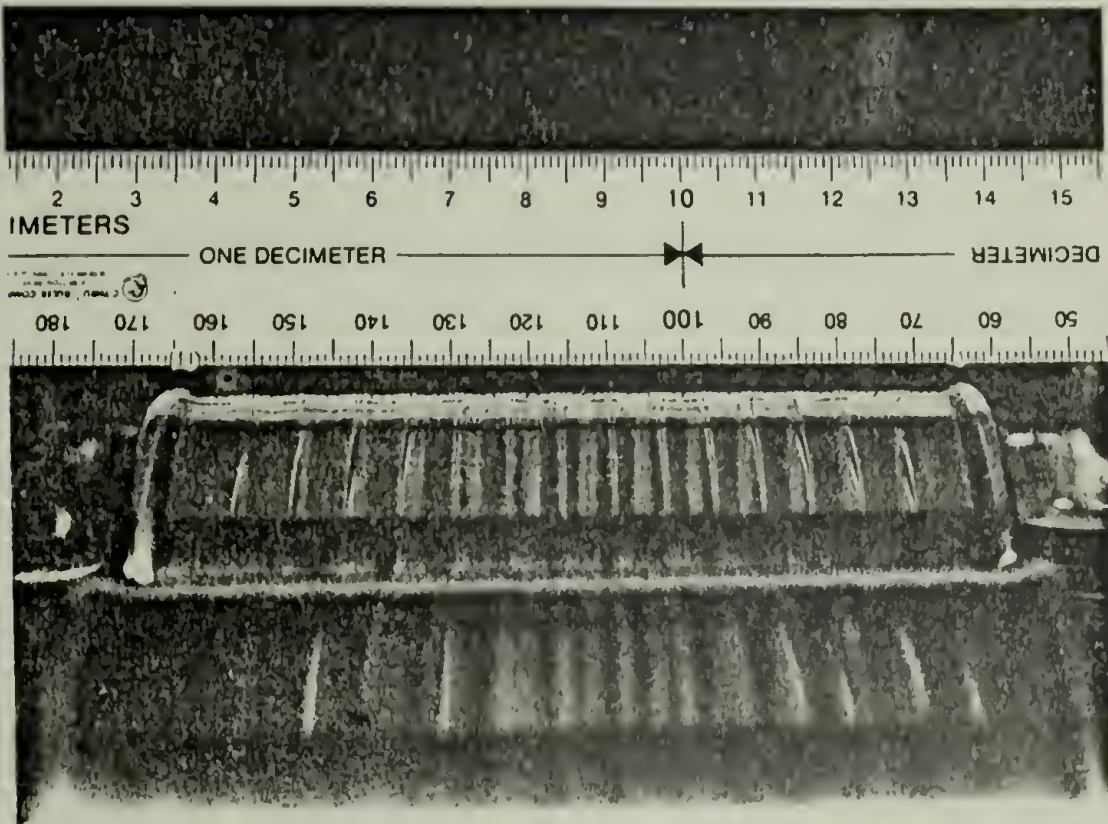
b
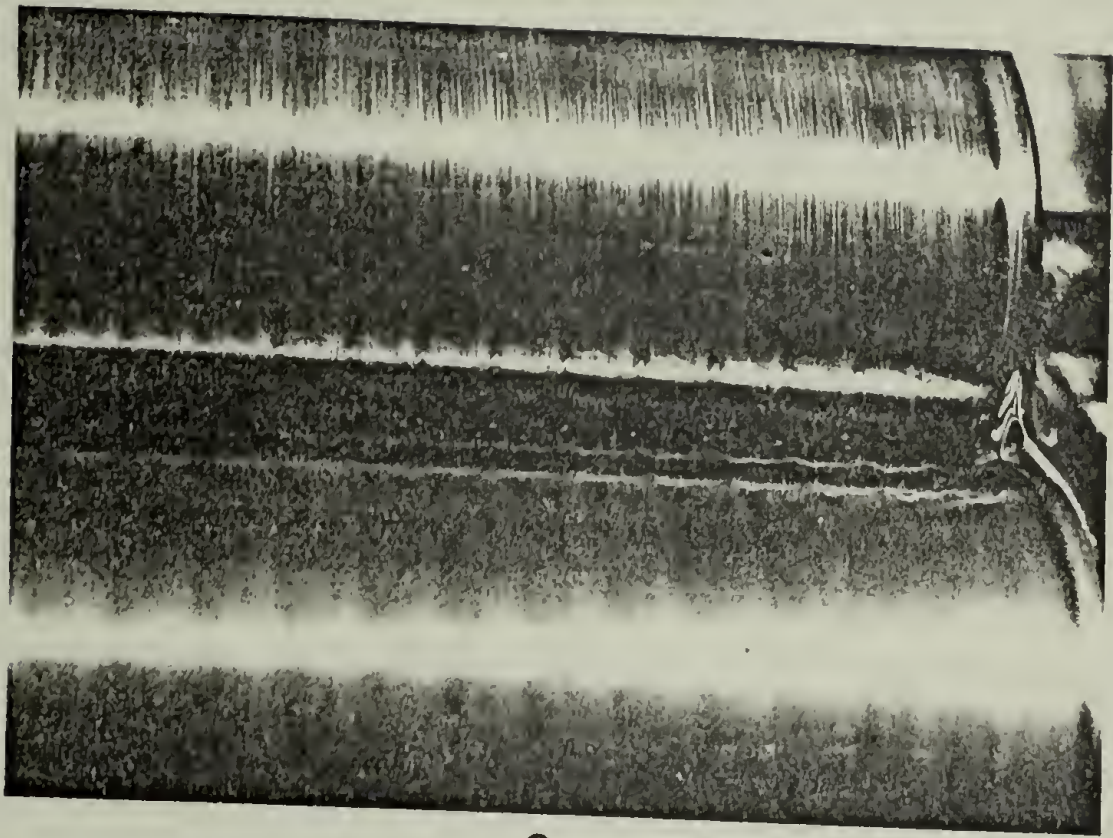
C

photographs waves near the edges of the rolls were excluded due to possible end effects. The final results are listed in Appendix A. and are presented in Figure VIII-12. The respective values of $(W/2H_0)$av. for Glycerin, Karo Syrup and GWS-0.90 are: 11.0, 9.7 and 16.0, which compares favorably with Mill and South's data (11.5-15.8). They noted that these numbers are independent of the capillary number for $N_{Ca} > 2.4$.

The data presented above can be similarly compared to Savage's theory (Part II) (1977b) which permits the determination of the wavenumber $(2\pi/W)$ as a function of the geometry (H_0/R) and the capillary number. Being formulated for the cylinder-plane geometry, Savage's theory needed some modification in order to be used in the case of counter-rotating rollers. These modifications have been worked out and are detailed in Appendix F. A comparison of the calculated $(W/2H_0)$'s to the observed values is presented in Figure VIII-5. It is noted that the calculated curves display a clear dependence on the capillary number unlike the observed values. Savage's theory should be commended, however, for approaching the observed values in the limit of small capillary numbers. Savage also observed a better fit of his data to the theory at low capillary numbers.

VIII.3 Observations on the Viscoelastic Ribbing Instability

As many coating materials are viscoelastic it would seem appropriate to extend the study of the ribbing phenomenon to viscoelastic fluids. This will be the subject of this and the following sections.

Figure VIII-5.   The normalized wavelength vs. the capillary number. Experimental data for Newtonian fluids are compared to the modified Savage (1977b) theory (the solid curves): See Table E-1.   (Key in Table VI-4.)
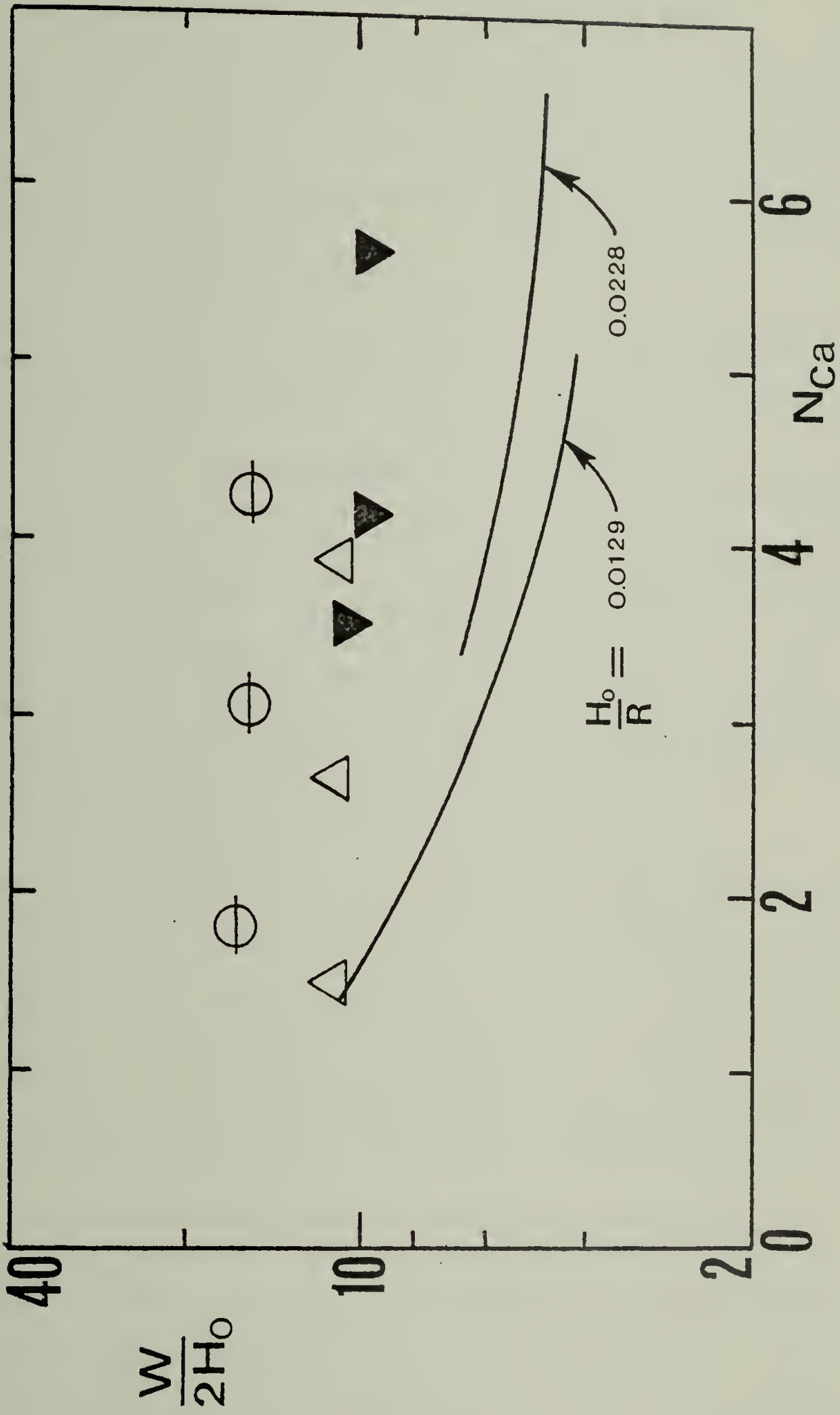
The following questions are posed from the outset:

1.   How do viscoelastic fluids compare phenomenologically to Newtonian fluids in the inducement and the nature of the ribbing instability?

2.   What are the dimensionless groups, viscoelastic and other, that govern the formation of ribs?

3.   What are the proper stability criteria for viscoelastic fluids? An attempt to answer these questions, at least partially, will be made in Sections 3 and 4.   Experimental observations on the ribbing phenomenon in viscoelastic systems are reported in this section, and the results are discussed and compared to corresponding observations in Newtonian systems. In Section 4 a simplified physical stability analysis is carried out with a modest attempt to elucidate the mechanism of rib formation and establish useful stability criteria for viscoelastic fluids.

The experimental procedure in this study follows closely the procedure described in the previous section, with viscoelastic fluids replacing the Newtonian fluids considered there.   A series of aqueous solutions of polyacrylamide in a concentration range of 0.15-0.75% by wt. were used.   As these materials are identical to those considered in Chapter VI the relevant information concerning these fluids together with their viscometric properties are given in VI.4.3.   A detailed description of the experimental system (counter-rotating rollers) can be found in VI.4.2.   Essentially, two pieces of information were sought in the course of this experiment,

1) the critical speed (U*) at which nonuniform coating first appeared, and

2) the wavelength of the unstable coating and its variation with speed.

The critical speed was determined, as before, by a careful observation of the concave interface between the rotating rollers while gradually increasing the speed of rotation.

This was repeated for each fluid at three different geometries (i.e., different H_0/R's). A common feature for all the viscoelastic fluids studied was the sharp transition from stable to unstable flow. In contrast to Newtonian fluids, the critical point was easily noticeable and the results obtained were highly reproducible. Table VIII-2 lists the measured critical speeds. In order to correlate these data in a coherent and meaningful way it is necessary to decide what are the important dimensionless groups that describe best the physical process considered.

In the Newtonian case, it was shown that the capillary number (or rather N_{Ca1}) governs the phenomenon of rib formation. From the observations on viscoelastic fluids it is evident that elasticity plays a major role in controlling the onset of ribbing. In addition, preliminary calculations showed that, unlike the Newtonian case, gravity and possibly inertia need to be considered in the assessment of the instability. Consequently, the following dimensionless groups are used for correlating the data:

the "recoverable shear": $\qquad SR(\dot{\gamma}) = \dfrac{\Psi_{12}(\dot{\gamma})}{2\eta(\dot{\gamma})}\dot{\gamma}$ $\qquad$ (VIII-4)

the gravity number: $\quad Ng(\dot{\gamma}) = \dfrac{\rho g H_0^2}{\eta(\dot{\gamma})U}$ $\qquad$ (VIII-5)

Table VIII-2

The Viscoelastic Ribbing Phenomenon:
Observed Critical Speeds

Fluid [1]	H_0/R	$U*^2$[rpm]
H-0. 15	0. 0129	100
"	0. 0228	152
H-0. 25	0. 0129	48
"	0. 0228	64
"	0. 0306	92
H-0. 35	0. 0129	28. 5
"	0. 0228	38. 5
"	0. 0306	51
H-0. 50	0. 0129	16.
"	0. 0228	22. 5
"	0. 0306	29
H-0. 75	0. 0129	9. 5
"	0. 0228	12. 5
"	0. 0306	15. 5
HS-0. 35	0. 0129	26. 5
"	0. 0228	37
"	0. 0306	50
HS-0. 50	0. 0129	17. 5
"	0. 0228	23. 5
"	0. 0306	29. 5

[1] More complete information for the fluids listed and a key to the codes is given in Table VI-4.

[2] $\pm$2, 3, standard deviationfor repetetive trials.

the modified capillary number:

$$N_{Ca1}(\dot{\gamma}) = \frac{\eta(\dot{\gamma})U}{\dot{\gamma}} \frac{R}{H_0}$$ (VIII-6)

and,

the Reynolds number:

$$N_{Re}(\dot{\gamma}) = \frac{H_0 U \rho}{\eta(\dot{\gamma})}$$ (VIII-7)

In addition, the geometrical shape factor, H_0/R, is considered.

Numerical evaluation of the various dimensionless groups is possible only after a nominal shear-rate has been specified, since the fluids under consideration have shear-rate dependent properties. Without an a-priori knowledge of the origin of the viscoelastic instability it is reasonable to select one of the following nominal shear-rates:

$$\dot{\gamma}_{N1} = \frac{U}{H_0}$$ (VIII-8)

and

$$\dot{\gamma}_{N2} = \frac{U}{(RH_0)^{1/2}}$$ (VIII-9)

$\dot{\gamma}_{N1}$ loosely represents shear-rates in the nip region, whereas $\dot{\gamma}_{N2}$ is a characteristic shear-rate for the separation region. Both shear-rates will be used for correlating the data and it will ultimately be decided, on the basis of the resulting correlations, which one is more appropriate.

Inasmuch as elasticity was found to have a strong effect on the critical speed, the recoverable shear, representing the relative elasticity of the fluid, was selected as a principal correlating parameter for the data. The

variation of S_R with the other dynamic parameters is presented in Figures VIII-6 to VIII-9 for both nominal shear-rates. Close examination of these figures reveals the following:

1. Surface-tension (or the capillary number) is apparently unimportant in the rib-formation process for the viscoelastic fluids studied. The fluids H-0.35 and H-0.50 are nearly identical rheologically to HS-0.35 and HS-0.50 respectively. However, the surface tensions of the latter fluids are about one-third those of the former (see Table VI4for details). The sizeable difference in surface tension had only a marginal effect on the critical speeds. This observation clearly illustrates the difference between Newtonian systems (where surface-tension is central) and the viscoelastic systems considered in this experiment.

2. On the basis of the "goodness of correlation" as judged by eye, $\dot{\gamma}_{N2}$ seems better suited than $\dot{\gamma}_{N1}$ for correlating the data. As was noted previously, $\dot{\gamma}_{N2}$ is representative of shear-rates in the neighborhood of the separation region. This may indicate that events in the separation region, rather than in the nip region, control the viscoelastic ribbing instability.

3. From the given correlations it appears that gravity and viscoelasticity govern the ribbing phenomenon. The apparent effect of viscoelasticity is to destabilize the flow, as small increase in polymer concentration resulted in a considerable reduction in the critical speed. Furthermore, the
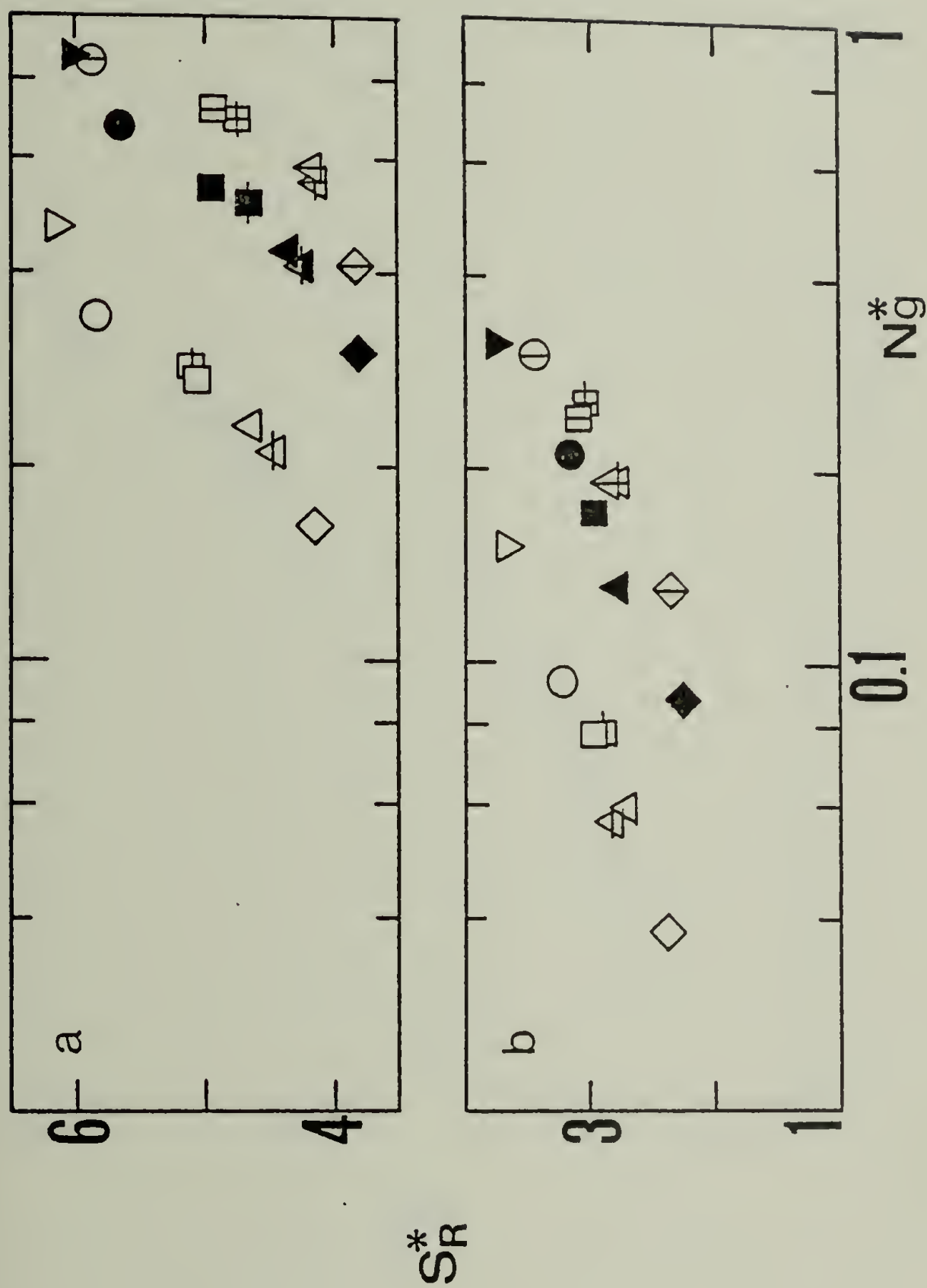
Figure VIII-6. The critical recoverable-shear vs. the critical gravity number. Experimental data for viscoelastic fluids presented for two nominal shear-rates: (a) $\dot{\gamma}_N = U/H_0$, (b) $\dot{\gamma}_N = U/(RH_0)^{1/2}$. (Key in Table VI-4.)
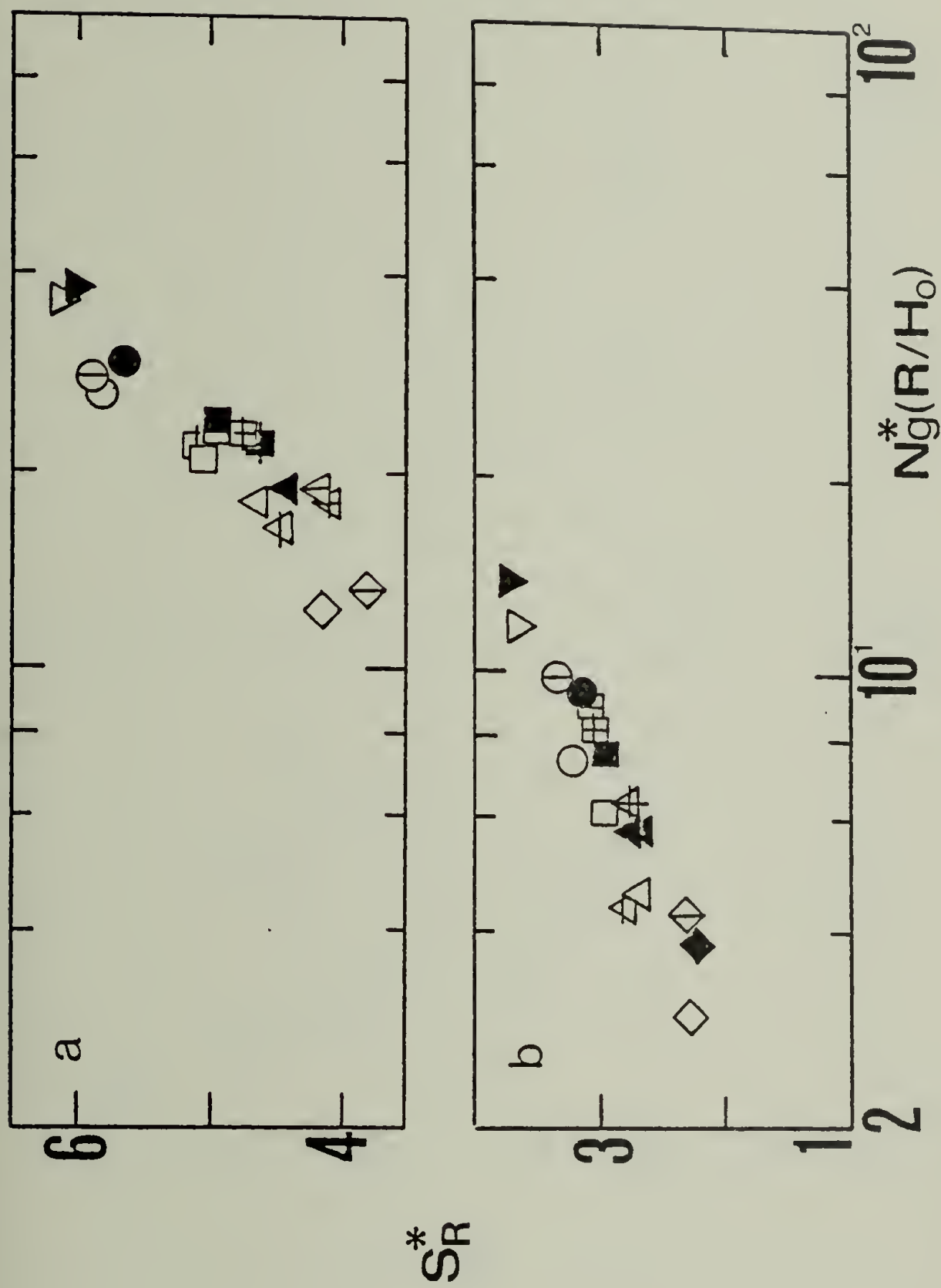
Figure VIII-7. The critical recoverable shear vs. the critical modified gravity number. Experimental data for viscoelastic fluids presented for two nominal shear-rates: (a) $\dot{\gamma}_N = U/H_0$, (b) $\dot{\gamma}_N = U/(RH_0)^{1/2}$. (Key in Table VI-4.)
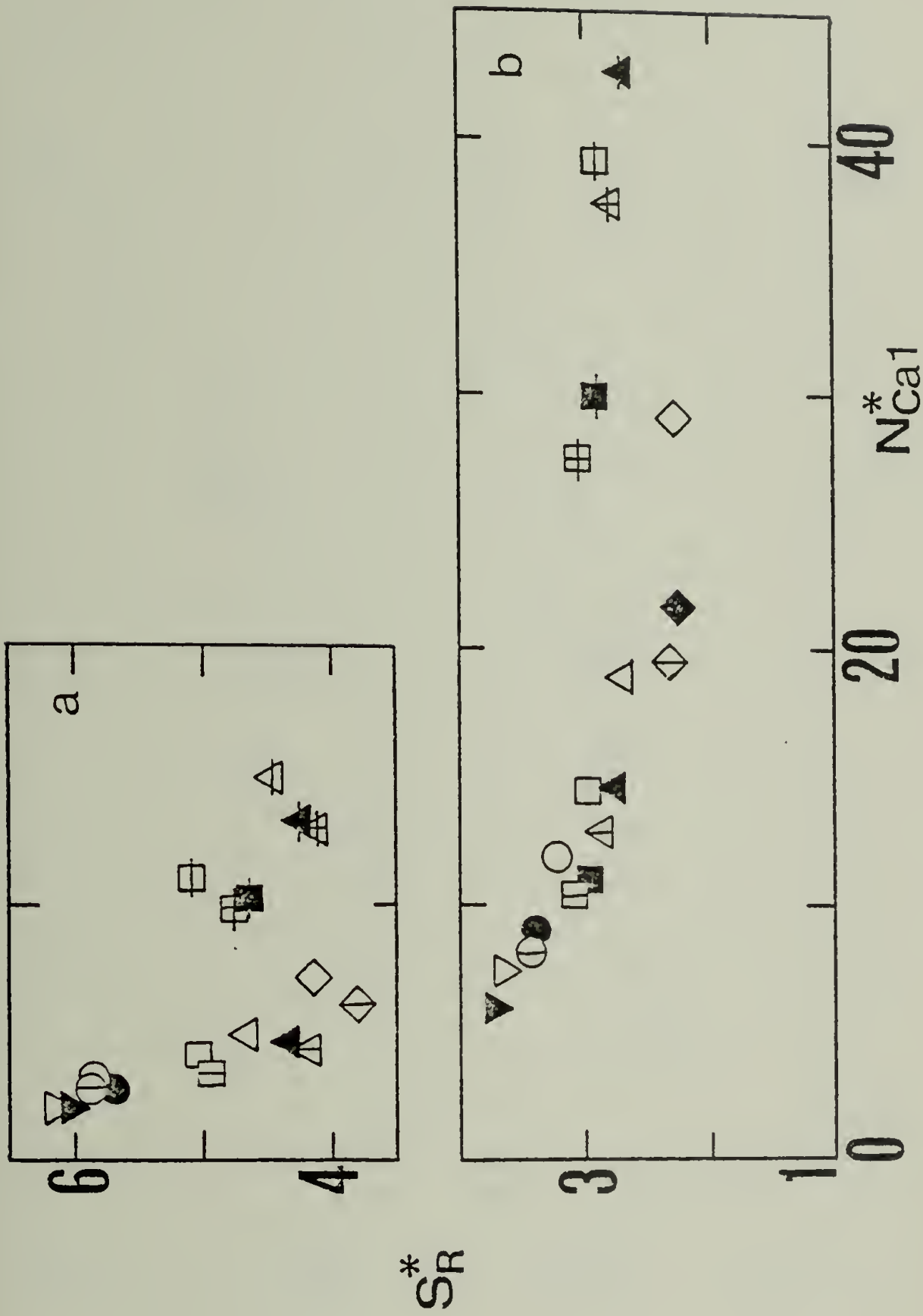
Figure VIII-8. The critical recoverable shear vs. the critical modified capillary number. Experimental data for viscoelastic fluids presented for two nominal shear rates: (a) $\dot{\gamma}_N = U/H_0$, (b) $\dot{\gamma}_N = U/(RH_0)^{1/2}$. (Key in Table VI-4.)
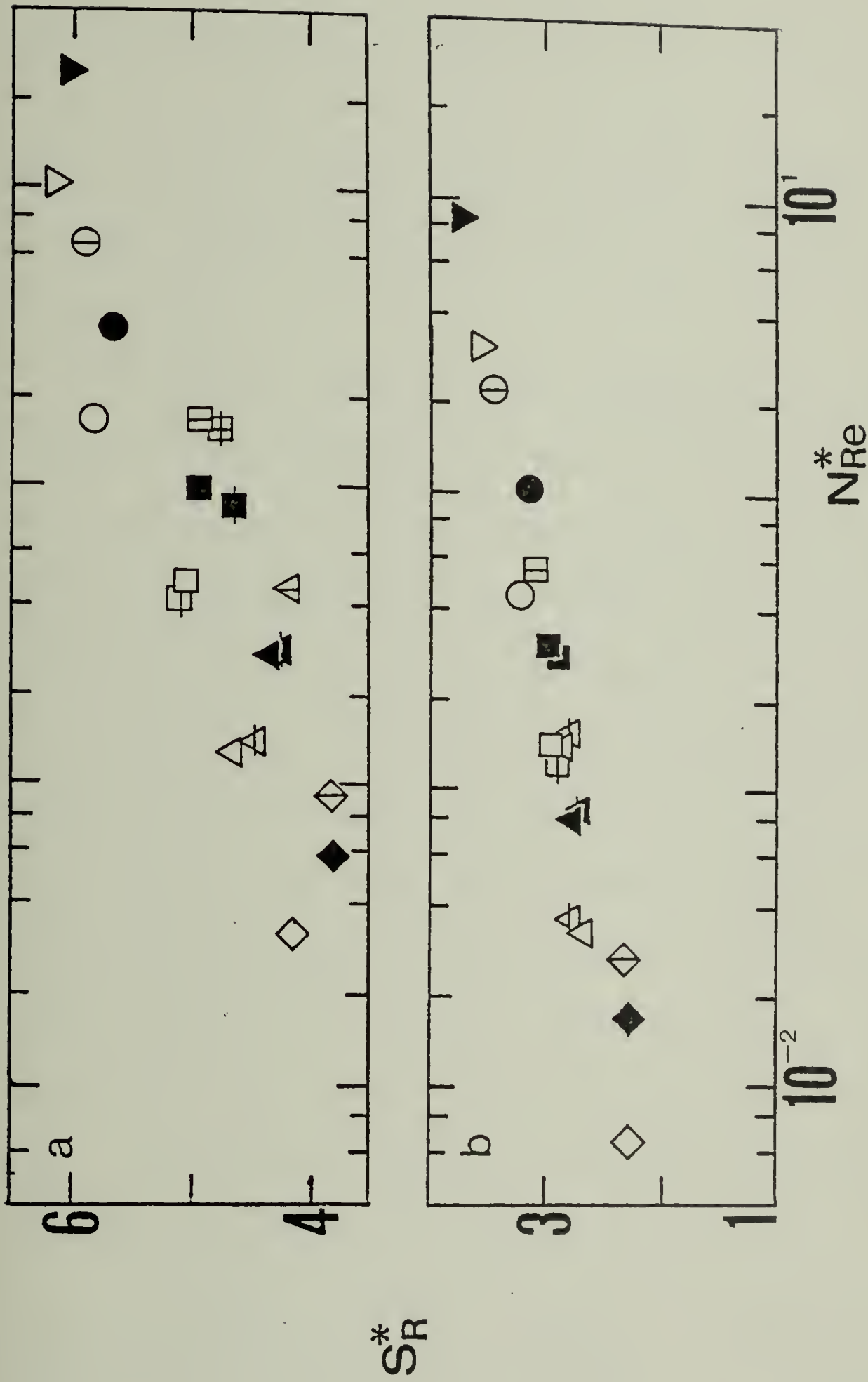
Figure VIII-9. The critical recoverable shear vs. the critical Reynolds number. Experimental data for viscoelastic fluids presented for two nominal shear-rates: (a) $\dot{\gamma}_N = U/H_0$, (b) $\dot{\gamma}_N = U/(RH_0)^{1/2}$. (Key in Table VI-4.)

observed N_{Ca1}^*'s (as calculated with both N_1 and N_2) were much lower

than those observed for Newtonian fluids. The gravity and, to a much

lesser extent, inertia seem to have a stabilizing effect. Seemingly,

$N_g^*(\frac{R}{H_0})$ is more appropriate than N_g^* to represent the effect of gravity since

the data, as correlated with this parameter, are less sparse and they show

a clearer trend.

Some distinct differences between Newtonian and viscoelastic fluids,

with regard to the transition from stable to unstable flow were cited and

discussed. These differences persist in the domain of unstable flow as is

evident from the photographs shown in Figure VIII-10. Upon the onset of

ribbing few wavy ripples appear in the center part of the interface between

the rotating rollers. As the speed is increased these waves start to

migrate towards the edges of the rollers and they are replaced by newly

formed ripples. The number of ribs is gradually increased with speed.

At high speeds the number of ribs stabilizes and they transform from

round wavelike ripples into sharp evenly spaced stripes. In the vicinity of

the separation region these stripes have the appearance of thin buttresses.

Only viscoelastic fluids, due to their ability to sustain normal stresses,

can allow the formation of such 'stable' liquid buttresses.

The Newtonian instability, as opposed to the viscoelastic one, is

characterized by a nearly constant wavelength that is attained shortly after

the onset. The ripples are round and wavy and their amplitude is generally

Figure VIII-10. Photographs of the ribbing phenomenon. (a) H-0.5, 50 rpm, set #2. (b) Glycerin, 50 rpm, set #2. (c) H-0.5, 100 rpm, set #2. (d) Glycerin, 100 rpm, set #2. (e) H-0.5, 100 rpm, set #2. (f) Glycerin, 100 rpm, set #2. (g) H-0.5, 100 rpm, set #2. (h) Glycerin, 100 rpm, set #2.
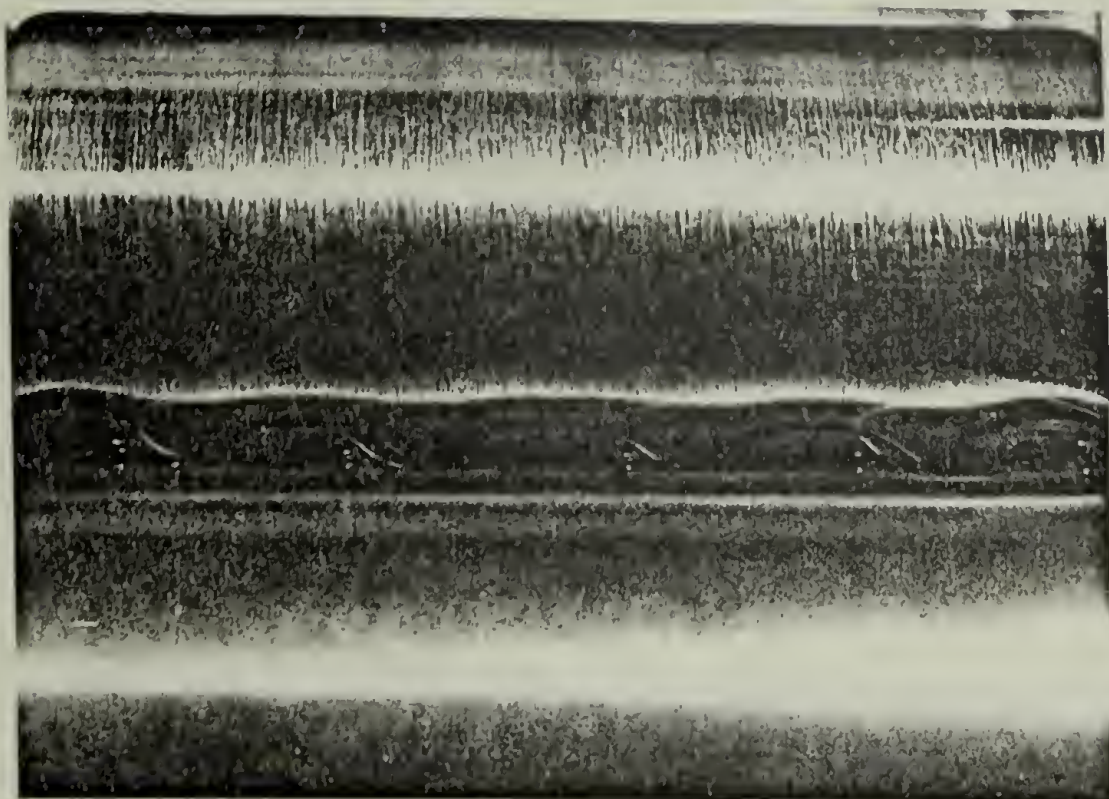
a
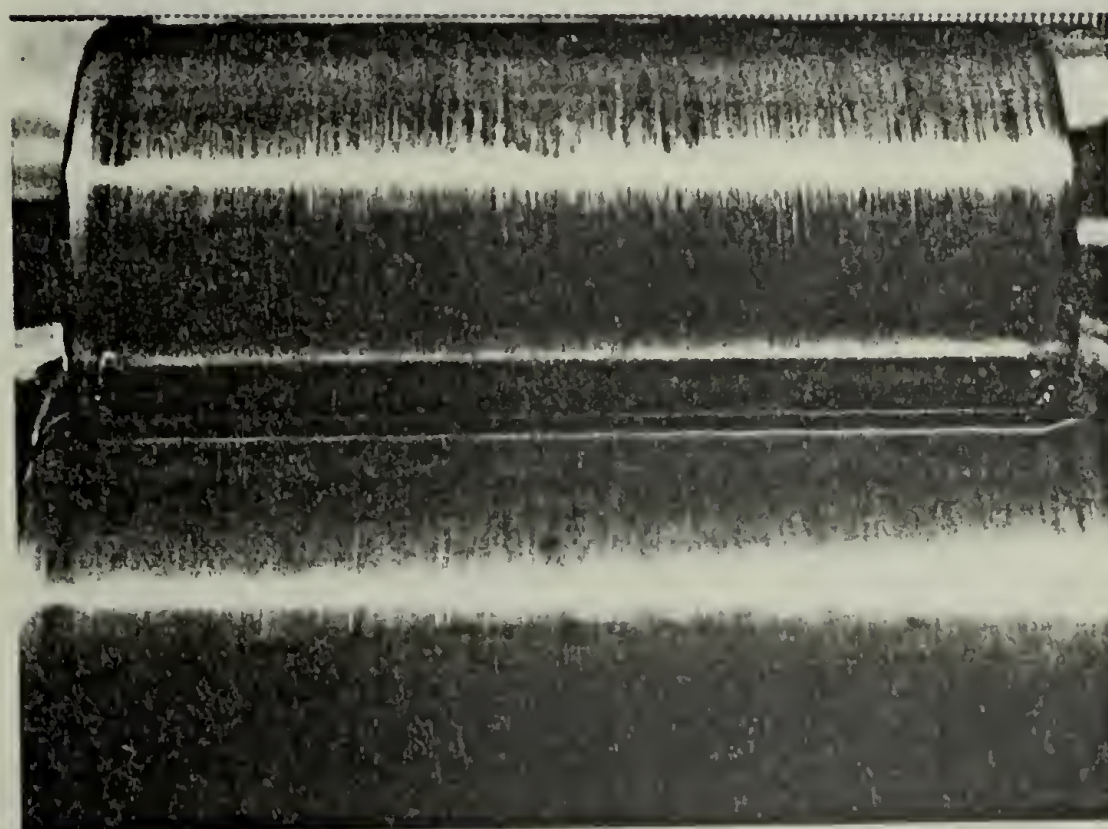
b
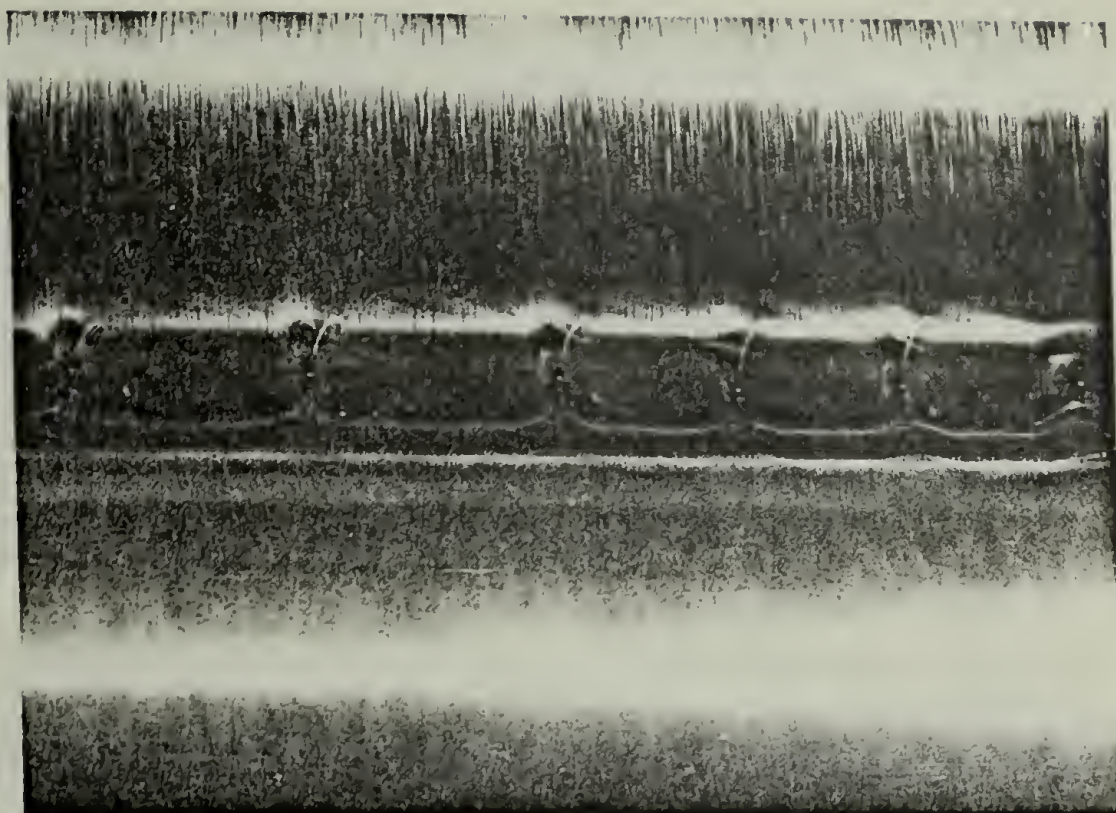
c
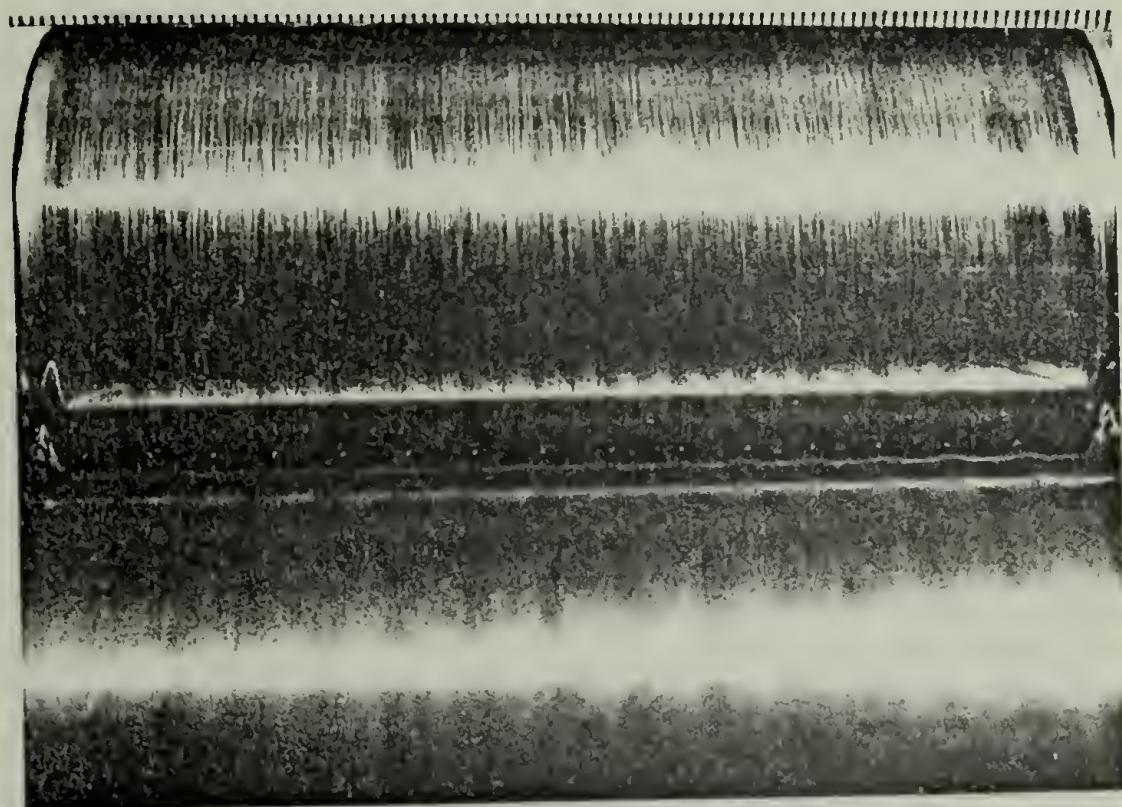
d
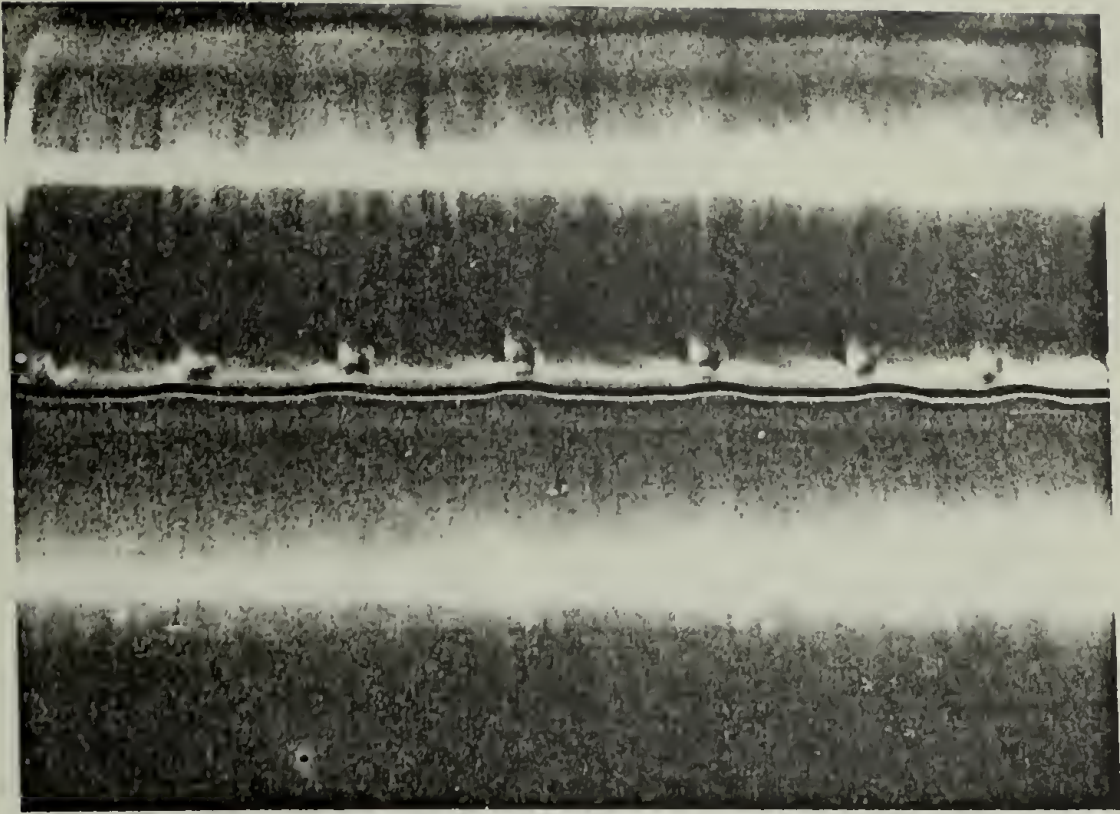
e
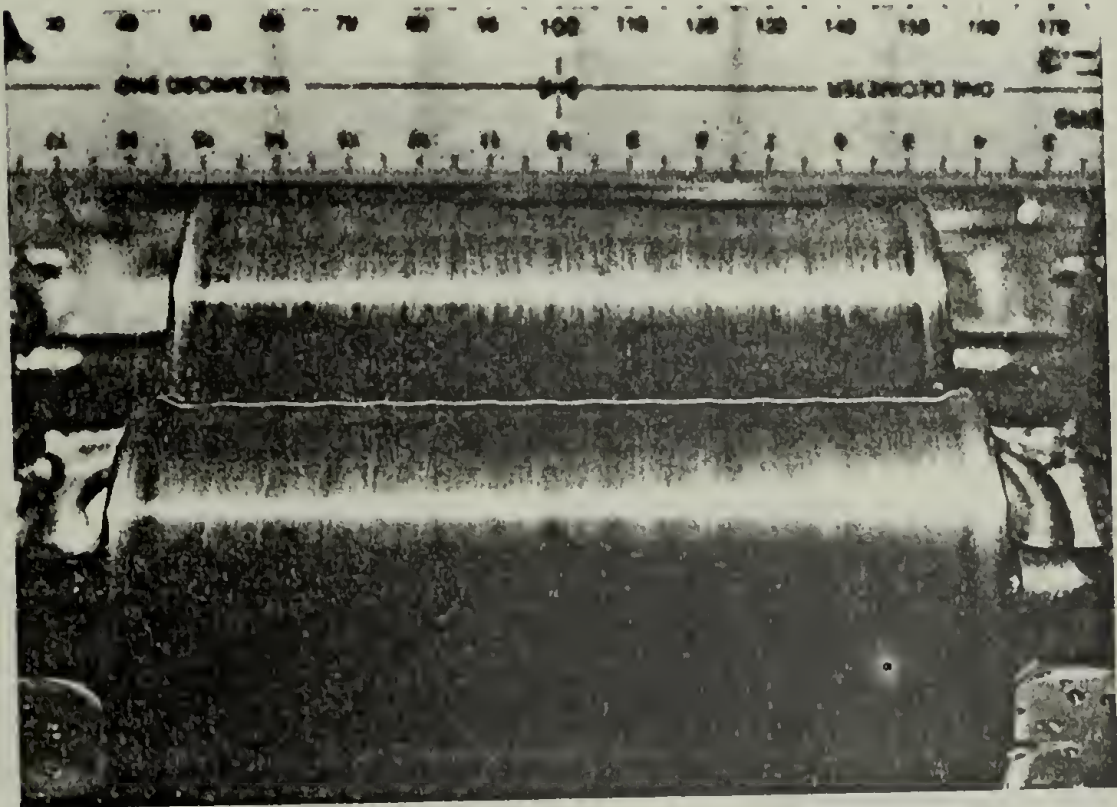
f
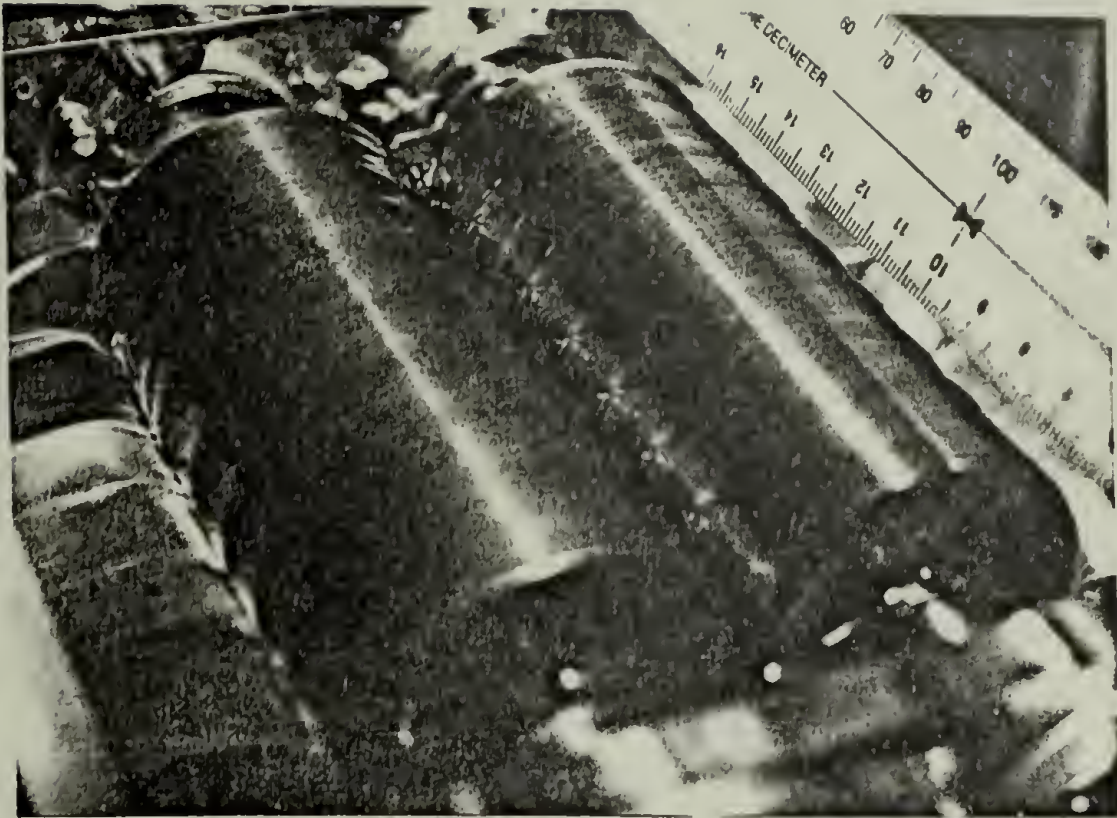
g
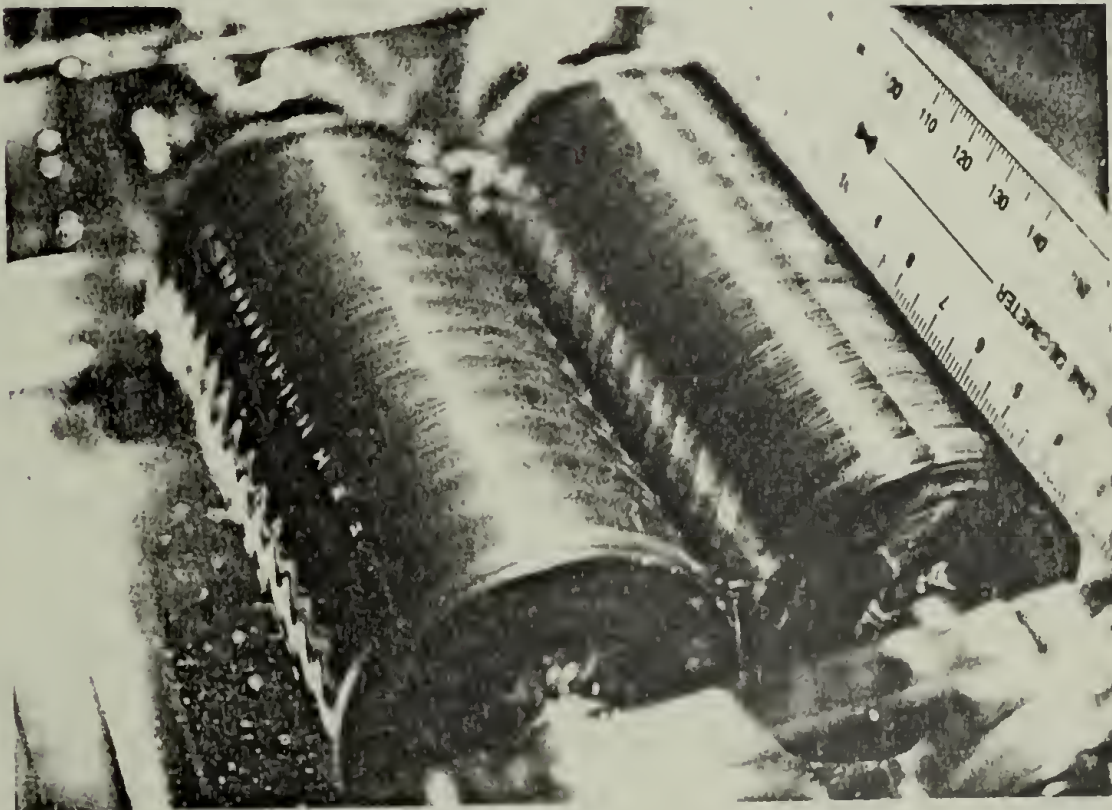
h

smaller than in the viscoelastic case.

As in the Newtonian experiment, wavelengths were measured photographically (see Section 2 for a detailed account of the procedure) and the results further demonstrate the distinct nature of the viscoelastic instability. The variation of the (normalized) wavelength $(W/2H_0)$ with speed for two viscoelastic fluids is shown in Figure VIII-11. Despite the sparsity of the data a clear trend emerges, and it shows a significant reduction in wavelength with speed. The results for H-0.35 are replotted in Figure VIII-12 and compared to the results for several Newtonian fluids. The Newtonian data are nearly stationary while the viscoelastic data show a clear variation with speed.

In summary, apparent phenomenological differences between Newtonian and viscoelastic fluids in the rib-formation process have been demonstrated. These differences are manifested by distinct critical conditions for transition from stable to unstable flow and by characteristic rib-patterns in the unstable flow domain. It is now necessary to have a closer look at the intricate interplay of physical forces participating in the process in order to account for the observed differences.

VIII.4. Physical Stability Analysis

VIII.4.1 General. The physical stability criterion, originally introduced by Pitts and Greiller (1961) and later employed by Savage (1977a), was found generally satisfactory in its ability to explain most of the features
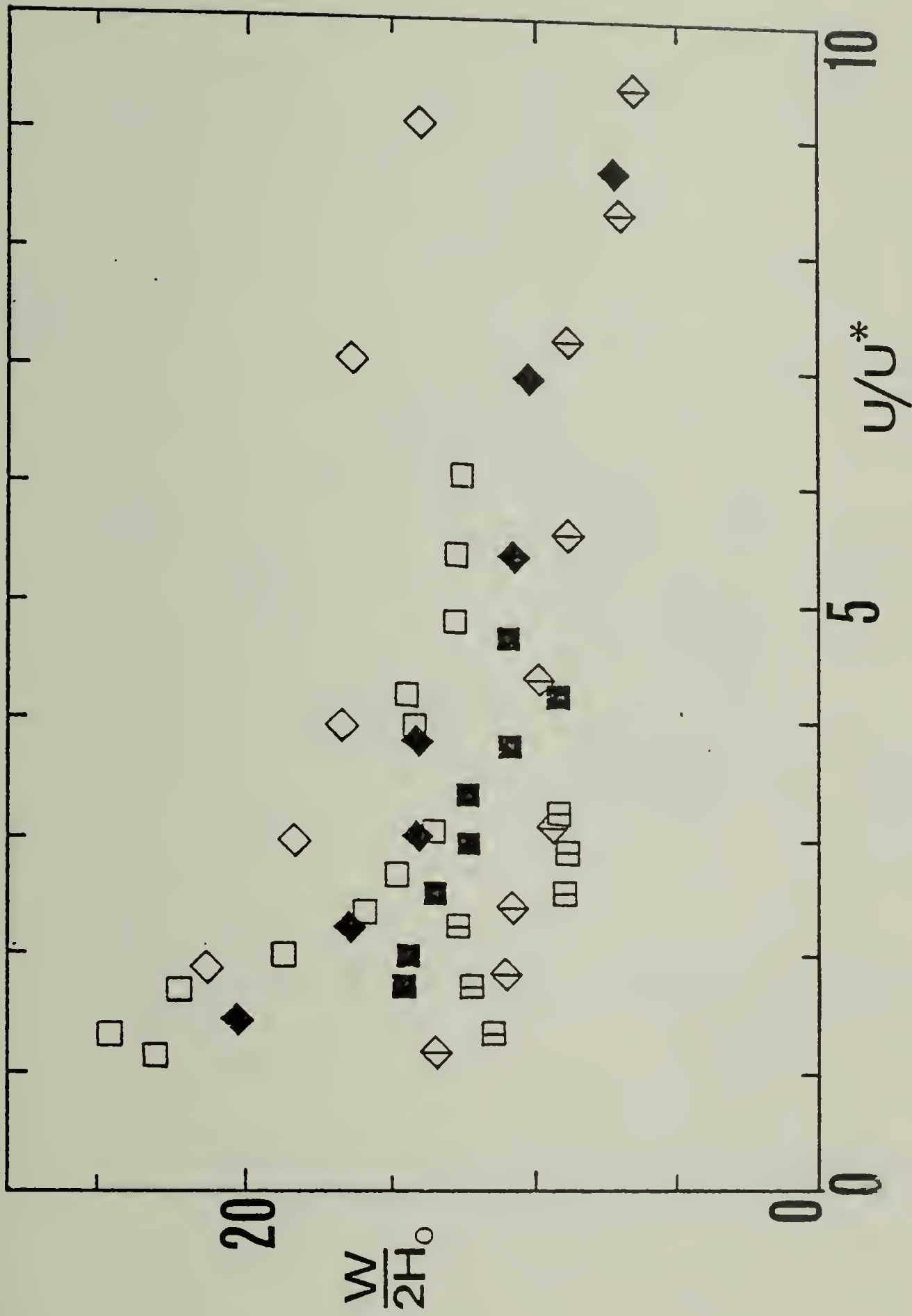
Figure VIII-11. The normalized wavelength vs. the reduced speed. Experimental data for two viscoelastic fluids. (Key in Table VI-4.)
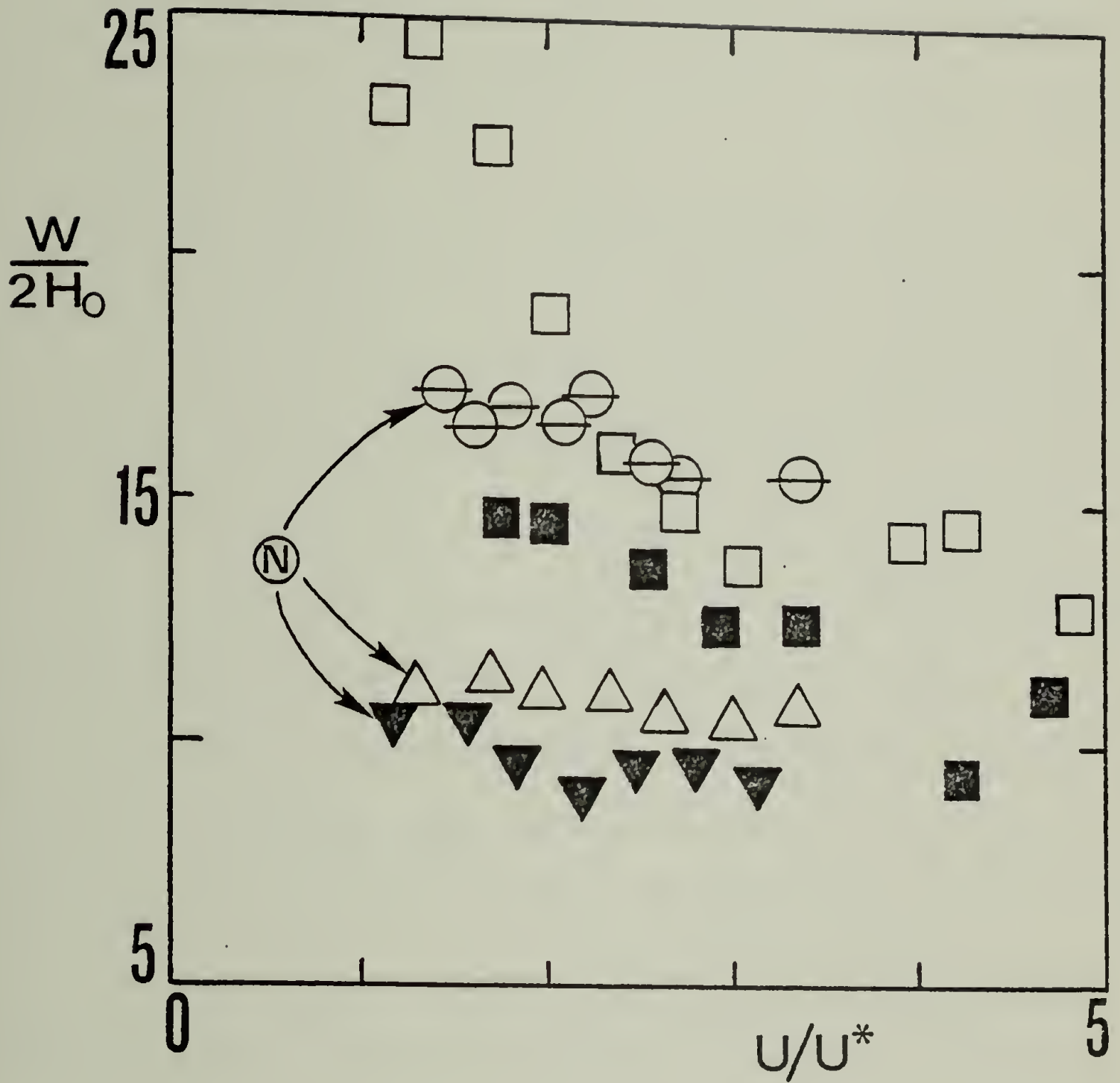
Figure VIII-12. The normalized wavelength vs. the reduced speed. Experimental data for a viscoelastic fluid and three Newtonian fluids. (Key in Table VI-4.)

observed in the Newtonian rib-formation process. This criterion is
reexamined and rederived here (as it was not strictly derived in Pitts and
Greiller's work) and it is later extended to a power-law fluid and a viscoe-
lastic second-order fluid.

Figure VIII-13 shows a cross section of the separation region as it
is projected on the xz plane (for $y = 0$). As before x is the direction of
flow and z is the neutral axis. The slight waviness of the separation line
is assumed to arise from some small physical disturbances. The objective
of this analysis is to determine under what conditions these perturbations
will decay or, conversely, when the waves will grow in amplitude away from
a smooth surface. It is reasonable to state a-priori that whenever the
pressure at point "1" (P_1) will be in excess of the pressure at point "2"
(P_2) there will be sideway motion of fluid from point "1" to point "2",
thereby causing the perturbation to grow. Note that points "1" and "2" are
both at a distance X_1 from the nip. Point "3" which is located on the
perturbed interface is removed an infinitesimal distance, dx, from point
"2". The pressures at all three points, evaluated by a simple force balance,
are:

$$P_1 = -\frac{\tau}{r} \tag{VIII-10}$$

$$P_3 = -\frac{\tau}{r} + \frac{d}{dx}\left(-\frac{\tau}{r}\right) dx \tag{VIII-11}$$

$$P_2 = -\frac{\tau}{r} + \frac{d}{dx}\left(-\frac{\tau}{r}\right) dx + \frac{dp}{dx} x_1 (-dx) \tag{VIII-12}$$
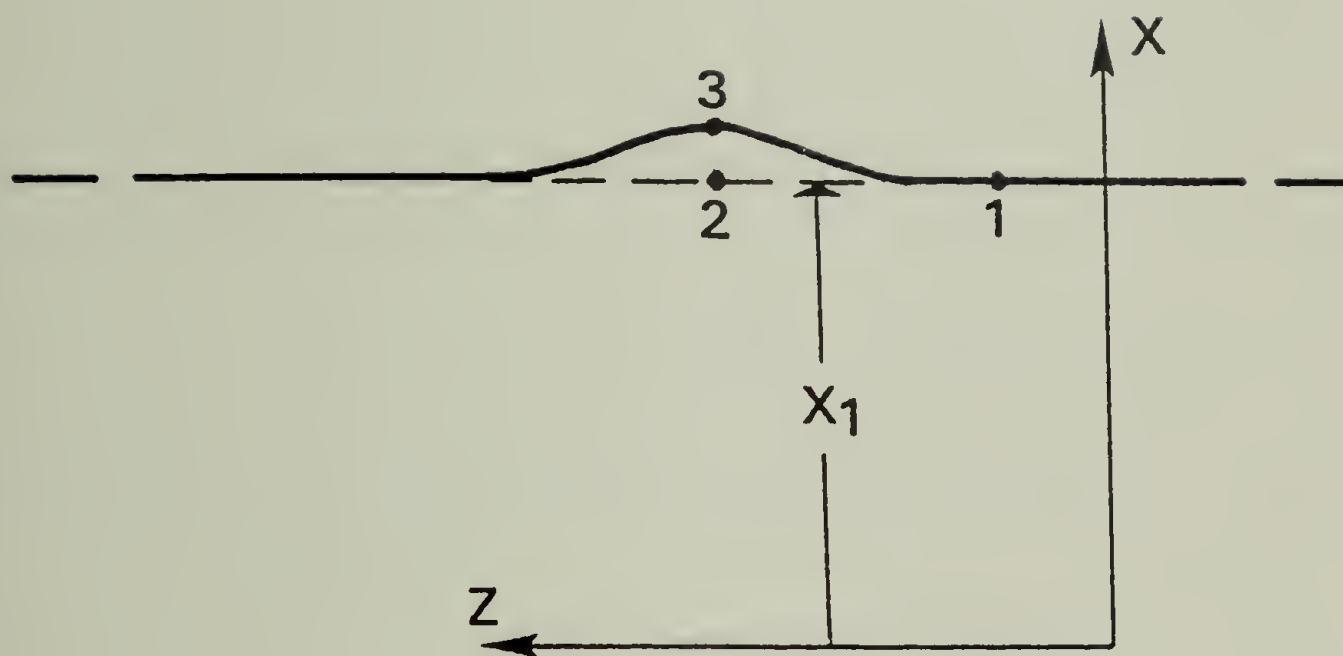
Figure VIII-13. A cross section of the separation region. The separation line (the heavy curve) is slightly perturbed by physical disturbances.

δ is the surface tension and r is the radius of curvature of the meniscus on the xy plane at point "1". (The contribution to the surface tension force from the curvature in the xz plane is ignored. This is justified so long as the initial disturbances are indeed small.) It follows that

$$\Delta P = P_1 - P_2 = [\frac{d}{dx} \cdot (\frac{\delta}{r}) + \frac{dP}{dx}\Big|_{x1}]\ dx$$

$$= [-\frac{\delta}{r^2}\ \frac{dr}{dx} + \frac{dP}{dx}\Big|_{x1}]\ dx \qquad \text{(VIII-13)}$$

and consequently the perturbation will decay whenever

$$\Delta P < 0$$

or

$$\frac{\delta}{r^2}\ \frac{dr}{dx} > \frac{dP}{dx}\Big|_{x1} \qquad \text{(VIII-14)}$$

Eq. (VIII-14) is the sought stability criterion for the system at hand. Without giving explicit expressions for the terms appearing in Eq. (VIII-14) it is possible to draw the following conclusions upon first examination of this criterion:

1. Stability is guaranteed for systems with negative pressure gradients in the vicinity of the separation region as the surface tension term is always positive. This conclusion is consistent with observation. Systems like blade-coaters and slider-bearings, for which the pressure gradients near the exit point are always negative, do not exhibit the ribbing instability.

2.   Surface tension has generally a stabilizing effect.   This too

conforms with experimental observations.

As was noted in Section 2 this criterion is <u>probably</u> a condition for

global stability rather than for neutral stability, i.e., it is a necessary

but not sufficient condition for ribbing to arise.   Hence, the merits of this

criterion should be judged accordingly.

VIII. 4. 2   <u>The purely viscous power-law fluid.</u>   The stability criterion,

Eq. (VIII-14), can easily be applied to a purely viscous power-law fluid.

Expression for the pressure-gradient of a power-law fluid in a system of

counter-rotating rollers has been derived and it is given in VI. 3. 2.   Using

this expression, pressure-gradients for Newtonian and power-law fluids can

be evaluated at the point of flow separation (x_1).   It is found that

$$\frac{d\,\pi_N}{d\,\xi}\bigg|_{\xi_1} = 0.131 \quad \text{for } n = 1 \text{ and } = 1.30$$

and

$$\frac{d\,\pi_{pl}}{d\,\xi}\bigg|_{\xi_1} = 0.208 \quad \text{for } n = 0.4 \text{ and } = 1.40$$

π and ξ are the dimensionless P and x and the values for λ were taken

from the "stable" roll coating analysis for $N_S \to 0$.   It can be shown that

in general,

$$\frac{d\,\pi_{pl}}{d\,\xi}\bigg|_{\xi_1} > \frac{d\,\pi_N}{d\,\xi}\bigg|_{\xi_1} \qquad \text{(VIII-15)}$$

Eqs. (VIII-14) and (VIII-15) imply that a power-law fluid will always be <u>less</u>

stable than a corresponding Newtonian fluid with identical surface tension.

As stated before, a corresponding Newtonian fluid has a viscosity equal to the apparent viscosity of the power-law fluid evaluated at $\dot{\gamma} = U/H_0$. The contribution of the surface tension term in Eq. (VIII-14) is expected to be comparable for both fluids.

In practice, many power-law fluids are also measureably elastic and it would seem natural to examine the effect of elasticity on the stability of the system. This and other effects are considered subsequently.

VIII. 4. 3 <u>The second-order fluid.</u> The stability criterion is now extended to a viscoelastic fluid. Eq. (VIII-14) is first modified by replacing the pressure with the z-component of the total stress ($- T_{zz} = p - \tau_{zz}$). Thus,

$$\frac{\dot{\gamma}}{r^2} \frac{dr}{dx} > - \left. \frac{d\, T_{zz}}{dx} \right|_{x_1} \qquad \text{(VIII-16)}$$

This equation, however, will reduce to Eq. (VIII-14) since $\tau_{zz} = 0$ for the system at hand.. In order to evaluate the dynamic term in Eq. (VIII-16) it is necessary to consider some viscoelastic constitutive equation. Due to the complexity of the problem it would seem reasonable to attempt an analysis with the relatively simple second-order fluid. The constitutive equation for this fluid has been discussed in Chapter IV.

In an instant <u>prior</u> to the onset of ribbing the flow is planar and creeping, thus the Giesekus-Tanner theorem, that was discussed and employed previously (IV. 2), is applicable and can be used for evaluating the pressure gradient in Eq. (VIII-16). Using the Giesekus-Tanner-Pipkin

equation the pressure gradient for the second-order fluid can be written as

$$\frac{dP}{dx} = \frac{dP^0}{dx} - \frac{\alpha_2}{\alpha_1} \left[\frac{du}{dx} \frac{dP^0}{dx} + u \frac{d^2P^0}{dx^2} \right]$$

$$- \frac{d}{dx} \left\{ (\alpha_{11} - \frac{1}{2}\alpha_2) \left[(\frac{\partial u}{\partial y})^2 + (\frac{\partial u}{\partial x})^2 \right] \right\}$$

(VIII-17)

where P^0 is the pressure distribution for a corresponding Newtonian fluid.

The dashed-underlined terms are negligible at or about the separation point

$(x = x_1, \ y = 0)$ where $u = \partial u/\partial y = 0$. The expression for the pressure

gradient is now modified to include gravity effects. The gravity term is

taken to be simply additive to the pressure-gradient and Eq. (VIII-17) takes

the form

$$\frac{dP}{dx} = \frac{dP^0}{dx} - \frac{\alpha_2}{\alpha_1} (\frac{du}{dx} \frac{dP^0}{dx}) - \rho g$$

(VIII-18)

(Recall that the gravity field acts in the $-x$ direction in the system of

counter-rotating rollers; see VI.3.3 for details.) Similar consideration of

the effect of inertia shows that inertia will have relatively little influence,

if any, on the dynamics of the rib-formation process since the leading

inertial term $\rho u (du/dx)$, will vanish identically at separation $(x = x_1, \ y = 0,$

$u = 0)$ where the pressure gradient is to be evaluated. Eq. (VIII-18) can

now be substituted into Eq. (VIII-16) and the stability criterion becomes

$$\frac{dP^0}{dx} \bigg|_{x_1} < \frac{\delta}{r^2} \frac{dr}{dx} + \frac{\alpha_2}{\alpha_1} (\frac{du}{dx} \frac{dP^0}{dx}) \bigg|_{x_1} + \rho g$$

(VIII-19)

This inequality is made dimensionless with the result

$$\frac{d\pi^0}{d\xi}\bigg|_{\xi_1} < \frac{1}{N_{Ca1}}\left(\frac{1}{a^2}\frac{da}{d\xi}\right) + S_R\left(\frac{d\varphi}{d\xi} \quad \frac{d\pi^0}{d\xi}\right)\bigg|_{\xi_1}$$

$$+Ng$$

$$(VIII-20)$$

where $a = r/(RH_0)^{1/2}$ and the various parameters are defined in Section 3.

(S_R has the form $\left[(\alpha_2)/(\alpha_1)\right]\left[(U)/(RH_0)^{1/2}\right]$. The definitions for the

dimensionless variables are given in the lubrication analysis, VI.2. Upon

substituting expressions for φ and $d\pi^0/d\xi$ (from the lubrication analysis),

Eq. (VIII-20) takes the form

$$3\frac{\sigma_1 - \lambda}{\sigma_1^3} < \frac{1}{N_{Ca1}}\left(\frac{1}{a^2}\frac{da}{d\xi}\right) + Ng$$

$$(VIII-21)$$

$$-S_R\frac{3\xi_1}{\sigma_1^5}\left(6\lambda\sigma_1 - 6\lambda^2 - \sigma_i^2\right)$$

where $\sigma_1 = \sigma(\xi_1)$.

This criterion can be made more explicit by using the relation $\sigma_1 = 3\lambda$

that has been derived in VI.2.2 and is a result of the Prandtl-Hopkins

separation condition. In addition, the surface tension term in the above

criterion can be evaluated using Pitts and Greiller's (1961) theory. Pitts

and Greiller's physical stability criterion (Eq. VIII-1) was found qualitatively

in reasonable agreement with observation even though it is quite far off

quantitatively from the observed behavior. This criterion can be conven-

iently incorporated in the present qualitative analysis to represent approx-

imately the effect of surface tension. With the proposed modifications the

stability criterion, Eq. (VIII-21), becomes

$$2 < \frac{1}{(N_{Ca1})^{1/2}} \ [14.1(3\lambda -1)]^{1/2} + Ng \ 9 \ \lambda^2$$

$$-S_R \ \frac{(6\lambda -2)^{1/2}}{3\lambda} \tag{VIII-22}$$

This expression is further complicated by the dependence of λ (the dimensionless flow-rate) on the parameters N_{Ca1}, Ng and possibly S_R.

One important consequence of the roll-coating analysis for the second-order fluid model (VI.2.3) was that the velocity field, and hence the flow-rate, of a second-order fluid in a roll-coating system is identical to that of a corresponding Newtonian fluid. This permits the use of the results for $\lambda = \lambda(N_S, Ng)$ that were derived for a purely viscous fluid in a system of counter-rotating rollers. The calculation of $\lambda = \lambda(N_S, Ng)$ is detailed in VI.3.3 and the results are given in Figure VI-14. Introducing $\lambda = \lambda(N_{Ca1}, Ng)$ into Eq. (VIII-22), where $N_{Ca1} = (1/N_S)(R/H_0)^{1/2}$, allows for a stability mapping of the flow domain. Such mapping is presented in Figure VIII-14 where S_R^* is plotted against N_g^* with N_{Ca1}^* as a parameter. This figure represents (physical) stability limits for a second-order fluid in a system of counter-rotating rollers; the regime below a curve is "stable" and the regime above the curve is "unstable". The general trends displayed by this result are in conformity with observation. Specifically, viscoelasticity (through S_R) has a destabilizing effect on the system while gravity (for $N_g < 0.3$) along with surface-tension are stabilizing. In the limit of a Newtonian gravity-free case (S_R, $N_g \rightarrow 0$) N_{Ca1}^* has the value of ~ 10 which is the result given by Pitts and Greiller. Also, it is found

that for $N_{Cal}^* \rightarrow \infty$ the system will be unstable for any value of N_g^*.

In view of the approximations made in deriving the above criterion it is not expected that it will be in a quantitative agreement with the experimental results which are presented in Section 3. Three points in particular may hinder such a quantitative fit. First, it is expected that the physical stability criterion provide global stability limits rather than neutral stability limits. Observed critical conditions are likely to fall closer to the neutral stability limit and as exemplified by the Newtonian data, the gap between these two limits may be considerable. Secondly, the fluids studied experimentally, and for that matter any common viscoelastic fluid, are not second-order fluids. Such constitutive approximation may be reasonable only in the limit of low deformation rates. Even though deformation-rates in the vicinity of the separation region (where the ribbing instability originates) are relatively small it is doubtful that common viscoelastic fluids will respond in a second-order fashion. (i.e., the actual deformation rates may not be sufficiently low). Finally, the exact role of surface tension is not completely resolved for Newtonian systems, let alone viscoelastic systems. Pitts and Greiller's criterion, used here, is known to be in poor agreement with observation. Yet, it was the only criterion that could be readily applied in this analysis.

One obvious failure of this theory is the excessive importance that it gives to surface tension. It was observed experimentally that surface

Figure VIII-14. The critical recoverable shear vs. the critical gravity number. Experimental data (Key in Table VI-4) are compared to theoretical stability limits. The solid curves are for $H_0/R = 0.01$ and the dashed curves are for $H_0/R = 0.04$.
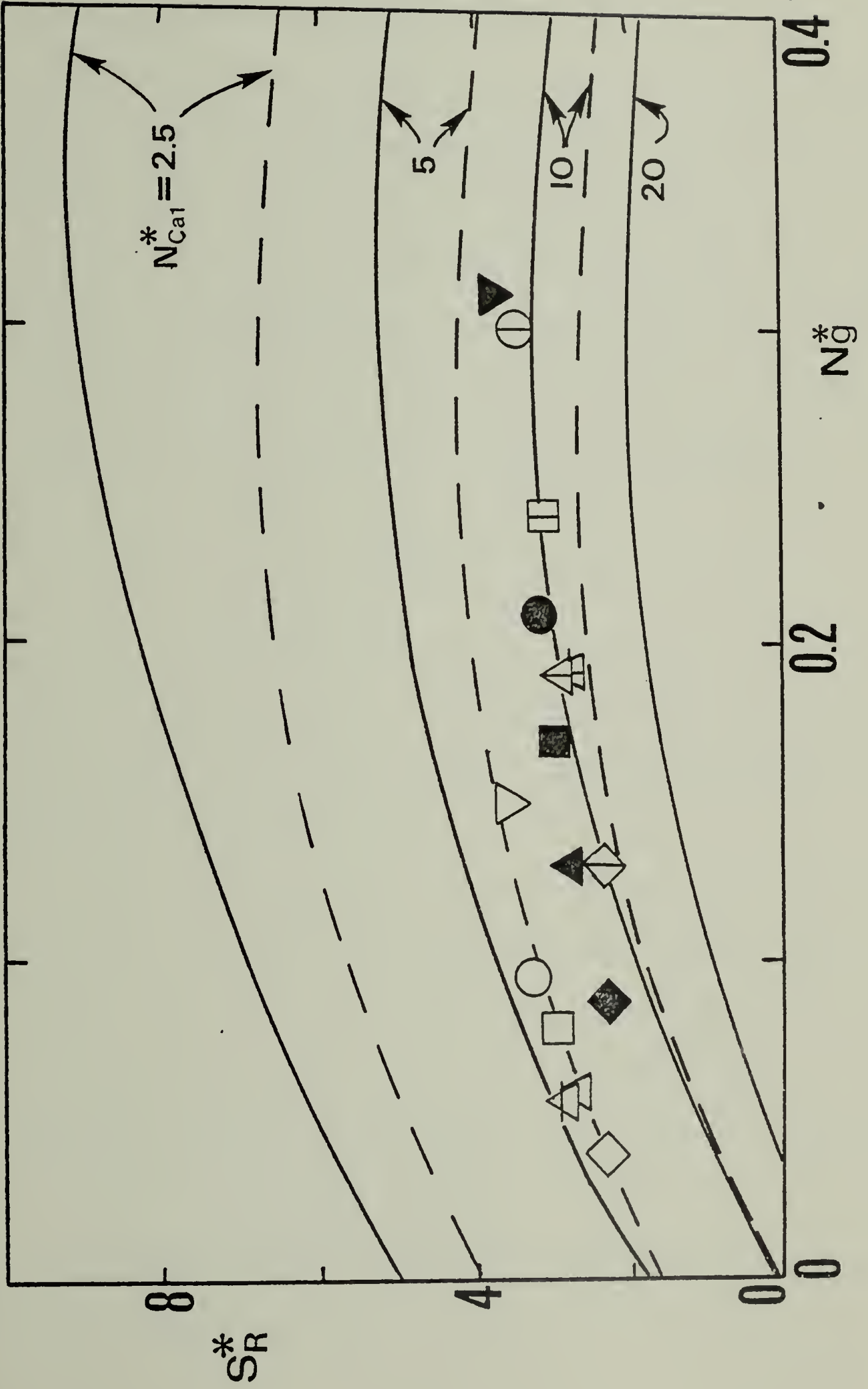
tension is secondary and has little effect on the critical conditions. The calculated values of N_{Ca1}^* (using $\dot{\gamma}_{N2}$) for the cases investigated range from 7 to 50, while the corresponding data points in Figure VIII-14 are clustered between the theoretical curves for $N_{Ca1}^* = 5$ and N_{Ca1}^*, 10. Otherwise, this simplified theory successfully predicts the correct trends. In face of all the approximations made the experimental results are in a reasonably good agreement with the theory with regard to the dependence of N_g^* on S_R^*. It is also worthy of note that this analysis gives

$$S_R = \frac{\alpha_2}{\alpha_1} \frac{U}{(RH_0)^{1/2}}$$

$$= \frac{\Psi_{12}}{2\eta} \dot{\gamma}_{N2}$$

Thus, according to this theory, $\dot{\gamma}_{N2}$ rather than $\dot{\gamma}_{N1}$ arises naturally as a parameter for correlating the data. Indeed, the experimental data are better correlated with $\dot{\gamma}_{N2}$.

Another interesting observation is that the data points in Figure VIII-14 are clearly separable for the three geometries considered ($H_0/R = 0.0129$, 0.0229, 0.0306). As seen, this behavior is consistent with the predictions of the theory; the direction of the effect of geometry for both theory and experiment is identical and the magnitude of this effect is comparable.

VIII.4.4 <u>Summary and discussion.</u> A simple stability criterion based on some plausible physical arguments has been derived and discussed. It was first applied to a purely viscous power-law fluid and later to a

viscoelastic second-order fluid. In both cases the non-Newtonian fluids were found less stable than the corresponding Newtonian fluids. With both effects, elasticity (S_R) and shear-thinning, causing "destabilization" it is expected that real viscoelastic fluids will be increasingly prone to the ribbing instability. In fact, the ribs are likely to appear at such an early stage that gravity effects are expected to be dominant. These theoretical results generally conform with the experimental observations presented in Section 3.

The stability model presented in this section should be put in the right perspective, however; it may well be an oversimplification of the actual situation especially as far as viscoelastic fluids are concerned. Hydrodynamic instabilities occuring in polymer processing (viscoelastic) systems are still far from being fully understood. Petrie and Denn (1976) in a comprehensive exposition on this subject point out that any generalizations concerning the behavior of polymeric systems, especially in stability problems, are "extremely dangerous" since the molecular topology of polymeric species may be in some cases of crucial importance. Indeed, instability behavior is, in some instances, a sensitive detector of variations in molecular structure. Such "topological effects" are sometimes overlooked by fluid dynamicists. Several classical stability problems, such as "melt fracture", are still subject to a number of conflicting interpretations. Petrie and Denn name few possible instability mechanisms for pressure driven flows of viscoelastic fluids. Some of them are: inherent constitutive instabilities,

hydrodynamic inertial instabilities, low Reynolds number instabilities, shear

waves (apparent slip at a solid wall) and die (or system) entry effects. In

the system considered herein, the presence of a free surface is an addition-

al potential source of instability; the behavior of viscoelastic fluids in the

vicinity of free surfaces is in itself poorly understood (Joseph and Beavers

1977).

The physical stability model that has been advanced in this section can

be categorized as a hydrodynamic (low Reynolds number) stability mechanism.

Other possible mechanisms, however, cannot be ruled out with complete

certainty.

In any case, the use of a roll-coater for an even deposition of a thin

fluid film seems feasible only at low speeds. If a uniform coating is

desired at high throughputs, a blade coater or a reverse-roll coater are to

be used as these devices do not exhibit the ribbing phenomenon for

sufficiently high speeds.

C H A P T E R IX

CONCLUSION

A comprehensive study of a subject as vast as coating flows requires major thrust efforts in areas as diverse as free surface hydrodynamics, lubrication theory, flow stability analysis, and weak and strong flow rheology. Naturally, in a single study such as this one can hope to touch upon only few of the many unresolved questions that need be considered. In this study attention was focused on a specific but important subclass of coating flows. These flows have been referred to as bounded coating flows and they are characterized by a lubrication-like kinematics and by the controlling effect of the dynamics in the bounded regimes on the performance of the corresponding systems.

The objective of this study was to establish useful performance relations for several technologically important systems via lubrication-based analyses accompanied by some simple experiments. A special consideration was given to the effect of fluid rheology. In a broader sense, this study was intended to serve as a groundwork and give an impetus to a more systematic and in-depth investigation of some important aspects of coating flows. Indeed, the major accomplishment of this work is in opening up some potential avenues for future research in this area. Before listing the research

topics that deserve further consideration it is useful to summarize briefly the important results of this work.

Two major coating systems were studied in detail: blade coating and roll coating. Some performance relations for a rigid planar blade coater have been derived for Newtonian, second-order and CEF fluids. The constitutive approximation utilized in this and other derivations is based on the purely viscous approach due to Tanner. These calculations specifically relate the coating thickness and the blade loading to the geometry of the system and the properties of the fluid. Experiments were conducted in which the coating thickness was measured for several fluids, both Newtonian and viscoelastic. The viscoelastic fluids produced a coating thickness that was consistently higher than in the Newtonian case. However, the observed difference was not statistically significant.

Performance relations have been derived for a sheet-and-roll system that is representative of roll coating operations. Analyses have been carried out for a power-law fluid, a second-order fluid, and a CEF fluid. Some of these analyses were extended to the system of half-immersed counter rotating rollers. This system was used in an experimental study of roll coating in which coating thickness data were gathered for Newtonian and viscoelastic fluids. Data for Newtonian fluids, both in gravity-free and gravity-controlled regimes, were found in satisfactory agreement with the lubrication solution. Similar experiments with viscoelastic fluids were not

conclusive because of the onset of the "ribbing instability" under relatively low speed conditions.

A brief study of a reverse-roll coating system was undertaken. A simple qualitative analysis for a Newtonian fluid was carried out yielding qualitative performance relations for the system. These relations were well reproduced experimentally.

An attempt to elucidate the dynamics in roll coating was made through a study of the submerged-roll system. This system was shown to be hydrodynamically similar to the sheet-and-roll system and it was also found amenable to experimental testing. An experimental study of the system was conducted in which pressure distributions were measured in the converging-diverging flow space for a Newtonian and a viscoelastic fluid. The Newtonian data were in agreement with a finite element solution of the problem. The results for the viscoelastic fluid, while qualitatively in conformity with the approximate theory, could not be evaluated because of a lack of an exact solution to the related problem.

The important question of stability in coating flows was considered through a study of the ribbing phenomenon. The related literature was surveyed and the few empirical and theoretical studies were critically assessed. Additional data for Newtonian fluids and some data for viscoelastic fluids have been reported. These data show some phenomenological as well as quantitative differences between Newtonian and viscoelastic systems. A

simple physical stability theory that is capable of explaining some of the observed differences has been presented.

The general conclusions that can be drawn from this study are:

1. The lubrication approach is useful in evaluating the performance of coating systems so long as the geometry of the system is consistent with the lubrication approximation.

2. Viscoelasticity has some effect on the performance of coating systems and it has a particularly strong influence on the stability of the systems.

3. As anticipated, the role of the free surface dynamics in the systems under consideration was at best secondary. Hence, these systems can be broadly classified as high capillary number systems.

While this study has covered some important topics within the context of coating flows, many areas were virtually untouched. Some immediate tasks for future research are summarized below.

The study of low capillary number systems is definitely one of the most important and challenging endeavors to be undertaken. While some analytical work on this subject has been reported (Ruschak 1974), further consideration of coating systems in which surface tension effects are dominant is needed. In particular, a careful study of the separation zone, both theoretical and experimental, will have to be undertaken. A relatively simple problem, for immediate consideration, is the one encountered in the

slot coating operation. Theoretical study of this problem will necessitate the use of advanced numerical techniques (such as FEM) modified to tackle free surface problems. Experimental investigation will require careful tracer studies of flow patterns in the separation zone and photographic studies of the shape of the liquid-air meniscus at separation. Such studies should eventually be extended to non-Newtonian fluids and to more complex geometries. This investigation can hopefully lead to separation boundary conditions for the Reynolds equation that are less questionalbe than the Coyne and Elrod conditions. The latter conditions are, at the moment, the best boundary conditions for separation cavitation. However, as was pointed out in IV.4, they are not completely satisfactory at low capillary numbers and they are flawed by some arbitrary assumptions.

A second subject that deserves further consideration is the study of coating systems with geometries that cannot be handled by the lubrication approach. This study will require the use of advanced numerical methods for dealing with the complex boundary-value problems for such systems; it also must be accompanied by careful experimental observations. A special consideration should be given to systems such as the knife coater, the blade coater (both rigid and flexible) with a large angle of inclination, and the reverse-roll coater. The latter system was considered in this study only superficially and it was noted that the lubrication approximation is quite limited in its ability to characterize the strongly two-dimensional

flow near the liquid-air meniscus. A more rigorous study of this system is clearly needed.

Another important problem that is not fully resolved is the question of coating flow stability. The ribbing phenomenon which is a common performance failure in coating operations was discussed in detail in Chapter VIII and it was concluded that a more rigorous consideration of this problem would be needed since the current theories are at best qualitative and they are in poor agreement with experimental observations. Also, the present body of experimental data is insufficient and more experiments with Newtonian and viscoelastic fluids need to be undertaken for a better understanding of the ribbing instability.

Because of the inherent difficulty in evaluating Deborah-number effects in flows with complex stretch histories such as bounded coating flows, these effects have been completely overlooked in this study. It was argued (in II. 4) that relaxation effects may be important in some instances in the systems under consideration and a rational approach to tackle this problem was proposed in II. 4. The importance of this question lies beyond the scope of coating flows. It was noted that the current understanding of viscoelastic lubrication flows is far from satisfactory, and that the study of relaxation effects in viscoelastic lubrication systems may well resolve some of the mysteries in the behavior of viscoelastic lubricants.

NOMENCLATURE

(i)

$\underset{\sim}{A}$ = The Rivlin-Ericksen tensors (sec^{-1}).

a = Dimensionless radius of curvature.

C = Constant of integration

$\underset{\sim}{C}$ = The Cauchy-Green tensor.

$\underset{\sim}{C^{-1}}$ = The Finger strain tensor

F = Dynamic loading per unit width (dyne cm^{-1})

g = Accelaration of gravity (cm sec^{-2})

H_0 = Characteristic film spacing (cm)

H_1 = Characteristic film spacing (cm)

H_f = Coating thickness on a forward roll in reverse-roll coating (cm)

H_r = Coating thickness on a reverse roll in reverse-roll coating (cm)

H_ω = Coating thickness (cm)

h = Lubricated film height (cm)

K = Geometric parameter of a blade coater (Def. Eq. V-4)

L = Characteristic length (cm)

$\dot{m}$ = Kinematic parameter (Def. Eq. II-9)

m' = The consistency index of the power-law fluid (poise sec^{1-n})

N_{Ca} = The capillary number (Def. P. 56)

N_{Ca1} = A modified capillary number (Def. Eq. VIII-1)

N_{Ca2} = A modified capillary number (Def. Eq. VIII-2)

N_{De} = The Deborah number (Def. Eq. II-28)

N_e = A viscoelastic parameter (Def. Eq. IV-15)

N_g = The gravity number (Def. Eq. VI-31)

N_{Re} = The Reynolds number (Def. Eq. VII-7)

N_S = The surface tension parameter (Def. Eq. VI-4)

N_{Tr} = The Trouton ratio (Def. Eq. III-4)

n = The power-law exponent

P = Pressure (dynes cm^{-2})

p = 3-n

Q = Flow-rate (cm^3 sec^{-1})

q = (1/n) + 1

R = Radius (cm)

r = Radius of curvature (cm)

S_R = The "recoverable shear" (Def. Eq. VIII-4)

s = The "backward running elapsed time" (sec)

$\underset{\sim}{T}$ = The total stress tensor (dyne cm^{-2})

t = Time (sec)

t_R = Relaxation time (sec)

U = Characteristic speed (cm sec^{-1})

U_f = Lateral speed of forward roll in reverse-roll coating (cm sec^{-1})

U_r = Lateral speed of reverse roll in reverse-roll coating (cm sec^{-1})

u = The x-component of the velocity vector (cm sec^{-1})

u^i = Velocity vector components (cm sec^{-1})

W = Wavelength of the ribbing instability (cm)

W_S = The Weissenberg number (Def. Eq. IV-15)

X = Hydrodynamic function (Def. V-19)

x = Primary flow coordinate (cm)

x^i = Cartesian coordinates (cm)

x_1 = Position of flow separation (cm)

Y = Hydrodynamic function (Def. Eq. V-20)

y = Cross film coordinate (cm)

z = Neutral axis (cm)

Greek

$\alpha_1, \alpha_2, \alpha_{11}$ = Parameters of the second-order fluid

β = Shape function for the separation geometry (Def. Eq. IV-22)

γ = Surface tension (dyne cm^{-1})

$\dot{\gamma}$ = Shear-rate (sec^{-1})

$\dot{\gamma}_1, \dot{\gamma}_2$ = kinematic parameters (sec^{-1})

$\underset{\sim}{\Delta}$ = The rate-of-deformation tensor (sec^{-1})

$\dot{\epsilon}$ = Strain rate (sec^{-1})

η = Dimensionless cross film coordinate

$\eta(\dot{\gamma})$ = The shear viscosity function (poise)

η_0 = Zero shear rate viscosity (poise)

η_{E_e} = Elongational viscosity (poise)

$\underset{\sim}{\Theta}$ = Dimensionless total stress tensor

k = Speed ratio in reverse roll coating.

λ = Dimensionless coating thickness and/or flow-rate per unit width.

μ = Newtonian viscosity (poise)

ν = Coating thickness ratio in reverse-roll coating

ξ = Dimensionless primary flow coordinate

ξ^i = Position coordinates for a fluid particle at past time t + s.

π = Dimensionless pressure

$\dot{\pi}$ = Dimensionless pressure gradient

ρ = Density (gr cm^{-3})

σ = Position of the lubricated film height (dimensionless)

$\underset{\sim}{\tau}$ = Dynamic stress tensor (dyne cm^{-2})

u = Dimensionless velocity component in the primary flow direction

$\bar{\phi}$ = Dimensionless loading per unit width

χ = Shape function for the separation region (Def. Eq. IV-23)

ψ_{12} = The first normal stress coefficient (poise sec)

ψ_{23} = The second normal stress coefficient (poise sec)

$\underset{\sim}{\omega}$ = Vorticity tensor (sec^{-1})

Roman

$\underset{\sim}{I}$ = The identity matrix

II_Δ = The second-invariant of the rate-of-deformation tensor (sec^{-2})

REFERENCES

Abdel-Khalik, S. I., O. Hassager and R. B. Bird, "Prediction of Melt Elasticity from Viscosity Data", Pol. Eng. Sci., 14, 12, 859 (1974)

Banks, W. H. and C. C. Mill, "Some Observations on the Behavior of Liquids Between Rotating Rollers", Proc. Royal Soc., A, 223, 414 (1954)

Bird, R. B., "Useful Non-Newtonian Models", Annual Review of Fluid Mechanics, 8, 13 (1976)

Bird, R. B., W. E. Stewart and E. N. Lightfoot, Transport Phenomena. John Wiley & Sons, New York (1960)

Bird, R. B., O. Hassager and S. I. Abdel-Khalik, "Co-rotational Rheological Models and the Goddard Expansion", AIChE J., 20, 6, 1041 (1974)

Bird, R. B., R. C. Armstrong and O. Hassager, Dynamics of Polymeric Liquids. Vol. 1. Fluid Mechanics. John Wiley & Sons, New York (1977a)

Bird, R. B., O. Hassager, R. C. Armstrong and C. F. Curtis, Dynamics of Polymeric Liquids. Vol. 2. Kinetic Theory. John Wiley & Sons, New York (1977b)

Birkhoff, G., "Free Boundary Problems for Viscous Flows in Channels", in: Cavitation in Real Liquids, R. Davis, ed., Elsevier Publishing Co., Amsterdam (1964)

Birkhoff, G. and D. F. Hays, "Free Boundaries in Partial Lubrication", J. Math. Phys. (MIT), 42, 2, 129 (1963)

Bliesner, W. C., "Basic Mechanisms in Blade Coating", Tappi, 54, 10 1673 (1971)

Booth, G. L., in: The Science and Technology of Polymer Films, Vol. 1, O. J. Sweeting, ed., Interscience Publishers, New York (1968)

Briston, J. H., Plastics Films, Iliffe Books, London (1974)

Cameron, A., Principles of Lubrication, Longmans, London (1966)

Canard, P., "Rheological Properties of Coating Colors at High Sheer Rates and Their Behavior in Blade Coaters", Tappi, 57, 11, 95 (1974)

Coleman, B. D. and W. Noll, "An Approximation Theorem for Functionals with Application in Continuum Mechanics", Arch. Rat. Mech. Anal., 6, 355 (1960)

Coyne, J. C. and H. G. Elrod Jr., "Conditions for the Rupture of a Lubricating Film. Part I: Theoretical Model", ASME Paper No. 69-Lub-3 (1969)

Coyne, J. C. and H. G. Elrod Jr., "Conditions for the Rupture of a Lubricating Film. Part II: New Boundary Conditions for Reynolds Equations", ASME Paper No. 70-Lub-3 (1970)

Criminale, W. O., J. L. Ericksen and G. L. Filbey Jr., "Steady Shear Flow of Non-Newtonian Fluids", Arch. Rat. Mech. Anal., 1, 410 (1958)

Crowley, D. G., F. C. Frank, M. R. Mackley and R. G. Stephenson, "Localized Flow Birefringence of Polyethylene Oxide Solutions in a Four Roll Mill", J. Polym. Sci. (Polymer Physics Ed.), 14, 1111 (1976)

Davies, M. J. and K. Walters, "The Behavior of Non-Newtonian Lubricants in Journal Bearings - A Theoretical Study", in: The Rheology of Lubricants, T. C. Davenport, ed., John Wiley & Sons, New York (1973)

Eckert, R. E. and E. J. Novotny Jr., "Ribbed Flow from a Float Channel", Nature Phys. Sci., 241, 147 (1973)

Floberg, L., "Cavitation in Lubricating Oil Films", in: Cavitation in Real Liquids, R. Davies, ed., Elsevier Publishing Co., Amsterdam (1964)

Floberg, L., "On Hydrodynamic Lubrication with Special Reference to Sub-cavity Pressures and Number of Streamers in Cavitation Regions", Acta Polytech. Scand., ME 19 (1965)

Floberg, L., "Sub-cavity Pressures and Number of Oil Streamers in Cavitation Regions with Special Reference to the Infinite Journal Bearing", Acta Polytech. Scand., ME 37 (1968)

Gains Jr., G. L., "Surface and Interfacial Tension of Polymer Liquids - A Review", Pol. Eng. Sci., 12, 1, 1 (1972)

Gatcombe, E. K., "Lubrication Characteristics of Involute Spur Gears. A Theoretical Investigation", Trans. ASME, 67, 177 (1945)

Graessley, W. W. and L. Segal, "Flow Behavior of Polystyrene Systems in Steady Shearing Flow, "Macromolecules, 2, 1, 49 (1969)

Greener, J. and S. Middleman, "Blade Coating of a Viscoelastic Fluid", Polymer Eng. Sci., 14, 11, 791 (1974)

Greener, J. and S. Middleman, "A Theory of Roll Coating of Viscous and Viscoelastic Fluids", Polymer Eng. Sci., 15, 1, 1 (1975)

Harnoy, A., "Stress Relaxation in Elastico-viscous Lubricants in Gears and Rollers", J. Fluid Mech., 76, 3, 501 (1976)

Higashitani, K. and A. S. Lodge, "Hole-Pressure Error Measurements in Pressure Generated Shear Flow", Trans. Soc. Rheol., 19, 2, 307 (1975)

Hirch, E. J., "Mechanical Models of Dilute Polymer Solutions for Strong Flows with Large Polymer Deformations", Proc. Int. Conf. C.N.R.S. Polymers and Lubrication, Brest, France (1974)

Hintermaier, J. C. and R. E. White, "The Splitting of a Water Film Between Rotating Rolls", Tappi, 48, 11, 617 (1965)

Hoffman, R. D. and R. R. Myers, "The Splitting of Thin Liquid Films. Cavitation Dynamics", Trans. Socl, Rheol., 6, 197 (1962)

Hopkins, M. R., "Viscous Flow Between Rotating Cylinders and a Sheet Moving Between Them", Brit. J. Appl. Phys., 8, 442 (1957)

Huebner, K. H., The Finite Element Method for Engineers, John Wiley & Sons, New York (1975)

Hutton, J. F., "The Rheology of Petroleum-Based Lubricating Oils and Greases: A Review", in: The Rheology of Lubricants, T. C. Davenport, ed., John Wiley & Sons, New York (1973)

Joseph, D. D. and G. S. Beavers, "Free Surface Problems in Rheological Fluid Mechanics", Rheol. Acta, 16, 169 (1977)

Langlois, W. E., Slow Viscous Flow, The Macmillan Co., New York (1964)

Leppard, W. R. and E. B. Christiansen, "Transient Viscoelastic Flow of Polymer Solutions", AICHE J., 21, 5, 999 (1975)

Lin, O. C. C., "Rheology and Surface Coatings", Chemtech, 51 (1975)

Marrucci, G. and G. Astarita, "Linear, Steady, Two-Dimensional Flows of Viscoelastic Liquids", AICHE J., 13, 5, 931 (1967)

McKelvey, J. M., Polymer Processing, John Wiley & Sons, New York (1962)

Metzner, A. B., "The Significant Rheological Characteristics of Lubricants", J. Lub. Tech., Trans. ASME, 90, 531 (1968)

Metzner, A. B., "Extensional Primary Field Approximations for Viscoelastic Media", Rheol. Acta, 10, 434 (1971)

Metzner, A. B., J. L. White and M. M. Denn, "Constitutive Equations for Viscoelastic Fluids for Short Deformation Periods and for Rapidly Changing Flows: Significance of the Deborah Number", AICHE J., 12, 5, 863 (1966)

Middleman, S., The Flow of High Polymers. Interscience Publishers, New York (1968)

Middleman, S., Fundamentals of Polymer Processing. McGraw-Hill Book Co., New York (1977)

Mill, C. C. and G. R. South, "Formation of Ribs on Rotating Rollers", J. Fluid Mech. 28, 3, 523 (1967)

Miller, J. C. and R. R. Myers, "A Photographic Study of Liquid Flow in a Role Nip", Trans. Soc. Rheol., 2, 77 (1958)

Modrak, J. P., "Effect of Coating Color Rheology on the Blade Coating Process", Tappi, 56, 10, 70 (1973)

Myers, R. R. and R. D. Hoffman, "The Distribution of Pressures in the Roll Application of Newtonian Fluids", Trans. Soc. Rheol., 5, 317 (1961)

Noll, W., "A Mathematical Theory of the Mechanical Behavior of Continuous Media", Arch. Rat. Mech. Anal., 2, 197 (1958)

Novotny, Jr., E. J. and R. E. Eckert, "Direct Measurement of Hole Error for Viscoelastic Fluids in Flow Between Infinite Parallel Plates", Trans. Soc. Rheol., 17, 2, 227 (1973)

Olabisi, O. and M. C. Williams, "Secondary and Primary Normal Stress, Hole Error, and Reservoir Edge Effects in Cone and Plate Flow of Polymer Solutions", Trans. Soc. Rheol., 16, 4, 727 (1972)

Padday, J. F., "Theory of Surface Tension. Part II", in: Surface and Colloid Science. Vol. I, Matijevic, E., ed., John Wiley & Sons, New York (1969)

Park, W. R. R., ed., Plastics Film Technology, Van Nostrand Reinhold Co., New York (1969)

Pearson, G. H., Elongational Flow of Polymer Solutions, Ph.D. Thesis, University of Massachusetts, Amherst (1975)

Pearson, J. R. A., "The Instability of Uniform Viscous Flow Under Rollers and Spreaders", J. Fluid Mech., 7, 4, 481 (1960)

Pearson, J. R. A., "The Lubrication Approximation Applied to Non-Newtonian Flow Problems: A Perturbation Approach", in: Nonlinear Partial Differential Equations, Ames W. F., ed., Academic Press, New York and London (1967)

Perry, J. H., Chemical Engineer's Handbook, 4th Ed., McGraw-Hill Book Co., New York (1963)

Petrie, C. J. S. and M. M. Denn, "Instabilities in Polymer Processing", AICHE J., 22, 2, 209 (1976)

Pinkus, O. and B. Sternlicht, Theory of Hydrodynamic Lubrication, McGraw-Hill Book Co., Inc., New York (1961)

Pipkin, A. C. and R. I. Tanner, "A Survey of Theory and Experiment in Viscometric Flows of Viscoelastic Liquids", Mechanics Today, 1, 262 (1972)

Pitts, E. and J. Greiller, "The Flow of Thin Liquid Films Between Rollers", J. Fluid Mech., 11, 33 (1961)

Reiner, M., "The Deborah Number", Physics Today, 17, 62 (1964)

Reiner, M., M. Hanin and A. Harnoy, "An Analysis of Lubrication with Elastico-Viscous Liquid", Isreal J. Tech., 7, 4, 273 (1969)

Riley, P. J., Part I. Hydrodynamic Stability of Time Dependent Flows, Ph.D. Thesis, University of Massachusetts, Amherst, (1975)

Roe, R. J., V. L. Bacchetta and P. M. G. Wong, "Refinement of Pendant Drop Technique for the Measurement of Surface Tension of Viscous Fluids", J. Phys. Chem., 71, 4190 (1967)

Ruschak, K. J., The Fluid Mechanics of Coating Flows, Ph.D. Thesis, University of Minnesota (1974)

Ruschak, K. J., and L. E. Seriven, "Developing Flow on a Vertical Wall", J. Fluid Mech., 81, 2, 305 (1977)

Savage, M. D., "Cavitation in Lubrication. Part I. On Boundary Conditions and Cavity-Fluid Interfaces", J. Fluid Mech., 80, 4, 743 (1977)

Savage, M. D., "Cavitation in Lubrication. Part II. Analysis of Wavy Interfaces", J. Fluid Mech., 80, 4, 757 (1977)

Sone, T. and M. Fukushima, "An Anomalous Flow During Rolling of Viscous Materials", in: Fourth Int. Congress on Rheology, Proceedings. Lee, E. H., ed., Brown University, Rhode Island (1965)

Stevenson, J. F., S. C. K. Chung and J. T. Jenkins, "Evaluation of Material Functions for Steady Elongational Flows", Trans. Soc. Rheol., 19, 3, 397 (1975)

Swift, H. W., "The Stability of Lubricating Films in Journal Bearings", Proc. Inst. Civil Engrs., London, 233, 267 (1932)

Tanner, R. I., "Full-Film Lubrication Theory for a Maxwell Liquid", Int. J. Mech., 1, 206 (1960)

Tanner, R. I., "Non-Newtonian Lubrication Theory and Its Application to the Short Journal Bearing", Aust. J. Appl. Sci., 14, 129-36 (1963)

Tanner, R. I., "Study of Anisothermal Short Journal Bearings with Non-Newtonian Lubricants", J. Appl. Mech., Trans. ASME, Ser. E, 32, 781 (1965)

Tanner, R. I., "Plane Creeping Flows of Incompressible Second-Order Fluids", Phys. Fluids, 9, 1246 (1966)

Tanner, R. I., "A Test Particle Approach to Flow Classification for Viscoelastic Fluids", AICHE J., 22, 5, 910 (1976)

Tanner, R. I., and R. R. Huilgol, "On a Classification Scheme for Flow Fields", Rheol. Acta, 14, 959 (1975)

Taylor, C. and P. Hood, "A Numerical Solution of the Navier-Stokes Equations Using the Finite Element Technique", Computers and Fluids, 1, 73 (1973)

Taylor, C. M., "Research Note: Separation Cavitation, Solutions for the Infinite Width Cyclinder-Phase and Journal- Bearing Configurations", J. Mech. Eng. Sci., 15, 3, 237 (1973)

Taylor, C. M., "Separation Cavitation in Lightly Loaded Fluid Film Bearings with Both Surfaces in Motion", J. Mech. Eng. Sci., 16, 3, 147 (1974a)

Taylor, C. M., "Film Rupture for a Lubricated Cylinder Lightly Loaded Against a Plane", J. Mech. Eng. Sci., 16, 4, 225 (1974b)

Taylor, G. I., "Cavitation of a Viscous Fluid in Narrow Passages", J. Fluid Mech., 16, 595 (1963)

Trusedell, C., "The Meaning of Viscometry in Fluid Dynamics", Annual Review of Fluid Mechanics, 6 (1974)

VanDyke, M., Perturbation Methods in Fluid Mechanics, Academic Press, New York (1964)

Walters, K., "New Concepts in Theoretical and Experimental Rheology", in: The Rheology of Lubricants, Davenport, T. C., ed., John Wiley & Sons, New York (1973)

Walters, K., Rheometry, John Wiley & Sons, New York (1975)

Williams, G. and R. I. Tanner, "Effects of Combined Shearing and Stretching in Viscoelastic Lubrication Flows", Trans. ASME, J. Lub. Tech., 217 (1970)

Williamson, A. S., "The Tearing of an Adhesive Layer Between Flexible Tapes Pulled Out Apart", J. Fluid Mech., 52, 4 (1972)

Windle, W. and K. M. Beazley, "The Mechanics of Blade Coating", Tappi, 50, 1, 1 (1967)

Windle, W. and K. M. Beazley, "The Role of Viscoelasticity in Blade Coating", Tappi, 51, 8, 340 (1968)

Yamada, Y., K. Ito, Y. Yokuchi and T. Ohtusbo, in: Finite Element Methods in Flow Problems, University of Alabama Press, Huntsville (1974)

A P P E N D I X A

EXPERIMENTAL DATA

The pertinent experimental data of this study are presented in this appendix in a tabular form. This presentation is complementary to the graphical presentation of the results in the text. Each table heading contains reference to the experimental section where a detailed account of the corresponding experiment is given. Experimental errors and standard deviations (for repetetive trials) where given were calculated in the usual manner (Perry 1963).

Table A-1

The Blade Coating Experiment (V. 3):
Coating Thickness Data

Fluid[1]	Blade Position[2]	H_∞ [3] [cm]	λ [4]
G	K-10	0.097	0.59 ± 0.05
G	K-13	0.107	0.72 ± 0.05
G	K-15	0.112	0.81 ± 0.06
G	K-18	0.114	0.88 ± 0.06
KS	K-10	0.095	0.57 ± 0.05
KS	K-13	0.102	0.69 ± 0.05
KS	K-16	0.109	0.81 ± 0.06
KS	K-18	0.107	0.83 ± 0.06
H-1.5	K-10	0.094	0.57 ± 0.05
H-1.5	K-13	0.117	0.79 ± 0.05
H-1.5	K-15	0.124	0.90 ± 0.06
H-1.5	K-16	0.120	0.89 ± 0.06
H-1.5	K-18	0.129	1.00 ± 0.06
H-1	K-18	0.124	0.96 ± 0.06
CMC-2.5	K-18	0.122	0.94 ± 0.06

[1] Key in Table V-2.

[2] Key in Table V-1.

[3] Arithmetic average of about eight multiple runs.

[4] Errors represent standard deviations for repetetive trials.

Table A-2

The Roll Coating Experiment (VI. 4):
Coating Thickness Data for Newtonian
Fluids in Gravity-Free Regime

Fluid[1]	μ^2[poise]	H_0/R	U[rpm]	H_∞^3[mils]	λ
G	11.4	0.0219	8.5	17.7	1.36
			13.5	17.5	1.35
			18	17.8	1.37
		0.0228	37.5	29.	1.29
			48	28.8	1.28
			57	29.1	1.29
			67	29.1	1.29
		0.0306	28	38.7	1.29
			37.5	38.8	1.29
			48	38.8	1.29
			67	38.6	1.29
GW-0.95	5.01	0.0129	18	17.1	1.31
			28	17.4	1.34
			37.5	17.0	1.31
			48	17.3	1.33
		0.0306	86.5	28.5	1.27
			76.5	29.1	1.29
			67	28.8	1.28
			57	28.7	1.28
			48	28.7	1.28
GW-0.90	2.08	0.0129	37.5	17.2	1.32
			57	17.2	1.32
			76.5	17.1	1.31
			97	17.4	1.34
		0.0228	57	28.1	1.25
			67	28.4	1.26
			76.5	28.3	1.26
			86.5	28.3	1.26
		0.0306	67	38.6	1.29
			76.5	38.6	1.29
			86.5	38.8	1.29
			97	38.8	1.29

Table A-2 Con't

Fluid[1]	μ[2][poise]	H_0/R	U[rpm]	H_∞[3][mils]	λ
GWS-0.90	2.50	0.0129	18	17.7	1.36
			28	17.5	1.35
			37.5	17.6	1.35
GW-0.75	0.51	0.0228	97	17.8	1.37
			120	16.9	1.30
			138	18.0	1.38
			155	17.5	1.35
MO	1.44	0.0129	18	17.4	1.34
			37.5	17.3	1.33
			57	17.0	1.31
			76.5	17.3	1.33
			97	17.5	1.35
		0.0228	181	29.0	1.29
			163	28.9	1.28
			146	28.9	1.28
			129	28.7	1.28

[1] Key in Table VI-4.

[2] Viscosities measured at the room temperature for the corresponding runs.

[3] ± 2 mils.

Table A-3

The Roll Coating Experiment (VI. 4):
Coating Thickness Data for Newtonian Fluids. Gravity Effects.

Fluid[1]	μ^2[poise]	H_0/R	U[rpm]	H_∞^3[mils]	λ
GW-0.90	2.08	0.0306	18	26.9	0.90
			28	32.2	1.07
			37.5	35.9	1.20
			48	37.2	1.24
			57	37.8	1.26
			67	38.6	1.29
			76.5	38.6	1.29
			86.5	38.8	1.29
			97	38.8	1.29
		0.0228	18	22.3	0.99
			28	25.9	1.15
			37.5	26.8	1.19
			48	27.3	1.21
			57	27.7	1.23
			67	27.7	1.23
			76.5	27.9	1.24
			86.5	28.4	1.26
			97	28.3	1.26
			112	28.4	1.26
GW-0.75	0.51	0.0306	18	8.9	0.30
			28	12.2	0.41
			37.5	14.9	0.50
			48	17.6	0.59
			67	21.4	0.71
			86.5	24.4	0.81
			112	27.0	0.90
			129	29.8	0.99
			146	31.6	1.05
			168	34.4	1.15
			190	35.1	1.17
MO	1.44	0.0306	18	22.0	0.73
			28	27.4	0.91
			37.5	31.2	1.04
			48	33.1	1.10
			57	34.3	1.14

Table A-3 Con't

Fluid[1]	μ[2][poise]	H_0/R	U[rpm]	H_∞[3][mils]	λ
MO	1.44	0.0306	67	35.3	1.18
			76.5	36.0	1.20
			86.5	36.8	1.23
			97	36.9	1.23
			112	36.9	1.23
			120	37.1	1.24
			129	37.6	1.25
			138	37.7	1.26
			146	37.7	1.26
		0.0228	28	25.1	1.12
			48	27.1	1.20
			67	27.9	1.24
			86.5	28.0	1.24
			112	28.2	1.25
			129	28.7	1.28
			146	28.9	1.28
			163	28.9	1.28
			181	29.0	1.29

[1] Key in Table VI-4.

[2] Viscosities measured at the respective room temperatures for the corresponding runs.

[3] $\pm$ 2 mils.

Table A-4

The Roll Coating Experiment (VI.4):
Coating Thickness Data for Viscoelastic Fluids

Fluid[1]	H_0/R	U[rpm]	H_∞^2[mils]	λ
H-0.15	0.0129	37.5	8.9	0.68
		48	8.6	0.66
		57	9.0	0.69
		67	9.1	0.70
		76.5	9.0	0.69
		86.5	9.1	0.70
		97	9.0	0.69
	0.0228	37.5	10.0	0.44
		48	10.7	0.48
		57	11.6	0.52
		67	12.4	0.55
		76.5	13.2	0.59
		86.5	13.6	0.60
		97	14.5	0.64
		112	14.9	0.66
		120	15.1	0.67
		129	15.7	0.70
		138	16.1	0.72
H-0.25	0.0129	18	10.2	0.78
		23	10.4	0.80
		28	10.5	0.81
		32.5	10.4	0.80
		37.5	10.2	0.78
		42.5	10.2	0.78
	0.0228	48	14.5	0.64
		52	14.3	0.64
		57	14.6	0.65
		62	14.5	0.64
	0.0306	62	20.6	0.69
		67	20.7	0.69
		71.5	20.9	0.70
		76.5	20.7	0.69
		81.5	20.8	0.69
		86.5	20.8	0.69

Table A-4 Con't

Fluid[1]	H_0/R	U[rpm]	H_∞[2][mils]	λ
H-0. 35	0. 0129	8. 5	9. 9	0. 76
		13. 5	10. 1	0. 78
		18	10. 0	0. 77
		23	10. 0	0. 77
	0. 0228	28	16. 0	0. 71
		32. 5	16. 4	0. 73
		37. 5	16. 5	0. 73
	0. 0306	37. 5	19. 2	0. 64
		42. 5	19. 3	0. 64
		48	19. 5	0. 65
H-0. 50	0. 0129	8. 5	11. 8	0. 91
		13. 5	11. 9	0. 91
	0. 0228	13. 5	16. 9	0. 75
		18	16. 9	0. 75
	0. 0306	13. 5	21. 2	0. 71
		18	22. 0	0. 73
		23	21. 7	0. 72
H-0. 75	0. 0129	8. 5	13. 0	1. 0
	0. 0228	8. 5	19. 0	0. 84
HS-0. 35	0. 0129	13. 5	11. 0	0. 85
		18	11. 1	0. 85
		23	11. 0	0. 85
	0. 0228	18	16. 7	0. 74
		23	16. 8	0. 75
		28	17. 1	0. 76
		32. 5	17. 0	0. 76
	0. 0306	18	17. 0	0. 57
		28	19. 0	0. 63
		37. 5	20. 7	0. 69

[1] Key in Table VI-4.

[2] ± 2 mils.

Table A-5

The Reverse-Roll Coating Experiment (VI.6):
Coating Thickness Data for Newtonian Fluids

Fluid[1]	μ^2[poise]	κ	$2H_0^3$[cm]	U_f[rpm]	H_f^4[mils]	ν
G	9.2	0.57	0.065	31.5	25.2	0.84 ± 0.06
				49	29.3	0.81 ± 0.05
				66	33.0	0.77 ± 0.05
				84	36.2	0.77 ± 0.04
				100	39.1	0.78 ± 0.04
				117	42.0	0.77 ± 0.04
		1.75	0.065	18	45.4	1.05 ± 0.05
				28	60.5	1.17 ± 0.04
				37.5	42.4	1.21 ± 0.04
				48	82.9	1.26 ± 0.04
				57	94.4	1.31 ± 0.03
				67	104.0	1.35 ± 0.03
		1.00	0.065	18	35.0	1.07 ± 0.07
				28	41.6	1.04 ± 0.05
				37.5	48.8	1.05 ± 0.05
				48	54.2	1.06 ± 0.04
		1.00	0.114	18	26.0	0.93 ± 0.07
				28	34.3	0.99 ± 0.06
				37.5	39.5	1.01 ± 0.05
				48	44.8	1.01 ± 0.05
				57	49.4	1.01 ± 0.04
				67	54.0	1.02 ± 0.04
		1.00	0.152	28	29.8	0.94 ± 0.07
				37.5	35.3	1.00 ± 0.06
				48	41.1	1.03 ± 0.05
				57	45.3	1.03 ± 0.05
				67	48.9	1.03 ± 0.05
GW-0.90	1.47	0.57	0.065	31.5	17.3	1.04 ± 0.05
				66	21.8	0.95 ± 0.09
				100	25.1	0.89 ± 0.07
				134	27.8	0.85 ± 0.06
				175	30.6	0.82 ± 0.05
		1.75	0.065	18	18.9	0.77 ± 0.08
				37.5	30.5	0.91 ± 0.06
				57	40.5	0.96 ± 0.05

Table A-5 Con't

Fluid[1]	μ[2][poise]	k	$2H_0$[3][cm]	Uf[rpm]	Hf[4][mils]	ν
GW-0.90	1.47	1.75	0.065	76.5	49.4	1.03 ± 0.04
				100	58.0	1.06 ± 0.04
		1.00	0.065	18	16.9	0.96 ± 0.12
				37.5	25.1	1.01 ± 0.09
				57	29.7	0.97 ± 0.07
				76.5	34.3	0.97 ± 0.06
				100	37.9	0.97 ± 0.05

[1] Key in Table VI-4.

[2] Viscosities measured at room temperature for the corresponding runs.

[3] ±0.005 cm

[4] ±2 mils.

Table A-6

The Submerged-Roll Experiment (VII. 3):
Newtonian Pressure Distribution

Fluid   : Karo Syrup

Viscosity :   19.7 poise at 27.8 $\pm$ 1.5°c

H_0 :   0.64 cm

R   :   10.70 cm

| Position | X [cm] | P^1 [cm CCl_4] at speed[2]: | | | |
		U_1	U_2	U_3	U_4
30	3.0	-1.2	-2.4	-3.6	-4.5
40	2.0	-1.5	-2.7	-3.9	-5.1
50	1.0	-1.0	-1.8	-2.6	-3.4
60	0.0	-0.2	-0.2	-0.3	-0.3
70	-1.0	1.4	2.6	4.3	5.3
80	-2.0	2.0	3.6	5.5	7.4
90	-3.0	1.9	3.5	5.2	7.1

[1] ρ_{CCl_4} = 1.58 g/cc;   P = $\pm$ 0.3 cm CCl_4

[2] U_1 = 24.4 rpm

U_2 = 45.4 rpm

U_3 = 67.4 rpm

U_4 = 87.6 rpm

Table A-7

The Submerged Roll Experiment (VII. 3):
Viscoelastic Pressure Distribution

Fluid   :   H-1

Temperature   : $27.0 \pm 2^{o}c$

H_0 :   0.19 cm

R   :   10.70 cm

Position	X [cm]	U[rpm]	P^1[cm CCl4]	Pe^2[cm CCl4]
130	-3.0	53.10	0.7	-0.16
120	-2.0	"	1.4	-0.02
110	-1.0	"	2.9	-0.40
100	0.0	"	0.8	-0.63
90	1.0	"	-2.6	-0.40
80	2.0	"	-2.1	-0.02
70	3.0	"	-1.1	-0.16
130	-3.0	89.22	1.4	-0.22
120	-2.0	"	2.7	-0.03
110	-1.0	"	4.1	-0.55
100	0.0	"	1.2	-0.90
90	1.0	"	-3.4	-0.55
80	2.0	"	-3.1	-0.03
70	3.0	"	-1.8	-0.22

[1] ρ CCl$_4$ = 1.58 g/cc,   P = $\pm$0.3 cm CCl$_4$

[2] Hole-Pressure error.   For discussion see VII.4.

Table A-8

The Newtonian Ribbing Phenomenon (VIII. 2):
Wavelength-Speed Data

Fluid[1]	μ^2[poise]	H_0/R	U[rpm]	U/U*	W /$2H_0$[3]
G	9.60	0.0129	37.5	1.29	11.1
			48	1.66	11.4
			57	1.97	11.1
			67	2.31	11.1
			76.5	2.64	10.7
			86.5	2.98	10.5
			97	3.34	10.8
KS	21.0	0.0228	57	1.84	9.6
			67	2.16	9.0
			76.5	2.47	9.5
			86.5	2.79	9.6
			97	3.13	9.2
			37.5	1.21	10.5
			48	1.55	10.5
GWS-0.90	2.50	0.0129	76.5	1.42	17.2
			86.5	1.60	16.5
			97	1.80	16.9
			112	2.07	16.6
			120	2.22	17.2
			129	2.39	15.7
			138	2.55	15.8
			146	2.70	15.4
			163	3.02	13.5
			181	3.35	15.4

[1] Key in Table VI. 4.

[2] Viscosities measured at the room temperature of the corresponding runs.

[3] Measured photographically.

Table A-9

The Viscoelastic Ribbing Phenomenon (VIII. 3):
Wavelength–Speed Data

Fluid[1]	H_0/R	U[rpm]	U /U*	$W/2H_0$ [2]
H-0.35	0.0129	32.5	1.14	23.1
		37.5	1.32	24.6
		48	1.68	22.3
		57	2.0	18.8
		67	2.35	16.0
		76.5	2.68	14.8
		86.5	3.03	13.7
		112	3.93	14.3
		120	4.21	14.5
		138	4.84	12.8
		155	5.44	12.8
		173	6.07	12.6
	0.0228	67	1.74	14.6
		76.5	1.99	14.5
		86.5	2.25	10.8
		97	2.52	13.6
		112	2.91	12.4
		129	3.35	12.5
		163	4.23	9.3
		181	4.70	11.1
	0.0306	67	1.31	11.5
		86.5	1.70	12.3
		112	2.20	12.8
		129	2.53	9.0
		146	2.86	8.9
		163	3.20	9.2
H-0.75	0.0129	13.5	1.42	29.2
		18	1.89	21.5
		28	2.95	18.5
		37.5	3.95	16.9
		48	5.05	19.1
		67	7.05	16.6
		86.5	9.10	14.2
		112	11.80	10.0
		129	13.58	10.6

Table A-9 Con't

Fluid[1]	H_0/R	U[rpm]	$U/U*$	$W/2H_0$ [2]
H-0.75	0.0129	146	15.39	10.2
		163	17.16	10.9
	0.0228	18	1.44	20.6
		28	2.24	16.7
		37.5	3.00	12.3
		48	3.84	12.3
		67	5.36	10.9
		86.5	6.92	10.4
		112	8.69	7.4
		129	10.32	7.6
		146	11.68	7.4
		163	13.04	8.2
		181	14.48	8.0
	0.0306	18	1.16	13.5
		28	1.81	11.2
		37.5	2.42	11.0
		48	3.10	9.5
		67	4.32	9.9
		86.5	5.58	9.0
		112	7.23	9.0
		129	8.32	7.1
		146	9.42	6.6

[1] Key in Table VI-4.

[2] Measured photograhically.

A P P E N D I X   B

VISCOMETRIC DATA

A tabular listing of the viscometric functions η and $\underline{\psi}_{12}$ for all the viscoelastic fluids used in this study is presented. These functions were measured by a Rheometrix Mechanical Spectrometer using a cone-and-plate mode. The geometric parameters for the set used in all the measurements are:

    diameter   -   100 mm

    cone angle -   0.040 rad.

    gap   -   0.050 mm

Inasmuch as the various solutions were prepared in a slightly different manner in each of the experiments conducted (see respective experimental sections), the corresponding experiments are specified in each of the tables presented below.

Errors arising from finite inertial effects were corrected using a well accepted formula for the inertial contribution to the normal force (Olabisi and Williams 1972, Walters 1975).

$$Fi = -\frac{3\pi \rho \Omega^2 R^2}{40} \qquad (B-1)$$

Ω is the rotational speed of the cone (in radians/sec.) and R is the cone radius. Eq. (B-1) can be easily written in terms of the first normal-stress

coefficient and for the system used one finds

$$\Psi_{12}\text{corr.} = \Psi_{12}\text{meas.} + 0.006 \text{ (in poise x sec.)} \tag{B-2}$$

Thus, the inertial correction should be considered only in the limit of

$$\Psi_{12}\text{meas.} \leq 0.1 \text{ poise x sec.}$$

Table B-1

Viscometric Data for H-1
(Blade Coating Experiment)

Temperature: 25.0°c

$\dot{\gamma}$ [sec^{-1}]	η [poise]	ψ_{12}[poise x sec]
0.025	300.0	-
0.04	281.2	-
0.0625	270.0	-
0.1	225.0	-
0.157	180.9	-
0.25	142.4	-
0.40	116.2	781.2
0.625	88.8	399.9
1.0	68.2	218.8
1.575	51.17	126.0
2.5	39.0	60.0
4.0	29.1	29.3
6.25	21.3	15.2
10.00	15.4	7.50
15.75	11.4	3.90
25.00	8.25	1.90
62.5	4.38	0.540
100.0	3.19	0.275
157.5	2.36	0.141

Table B-2

Viscometric Data for H-1.5
(Blade Coating Experiment)

Temperature: 25.0°c

$\dot{b}$ [sec^{-1}]	η[poise]	Ψ_{12}[poise x sec]
0.025	824.0	-
0.04	795.0	-
0.0625	718.4	-
0.157	451.4	-
0.25	344.4	-
0.4	299.5	234.2
1.0	138.6	530.8
1.575	100.2	304.0
2.5	76.4	139.9
6.25	39.5	32.0
10.0	28.5	15.0
15.75	20.2	7.50
25.0	14.6	3.80

Table B-3

Viscometric Data for CMC-2.5
(Blade Coating Experiment)

Temperature: 25.0°c

$\dot{\gamma}$ [sec^{-1}]	η [poise]	Ψ_{12}[poise x sec]
0.1575	47.6	–
0.25	45.0	–
0.40	42.2	–
0.625	39.0	–
1.0	35.6	–
1.575	32.1	75.6
2.5	28.5	40.0
4.0	23.9	19.5
6.25	21.0	8.48
10.0	16.5	3.44
15.75	13.81	–
25.0	11.4	0.600
40.0	9.56	0.312

Table B-4

Viscometric Data for H-0.15
(Roll Coating Experiment)

Temperature: 26.0°c

$\dot{\gamma}$ [sec^{-1}]	η [poise]	ψ_{12} [poise x sec]
10.0	0.940	0.380[1]
15.75	0.710	0.210[1]
25.0	0.600	0.130[1]
40.0	0.420	0.065[1]
62.5	0.330	0.036[1]
100.0	0.280	0.020[1]
157.5	0.210	0.011[1]
250.0	0.172	–

[1] Corrected for inertial effects.

Table B-5

Viscometric Data for H-0.25
(Roll Coating Experiment)

Temperature: 23.0°c

$\dot{\gamma}$ [sec^{-1}]	η [poise]	ψ_{12}[poise x sec]
1.0	7.50	25.0
1.575	5.95	12.6
2.5	4.50	6.00
4.0	3.75	3.51
6.25	3.00	1.92
10.0	2.25	1.00
15.75	1.67	0.530
25.0	1.29	0.280[1]
40.0	0.980	0.150[1]
62.5	0.750	0.083[1]
100.0	0.562	0.045[1]
157.5	0.460	0.025[1]
250.0	0.340	0.014[1]

[1] Corrected for inertial effects.

Table B-6

Viscometric Data for H-0.35
(Roll Coating Experiment)

Temperature: 23.0°c

$\dot{\gamma}$ [sec^{-1}]	η [poise]	Ψ_{12}[poise x sec]
0.4	14.1	117.2
0.625	13.2	64.0
1.0	13.1	37.5
1.575	9.52	20.2
2.5	6.75	11.0
4.0	5.34	6.05
6.25	3.72	3.12
10.0	3.37	1.50
15.75	2.48	0.831
25.0	1.87	0.450[1]
40.0	1.50	0.240[1]
62.5	1.17	0.131[1]
100.0	0.862	0.070[1]
157.5	0.678	0.038[1]
250.0	0.510	0.021[1]

[1] Corrected for inertial effects.

Table B-7

Viscometric Data for HS-0.35
(Roll Coating Experiment)

Temperature: 24.5°c

$\dot{\gamma}$ [sec^{-1}]	η [poise]	Ψ_{12}[poise x sec]
0.4	14.0	109.4
0.625	12.0	64.0
1.0	13.1	35.0
1.575	9.52	21.2
2.5	6.75	11.6
4.0	5.34	5.78
6.25	4.20	2.88
10.0	3.37	1.45
15.75	2.48	0.786
25.0	1.87	0.450[1]
40.0	1.45	0.237[1]
62.5	1.14	0.131[1]
100.0	0.862	0.070[1]
157.5	0.643	0.038[1]

[1] Corrected for inertial effects.

Table B-8

Viscometric Data for H-0.5
(Roll Coating Experiment)

Temperature: 23.0°c

$\dot{\gamma}$ [sec^{-1}]	η [poise]	Ψ_{12} [poise x sec]
0.25	37.5	300.0
0.40	37.5	156.2
0.625	30.0	96.0
1.0	22.5	68.8
1.575	16.7	37.8
2.5	12.9	20.0
4.0	9.84	10.2
6.25	7.20	5.44
10.0	5.25	2.75
15.75	4.05	1.41
25.0	3.22	0.750[1]
40.0	2.44	0.400[1]
62.5	1.80	0.217[1]
100.0	1.29	0.111[1]
157.5	1.01	0.060[1]
250.0	0.750	0.032[1]

[1] Corrected for inertial effects.

Table B-9

Viscometric Data for HS-0.5
(Roll Coating Experiment)

Temperature: 25.0°c

$\dot{\gamma}$ [sec^{-1}]	η [poise]	Ψ_{12} [poise x sec]
0.25	37.5	320.0
0.40	37.5	218.7
0.625	33.0	140.8
1.0	24.4	72.5
1.575	17.9	42.3
2.5	12.0	20.0
4.0	9.84	10.2
6.25	7.80	5.28
10.0	5.62	2.69
15.75	4.17	1.41
25.0	3.30	0.770[1]
40.0	2.53	0.408[1]
62.5	1.83	0.217[1]
100.0	1.39	0.108[1]
157.5	1.07	0.060[1]

[1] Corrected for inertial effects.

Table B-10

Viscometric Data for H-0.75
(Roll Coating Experiment)

Temperature: 23.0°c

$\dot{\gamma}$ [sec^{-1}]	η [poise]	Ψ_{12} [poise x sec]
0.0625	150.0	–
0.1	150.0	1250'
0.1575	119.1	1512'
0.25	90.0	860.0
0.4	75.0	507.0
0.625	50.6	320.0
1.0	45.0	150.0
1.575	33.3	73.1
2.5	25.5	34.0
4.0	18.7	16.8
6.25	14.4	9.44
10.0	10.5	4.94
15.75	7.38	2.59
25.0	5.70	1.36
40.0	4.12	0.680
62.5	3.00	0.380
100.0	2.25	0.193[1]
157.5	1.67	0.106[1]
250.0	1.20	0.056[1]

[1] Corrected for intertial effects

Table B-11

Viscometric Data for H-1
(Sumberged Roll Experiment)

Temperature: 27.0°c

$\dot{\gamma}$ [sec^{-1}]	η [poise]	Ψ_{12}[poise x sec]
1.0	45.0	60.0
1.575 ·	33.3	34.3
2.5	24.0	19.2
4.0	18.0	10.9
6.25	13.4	6.40
10.0	10.2	3.20
15.75	7.62	1.79
25.0	6.12	0.960
40.0	4.42	0.510
62.5	3.48	0.280[1]
100.0	2.62	0.150[1]
157.5	1.95	0.077[1]
250.0	1.44	0.042[1]

[1] Corrected for inertial effects.

A P P E N D I X C

PERTURBATION ANALYSES

C.1   Preliminaries

The (approximate) solution of the dynamic equation, Eq. (IV-2), combined with the empirical viscosity model (Eq. IV-12), can be carried out conveniently using a regular perturbation technique. The essentials of the perturbation scheme are presented and discussed in IV.3.

The perturbation solution, though conceptually simple, can be in some cases quite involved algebraically. For systems in which the velocity field does not possess a plane (or axis) of symmetry, for example, the solution is particularly lengthy. Two such systems were encountered in the course of this study: the rigid planar blade coater and the submerged roll. In both systems, the analytical solution is hampered by the need to integrate functions that contain absolute-value operators. This difficulty can be overcome by dividing the flow domain into zones which are characterized by the general shape of the local Newtonian velocity profile. The perturbation analysis is then carried out separately for each zone with the condition that all the hydrodynamic functions are continuous across the zone boundaries.

The analysis begins with Eq. (IV-16) which reads:

$$\frac{d\varphi}{d\eta} = (\dot{\kappa}\eta + C)\left[1 + N_e\left(\left|\frac{d\varphi}{d\eta}\right|\right)^{1-n}\right] \tag{C-1}$$

N_e is a viscoelastic characteristic of the system and it is utilized in this analysis as a perturbation parameter. All the dependent variables in Eq. (C-1) are linearized in the following manner

$$\varphi = \varphi^0 + N_e \varphi^1 + \ldots \tag{C-2}$$

$$\dot{\pi} = \dot{\pi}^0 + N_e \dot{\pi}^1 + \ldots \tag{C-3}$$

$$C = C^0 + N_e C^1 + \ldots \tag{C-4}$$

and also

$$\lambda = \lambda^0 + N_e \lambda^1 + \ldots \tag{C-5}$$

where λ is a dimensionless flow rate defined by

$$\lambda = \int_0^{\sigma} \varphi \, d\eta$$

$\eta = 0$ and $\eta = \sigma$ are the positions of the lower and upper boundaries of the system.

The linearized functions are introduced back into Eq. (C-1) and after equating the first-order terms one is left with a first-order equation to be solved. The boundary conditions for the first-order functions appearing in this equation can be formulated by assuming that these functions vanish identically on the system boundaries where the zeroth-order functions meet exactly the physical boundary conditions. This is a common practice in regular perturbation analyses.

Finally, it is useful to define the following functions

$$X \equiv - \frac{\dot{\pi}^0 \sigma}{2} + \frac{1}{\sigma} \tag{C-6}$$

and

$$Y = \frac{\dot{\kappa}^0 \mathcal{S}}{2} + \frac{1}{\mathcal{S}} \tag{C-7}$$

Both are used for characterizing the various zones in the corresponding flow domains.

Complete perturbation solutions of the blade coating problem and the submerged-roll problem are presented below.

C.2 The Rigid Planar Blade Coater

The various physical considerations of this problem are discussed in V.2. It was found that the Newtonian velocity distribution for this system has the form

$$\varphi^0 = \frac{1}{2} \dot{\kappa}^0 \eta^2 - Y\eta + 1 \tag{C-8}$$

or

$$\frac{d\varphi^0}{d\eta} = \dot{\kappa}^0 \eta - Y \tag{C-9}$$

From inspection of Eq. (C-9) it is seen that the velocity profile in this system can have three general shapes. These possible shapes are presented schematically in Figure C-1. Conditions for each such configuration can be easily derived in terms of the functions X and Y. It is found that,

$$\text{in Zone A} \quad : \quad X > 0, \ Y > 0 \tag{C-10}$$

$$\text{in Zone B} \quad : \quad X < 0, \ Y > 0 \tag{C-11}$$

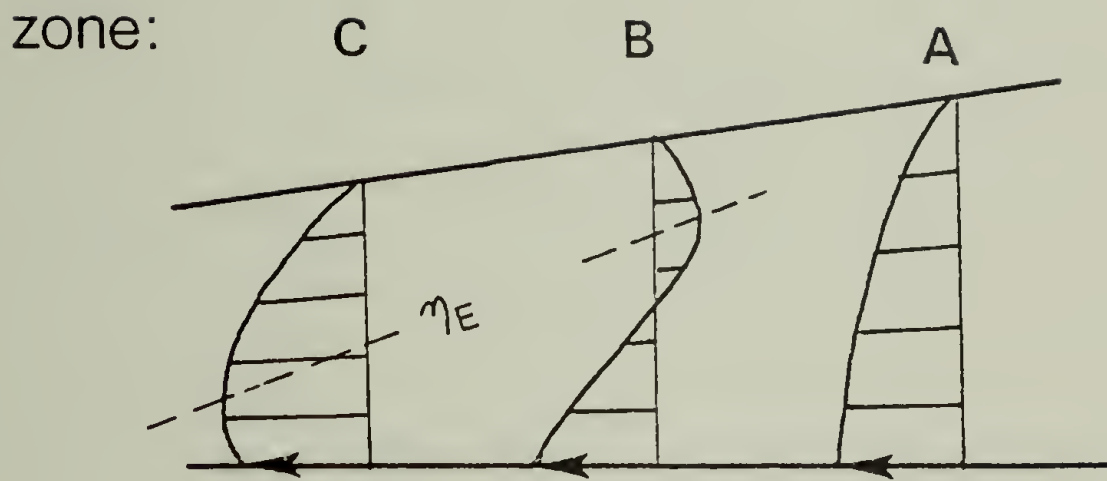$$\text{and} \quad \text{in Zone C} \quad : \quad X > 0, \ Y < 0 \tag{C-12}$$

Figure C-1. The rigid planar blade coater: possible velocity profiles.

These are necessary and sufficient conditions.

<u>Zone A.</u> Introducing the linearized functions into Eq. (C-1) and equating first-order terms, one finds

$$\frac{d\varphi_A^1}{d\eta} = \dot{\kappa}_A^1 \eta + C_A^1 + (\dot{\kappa}^0\eta - Y)\left|\frac{d\varphi^0}{d\eta}\right|^{1-n} \tag{C-13}$$

Since $d\varphi^0/d\eta < 0$ in Zone A one can write

$$\frac{d\varphi_A^1}{d\eta} = \dot{\kappa}_A^1 \eta + C_A^1 - (Y - \dot{\kappa}^0\eta)^{2-n} \tag{C-14}$$

and integration gives

$$\varphi_A^1 = \dot{\kappa}_A^1 \frac{\eta^2}{2} + C_A^1\eta + \frac{1}{p\dot{\kappa}^0}(Y - \dot{\kappa}^0\eta)^p + C_A' \tag{C-14}$$

where C_A' is a constant of integration. C_A' and C_A^1 can be determined by specifying:

$$\varphi_A^1 = 0 \quad @ \quad \eta = \varsigma$$

and $\tag{C-16}$

$$\varphi_A^1 = 0 \quad @ \quad \eta = 0$$

and it follows that

$$\varphi_A^1 = \dot{\kappa}_A^1 \frac{\eta^2}{2} - \frac{\eta}{\varsigma}\left[\dot{\kappa}_A^1 \frac{\varsigma^2}{2} + \frac{X^p - Y^p}{p\dot{\kappa}^0}\right]$$

$$\tag{C-17}$$

$$+ \frac{1}{p\dot{\kappa}^0}(Y - \dot{\kappa}^0\eta)^p - \frac{Y^p}{p\dot{\kappa}^0}$$

λ^1 can now be evaluated from integration of φ^1, and after some rearrangements it is found that

$$\dot{\mathcal{R}}\,^1_A = -12\frac{\lambda^1}{\delta^3} - \frac{G}{\delta^{2p}\,\dot{\mathcal{R}}\,^0}\,[X^p + Y^p]$$

$$- \frac{12}{\delta^3\,\dot{\mathcal{R}}\,^{02}p\,(p+1)}\cdot[X^{p+1} - Y^{p+1}] \tag{C-18}$$

<u>Zone B.</u> The analysis begins again with Eq. (C-13). However, since $d\,\varphi^0/d\eta$ is not monotonous across the film in this zone, it is necessary to divide the flow cross-section into two regions: region B1 corresponds to $\eta < \eta_E$ where $d\,\varphi^0/d\eta < 0$ and region B2 corresponds to $\eta > \eta_E$ where $d\,\varphi^0/d\eta > 0$. Separate integrations of Eq. (C-13) for each region give

$$\varphi^1_{B1} = \dot{\mathcal{R}}\,^1_B\,\frac{\eta^2}{2} + C^1_{B1}\eta + \frac{1}{p\,\dot{\mathcal{R}}\,^0}\,(Y - \dot{\mathcal{R}}\,^0\eta)^p + C'_{B1} \tag{C-19}$$

and

$$\varphi^1_{B2} = \dot{\mathcal{R}}\,^1_B\,\frac{\eta^2}{2} + C^1_{B2}\eta + \frac{1}{p\,\dot{\mathcal{R}}\,^0}\,(\dot{\mathcal{R}}\,^0\eta - Y)^p + C'_{B2} \tag{C-20}$$

The constants of integration C^1_{B1}, C'_{B1}, C^1_{B2}, C'_{B2} are determined from the following boundary conditions

$$\varphi^1_{B1} = 0 \qquad @ \quad \eta = 0$$

$$\varphi^1_{B2} = 0 \qquad @ \quad \eta = \delta$$

$$\varphi^1_{B1} = \varphi^1_{B2} \qquad @ \quad \eta = \eta_E$$

$$\frac{d\,\varphi^1_{B1}}{d\eta} = \frac{d\,\varphi^1_{B2}}{d\eta} \qquad @ \quad \eta = \eta_E$$

$$\tag{C-21}$$

The last two are continuity conditions. Finally, the following expressions for φ_{B1}^1 and φ_{B2}^1 are obtained

$$\varphi_{B1}^1 = \dot{\mathcal{R}}_B^1 \frac{\eta^2}{2} - \frac{\eta}{\varsigma} [\dot{\mathcal{R}}_B^1 \frac{\varsigma^2}{2} + \frac{(-X)^p - Y^p}{p \dot{\mathcal{R}}^0}]$$
$$+ \frac{1}{p \dot{\mathcal{R}}^0} (Y - \dot{\mathcal{R}}^0 \eta)^p \tag{C-22}$$

and

$$\varphi_{B2}^1 = \dot{\mathcal{R}}_B^1 \frac{\eta^2}{2} - \frac{\eta}{\varsigma} [\dot{\mathcal{R}}_B^1 \frac{\varsigma^2}{2} + \frac{(-X)^p - Y^p}{p \dot{\mathcal{R}}^0}]$$
$$+ \frac{1}{p \dot{\mathcal{R}}^0} (\dot{\mathcal{R}}^0 \eta - Y)^p \tag{C-23}$$

Again, $\dot{\lambda}^1$ is evaluated by integration of φ_B^1 across the film, that is

$$\lambda^1 = \int_0^{\eta_E} \varphi_{B1}^1 \, d\eta + \int_{\eta_E}^{\varsigma} \varphi_{B2}^1 \, d\eta \tag{C-24}$$

and after some rearrangements, the following expression for $\dot{\mathcal{R}}_B^1$ is found

$$\dot{\mathcal{R}}_B^1 = -\lambda^1 \frac{12}{\varsigma^3} - \frac{6}{\varsigma^2 p \dot{\mathcal{R}}^0} [(-X)^p + Y^p]$$
$$+ \frac{12}{\varsigma^3 \dot{\mathcal{R}}^{02} p(p+1)} [(-X)^{p+1} + Y^{p+1}] \tag{C-25}$$

Zone C. The analysis in this case follows closely the analysis for Zone B and the results for φ^1 and $\dot{\mathcal{R}}^1$ can be obtained by inspection. In this zone, region C_1 corresponds to $\eta < \eta_E$ where $d\varphi^0/d\eta > 0$ and region C_2 corresponds to $\eta > \eta_E$ where $d\varphi^0/d\eta < 0$.

The first-order functions for Zone C are as follows:

$$\varphi^1_{C1} = \dot{\mathcal{R}}^1_C \frac{\eta^2}{2} - \frac{\eta}{6} [\dot{\mathcal{R}}^1_C \frac{\varsigma^2}{2} + \frac{X^p-(-Y)^p}{p}_0]$$

$$+ \frac{1}{p\dot{\mathcal{R}}^0} (\dot{\mathcal{R}}^0 \eta - Y)^p - \frac{1}{p\dot{\mathcal{R}}^0} (- Y)^p \qquad (C-26)$$

$$\varphi^1_{C2} = \dot{\mathcal{R}}^1_C \frac{\eta^2}{2} - \frac{\eta}{6} [\dot{\mathcal{R}}^1_C \frac{\varsigma^2}{2} - \frac{X^p-(-Y)^p}{p\dot{\mathcal{R}}^0}]$$

$$+ \frac{1}{p\dot{\mathcal{R}}^0} (Y - \dot{\mathcal{R}}^0_\eta)^p - \frac{1}{p\dot{\mathcal{R}}^0} (-Y)^p \qquad (C-27)$$

and

$$\dot{\mathcal{R}}^1_C = -\lambda^1 \frac{12}{\varsigma^3} - \frac{6}{\varsigma^2 p \dot{\mathcal{R}}^0} [X^p + (-Y)^p]$$

$$- \frac{12}{\varsigma^3 \dot{\mathcal{R}}^{02} p(p+1)} [X^{p+1} + (-Y)^{p+1}] \qquad (C-28)$$

Once expressions for $\dot{\mathcal{R}}^1$ are on hand it is possible to solve for λ^1 by specifying in addition that

$$\mathcal{R}^0(1) + N_e \mathcal{R}^1(1) = 0 \qquad (c-29)$$

This additional constraint yields (see Eq. V-31)

$$\lambda^1 = \frac{K^2}{6(K+1)} \dot{\mathcal{R}}^1(1) \qquad (C-30)$$

This equation needs to be solved simultaneously with the equations for $\dot{\mathcal{R}}^1$.

Such solution has been carried out via successive approximations and the

final results for $\lambda^1(K,\eta)$ and for $\mathcal{R}(N_e, K, \eta)$ are presented in V.2.3.

C.3   The Submerged-Roll System

A physical statement of this problem is given in VII. 2.   The Newtonian velocity distribution in the submerged-roll system was found to have the form

$$0 = \frac{\dot{\mathcal{R}}^0 \eta^2}{2} + X\eta \tag{C-31}$$

or

$$\frac{d\varphi^0}{d\eta} = \dot{\mathcal{R}}^0 \eta + X \tag{C-32}$$

In this case, the velocity profile can assume two distinct shapes.   These cases are presented in Figure C-2 and it can be shown, using the expression for $\dot{\mathcal{R}}^0$, that these are the only physically admissible forms of the velocity profile.   The zones corresponding to these profiles are distinguished by the following conditions

in Zone A   : $X > 0$, $Y > 0$ $\tag{C-33}$

(and it corresponds to $\mathcal{S} < 2$)

and   in Zone B   : $X < 0$, $Y > 0$ $\tag{C-34}$

(and it corresponds to $\mathcal{S} > 2$).

As before, these are necessary and sufficient conditions.

Zone A.   Introducing the expanded functions into Eq. (C-1) and equating first-order terms yields the following first-order equation,

$$\frac{d\varphi_A^1}{d\eta} = \dot{\mathcal{R}}_A^1 \eta + C_A^1 + (\dot{\mathcal{R}}^0 \eta + X)\left(\frac{d\varphi^0}{d\eta}\right)^{1-n} \tag{C-35}$$
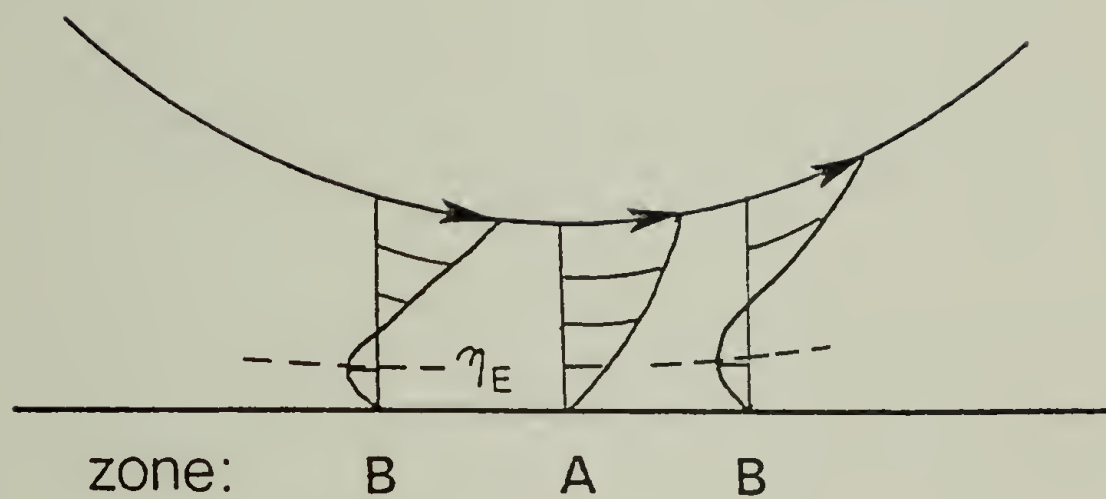
Figure C-2. The submerged-roll system: possible velocity profiles.

This equation is equivalent to Eq. (C-13) in the analysis for the blade coater. Since $d\varphi^0/d\eta > 0$ in Zone A one can write,

$$\frac{d\varphi_A^1}{d\eta} = \dot{\pi}_A^1 \eta + C_A^1 + (\dot{\pi}_A^0 \eta + X)^{2-n} \qquad \text{(C-36)}$$

and integration gives

$$\varphi_A^1 = \dot{\pi}_A^1 \frac{\eta^2}{2} + C_A^1 \eta + \frac{1}{p\dot{\pi}^0}(\dot{\pi}^0\eta + X)^p + C_A' \qquad \text{(C-37)}$$

Specifying

$$\varphi_A^1 = 0 \qquad @ \ \eta = 0$$

and

$$\varphi_A^1 = 0 \qquad @ \ \eta = \varsigma \qquad \text{(C-38)}$$

allows the evaluation of the integration constants C_A^1 and C_A' and it follows that

$$\varphi_A^1 = \dot{\pi}_A^1 \frac{\eta^2}{2} - \frac{\eta}{\varsigma}\left(\frac{\dot{\pi}_A^1 \varsigma^2}{2} - \frac{X^p - Y^p}{\dot{\pi}^0 p}\right)$$

$$+ \frac{1}{p\dot{\pi}^0}(\dot{\pi}^0\eta + X)^p - \frac{X^p}{p\dot{\pi}^0} \qquad \text{(C-39)}$$

Integration of φ_A^1 with respect to η across the film gives an expression for λ^1 which can be rearranged to

$$\dot{\pi}_A^1 = -\lambda^1 \frac{12}{\varsigma^3} - \frac{6}{\varsigma^2 p\dot{\pi}^0}[X^p + Y^p]$$

$$- \frac{12}{\varsigma^3 \dot{\pi}^{02}p(p+1)}[X^{p+1} - Y^{\bar{p}+1}] \qquad \text{(C-40)}$$

Zone B. In order to integrate Eq. (C-35) it is necessary to distinguish between two regions since φ^0 is not a monotonous function in this zone. In region B1 $d\varphi^0/d\eta < 0$ ($\eta < \eta_E$) and in region B2 $d\varphi^0/d\eta > 0$ ($\eta > \eta_E$). Eq. (C-35) can now be integrated separately in each region to give

$$\varphi^1_{B1} = \dot{\mathcal{K}}^1_B \frac{\eta^2}{2} + C^1_{B1} \eta + \frac{1}{\dot{\mathcal{K}}^0 p} (- \dot{\mathcal{K}}^0 \eta - X)^p + C'_{B1}$$

(C-41)

and

$$\varphi^1_{B2} = \dot{\mathcal{K}}^1_B \frac{\eta^2}{2} + C^1_{B2} \eta + \frac{1}{\dot{\mathcal{K}}^0 p} (\dot{\mathcal{K}}^0 \eta + X)^p + C'_{B2}$$

(C-42)

As before, the various integration constants are evaluated using the following conditions

$$\varphi^1_{B1} = 0 \qquad @ \qquad \eta = 0$$

$$\varphi^1_{B2} = 0 \qquad @ \qquad \eta = \mathcal{L}$$

$$\varphi^1_{B1} = \varphi^1_{B2} \qquad @ \qquad \eta = \eta_E$$

and

$$\frac{d\varphi^1_{B1}}{d\eta} = \frac{d\varphi^1_{B2}}{d\eta} \qquad @ \qquad \eta = \eta_E$$

and it follows that

$$\varphi^1_{B1} = \dot{\pi}^1_B \frac{\eta^2}{2} - \frac{\eta}{\varsigma} \left[\frac{\dot{\pi}^1_B \varsigma^2}{2} - \frac{(-X)^p - Y^p}{\pi^0 p} \right]$$

$$+ \frac{1}{\pi^0 p} (-\dot{\pi}^0 \eta - X)^p - \frac{1}{\pi^0 p} (-X)^p \qquad \text{(C-44)}$$

and

$$\varphi^1_{B2} = \dot{\pi}^1_B \frac{\eta^2}{2} - \frac{\eta}{\varsigma} \left[\frac{\dot{\pi}^1_B \varsigma^2}{2} - \frac{(-X)^p - Y^p}{\pi^0 p} \right]$$

$$+ \frac{1}{\pi^0 p} (\dot{\pi}^0 \eta + X)^p - \frac{1}{\pi^0 p} (-X)^p \qquad \text{(C-45)}$$

λ^1 can now be evaluated using Eq. (C-24) and after some rearrangements it is found that

$$\dot{\pi}^1_B = -\lambda^1 \frac{12}{\varsigma^3} - \frac{6}{\varsigma^2 \pi^0 p} [(-X)^p + Y^p]$$

$$+ \frac{12}{\pi^{02} \varsigma^3 p(p+1)} [(-X)^{p+1} + Y^{p+1}] \qquad \text{(C-46)}$$

At this stage the equations for $\dot{\pi}^1$ contain an unknown quantity, λ^1. Thus, in order to solve for π^1 it is necessary to consider an additional constraint. One such constraint can be supplied by the statement

$$\pi^1(1) = 0 \qquad \text{(C-47)}$$

This statement is physically reasonable since it is expected that the pressure function would be anti-symmetric relative to the geometric axis of symmetry ($\int = 0$). (See VII. 2. 3 for further considerations).

It is now possible to evaluate π^1 by solving Eq. (C-47) simultaneously with the equations for $\dot{\pi}^1$. Such a solution was carried out by

successive approximations with a result for $\lambda^1(n)$. The solution for

$\lambda^1(n)$ is presented in Figure C-3. With λ^1 on hand it is possible to

calculate the pressure distribution by numerical integration of the expres-

sions for $\dot{\pi}^1$. Several pressure distributions for the submerged-roll

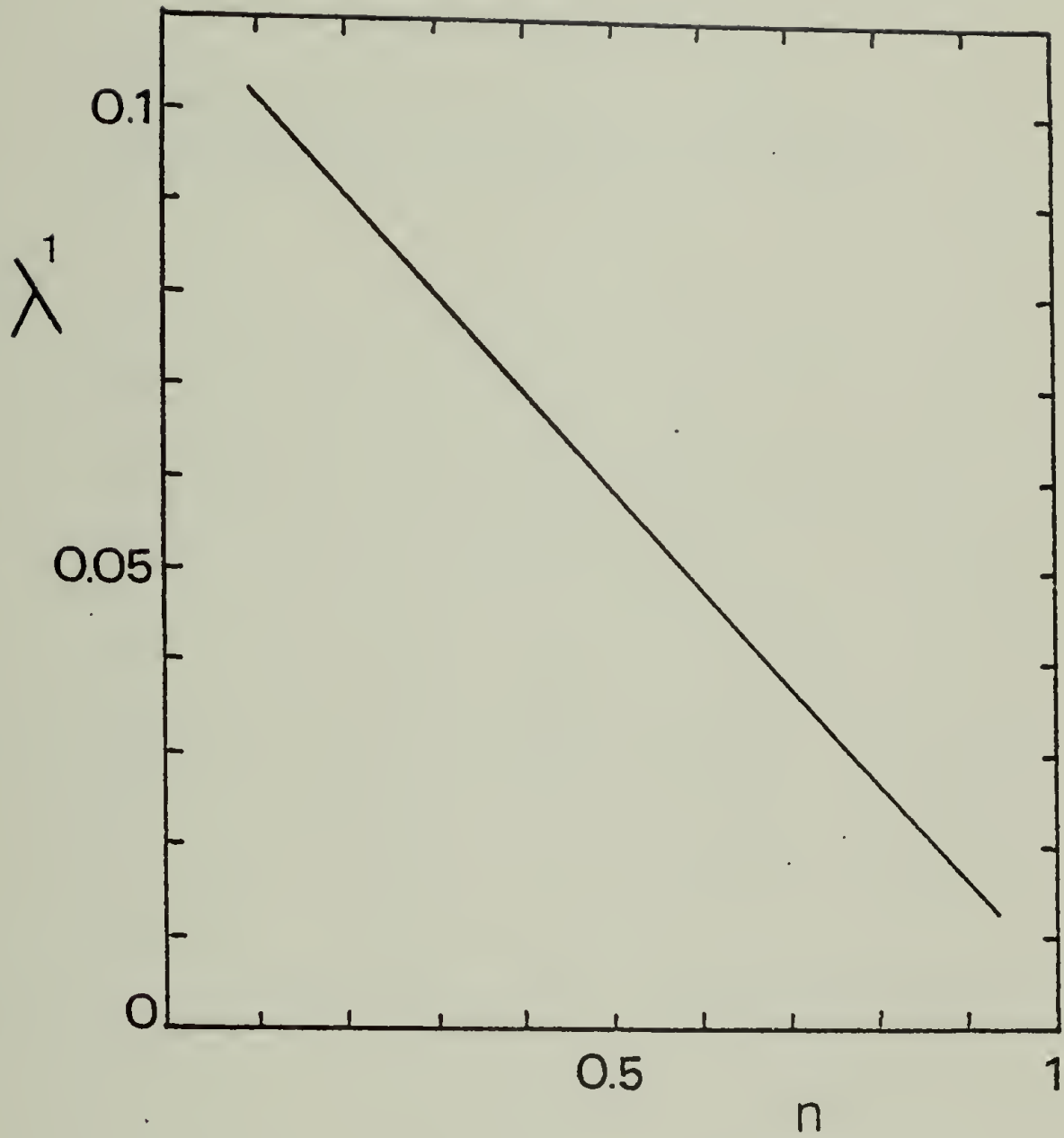system, based on this calculation, are presented in VII.2.3.

Figure C-3.   The first-order flow-rate function vs. the power law index.
Perturbation analysis result for a CEF fluid in a submerged-
roll system.

A P P E N D I X D

A FINITE ELEMENT (FEM) SOLUTION OF
THE CREEPING PLANAR FLOW PROBLEM

D. 1 Scope

The lubrication approximation was employed in the current study for

solving the flow equations for the systems under consideration. It was

shown that this approximation essentially transforms a two-dimensional flow

into a unidirectional flow, thereby allowing a straightforward solution of

the dynamic equation (at least for Newtonian fluids). Some degree of arbi-

trariness, however, is involved in the application of the lubrication assump-

tions and it is clearly of interest to assess the error associated with such

approximation. The most direct way for assessing the validity of the

lubrication solution is to solve the full (planar) creeping flow problem for

the pertinent geometries and compare the result with the approximate

solution. Since a simple analytical solution of the planar flow equations is

not possible (for the geometries considered) one has to resort to some

effective numerical technique.

The finite-element method (FEM) is an extremely versatile numerical

tool and it is particularly adaptive to boundary-value problems with complex

geometries. This method was selected for solving the two-dimensional flow

equations and it is applied for two systems: the rigid planar blade coater

and the submerged-roll system. Physical statements of the corresponding problems are given in Chapters V and VII respectively. In both cases the solution is carried out for geometries similar to the corresponding experimental geometries.

The FEM approach for solving the slow viscous flow problem is presented and discussed in D.2. Subsequently, in D.3 and D.4 the FEM models are introduced and the numerical results are presented. The computer code for the FEM scheme is given in D.5.

D.2 Slow Viscous Flow and the FEM Approach

Creeping planar flow systems are governed by the following equations (in cartesian coordinates),

Continuity:

$$\frac{\partial u}{\partial x} + \frac{\partial v}{\partial y} = 0 \tag{D-1}$$

Momentum:

$$\frac{\partial P'}{\partial y} = (\frac{\partial^2 u}{\partial x^2} + \frac{\partial^2 u}{\partial y^2}) \tag{D-2}$$

$$\frac{\partial P'}{\partial y} = (\frac{\partial^2 v}{\partial x^2} \quad \frac{\partial^2 v}{\partial y^2}) \tag{D-3}$$

P' is a viscosity normalized pressure and u and v are the x- and y-components of the velocity vector. The objective of the FEM analysis is to evaluate the unknown functions P', u and v throughout the flow domain subject to the above equations. There are several ways in which the FEM equations

can be formulated for slow viscous flow problems. In this analysis a "pressure and velocity" formulation is adopted following a procedure outlined by Yamada et al. (1974) and Huebner (1975).

The finite element solution begins by dividing the flow domain into arbitrarily shaped small subdomains that contain three or more nodes. These subdomains are called finite elements. All three hydrodynamic functions are then approximated over a single element domain by suitable interpolation functions whose coefficients are the unknown nodal values of the unknown functions. This can be written in the form

$$u^{(e)} \; = \; \lfloor N \rfloor \{u\} \tag{D-4}$$

$$v^{(e)} \; = \; \lfloor N \rfloor \{v\} \tag{D-5}$$

$$\overset{!}{P}{}^{(e)} \; = \; \lfloor N^e \rfloor \{P\} \tag{D-6}$$

$u^{(e)}$, $v^{(e)}$ and $\overset{!}{P}{}^{(e)}$ are the approximate functions over the domain of element (e). $\lfloor N \rfloor$ and $\lfloor N^e \rfloor$ are row vectors with components which are the nodal interploation functions for the velocity and the pressure respectively. $\{u\}$, $\{v\}$ and $\{P\}$ are column vectors of the nodal degrees-of-freedom (DOF).

The governing equations are now transformed into a set of algebraic equations for a single element using the method of weighted residuals combined with Galerkin's criterion. This criterion is applied in a node i of element (e) in the following manner:

$$\int_{(e)} \Lambda_i \ [\frac{\partial^2 u^{(e)}}{\partial x^2} + \frac{\partial^2 u^{(e)}}{\partial y^2} - \frac{\partial P^{(e)}}{\partial x}] \ dxdy = 0 \tag{D-7}$$

$$\int_{(e)} \Lambda_i \ [\frac{\partial^2 v^{(e)}}{\partial x^2} + \frac{\partial^2 v^{(e)}}{\partial y^2} - \frac{\partial P^{(e)}}{\partial y}] \ dxdy = 0 \tag{D-8}$$

$$\int_{(e)} \Lambda_i^p \ [\frac{\partial u^{(e)}}{\partial x} + \frac{\partial v^{(e)}}{\partial y}] \ dxdy = 0 \tag{D-9}$$

Insertion of Eqs. (D-3) – (D-5) into Eqs. (D-6) – (D-8) and integrating by parts yields a set of linear equations which can be written in the form

$$[S]^{(e)} \ \{Z\}^{(e)} = \{R\}^{(e)} \tag{D-10}$$

$[S]^{(e)}$ is a stiffness matrix for element (e), $\{Z\}^{(e)}$ is the vector of nodal unknowns and $\{R\}^{(e)}$ is a reaction vector which results from the integration by parts. From considerations of computational consistency Λ_i should be higher by one order than Λ_i^p (Taylor and Hood 1973). Thus it is natural to choose Λ_i to be quadratic and Λ_i^p to be linear interpolation functions. Further, if the elements are chosen to be triangular in shape, the various DOF are distributed among the nodes as follows:
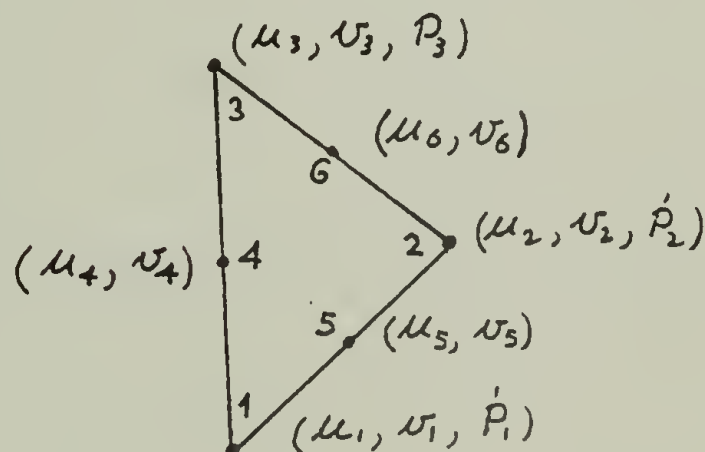
In this element nodes 1, 2, 3 are considered primary nodes. For this case Eq. (D-9) can be written in the form

$$
\begin{bmatrix}
\begin{matrix} 6\times6 \\ [K_1] \end{matrix} & \begin{matrix} 6\times6 \\ [0] \end{matrix} & \begin{matrix} 6\times3 \\ [K_2] \end{matrix} \\
\\
\begin{matrix} 6\times6 \\ [0] \end{matrix} & \begin{matrix} 6\times6 \\ [K_1] \end{matrix} & \begin{matrix} 6\times3 \\ [K_3] \end{matrix} \\
\\
\begin{matrix} 3\times6 \\ [K_2] \end{matrix} & \begin{matrix} 3\times6 \\ [K_3] \end{matrix} & \begin{matrix} 3\times3 \\ [0] \end{matrix}
\end{bmatrix}
\begin{Bmatrix} u_1 \\ \cdot \\ u_6 \\ v_1 \\ \cdot \\ \cdot \\ v_6 \\ P_1 \\ P_2 \\ P_3 \end{Bmatrix}
=
\begin{Bmatrix} R_2 \\ \cdot \\ \cdot \\ \cdot \\ \cdot \\ R_{12} \\ 0 \\ 0 \\ 0 \end{Bmatrix}
\tag{D-11}
$$

where

(a) $\displaystyle K_{1ij} = \int_{(e)} \left(\frac{\partial \Lambda_i}{\partial x} \frac{\partial \Lambda_j}{\partial x} + \frac{\partial \Lambda_i}{\partial y} \frac{\partial \Lambda_j}{\partial y} \right) dxdy$

(b) $\displaystyle K_{2ij} = -\int_{(e)} \frac{\partial \Lambda_i}{\partial x} \Lambda_j^p \, dxdy$

(c) $\displaystyle K_{3ij} = -\int_{(e)} \frac{\partial \Lambda_i}{\partial y} \Lambda_j^p \, dxdy$

(d) $\displaystyle R_i = \int_c \Lambda_i X^* \, ds \qquad\qquad i = 1, \ldots, 6$

(e) $\displaystyle R_i = \int_c \Lambda_i Y^* \, ds \qquad\qquad i = 7, \ldots, 12$

R_i are evaluated along the system boundaries and

$$ X^* = \nabla u^{(e)} \underset{\sim}{n} - n_x P^{(e)} $$

$$ Y^* = \nabla u^{(e)} \underset{\sim}{n} - n_y P^{(e)} $$

$\underset{\sim}{n}$ $(= n_x i + n_y j)$ is an otward unit normal to a boundary segment $d\underline{s}$.

One is now left with the task of selecting proper interpolation functions so that the various terms in Eq. (D-10) can be evaluated explicitly. It is convenient to write these functions in terms of natural coordinates, L_i (see Huebner 1975, Chapter 5). For a triangular element, a proper set of interpolation functions is as follows:

(a) $\Lambda_1 = L_1^2 - L_1 (L_2 + L_3)$

(b) $\Lambda_2 = L_2^2 - L_2 (L_1 + L_3)$

(c) $\Lambda_3 = L_3^2 - L_3 (L_1 + L_2)$

(d) $\Lambda_4 = 4 L_1 L_3$ (D-12)

(e) $\Lambda_5 = 4 L_1 L_2$

(f) $\Lambda_6 = 4 L_2 L_3$

(g) $\Lambda_i^p = L_i$

where

$$L_1 = \frac{1}{2D} (a_1 + b_1 x + C_1 y)$$

$$L_2 = \frac{1}{2D} (a_2 + b_2 x + C_2 y)$$

$$L_3 = \frac{1}{2D} (a_3 + b_3 x + C_3 y)$$

D is an area of triangle 1-2-3,

$$a_1 = x_2 y_3 - x_3 y_2$$

$$b_1 = y_2 - y_3$$

$$c_1 = x_3 - x_2$$

and the other coefficients are obtained by cyclic permutation.

By inserting the chosen interpolation functions into the integrals in Eq. (D-11) all the terms in Eq. (D-10) can be evaluated; the integration is tedious but direct. From here the solution proceeds in the usual FEM fashion. This is summarized by a computer algorithm presented in Figure D-1.

D. 3 The Rigid Planar Blade Coater

The FEM model for this problem is presented in Figure D-1. The dimensions of the system are: $H_0 = 0.5$, $H_1 = 3.5$, and $L = 30$. (in arbitrary units) using the nomenclature of Chapter V. These dimensions correspond to $K = 7.0$ and a blade angle of $5°43'$. The model consists of 28 elements and a total of 174 DOF.

The following boundary conditions are applied:

(a) $u = 1$, $v = 0$ @ $y = 0$

(b) $u = 0$, $v = 0$ @ $y = H$ (position of blade surface)

(c) $\dfrac{\partial u}{\partial n} = \dfrac{\partial v}{\partial n} = 0$ @ $x = 0$, $x = L$ .... (D-13)

(d) $P = 0$ @ $\dot{x} = 0$, $x = L$

Figure D-1.   A computer algorithm for the finite element solution.

```
┌─────────────┐
│    START    │
└─────────────┘
       │
       ▼
┌───────────────────────┐
│      Data input:      │
│  geometry,  topology  │
└───────────────────────┘
       │
       ▼
┌───────────────────────────────────┐
│     Evaluate stiffness matrices   │
│  for all the elements in the system │
└───────────────────────────────────┘
       │
       ▼
┌───────────────────────────────────┐
│        Assemble the elements to   │
│   obtain a global stiffness matrix │
└───────────────────────────────────┘
       │
       ▼
┌───────────────────────────┐
│   Modify reaction vector and │
│   global stiffness matrix to  │
│    account for boundary       │
│        conditions             │
└───────────────────────────┘
       │
       ▼
┌───────────────────────────┐
│   Solve the modified global  │
│    matrix equations by a     │
│  'linear equations solver'   │
│         routine              │
└───────────────────────────┘
       │
       ▼
┌───────────────────────────┐
│     Print final results     │
└───────────────────────────┘
       │
       ▼
┌─────────────┐
│     END     │
└─────────────┘
```
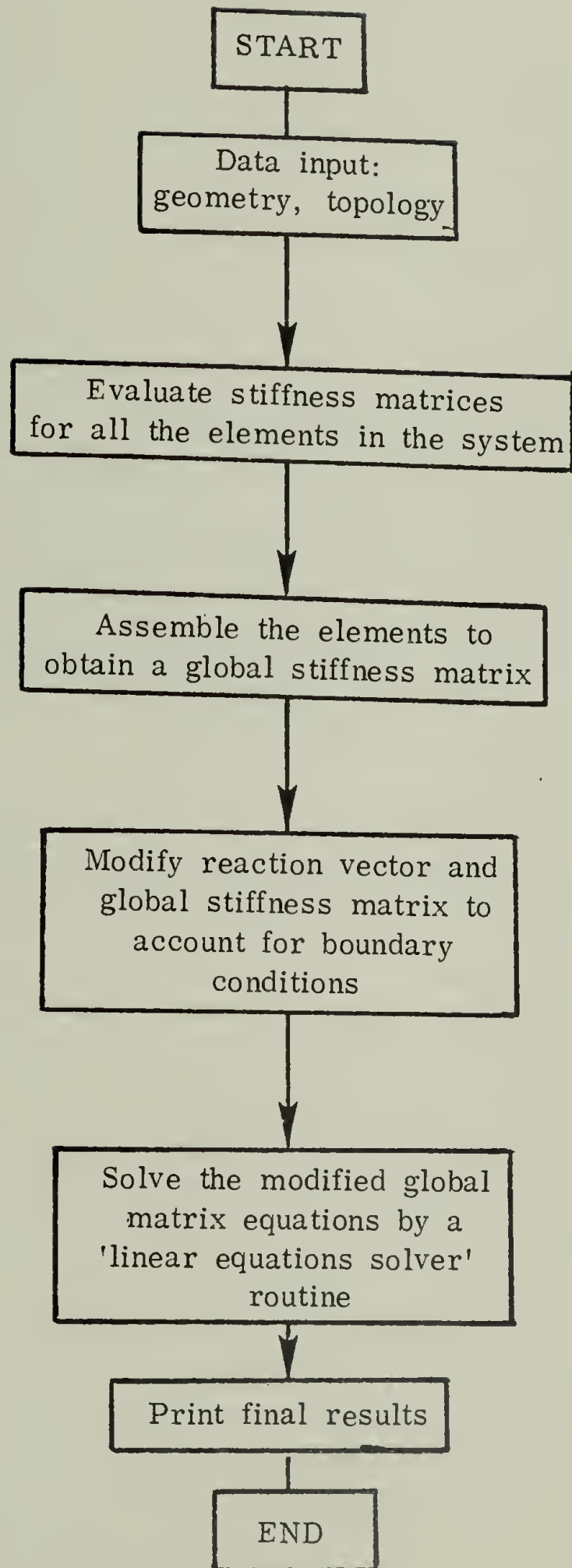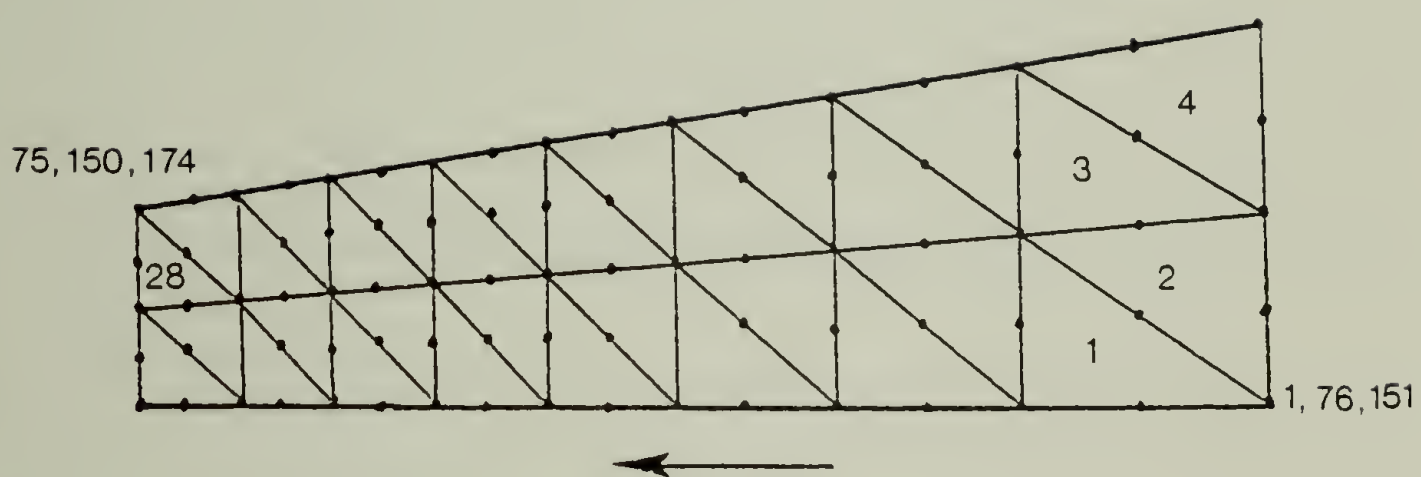
Figure D-2.   A FEM model for the blade coating problem (not to scale).

The physical basis for these conditions has been discussed in V. 2.

The numerically calculated pressure distribution is shown in Figure V-12 together with the lubrication solution. Since slight variation of the pressure across the film was obtained (i.e., $\partial P/\partial y$ is indeed much smaller than $\partial P/\partial x$) the values shown in Figure V-12 represent the average pressures for any x-position. As seen, the "numerical" distribution is in excellent agreement with the lubrication solution for the geometry considered. Also, as expected, the velocity field and, hence, the flow rate as predicted by the lubrication solution match closely the "more exact" numerical solution.

D. 4   The Submerged-Roll System

The FEM model for the submerged-roll system is shown in Figure D-3. The geometric parameters for this model are $H_0 = 0.32$ and $R = 5.35$ (in arbitrary units) using the terminology of Chapter VII. Thus, H_0/R for this case is identical to that value for the experimental setting in the run with the Newtonian fluid (see VII. 3). The symmetry of the system about the nip position allows the consideration of only one half of the flow space thereby reducing considerably the number of DOF to be determined.

The boundary conditions for this system are as follows:
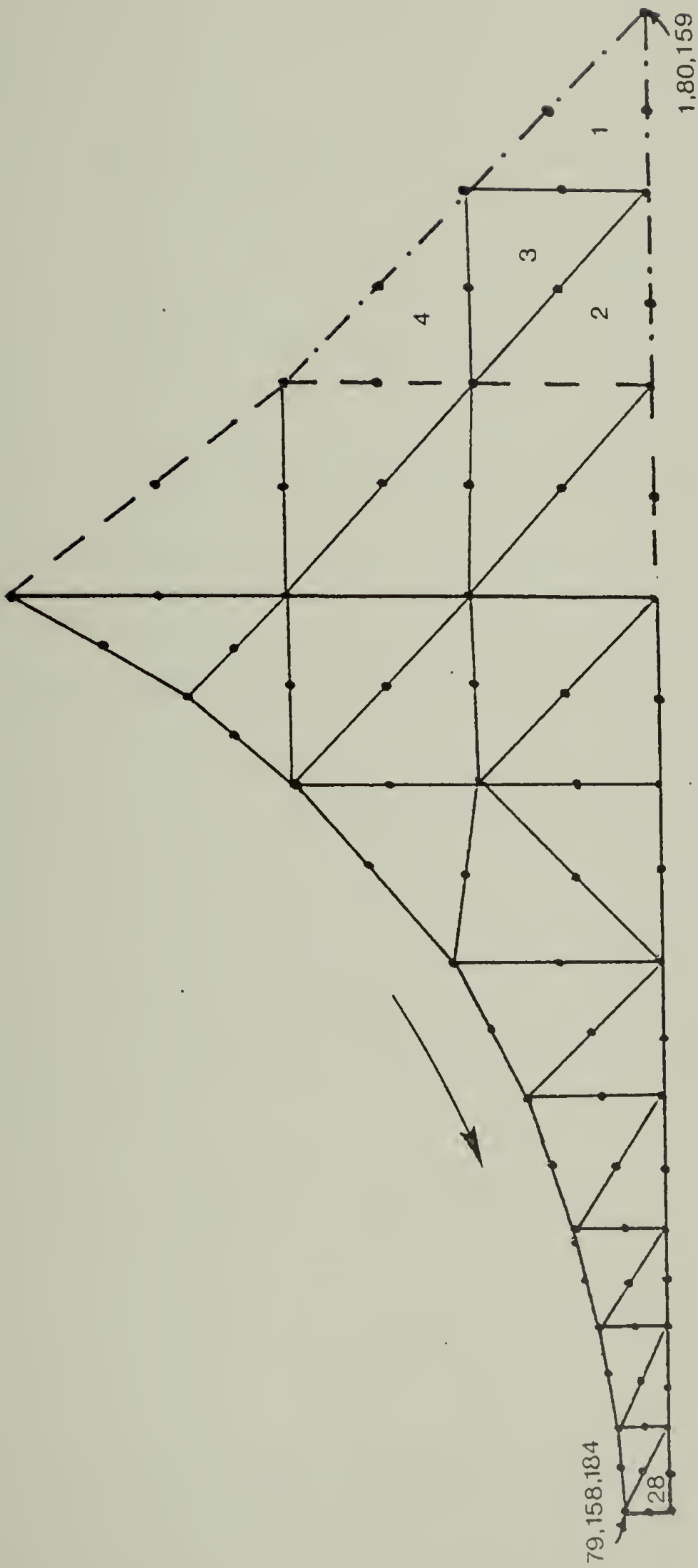
Figure D-3. FEM models for the submerged-roll problem. First model ———, second model ———, third model ——— · ——— ·

(a) $u = v = 0$ @ $y = 0$

(b) $u\underline{i} + v\underline{j} = 1$ @ $y = H$ (position of roll surface)

(c) $\dfrac{\partial u}{\partial n} = \dfrac{\partial v}{\partial n} = 0$ @ $x = 0$, along E   (D-14)

(d) $P = 0$ @ $x = 0$, along E

E is a cross-section of the flow space "far" upstream from the nip whose

position is yet unspecified. By the term "far" is meant a point or a

plane sufficiently removed from the nip region such that the local hydro-

static pressure is unaffected by the hydrodynamic events in the converging

flow space. In order to determine the position of E without increasing

substantially the number of elements, it is necessary to consider a

reasonable model and then expand it several times by some increment

until the pressure distribution is not affected by the expansion. Three

such models were considered in this study as seen in Figure D-3. Each

expansion required the addition of several elements and degrees-of-

freedom. The number of elements and degrees-of-freedom for each model

are given below:

Model	Elements	DOF
1st	19	136
2nd	24	161
3rd	28	184

The second boundary condition for the pressure $(P(0)=0)$ is based on

symmetry considerations. This point is discussed in Chapter VII.
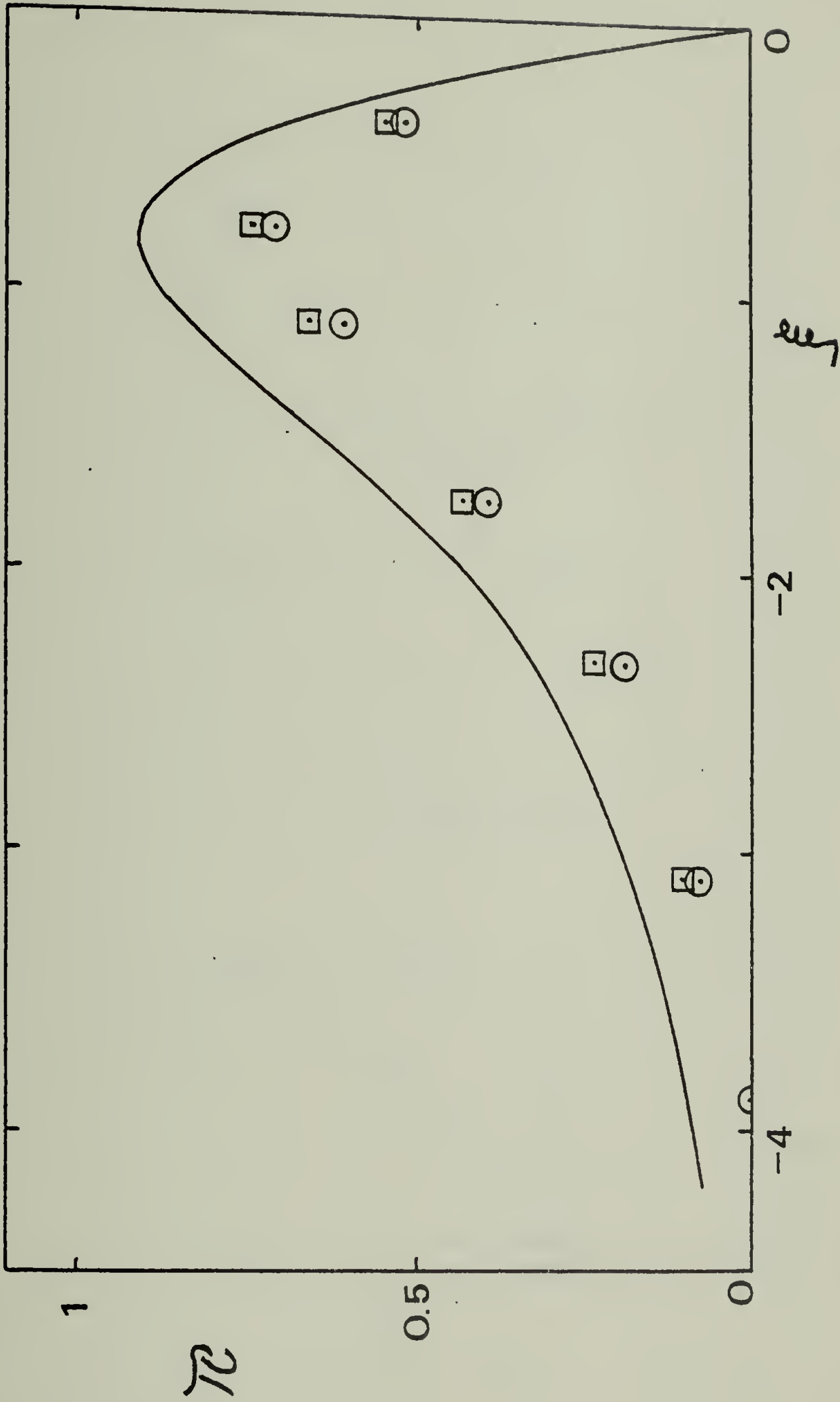
Figure D-4. Pressure distributions for a Newtonian fluid in the submerged-roll system. Calculations by FEM ($\odot$ – 1st model, $\boxdot$ – 2nd and 3rd models) are compared to the Newtonian lubrication solution (the solid curve).
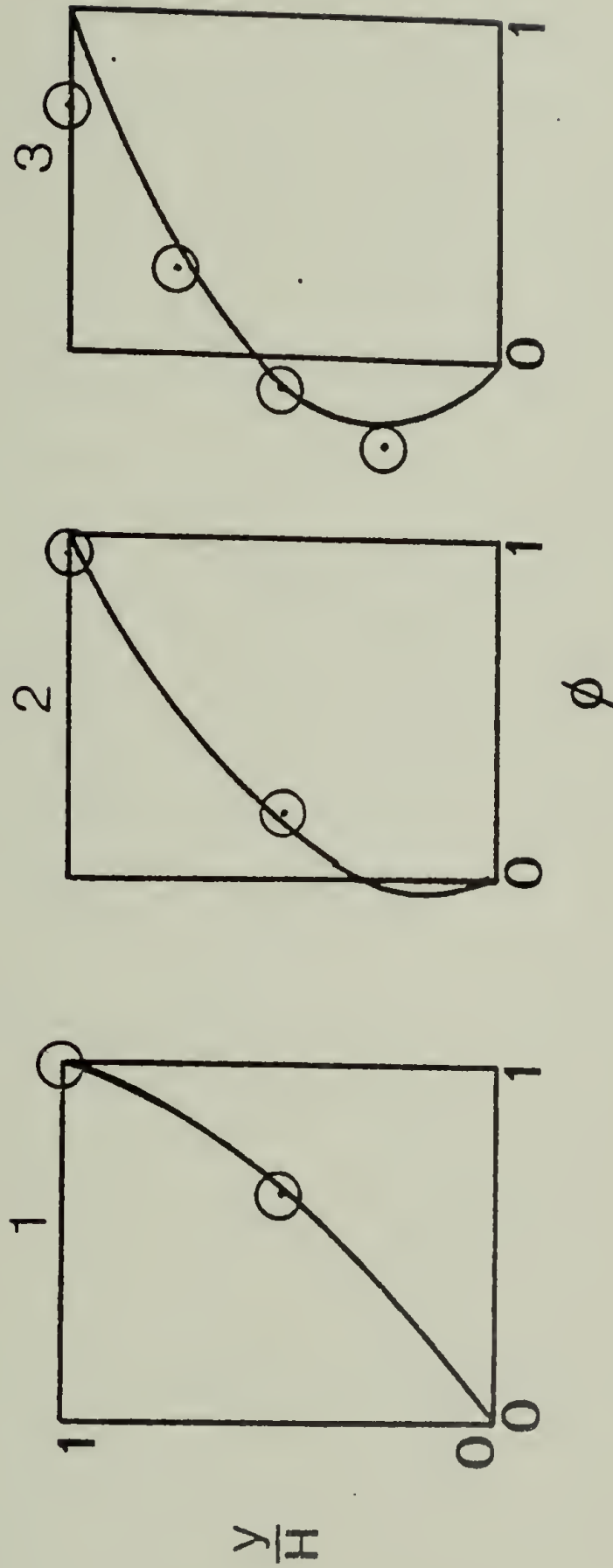
Figure D-5. Velocity profiles for a Newtonian fluid in the submerged-roll system at several axial positions: 1. $f = -0.388$, 2. $f = -1.75$, 3. $f = -3.10$. Calculation by FEM (3rd model) is compared to the lubrication solution (the solid curves).

The calculated pressure distributions are presented in Figure D-3 in terms of the dimensionless variables defined in VII. 2. Inasmuch as the variation of the pressure across the film was relatively small, the results in Figure D-3 represent pressure values that are averaged for each x-position. It was found that the pressure distributions for the first and second models differed by ~ 0.05 using the units of Figure D-4. However, the second and third models gave nearly identical values. The final results (for the 3rd model) are still lower than the lubrication solution. It seems that this difference is primarily due to incorrect upstream boundary conditions for the pressure in the lubrication analysis rather than the two-dimensional nature of the flow. Numerically calculated velocity profiles (u (x, y)) were found nearly identical to the velocity field predicted by the lubrication solution (see Figure D-5).

D. 5 The Computer Program

The computer program for the finite element scheme is based on the algorithm presented in Figure D-1. This program is written in FORTRAN for the CYBER 74 (CDC) system in the University of Massachusetts in Amherst. The various codes are defined and explained in the body of the program. Also, comment statements are added prior to any major operation to assist in following the logic and structure of the program. The solution of the global matrix equations is carried out by the subroutine MATINV that is available in the computer library of the University of Massachusetts.

```
         PROGRAM FEMB              74/74    OPT=1                    FTN 4.6+452              77/1

      C  PROGRAM FEMB
      C  FINITE ELEMENT SOLUTION OF THE SLOW VISCOUS FLOW PROBLEM
      C            VELOCITY-PRESSURE FORMULATION
      C
      C      E IS THE ELEMENT STIFFNESS MATRIX
      C      G IS THE GLOBAL STIFFNESS MATRIX
      C   JTOP IS THE TOPOLOGY ARRAY WHICH TRANSFORMS LOCAL DOF INTO GLOBAL DOF
      C      R IS THE REACTION VECTOR
      C   XC AND YC ARE X- AND Y- POSITIONS OF PRIMARY NODES
      C     NB IS A VECTOR THAT LISTS ALL THE DOF ON THE BOUNDARIES
      C      B IS A VECTOR THAT LISTS ALL THE BOUNDARY CONDITIONS
      C   J1,J2,J3 ARE THE GLOBAL PRIMARY NODES PER ELEMENT
      C      D2S=THE AREA OF AN ELEMENT
      C   NCDF=NUMBER OF DEGREES OF FREEDOM
      C   NPRIM=NUMBER OF PRIMARY NODES
      C   NEL=NUMBER OF ELEMENTS
      C   NBCUND=NUMBER OF BOUNDARY CONDITIONS
      C   NODES=TOTAL NUMBER OF NODES
      C
      C  PROGRAM FEMB(INPUT,OUTPUT)
         DIMENSION E(15,15)
         COMMON G(174,174)
         DIMENSION JTOP(30,15),XC(30),YC(30)
         DIMENSION R(200),B(100),NB(100),NE(100)
      C
         F1(X,Y,Z)= (3.*(X**2)-(2.*X-Y-Z)*(Y+Z))/24.
         F2(X,Y,Z)=((X**2)+(Y+Z)**2)-2.*(Z**2)-2.*X*Y+2.*Y*Z+2.*X*Z)/48.
         F3(X,Y,Z)= (-(X**2)+2.*X*Y+X)*(Y+Z))/12.
         F4(X,Y,Z)= -(X*(Y+Z)+(Y+Z)**2)/12.
         F5(X,Y,Z)= 2.*(X*Y+Y**2+X**2)/3.
         F6(X,Y,Z)= (X**2+X*Y+X*Z+2.*Y*Z+2.*Y*Z)/3.
      C
      C  DATA INPUT
```

```fortran
      READ 3,NDOF,NPRIM,NEL,NBOUND,NODES
      CALL SINDEX(NDOF,NPRIM,NEL,NBOUND,JTOP,XC,YC,R,B,NB)
      READ 1,((JTOP(II,JJ),JJ=1,NPRIM),II=1,NEL)
      READ 2,((XC(II),II=1,NPRIM)
      READ 2,((YC(K),K=1,NBOUND)
      READ 1,(NB(K),L=1,NBOUND)
    1 FORMAT(15(I3,,1X),21X)
    2 FORMAT(15(F5.2,1X),15X)
    3 FORMAT(5(I3,1X))
   20 FORMAT(//,5X,15HSYSTEM-TOPOLOGY,//,1X,7HELEMENT,2X,
     $ U2  U3  U4  U5  U6  V1  V2  V3  V4  V5  V6  P1  P2  P3/)
      DO 100 II=1,NEL
      PRINT 4,II,(JTOP(II,JJ),J=1,15)
    4 FORMAT(4X,I2,2X,15I4)
  100 CONTINUE
   21 FORMAT(///,5X,15HSYSTEM-GEOMETRY,//,2X,4HNODE,6X,1HX,7X,1HY/)
      DO 110 K=1,NPRIM
      PRINT 5,K,XC(K),YC(K)
    5 FORMAT(3X,I2,4X,F6.3,3X,F5.3,/)
  110 CONTINUE
      DO 120 K1=1,NDCF
      DO 120 K2=1,NDCF
      G(K1,K2)=0.
  120 CONTINUE
C
C     ELEMENT MATRIX CALCULATION AND GLOBAL MATRIX ASSEMBLY
C
      DO 130 I=1,NEL
      JJ1=JTOP(III,13)-2*NODES
      JJ2=JTOP(III,14)-2*NODES
      JJ3=JTOP(III,15)-2*NODES
      B1=YC(JJ2)-YC(JJ3)
      B2=YC(JJ3)-YC(JJ1)
      B3=YC(JJ1)-YC(JJ2)
      CC1=XC(JJ3)-XC(JJ2)
      CC2=XC(JJ1)-XC(JJ3)
      CC3=XC(JJ2)-XC(JJ1)
      C=0.5*(XC(JJ2)*(YC(JJ3)-YC(JJ1))+XC(JJ3)*(YC(JJ1)-YC(JJ2))
     $  +YC(JJ1)*(XC(JJ3)-XC(JJ2)))
      DO 140 K1=1,15
      DO 140 K2=1,15
      E(K1,K2)=0.
```

```
140 CONTINUE
    E(1,1)=(F1(B1,B2,B3)+F2(C1,C2,C3))/D
    E(1,2)=(F2(B1,B2,B3)+F3(C1,C3,C2))/D
    E(1,3)=(F3(B1,B3,B2)+F4(C1,C3,C2))/D
    E(1,4)=(F3(B2,B3,B1)+F3(C1,C3,C2))/D
    E(1,5)=(F4(B2,B3,B1)+F3(C1,C2,C3))/D
    E(2,2)=(F1(B1,B3)+F2(C2,C1,C3))/D
    E(2,3)=(F2(B3,B1)+F4(C2,C3,C1))/D
    E(2,4)=(F4(B2,B3,B1)+F3(C2,C1,C3))/D
    E(2,5)=(F3(B2,B3,B1)+F3(C2,C3,C1))/D
    E(3,3)=(F1(B3)+F2(C3,C1,C2))/D
    E(3,4)=(F3(B1,B3)+F4(C3,C2,C1))/D
    E(3,5)=(F4(B2,B3)+F3(C3,C1,C2))/D
    E(4,4)=(F3(B3,B1)+F5(C1,C3))/D
    E(4,5)=(F4(B1,B3)+F6(C3,C1,C2))/D
    E(5,5)=(F6(B1,B3)+F5(C1,C2))/D
    E(6,6)=(F6(B2,B1,B3)+F5(C2,C1,C3))/D
    E(6,13)=(E1,B2)/6.
    E(7,8)=(B2+B3)/6.
    E(7,10)=(B2,B1)/6.
    E(7,12)=(B2+B3)/6.
    E(7,14)=(-C1+C2+C3)/12.
    E(7,15)=(C1+C2+C3)/24.
```

```
      E(8,8)==E(2,2)
      E(8,9)==E(2,3)
      E(8,10)==E(2,4)
      E(6,11)==E(2,5)
      E(8,12)==E(2,6)
      E(8,13)==E(7,14)
      E(8,14)==(-C2+C1+C3)/12.
      E(8,15)==E(7,14)
      E(9,9)==E(3,3)
      E(9,10)==E(3,4)
      E(9,11)==E(3,5)
      E(9,12)==E(3,6)
      E(9,13)==E(7,14)
      E(9,14)==E(7,14)
      E(9,15)==(-C3+C1+C2)/12.
      E(10,10)==E(4,4)
      E(10,11)==E(4,5)
      E(10,12)==E(4,6)
      E(10,13)==(2.*C3+C1)/6.
      E(10,14)==(C3+C1)/6.
      E(10,15)==(2.*C1+C3)/6.
      E(11,11)==E(5,5)
      E(11,12)==E(5,6)
      E(11,13)==(2.*C2+C1)/6.
      E(11,14)==(2.*C1+C2)/6.
      E(11,15)==(C1+C2)/6.
      E(12,12)==E(6,6)
      E(12,13)==(C2+C3)/6.
      E(12,14)==(2.*C3+C2)/6.
      E(12,15)==(2.*C2+C3)/6.
      DO 150 K3=2,15
      K5=K3-1
      DO 150 K4=1,K5
      E(K3,K4)=E(K4,K3)
  150 CONTINUE
      DO 130 I2=1,15
      J1=JTCP(I1,I2)
      DO 130 I3=1,15
      J2=JTCP(I1,I3)
      G(J1,J2)=G(J1,J2)+E(I2,I3)
```

```fortran
130   CONTINUE
C
C     INSERTION CF BOUNDARY CONDITIONS
      WRITE 15
15.   FORMAT(//5X,*BOUNDARY CONDITIONS*,//,3X,3HDOF,
     $3X,*BOUNDARY VALUE*/)
      PRINT 16,(NB(I),B(I),I=1,NECUND)
16.   FORMAT(3X,I3,EX,F6.3/)
      DO 180 I=1,NCCF
      R(I)=0.
180   CONTINUE
C
C     MCDIFICATION CF REACTION VECTCR R
      DO 210 L1=1,NDOF
      DO 250 L2=1,NECUND
      IF(L1.NE.NB(L2))GOTO 250
      R(L1)=B(L2)
      GOTO 210
250   CONTINUE
      DO 230 L3=1,NDOF
      DO 240 L4=1,NECUND
      IF(L3.NE.NB(L4))GOTO 240
      R(L1)=R(L1)-G(L1,L3)*B(L4)
      GOTO 230
240   CONTINUE
230   CONTINUE
210   CONTINUE
C
C     MCDIFICATION OF GLOBAL MATRIX G
      DO 190 L1=1,NECUND
      DO 260 L2=1,NDOF
      G(NB(L1),L2)=0.
      G(L2,NB(L1))=0.
260   CONTINUE
      G(NB(L1),NB(L1))=1.
190   CONTINUE
C
C     SCLUTION OF THE MATRIX EQUATIONS (G*X=R) BY MATINV
      CALL MATINV(G,NDOF,R,1,DETERM,NDOF)
      PRINT 12,DETERM
12    FORMAT(//,5X,20HDETERMINANT CF G IS ,E9.3///)
```

```fortran
C
C      BAND-WIDTH DETERMINATION
C
       IBAND=0
       DO 400 M=1,NCOF
       DO 410 M1=M,NCOF
410    IF (G(M,M1).NE.0.) IROW=M1-M
       IF (IBAND.LT.IROW) IBAND=IROW
400    CONTINUE
       PRINT 13,IBAND
13     FORMAT(///,5X,24HHALF BAND WIDTH OF G IS ,I3///)
       PRINT 8
8      FORMAT(////,20X,13HFINAL-RESULTS///10X,4HNODE
      $,7X,4HV(X),8X,4HV(Y)//)
       DO 300 K=1,NODES
       K1=K+NODES
       PRINT 9,K,R(K),R(K1)
9      FORMAT(11X,I3,5X,F7.4,5X,F7.4/)
300    CONTINUE
       PRINT 10
10     FORMAT(//6X,12HPRIMARY-NODE,5X,19HNORMALIZED-PRESSURE//)
       DO 310 K1=1,NPRIM
       K=K1+2*NODES
       PRINT 11,K1,R(K)
11     FORMAT(11X,I3,17X,F8.4/)
310    CONTINUE
       STOP
       END
```

```
      SUBROUTINE MATINV (A,NSUB,B,MSUB,DET,NMAX)
C
C     MATRIX INVERSION WITH ACCOMPANYING SOLUTION OF LINEAR EQUATIONS
C
      DIMENSION A(NMAX,NSUB), B(NMAX,MSUB)
      DIMENSION PIVOT(174)
      DIMENSION IPIVOT(174), INDEX(174)
      EQUIVALENCE (PIVOT,INDEX),(PIVOT,IPIVOT)
      DATA (ISHIFT=4096), (MASK=0000000077777777B)
C
      N=NSUB
      M=MSUB
C
C     INITIALIZATION
C
      DETERM=1.0
      DO 20 I=1,N
      IPIVOT(I)=0
   20 CONTINUE
      DO 550 I=1,N
C
C     SEARCH FOR PIVOT ELEMENT
C
      AMAX=0.0
      DO 105 J=1,N
      TEMP=IPIVOT(J).AND..NOT.MASK
      IF(TEMP)105, 60
   60 DO 100 K=1,N
      TEMP=IPIVOT(K).AND..NOT.MASK
      IF(TEMP)100, 80
   80 TEMP=ABS(A(J,K))
      IF(TEMP-AMAX) 100, 85, 85
   85 IROW=J
      ICOLUM=K
      AMAX=TEMP
  100 CONTINUE
  105 CONTINUE
      INDEX(I)=INDEX(I) + (ISHIFT*IROW+ICCLUM)
      J=IROW
      AMAX=A(J,ICOLUM)
      DETERM=AMAX*DETERM
```

355

```fortran
C
C     RETURN IF MATRIX IS SINGULAR
C
      IF (DETERM) 110, 600
C
  110 PIVOT(ICOLUM)=INDEX(ICCLUM).OR.AMAX.AND..NOT.MASK
C
C     INTERCHANGE ROWS TO PUT PIVOT ELEMENT ON DIAGONAL
C
  140 IF (IROW-ICOLUM) 140, 260
      DETERM=-DETERM
      DO 200 K=1,N
      SWAP=A(J,K)
      A(J,K)=A(ICOLUM,K)
      A(ICOLUM,K)=SWAP
  200 CONTINUE
      IF(M.EG.0) GOTO 251
      DO 250 K=1,M
      SWAP=B(J,K)
      B(J,K)=B(ICOLUM,K)
      B(ICOLUM,K)=SWAP
  250 CONTINUE
  251 CONTINUE
C
C     DIVIDE PIVOT ROW BY PIVOT ELEMENT
C
  260 K=ICOLUM
      A(ICCLUM,K)=1.0
      DO 350 K=1,N
      A(ICCLUM,K)=A(ICOLUM,K)/AMAX
  350 CONTINUE
      IF(M.EQ.0)GOTO 371
      DO 370 K=1,M
      B(ICOLUM,K)=B(ICOLUM,K)/AMAX
  370 CONTINUE
  371 CONTINUE
C
C     REDUCE NON-PIVOT ROWS
C
  400 DO 550 J=1,N
      IF(J-ICOLUM) 400, 550
      T=A(J,ICOLUM)
      A(J,ICOLUM)=0.0
      DO 450 K=1,N
      A(J,K)=A(J,K)-A(ICOLUM,K)*T
```

```
450   CONTINUE
      IF(M.EQ.0)GOTO 501
      DO 500 K=1,M
      B(J,K)=B(J,K)-B(ICOLUM,K)*T
500   CONTINUE
501   CONTINUE
550   CONTINUE
C
C        INTERCHANGE COLUMNS
600   DO 710 I=1,N
      I1=N+1-I
      IRC=INDEX(I1).AND.MASK
      K=IRC/ISHIFT
      ICOLUM=IRC-K*ISHIFT
      IF (K-ICOLUM) 650, 710
650   DO 705 J=1,N
      SWAP=A(J,K)
      A(J,K)=A(J,ICOLUM)
      A(J,ICOLUM)=SWAP
705   CONTINUE
710   CONTINUE
C
740   DET=DETERM
      RETURN
      END
```

A P P E N D I X E

APPLICATION OF THE COYNE AND ELROD (CE) SEPARATION CONDITIONS TO THE SYSTEM OF PARTIALLY IMMERSED COUNTER-ROTATING ROLLERS

E.1 Scope

This appendix outlines the way by which the CE conditions (Coyne and Elrod 1969, 1970; see also IV.4) are applied in the system of partially immersed counter-rotating rollers. The first part, E.2, deals with the stable flow problem and a relation for the position of film separation is obtained. In the second part (E.3) a critical condition for stability is derived based on Savage's theory (Savage 1977a). A linear stability analysis for the system of counter-rotating rollers is presented in E.4 in a manner that parallels Savage's (1977b) work. This analysis yields an algebraic equation for the wavenumber. The terminology and nomenclature, in this appendix, follow VI.3 and VIII.2.

E.2 Stable Flow

The Coyne and Elrod theory yields two functions that are characteristic of the separation region in a partial film lubrication system. These functions are:

$$\beta = \frac{\lambda}{\sigma_1} = \beta \, (N_{ca}, \; N_g, \; N_{Re}) \tag{E-1}$$

and,

$$\chi = \frac{r}{\xi_1 H_0} = \chi(N_{Ca}, N_g, N_{Re})$$

(E-2)

As specified, both β and χ are dependent upon three dynamic parameters. However, in the present calculation gravity and inertia effects are not considered.

From the lubrication analysis (VI.3) the pressure-gradient in the bounded regime (for $n = 1.0$) is given by

$$\dot{\pi} = \frac{3}{\xi^2} (1 - \frac{\lambda}{\xi})$$

(E-3)

or, using Eq. (E-1),

$$\dot{\pi} = \frac{3}{\xi^2} (1 - \frac{\beta \xi_1}{\xi})$$

(E-4)

From a simple force balance the pressure at separation ($\xi = \xi_1$) is,

$$\pi_1 = - N_S \frac{1}{\chi \xi_1}$$

(E-5)

where the radius of curvature (r) has been evaluated using Eq. (E-2). Eqs. (E-4) and (E-5) are, in fact, the CE boundary conditions. ξ_1, the point of separation, is the only unknown so far and it can be evaluated by equating the upstream pressure to the pressure specified at separation. Thus,

$$\int_{-\infty}^{\xi_1} \dot{\pi} d\xi = \pi_1$$

(E-6)

The integration in Eq. (E-6) can be carried out analytically by using the transformation $\xi^2 = 2\tan^2\alpha$. Eventually, the following equation for α_1 ($=\tan^{-1}\xi_1/\sqrt{2}$) is obtained,

$$-\frac{\sqrt{2}}{6}\frac{N_S}{\varkappa}\cos^2\alpha_1 - \frac{\alpha_1}{2} - \frac{\pi}{4} - \frac{\sin 2\alpha_1}{4}$$

$$+ \frac{\beta}{\cos^2\alpha_1}\left(\frac{3\alpha_1}{8} + \frac{3\pi}{16} + \frac{\sin 2\alpha_1}{4} + \frac{\sin 4\alpha_1}{32}\right) = 0 \tag{E-7}$$

This transcendental equation in α_1 was solved graphically and the results in terms of ξ_1 are given in Figure E-1 where β (N_{Ca}) and $\varkappa$ (N_{Ca}) were taken from Coyne and Elrod's work. The results can be easily cast in the form of a λ ($= \beta/\cos^2\alpha_1$) vs. N_S curve which can be compared to the corresponding curve for the approximate separation model discussed in Chapter VI. Such comparison is presented in Figure VI-16.

E.3 Stability Criterion for the Ribbing Phenomenon

This derivation follows closely Savage's (1977a) work. Savage has derived an explicit stability criterion for the cylinder-plane system (rotating cylinder parallel to a stationary plane). However, his derivation for the system of partially immersed counter-rotating rollers is not complete and it is rederived here in full. Pitts and Greiller's physical stability criterion (VIII. 4) reads,

$$\left.\frac{dP}{dx}\right|_{x_1} < \frac{\tau}{r^2}\left.\frac{dr}{dx}\right|_{x_1} \tag{E-8}$$

Figure E-1. β, χ and ξ_1 (the position of film separation) vs. the capillary number. The functions β and χ are extracted from Coyne and Elrod's work (1969, 1970). ξ_1 is calculated for the system of partially immersed counter rotating rollers (——— $H_0/R = 0.005$, - - - - $H_0/R = 0.05$).
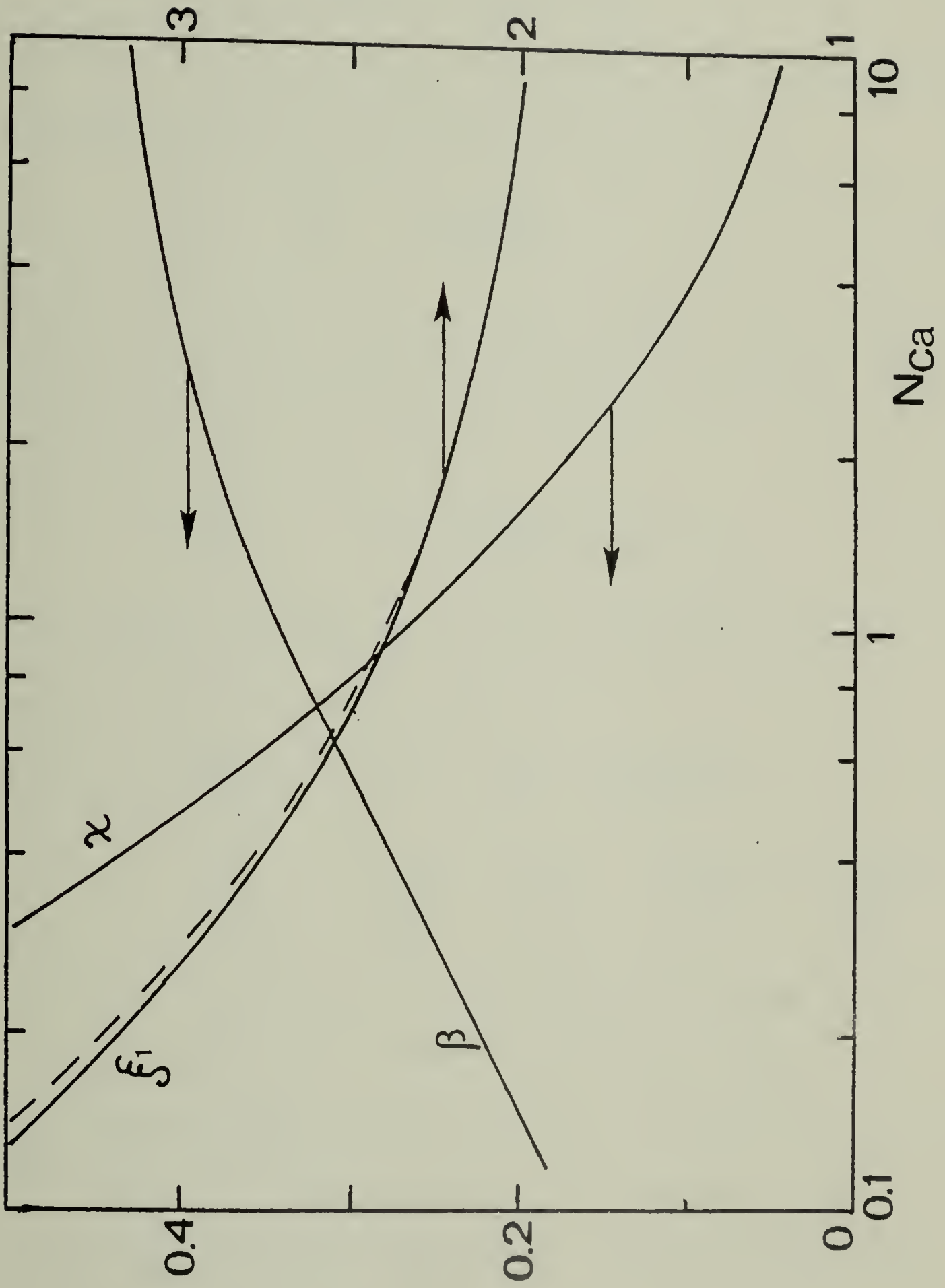
or, in dimensionless form,

$$\dot{\pi}_1 \; < \; \frac{N_S}{\mathcal{X}\mathcal{6}_1{}^2} \; \frac{d}{d\xi} \; (\mathcal{6})\Big|_{\xi_1} \tag{E-9}$$

After some algebraic manipulations using Eqs. (E-2), (E-4) and (E-9), the following expression for the stability limit is obtained,

$$N_S{}^* \; = \; \frac{3\sqrt{2}}{2} \; \frac{\mathcal{X}^*(1-\beta^*)}{\tan\alpha_1^*} \tag{E-10}$$

where the superscript * denotes critical conditions. Eq. (E-10) can be written as a relation between the geometric parameter H_0/R and the critical capillary number, N_{Ca}^*, in the form

$$\frac{H_0}{R} \; = \; \frac{9}{2} \; \Big[\frac{\mathcal{X}^*(1-\beta^*)}{\tan\alpha_1^*} \; N_{Ca}^* \Big]^2 \tag{E-11}$$

This equation is coupled with Eq. (E-7) for α_1 that is still valid. Combination of Eqs. (E-7) and (E-11) gives,

$$(\beta^*-1) \; \frac{\cos^2\alpha_1^*}{2\tan\alpha_1^*} \; = \; \frac{\pi}{4} \; + \; \frac{\alpha_1^*}{2} \; + \; \frac{\sin 2\alpha_1^*}{4} \tag{E-12}$$

$$- \; \frac{\beta^*}{\cos^2\alpha_1^*} \; \Big(\frac{3\pi}{16} \; + \; \frac{3\alpha_1^*}{8} \; + \; \frac{\sin 2\alpha_1^*}{4} \; + \; \frac{\sin 4\alpha_1^*}{32} \Big)$$

This equation gives the relationship between α_1^* and β^* which is presented in Figure E-2 . Since β^* is a known function of N_{Ca}^* (or $\mathcal{X}^*$) it is possible to solve Eq. (E-11) for H_0/R. The relation between H_0/R and N_{Ca}^* constitutes a stability criterion for the system of partially immersed counter rotating rollers. This criterion is plotted in Figure VIII-3.
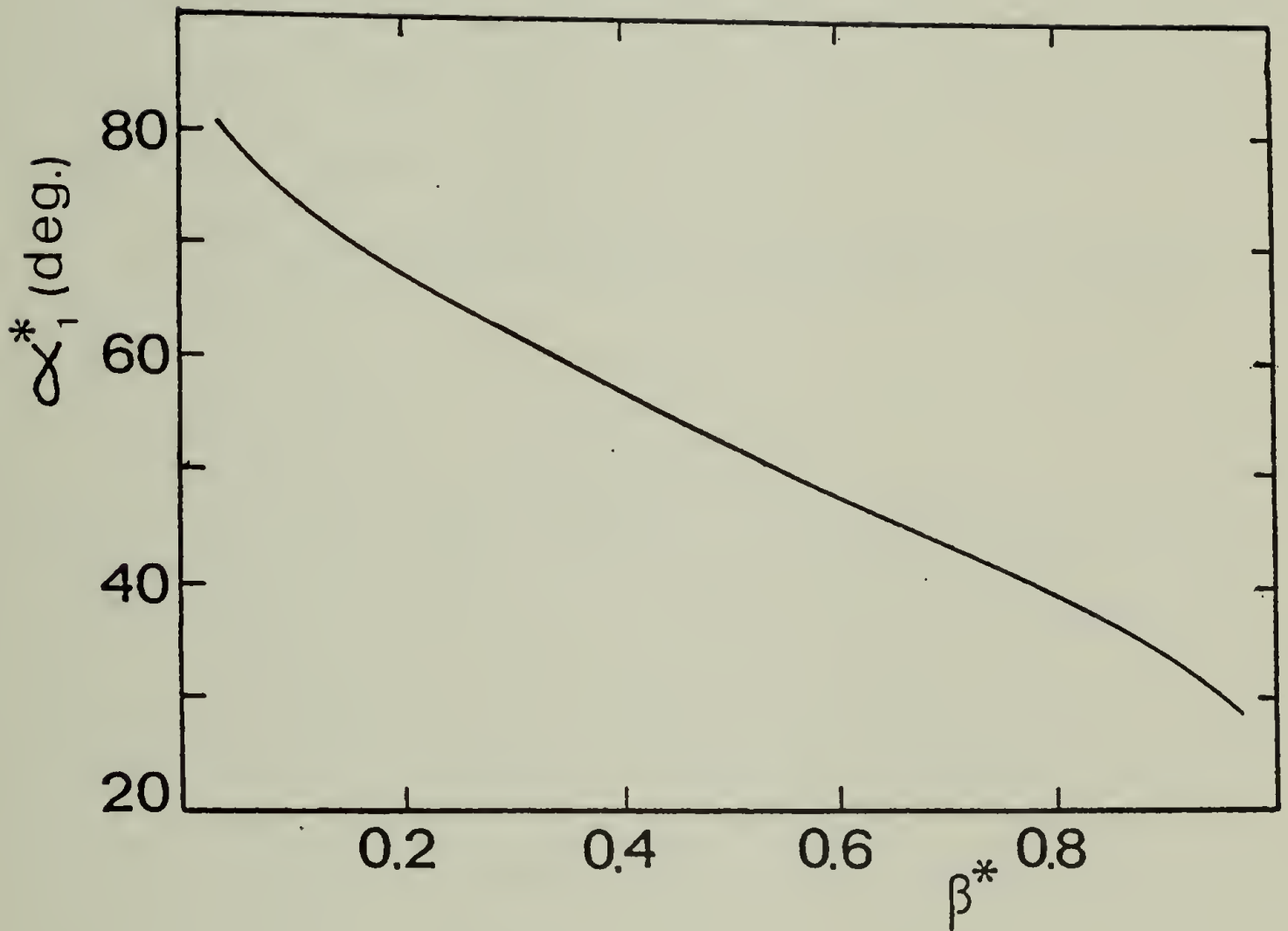
Figure E-1. The position of film separation under critical conditions vs. the function β^*. Calculations are for the system of partially immersed counter rotating rollers.

E.4   A Linear Stability Analysis

In the second part of Savage's work (1977b) a linear stability analysis is carried out for a cylinder-plane geometry. This analysis results in a second-order ordinary differential equation combined with a set of boundary conditions that are based on Coyne and Elrod's theory. A solution to this equation yields a relation between the wavenumber, $\mathcal{N}^{\circ}$, the geometry (H_0/R) and the capillary number.

In the unstable flow domain the pressure function is assumed to be expressed by

$$P(x,z) = P^0(x) + \epsilon G(x)\sin \mathcal{N}z \tag{E-13}$$

where $P^0(x)$ is the pressure function in the unperturbed case, ϵ is the magnitude of the perturbation ($\epsilon \ll X_1$) and $G(x)$ is an unspecified function. The objective of this analysis is to determine both $\mathcal{N}$ and $G(x)$. As this analysis (for the system of counter-rotating rollers) parallels Savage's treatment, the resulting boundary-value problem is presented without derivation. Essentially Eq. (E-13) is introduced into the governing equations of motion and after some manipulations the following differential equation is obtained.

$$\frac{d^2g}{d\xi^2} + \frac{3\xi}{1 + 1/2\,\xi^2}\,\frac{dg}{d\xi} - N^2 g = 0 \tag{E-14}$$

where

$$g(\xi) = G(x)\,\frac{\epsilon_1{}^2\,H_0{}^2}{3\mu U}$$

and
$$N^2 = \mathcal{N}^2(RH_0)$$

This equation is evidently slightly different from the equation given by Savage due to the geometric differences between the systems considered. Eq. (E-14) is accompanied by the following boundary conditions

$$g(-\infty) = 0 \tag{E-15}$$

$$g(\xi_1) = \beta - 1 + \frac{1}{3N_{Ca}\chi} \left(\frac{H_0}{R}\right) \xi_1$$

$$\tag{E-16}$$

$$+ \frac{1}{3N_{Ca}} \left(\frac{H_0}{R}\right) N^2 (1 + \tfrac{1}{2}\xi_1^2)^2$$

and

$$\frac{dg}{d\xi}\bigg|_{\xi_1} = -\frac{\xi_1}{1 + 1/2\,\xi_1^2} \tag{E-17}$$

In addition, the position of flow separation (ξ_1) is given by Eq. (E-7) which is assumed to be still valid. Eq. (E-15) results from specifying zero pressure at the system inlet. Eq. (E-16) is a force balance at separation and Eq. (E-17) is a statement of conservation of mass.

The boundary-value problem defined by Eqs. (E-14) – (E-17) and (E-7) is clearly too complex to be handled by exact analytical methods. Savage showed, however, that the expression

$$g(\xi) = g(\xi_1) \exp[w(\xi - \xi_1)] \tag{E-18}$$

is a reasonable approximation of the exact solution for g. In order to satisfy Eq. (E-14) w should have the form

$$w = -k + [k^2 + N^2]^{1/2} \tag{E-19}$$

where

$$k = \frac{3}{2} \frac{\xi_1}{1 + 1/2\,\xi_1^2}$$

Also $g(\xi_1)$ is given by Eq. (E-16). Finally, using Eq. (E-17), the following cubic equation in w is found

$$w^3 + 2\,k\,w^2 - l\,w + m = 0$$

where

$$l = \frac{3N_{Ca}(1-\beta) - \frac{1}{\mathscr{X}}\left(\frac{H_0}{R}\right)^{1/2}\xi_1}{\frac{H_0}{R}(1 + 1/2\,\xi_1^2)^2}$$

and

$$m = \frac{3N_{Ca}\,\xi_1\,\beta}{\frac{H_0}{R}(1 + 1/2\,\xi_1^2)^3} .$$

Once the coefficients k, l and m are known, the equation can be solved graphically for w. These coefficients can be determined, using Coyne and Elrod's theory, for any specified N_{Ca} and H_0/R (see Figure E-1). As was pointed out by Savage, only one solution (out of the three possible) is physically admissible. This solution yields the wavenumber for a particular set of H_0/R and N_{Ca}.

Some calculated values of $\mathscr{N}$ for the data given in VIII.2 are listed in Table E-1. A comparison of these values, expressed as normalized wavelengths, to the measured values is presented in Figure VIII-5.

Table E-1

Results of Wavenumber Calculations
Using the Modified Savage Theory

Fluid[1]	H_0/R	U[rpm]	N_{Ca}	β^2	$\varkappa^2$	f_1^2	w	$W/2H_0$
G	0.0129	37.5	1.51	0.36	0.21	2.25	1.875	10.81
"	"	67	2.67	0.40	0.13	2.15	3.15	6,85
"	"	97	3.90	0.41	0.10	2.10	4.55	5.03
KS	0.0228	48	3.52	0.405	0.11	2.05	2.35	6.47
"	"	57	4.18	0.41	0.09	2.05	2.70	5.84
"	"	76.5	5.61	0.42	0.07	2.05	3.35	4.90
GWS-0.90	0.0129	76.5	1.80	0.38	0.185	2.20	2.25	8.99
"	"	129	3.03	0.40	0.12	2.10	3.75	5.97
"	"	181	4.25	0.415	0.09	2.05	4.875	4.71

[1] Physical properties for the fluids listed are given in Tables VI-4 and A-8.

[2] Extracted from Figure E-1.